Molecular Mechanisms of Intercellular Coupling among Peripheral Circadian Oscillators

DISSERTATION

zur Erlangung des akademischen Grades

Doctor rerum naturalium (Dr. rer. nat.)

im Fach Biologie mit der Spezialisierung Molekularbiologie

eingereicht an der

Lebenswissenschaftlichen Fakultät der Humboldt-Universität zu Berlin

von

M.Sc. Anna-Marie Finger

Präsidentin der Humboldt-Universität zu Berlin

Prof. Dr.-Ing. Dr. Sabine Kunst

Dekan der Lebenswissenschaftlichen Fakultät der Humboldt-Universität zu Berlin

Prof. Dr. Bernhard Grimm

Gutachter/innen

1. Prof. Dr. Hanspeter Herzel
2. Prof. Dr. Achim Kramer
3. David Gatfield, PhD

Tag der mündlichen Prüfung: 19.06.2020

Abstract

Circadian clocks have evolved as endogenous timekeepers, allowing living beings to anticipate and adapt to daily environmental changes (Zeitgebers), most importantly the light-dark cycle. Mammalian circadian systems constitute hierarchically organized networks of cell-autonomous oscillators. On the cellular level, circadian rhythms are driven by intertwined feedback loops between clock genes and their own protein products. On the tissue level, oscillations are generated by ensembles of cell-autonomous oscillators, which need to be synchronized to maintain coherent network rhythmicity. On the system level, a central “pacemaker” is located in the suprachiasmatic nucleus (SCN) of the hypothalamus and ensures entrainment of subsidiary body clocks to the light-dark cycle, as well as correct phase alignment among them. Within the SCN, individual neuronal oscillators are strongly coupled to sustain synchronized and robust tissue rhythms. Such robust rhythmicity is indispensable for the temporal coordination of biological organ functions and circadian physiology and its disruption has been associated with diverse human pathologies.

Evidence supporting the independence of synchronized peripheral tissue rhythms has accumulated over the last years. Nevertheless, existence, let alone molecular mechanisms and functional role of intercellular coupling among peripheral circadian oscillators remain highly debated. Here we provide additional evidence for the existence of intercellular coupling, using U-2 OS cells as model of peripheral circadian oscillators. Moreover, our results indicate that peripheral circadian oscillators couple via the exchange of secreted signaling molecules, namely growth factors. To our knowledge, we are the first to have identified a potential mechanism of peripheral coupling, as well as to show that perturbation of this mechanisms results in weakened rhythmicity of peripheral circadian oscillator networks. In other words, our findings demonstrate that coupling via the TGF-β pathway promotes synchronization among peripheral circadian oscillators, characterized by high-amplitude and lowly damped network rhythms, as well as robustness against perturbation by Zeitgeber stimuli. We suggest that peripheral coupling plays an important role for the entrainment of peripheral tissue clocks to incoming SCN-derived or external signals, as well as for the temporal coordination of their rhythmic biological functions.

Zusammenfassung

Zirkadiane Uhren sind körpereigene „Zeitmess-System“, welche sich evolutionär entwickelt haben. Sie ermöglichen lebenden Organismen die Antizipation von und die Anpassung an periodisch widerkehrende Umgebungsbedingungen (Zeitgeber), insbesondere den Licht-Dunkel Rhythmus. Zirkadiane Netzwerke in Säugetieren sind hierarchisch aufgebaut. Auf zellulärer Ebene ergeben sich zirkadiane Oszillationen aus sogenannten „Transkriptions-Translations-Rückkopplungsschleifen“ zwischen Uhr-Genen und deren eigenen Proteinprodukten. Auf Gewebseben müssen selbsterhaltende Einzelzelloszillatoren ihre Rhythmen synchronisieren, um robuste Gewebeoszillationen zu erhalten. Auf systemischer Ebene gewährleistet eine sogenannte „Schrittmacher-Uhr“, welche sich im Nucleus suprachiasmaticus (SCN) des Hypothalamus befindet, die Anpassung an den Licht-Dunkel Rhythmus, als auch die Abstimmung zirkadianen Rhythmen untergeordneter Gewebeuhren aufeinander. Innerhalb des SCN sind neuronale Einzeloszillatoren stark miteinander gekoppelt, um synchronisierte und robuste Geweberhythmik zu erzeugen. Solch robuste Rhythmik ist entscheidend für die zeitliche Koordination zirkadianer Organfunktionen und für die Gesundheit des Organismus. Störungen und Fehljustierungen der Gewebeuhren untereinander konnten bereits mit verschiedensten Pathologien assoziiert werden.

Neuste Forschungsergebnisse weisen zunehmend darauf hin, dass synchronisierte zirkadiane Rhythmik peripherer Gewebeuhren unabhängig vom SCN erhalten bleibt. Nichtsdestotrotz ist die Existenz, sowie Mechanismen und funktionale Bedeutung interzellulärer Kopplung peripherer Einzeloszillatoren noch immer umstritten. Die hier präsentieren Ergebnisse, basierend auf Kopplungsstudien in einem Model peripherer Gewebeuhren (U-2 OS Zellen), liefern weitere Hinweise darauf, dass periphere Gewebeoszillatoren miteinander koppeln. Weiterhin zeigen sie, dass diese Kopplung auf dem Austausch sekretierter Signalmoleküle, sehr wahrscheinlich Wachstumsfaktoren, beruht. Unserer Erkenntnis nach, ist diese Studie die erste, welche einen potentiellen Mechanismus interzellulärer Kopplung zwischen peripheren Gewebeoszillatoren identifiziert, sowie dessen Bedeutung für den Erhalt robuster Rhythmik auf Netzwerkebene dargestellt hat. Anders gesagt, diese Studie zeigt, dass periphere Kopplung mittels TGF-β Signalweg, die Synchronisation peripherer Oszillatoren ermöglicht und somit hoch-amplitudige und gering gedämpfte zirkadiane Geweberhythmik fördert, als auch die Widerstandsfähigkeit gegenüber

Zeitgeber Impulsen erhöht. Wir nehmen an, dass interzelluläre Kopplung zwischen Einzelzelloszillatoren innerhalb peripherer Gewebe eine wichtige Rolle für die Anpassung an rhythmische intrinsische oder extrinsische Signale, sowie für die zeitliche Koordinierung zirkadianer Organfunktionen und die Gesundheit des Organismus spielt.

„Das Schönste, was wir erleben können, ist das Geheimnisvolle“ (Albert Einstein)

Contents

Abstract ..... **iii**

Zusammenfassung ..... **iv**

List of Figures ..... **xii**

Supplementary Figures ..... **xiii**

List of Tables ..... **xv**

List of Equations ..... **xvi**

1 Introduction **1**

1.1 Introduction to chronobiology *1*

1.1.1 History and basic concepts of chronobiology 1

1.1.2 Properties of circadian rhythms 5

1.1.3 Evolutionary conservation of circadian rhythms 8

1.2 The mammalian circadian system *9*

1.2.1 Organization of the mammalian circadian system 9

1.2.2 SCN, the master clock? 11

1.2.3 Peripheral clocks, slave oscillators? 14

1.2.4 The molecular clock machinery in mammals 16

1.3 Entrainment of mammalian circadian clocks *19*

1.3.1 Entrainment from a theoretical perspective 20

1.3.2 Entrainment to the light-dark cycle 21

1.3.3 Entrainment of peripheral circadian clocks 25

1.4 Intercellular coupling *27*

1.4.1 Coupling from a theoretical perspective 27

1.4.2 Coupling in the central clock 31

1.4.3 Coupling in peripheral clocks 33

1.5 Circadian alignment and physiology *35*

1.5.1 The synchronized state: circadian physiology 37

1.5.2 The desynchronize state: circadian pathology 38

1.6 Secretory pathway 39

1.6.1 Secretory pathway and circadian clocks 39

1.6.2 TGF-β family 40

1.6.3 TGF-β secretion and signaling 42

1.6.4 TGF-β and circadian clocks 45

1.7 Aim of the study 46

2 Materials and Methods 48

2.1 Materials 48

2.1.1 Animal strains 48

2.1.2 Mammalian cell lines and primary cells 48

2.1.3 Bacterial cell lines 53

2.1.4 Culture media 54

2.1.5 Vectors 55

2.1.6 Antibodies 56

2.1.7 Enzymes 56

2.1.8 Buffers and solutions 57

2.1.9 Reagents 59

2.1.10 Kits 60

2.1.11 Primers and Oligos 61

2.1.12 Special equipment 62

2.1.13 (Electronic) devices 63

2.1.14 Databases, software and distributions 64

2.1.15 Company register 66

2.2 Methods 68

2.2.1 Animal based procedures 68

2.2.2 Cell culture procedures 70

2.2.3 Bacterial cell based procedures 72

2.2.4 Imaging methods 73

2.2.5 Genetic and pharmacological perturbation of mammalian cells 74

2.2.6 Stimulations 76

2.2.7 Special cell culture assays 79

2.2.8 RNA and DNA based procedures 82
2.2.9 Cloning of pLenti6_7xmutCRE:Luc 84
2.2.10 Protein based methods 87
2.2.11 Data analysis 90

3 Results 95

3.1 Circadian rhythms depend on culture density 95

3.2 Peripheral circadian oscillators (weakly) couple 99

3.3 Paracrine factors modulate circadian dynamics and induce specific transcriptional profiles 106

3.4 Secreted factors are proteins 114

3.5 Secreted TGF-β is important for normal circadian dynamics 120

3.6 TGF-β signaling pathway promotes intercellular coupling 128

4 Discussion 132

4.1 Peripheral coupling: state of the art 132

4.2 Key findings discussed 134
4.2.1 Peripheral circadian oscillators are coupled 134
4.2.2 Coupling is mediated by paracrine signaling factors 141
4.2.3 TGF-β is a potential peripheral coupling factor 146

4.3 Limitations and perspectives 155

4.4 Conclusions 160

5 Bibliography 164

6 Appendix I

Supplementary Figures I

Open Data IX
RNA sequencing IX
Mass spectrometry IX

Standard Operating Procedures X

Vector maps XIII

List of Abbreviations ..... **XXII**

Publications and distinctions ..... **XXIX**

Publications XXIX
Conference contributions XXIX
Fellowships, and awards XXX
Professional experiences XXX

Acknowledgement ..... **XXXI**

Declaration of Authorship ..... **XXXII**

List of Figures

FIGURE 1-1: REPRESENTATION OF CIRCADIAN CLOCK SYSTEMS 6
FIGURE 1-2: SCHEMATIC REPRESENTATION OF A DAMPED CIRCADIAN OSCILLATION 7
FIGURE 1-3: ORGANIZATION OF THE MAMMALIAN CIRCADIAN SYSTEM 10
FIGURE 1-4: THE MAMMALIAN CORE CLOCK NETWORK 18
FIGURE 1-5: THEORETICAL CONCEPTS OF ENTRAINMENT 21
FIGURE 1-6: TYPES OF PHASE RESPONSE CURVES (PRCS) 23
FIGURE 1-7: COUPLING IN THE SCN 32
FIGURE 1-8: STATES OF CIRCADIAN (DE)SYNCHRONY 36
FIGURE 1-9: PHYLOGENETIC TREE OF THE 33 (HUMAN) TGF-B FAMILY POLYPEPTIDES 41
FIGURE 1-10: TGF-β SECRETION AND SIGNALING 44
FIGURE 3-1: U-2 OS CIRCADIAN RHYTHMICITY DEPENDS ON CULTURE DENSITY 96
FIGURE 3-2: U-2 OS TRANSCRIPTIONAL PROFILES DEPEND ON CULTURE DENSITY 98
FIGURE 3-3: CO-CULTURED POPULATIONS OF U-2 OS CELLS DISPLAY WEAK INTERCELLULAR COUPLING WITH RESPECT TO PHASE AND PERIOD 103
FIGURE 3-4: CO-CULTURED POPULATIONS OF U-2 OS CELLS DISPLAY WEAK INTERCELLULAR COUPLING WITH RESPECT TO AMPLITUDE AND DAMPING 106
FIGURE 3-5: FACTORS SECRETED BY PERIPHERAL CIRCADIAN OSCILLATORS PHASE SHIFT CIRCADIAN RHYTHMS 108
FIGURE 3-6: FACTORS SECRETED BY PERIPHERAL CIRCADIAN OSCILLATORS MODULATE CLOCK GENE EXPRESSION AND ACTIVATE CRE ENHANCER ELEMENTS 111
FIGURE 3-7: FACTORS SECRETED BY PERIPHERAL CIRCADIAN OSCILLATORS INDUCE SPECIFIC TRANSCRIPTIONAL PROFILES 113
FIGURE 3-8: ACTIVE COMPONENTS IN CONDITIONED MEDIUM DISPLAY CHARACTERISTICS OF PROTEINS 116
FIGURE 3-9: ACTIVE AND SECRETED CM FACTORS IDENTIFIED BY CHROMATOGRAPHY AND MASS SPECTROMETRY 119
FIGURE 3-10: TGF-β ACTS AS ACTIVE CM FACTOR WITH RESPECT TO CRE ACTIVATION AND PER2 INDUCTION 121
FIGURE 3-11: GENETIC PERTURBATION OF TGF-β SIGNALING ALTERS CRE TRANSCRIPTIONAL ACTIVATION AND CIRCADIAN DYNAMICS 124

FIGURE 3-12: PHARMACOLOGICAL PERTURBATION OF TGF-β SIGNALING ALTERS CRE TRANSCRIPTIONAL ACTIVATION, CIRCADIAN DYNAMICS, AND PHASE RESPONSES TO CM 127
FIGURE 3-13: PHARMACOLOGICAL PERTURBATION OF TGF-β SIGNALING ATTENUATES INTERCELLULAR COUPLING 130
FIGURE 4-1: PHASE RESPONSE CURVE OF TGF-β AND ACTIVIN 148
FIGURE 4-2: ENHANCER ELEMENTS IN PERIOD PROMOTERS AND IN THE 7XCRE:LUC REPORTER CONSTRUCT 152
FIGURE 4-3: MODEL OF TGF-β COUPLING AMONG PERIPHERAL CIRCADIAN OSCILLATORS 161

Supplementary Figures

FIGURE 6-1: U-2 OS CIRCADIAN RHYTHMICITY DEPENDS ON CULTURE DENSITY I
FIGURE 6-2: CO-CULTURED POPULATIONS OF U-2 OS CELLS DISPLAY WEAK INTERCELLULAR COUPLING WITH RESPECT TO PHASE II
FIGURE 6-3: FACTORS SECRETED BY PERIPHERAL CIRCADIAN OSCILLATORS MODULATE CIRCADIAN DYNAMICS IV
FIGURE 6-4: PROTEIN CONTENT OF SIZE FRACTIONATED CONDITIONED AND CONTROL MEDIUM V
FIGURE 6-5: GENETIC PERTURBATION OF TGF-β SIGNALING PATHWAY ALTERS CIRCADIAN DYNAMICS VI
FIGURE 6-6: PHARMACOLOGICAL PERTURBATION OF TGF-β SIGNALING PATHWAY ALTERS CIRCADIAN DYNAMICS VII
FIGURE 6-7: PHARMACOLOGICAL PERTURBATION OF TGF-β SIGNALING ATTENUATES INTERCELLULAR COUPLING VIII
FIGURE 6-8: STANDARD OPERATING PROCEDURE FOR LENTIVIRUS PRODUCTION X
FIGURE 6-9: STANDARD OPERATING PROCEDURE FOR RNA INTERFERENCE SCREENS XII
FIGURE 6-10: VECTOR MAP OF PLENTI6_PER2:LUC XIII
FIGURE 6-11: VECTOR MAP PABHYGRO_BMAL1:LUC XIV
FIGURE 6-12: VECTOR MAP OF PLENTI6_7XCRE:LUC XV
FIGURE 6-13: VECTOR MAP PLENTI6_7XMUTCRE:LUC XVI
FIGURE 6-14: VECTOR MAP PSTARPROM_7XSRE:LUC XVII
FIGURE 6-15: VECTOR MAP PUC57_7XMUTCRE XVIII

FIGURE 6-16: VECTOR MAP PGIPZ XIX
FIGURE 6-17: VECTOR MAP PMD2G XX
FIGURE 6-18: VECTOR MAP PSPAX XXI

List of Tables

TABLE 2-1: CELL CULTURE NUMBERS 71
TABLE 2-2: SEEDING NUMBERS OF PHASE-PULLING EXPERIMENTS 80
TABLE 2-3: TEMPERATURE PULSE PROTOCOL (JUMO IMAGO) 82
TABLE 2-4: MASTERMIX PREPARATION FOR REVERSE TRANSCRIPTION 83
TABLE 2-5: RESTRICTION ENZYME DIGEST USING APAI AND NHEI-HF 85
TABLE 2-6: MASCOT SEARCH PARAMETERS 93

List of Equations

EQUATION 1: HARMONIC REGRESSION FUNCTION TO FIT A COSINE CURVE TO A TIMESERIES…7
EQUATION 2: FUNCTION FOR DETERMINING CELLULAR CONCENTRATIONS……..…71
EQUATION 3: CHRONOSTAR ALGORITHM……..……91

1 Introduction

1.1 Introduction to chronobiology

“Whether we measure, hour by hour, the number of dividing cells in any tissue, the volume of urine excreted, the reaction to a drug, or the accuracy and the speed with which arithmetical problems are solved, we usually find that there is a maximum value at one time-of-day and a minimum value at another.” [1]

As Jürgen Aschoff described, most living organisms exhibit daily changes in their physiology, cognitive ability, and behavior. These changes are driven by underlying circadian rhythms, which are generated by endogenous, self-sustained, and temperature-compensation oscillations with an ~24 hour period. Chronobiology is the study of such endogenous rhythmic biological processes in adaptation to periodically reoccurring environmental conditions, including solar, lunar, and tidal cycles but also changes in our daily lives. The mammalian circadian system acts as endogenous timekeeper, allowing organisms to anticipate and adapt to rhythmic environmental changes, most importantly the light-dark cycle. Modern lifestyle can perturb the intricate balance between circadian and exogenous rhythms, resulting in pathologies associated with so-called circadian disruption. Thus, based on the interconnection between circadian rhythmicity and health, chronobiology has evolved into one of the most interdisciplinary research fields, receiving more and more attention from other disciplines.

1.1.1 History and basic concepts of chronobiology

Already in the mid 18th century both Jean-Jacques d'Ortous de Mairan and Carl Linnaeus discovered daily rhythms in opening and closing of leaves in plants. Carl Linnaeus invented the “flower clock”, a clock to predict time, based on flowering time across the solar day. While Linnaeus studied flowering under light-dark conditions, de Mairan discovered that even in constant darkness “[*Mimosa pudica*] opens very appreciably during the day, and at evening folds up again for the night” [2]. Thirty years later Duahmel de Monceau and Zinn demonstrated that rhythmic leaf movement is not only independent of light but also of ambient temperature, suggesting that it is indeed

driven by endogenous rhythmic processes [3]. In the 1830s, De Candolle showed that leaflet movement maintains a rhythm of approximately but not exactly 24 hours under constant light conditions [4], indicating that it is governed by a “free-running” (= not entrained to external cycles) rhythm. Nevertheless, despite these observations, it was not until 100 years later that biological clocks were accepted as endogenous drivers of daily oscillations. As well as that these oscillations can be detected in a multitude of living organisms, including bacteria, fungi, plants, insects, and vertebrates, regulating rhythmic behavior and physiology in adaptation to reoccurring environmental cycles [5]–[12]. In the early 1930s, Erwin Bünning demonstrated that periods of biological rhythms are inheritable in bean plants [13]. His finding led to a paradigm shift from the “hourglass hypothesis”, describing biological rhythms as entirely driven by external light-dark cycles, towards “Bünning’s hypothesis”. Bünning proposed that rhythmicity derives from endogenous biological rhythms, which synchronize to photoperiodic stimuli [14]. In 1959, Franz Halberg introduced the term “circadian” (*circa* = around/approximately, *dies* = day) to describe biological rhythms with a period of about 24 hours [15] and later helped to develop the cosinor procedure for describing circadian oscillations by mathematical fitting of cosine waves [16].

Breakthroughs in understanding the molecular basis of biological/circadian rhythms were made in the late 20th century. Back then chronobiology started to develop into an independent field of research based on the concept that clock genes act as drivers of endogenous biological rhythms. In 1971, Konopka and Benzer were the first to study clock mutants in *Drosophila melanogaster.* Their research led to the discovery of the *Period* gene [17], which was further isolated, and characterized as first clock gene by Jeffrey Hall, Michael Rosbash, and Michael Young in the 1980s [18]. A few years later Ralph and Menaker discovered that a single gene mutation, called tau mutation, affects the circadian period in hamsters. This suggested that indeed single genes govern circadian rhythm generation [19]. In 1994, Takahashi et al. identify the first mammalian clock gene, called *Clock*, by a mutagenesis screen and showed that mutation of this gene results in aberrant or even arrhythmic behavior of mice [20]. As more and more clock genes were discovered in multiple organisms, the concept of self-sustained transcriptional translational feedback loops (TTFL) as central component of biological circadian clocks emerged [21]. This introduced a new paradigm in chronobiology,

suggesting that all circadian clocks use the same molecular design principle for the generation of self-sustained circadian rhythms.

Besides their molecular makeup, entrainment of circadian rhythms to environmental light-dark cycles constitute a fundamental feature of the mammalian circadian system. In the 1960s, Bünning's concept of synchronization between endogenous and exogenous rhythms was refined by Jürgen Aschoff and Collin Pittendrigh, who studied entrainment (or period/phase adaptation) of circadian clocks to environmental "Zeitgebers*"* (= German meaning "time giver", introduced by Jürgen Aschoff in the 1960s) [22]. As Daan (2001) described, entrainment is an essential characteristic for circadian clock systems that "requires the sensitivity of endogenous oscillators toward particular environmental cues, as well as insensitivity towards others" [23]. Adaptation to photic information was thought to be achieved via the eyes and downstream light-sensitive entity. In 1972, Moore and Lenn discovered a projection from the retina to the suprachiasmatic nucleus (SCN) of the anterior hypothalamus [24], a region that had previously been shown to be involved in sleep-wake cycle and rhythm regulation [25], [26]. In the same year, Moore, Eichler, and Zucker performed lesion experiments, demonstrating that the SCN is required for hormone, activity, and feeding rhythms in rats [27], [28]. These findings paved the way for recognizing the SCN as "master pacemaker" in mammals. In following years, explanation experiments demonstrated autonomy of the SCN, with respect to daily rhythms in electrical firing and neurotransmitter release [29]–[32]. In the 1990s, Ralph et al. strengthened the role of the SCN acts as pacemaker clock by elegant transplantation experiments, showing that transplanted SCN restores behavioral rhythmicity of SCN-lesioned hamsters with the free-running period of the donor [33]. Nevertheless, since Aschoffs' and Pittendrighs' initial studies a number of photic and non-photic entrainment signals has been described. Especially the dissonance among different Zeitgeber signals, with regard to pathologies arising from circadian disruption (for details see 1.5), has become of large interest within recent years.

From a methodological standpoint important progress was made in the late 20th /early 21st century. The identification of clock genes was applied to the development of real-time imaging techniques enabling the tracking of biological rhythms in single cells, populations of oscillators or even entire organisms [34]–[36]. In 1993, Welsh et al., by

long-term recording of electrical activity from individual dissociated SCN neurons, demonstrated that single cell oscillators in the SCN maintain cell-autonomous free-running rhythms of electrical firing [37]. A few years later, rhythms of clock gene and protein expression were detected in peripheral tissues and shown to persist in culture [38]–[40]. These findings initiated a series of studies culminating in the finding that 3-10% of all genes are transcribed rhythmically and in a cell-autonomous and tissue-specific fashion [41]–[46]. Almost 10 years after Welsh's experiment, real-time bioluminescence imaging of luciferase reporter genes/proteins helped to show that also single cell oscillators in non-SCN tissues exhibit cell-autonomous and self-sustained rhythms [47], [48]. Moreover, peripheral tissues were demonstrated to display persistent and SCN-independent circadian rhythmicity ex vivo [35] and in vivo [36]. Since then, new ideas of non TTFL driven oscillations have been proposed. In 2005, Kondo et al. showed that circadian rhythms can be reconstituted in a test tube using only cyanobacterial proteins and ATP [49]. In 2011, O'Neill and Reddy reported that ~24 hour redox cycles drive circadian rhythms in non-nucleated red blood cells [50]. Together these findings resulted in yet another paradigm shift in the field of chronobiology, accepting that autonomous circadian oscillators can be found in virtually all cells, as well as suggesting that the SCN, rather than as pacemaker, acts as orchestrater of peripheral tissue clocks.

Identification of self-sustained cellular oscillations in almost every tissue of the mammalian system posed the question of interoscillator communication mechanisms among these oscillators. While this topic will be discussed in more detail below, it should be mentioned that, in 1996, Silver et al. demonstrated that encapsulated SCN transplants sustain circadian rhythmicity by diffusible signals [51]. Almost 10 years later, single cell imaging helped to show that heterogeneous single oscillators within the SCN couple to produce synchronized network rhythmicity [52]. Secreted neuropeptides, most importantly vasoactive intestinal polypeptide (VIP) and arginine vasopressin (AVP), have been shown to be required for synchronization of SCN neurons, as well as rhythmic behavior [53]–[56]. Moreover, intercellular coupling within the SCN has been demonstrated to play an important role for robust tissue rhythmicity and response to Zeitgeber signals [57]–[59]. Whether or not peripheral circadian oscillators couple with each other is still debated. In 2007 Lui et al. reported that intercellular coupling in the SCN, but not in peripheral tissues, maintains network

rhythmicity despite aberrant single cell oscillators [60]. Other studies have suggested that peripheral oscillators exchange paracrine signals to enhance rhythmicity of neighboring cells [61]–[63]. With the help of in vivo bioluminescence imaging Saini et al. (2013) were able to show that peripheral circadian clocks are able to maintain synchronized circadian rhythmicity under constant conditions and independently of the SCN [36]. Thus, the existence and the functional role of intercellular coupling within peripheral tissues remains one of the prevailing questions of chronobiological research.

Within the last years, contemporary chronobiology has been concerned with circadian rhythmicity on a system-level. Questions relating circadian clocks to an organism's behavior and well-being, as well as to the temporal coordination of circadian physiology under modern living conditions have become "hot topics" in the field. Especially the relevance of mutual interactions between individual body clocks for normal circadian rhythms, as well as health consequences arising from perturbations of such interactions will likely be addressed in the future.

1.1.2 Properties of circadian rhythms

According to the dictionary biological clocks are "inherent timing mechanism in living system[s], inferred to exist to explain the timing or periodicity of various behaviors, physiological states and processes" [64]. Such clocks generate oscillations with circadian (period 24 $\pm$ 4 hours), ultradian (period < 20 hours), or infradian (period > 28 hours) periods. For example, sleep (90-120 minutes) and menstrual cycles (28 days), constitute ultradian or infradian rhythms, respectively. Thus, even though the term "biological clock' emphasizes the importance of endogenous rhythm generation and time measurement, it fails to clearly distinguish circadian oscillations from other intrinsic rhythmic biological processes. Therefore, the field of chronobiology has agreed on three properties that clearly define circadian rhythms:

(i) They oscillate with self-sustained endogenous periods of about 24 $\pm$ 4 hours, which are maintained even under constant conditions (also called free-running period)

(ii) They are able to entrain to rhythmically reoccurring (environmental) Zeitgebers within given period ranges, i.e. they can adapt their period and phase to align with the external rhythms

(iii) They are temperature-compensated, i.e. their free-running period remains unchanged despite variations in ambient temperature

To fulfill these criteria, circadian clock systems follow a general design principle, which, according to Kuhlman et al. (2018), can be broken down into three basic elements: an input pathway, a central oscillator, and an output pathway [65] (Figure 1-1). The pacemaker can either be a single superordinate oscillator or a network of tightly coupled oscillators. On the one hand the pacemaker needs to be entrainable to environmental timing cues via the temporally gated regulation of input pathways by external Zeitgebers. One the other hand, the pacemaker must be able to synchronize subordinate oscillators via the regulation of output pathways that drive the temporal coordination of circadian behavior, physiology, and metabolism. Additionally, in complex organisms, circadian clocks likely incorporate multiple interlocked feedback loops that fine-tune interactions between external and internal rhythms, as well as between pacemaker and inferior oscillators.

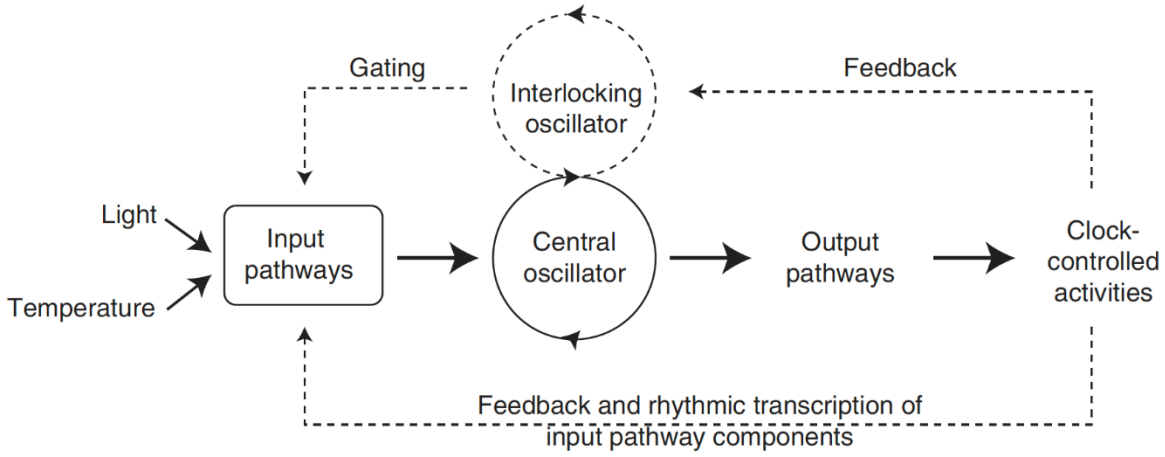

Figure 1-1: Representation of circadian clock systems

Circadian clock systems can be depicted as networks of input pathways, central oscillator (pacemaker), and output pathways. Central oscillators generate the endogenous rhythm and must be able to synchronize to environmental Zeitgebers via the input pathways. Consequently, pacemakers drive output pathways and clock-controlled activities via the synchronization of downstream oscillators. Additionally, intertwined negative and positive feedback loops (dashed lines) influence the interaction of the three basic circadian clock elements. (adapted from [65])

The particular beauty of circadian rhythms, on single cell and on network level, is their harmonic motion, allowing to describe them by sinusoidal equations. Consequently, a defined set of "circadian parameters" arises upon mathematical fitting of circadian data to cosine functions (Equation 1): amplitude, period (frequency), phase, and damping.

$$x(t) = e^{-dt} * A * \cos(\omega t - \phi) \quad (1)$$

A = amplitude
d = damping constant
ω = frequency = 2π/period
ϕ = phase
t = time

By convention parameters are defined as follows (Figure 1-2): amplitude is the half-difference between peak and trough of one oscillatory cycle. Circadian period (also called τ) is the duration of one complete cycle or in other words, the time difference between two consecutive peaks. Phase is the time difference between a reference time point and any other given time point within one oscillatory cycle. However, often phase is defined as so-called acro-phase, i.e. the time at which the peak of one cycle occurs. Damping is the exponential decay rate of the amplitude over the course of the oscillation. Additionally, the frequency of an oscillation is the number of cycles within a given time interval, which for circadian oscillations is defined as reciprocal of the period (frequency = 1/period), e.g. 24^{-1} hours.

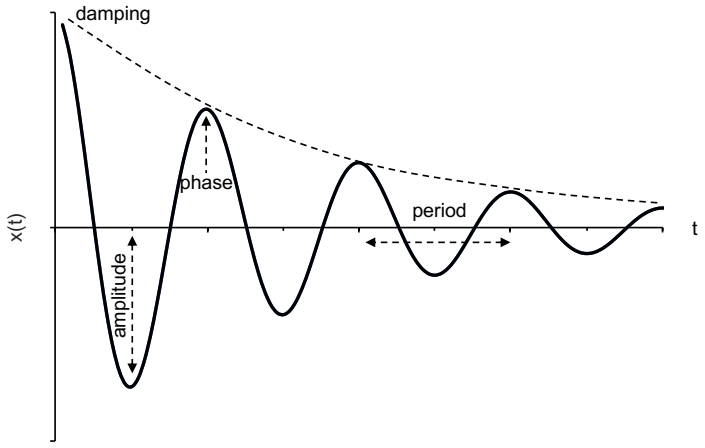

Figure 1-2: Schematic representation of a damped circadian oscillation

Circadian oscillations can be represented by cosine wave functions, which describe periodic motions by a defined set of parameters: amplitude, period, phase, and damping.

1.1.3 Evolutionary conservation of circadian rhythms

According to Darwin's theory biological traits exhibit inheritable variation. If variations provide a selective advantage in a given environmental niche, they are more likely to be passed on to offspring and to manifest in the gene pool [66]. Thus, what selective advantage did circadian rhythms provide to organisms to prevail during evolution?

Circadian clocks are able to entrainment to environmental cycles. Period and phase adaptation to external rhythms guarantees the temporal coordination of behavior and physiology with ambient conditions [22]. Thereby, circadian rhythms provide an extrinsic advantage. This may have promoted fitness of circadian organisms by scheduling behavior and physiology at times of the day when the likelihood of finding food, meeting fellows, mating, or avoiding harmful environmental conditions and predators would be increased [67]. Moreover, circadian clocks maintain rhythmicity even despite absence of environmental entrainment signals (free-running rhythms). Self-sustainment of circadian rhythms provides an intrinsic advantage [68], which may have promoted fitness of circadian organisms by synchronization of internal processes and coordination of rhythmic biological functions such as sleep, feeding, metabolism, cardiac and immune functions [67].

Many experimental studies have been conducted to support the concept of an adaptive advantage of circadian clocks. One of the most prominent studies was performed by the Johnson laboratory in 2004. They demonstrated that photosynthetic cyanobacteria with circadian periods matching the environmental period possess a fitness advantage over strains with circadian periods longer or shorter than the external period [69]. Other studies have shown that SCN lesion under natural conditions results in reduced survival due to increased predator attacks or mistiming of hibernation [70]–[72]. Housing of laboratory animals under abnormal light dark cycles has been shown to result in reduced longevity [73]. Additionally, many species appear to maintain circadian rhythmicity for generations even if they are raised under constant environments, supporting the concept of an intrinsic selective advantage [74]–[76].

1.2 The mammalian circadian system

Almost all living organisms possess circadian clocks coordinating their behavior and physiology. Even though studying circadian processes in lower organisms has largely increased the knowledge about circadian clocks in higher vertebrates, the work presented here is focused on the investigation of the mammalian circadian system. Especially the molecular machinery regulating circadian oscillations from single cell to network level.

1.2.1 Organization of the mammalian circadian system

Mammalian circadian clocks are composed of manifold single cell circadian oscillators organized into various tissue networks, hierarchically arranged to constitute the mammalian circadian clock system (Figure 1-3). While locomotor activity, cognition, and behavior are mainly governed by central oscillators, oscillators in the periphery modulate physiological and metabolic functions of peripheral tissues.

External Zeitgebers are perceived by body clocks (Figure 1-3). Most importantly, the light-dark cycle gives input to the suprachiasmatic nucleus (SCN), formed by a bilateral neuronal cluster in the anterior hypothalamus of the brain. Since the 1970s the SCN is considered the master pacemaker because ablation and transplantation experiments have demonstrated its necessity for circadian rhythm generation, as well as for rhythmic behavior, hormone secretion, and entrainment to light-dark cycles [27], [28], [33], [77]. As mentioned above, the SCN is required for photic entrainment of the endogenous rhythm to the environmental light-dark cycle. Diurnal changes in light intensity are perceived primarily by melanopsin-expressing intrinsically photosensitive retinal ganglion cells (ipRGCs) in the retina [78], [79]. These cells pass on photic information to the SCN via the retinohypothalamic tract (RHT) [80]. Light invoked electrical signals reach the SCN, are transformed into biochemical signals, and induce time-dependent phase resetting of the central pacemaker, which guarantees daily (phase and period) adaptation to the environmental cycle.
More recently, gene expression studies and the development of bioluminescent reporter genes enabled to shown that circadian rhythmicity persists also outside the brain. Oscillations were detected in tissue explants, as well as primary and

immortalized cells [38], [39]. Transcriptomic studies revealed that the expression of ≥ 10% of genes in peripheral tissues are regulated rhythmically but with very small overlap between individual tissues [43], [46], [81]. While both, behavioral and underlying SCN rhythmicity have been shown to oscillate robustly under constant conditions, rhythms of peripheral tissue explants ex vivo and in vitro have been found to dampen out over time. This suggested that peripheral circadian clocks are inferior to the central pacemaker [39]. Indeed, peripheral clocks receive SCN derived neuronal, hormonal, and temperature information, which act as synchronizing signals to establish physiologically required phase relationships among them [82]–[84]. Nevertheless, despite responses to SCN output signals, peripheral circadian oscillators are also able to entrain directly to external Zeitgebers, most importantly feeding fasting cycles. Interestingly, feeding derived signals not only entrain peripheral rhythms but can uncouple them from the control of the pacemaker [85].

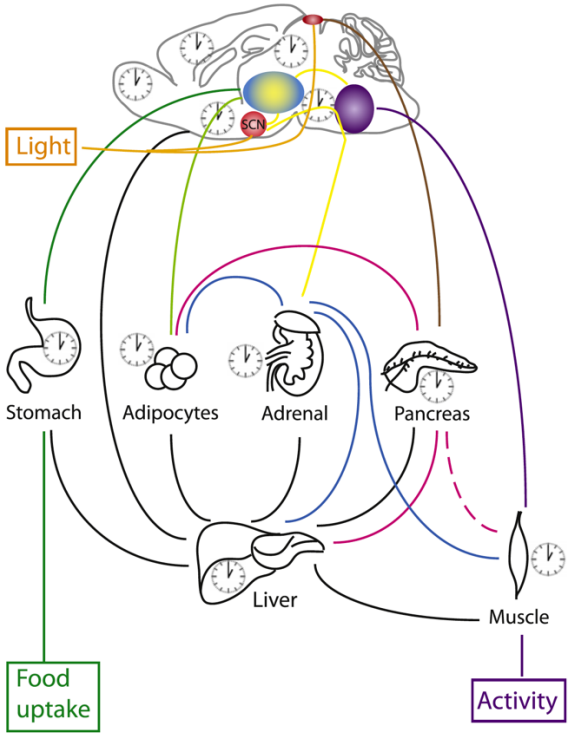

Figure 1-3: Organization of the mammalian circadian system

Circadian clocks are found in virtually all cells across the body. The master pacemaker is located in the SCN and synchronizes other central and peripheral clocks via humoral and neuronal routes. SCN and pineal gland (red ovals) are responsive to light (orange box and lines). Peripheral organs are responsive to non-photic signals, e.g. feeding and activity (green and purple box and lines). Feedback regulations among tissue clocks exist: hormonal (brown = melatonin, dark green = ghrelin, light green = leptin, pink solid = insulin/glucagon, pink hatched = insulin, blue = adrenalin), metabolic (black = carbohydrates, fatty acids, amino acids), and neuronal connections (purple) are depicted. (adapted from [86])

In agreement with the Kuhlman model (Figure 1-1), the mammalian circadian system consists of hierarchically organized clocks: a pacemaker clock in the SCN and subsidiary clocks in the rest of the body. On tissue level, these body clocks are organized as networks of cell-autonomous oscillators. Neuronal oscillators in the SCN have been shown to tightly couple in order to sustain synchronized network rhythmicity (for details see 1.4). Whether cell-autonomous oscillators within peripheral clocks couple or if synchronized tissue rhythmicity depends on SCN derived input signals is still debated. Consistent with Kuhlman et al. (2018), mammalian circadian clocks entrain to external input signals. The SCN receives photic input signals and entrains body clocks to the environmental light-dark cycle. However, in contrast to this theoretical model, also non-pacemaker clocks entrain to non-photic input signals. Nevertheless, the SCN seems to be required for the orchestration of other body clocks in order to coordinate rhythmic physiological functions (outputs). Feedback regulations of the mammalian circadian system, either among individual body clocks or between endogenous rhythms and exogenous Zeitgebers, are believed to exist but are not well understood.

1.2.2 SCN, the master clock?

In 1960, Pittendrigh proposed that transients following Zeitgeber perturbations may be explained by a coupled two-oscillator model: a pacemaker receiving input signals and another reacting to pacemaker signals [87]. However, it took almost 30 more years until the suprachiasmatic nucleus (SCN) was accepted as master pacemaker (for review see [88]). Initial lesion experiments identified the SCN as two bilaterally paired clusters of ~20.000 densely packed neurons located superior to the optic chiasm. This region was shown to be required for hormone, activity and feeding rhythms in rats [24], [27], [28]. Elegant explanation and transplantation experiments, demonstrating autonomous rhythmicity [29]–[32] and pace-making function [33], consolidated the role of the SCN as master clock and sole driver of all body rhythms. However, in 2004, three independent groups were demonstrated that peripheral circadian oscillators display autonomous and self-sustained circadian rhythmicity ex vivo and in vitro [35], [47], [48], [89]. Almost 10 years later, the independence of peripheral tissue oscillations of rhythmic SCN derived (and environmental) signals was demonstrated in vivo [36], [90]. These findings shifted the role of the SCN from a master pacemaker to an

orchestrater of other body clocks. Nevertheless, unlike any other body clock, the SCN is indispensable for photic entrainment and transmission of light-dark signals to downstream tissue oscillators.

Each neuronal cluster of the SCN is divided into a core region and a shell region. The core region is closely located to the optic chiasm and receives direct input from the retinohypothalamic tract (RHT) [80]. The shell region receives input from the hypothalamus, limbic areas, as well as the SCN core region [80]. External time, in form of photic signals, is perceived by ocular opsin photoreceptors and, via the melanopsin expression retinal ipRGCs, transmitted to the SCN [91]. The RHT originates from the retina and forms synapses with SCN neurons, where the neurotransmitters pituitary adenylate cyclase-activating polypeptide (PACAP) and glutamate are released to transform electrical into biochemical signals [92]. Activation of their respective receptors (GluR and PAC1) induces kinase signaling pathways resulting in the rapid induction of so-called immediate early genes (e.g. *c-fos, fos-B, c-myc, c-jun, jun-B*), including components of the core clock machinery (*Per1/2*) [93], [94]. Ionotropic GluRs function as voltage-gated ion channels, metabotropic GluRs and PAC1 as G-protein coupled receptors (GPCR). Thus, several downstream signaling cascades may be activated by glutamate and PACAP. The most accepted pathways include voltage-gated calcium (Ca^{2+}) channel and Gα GPCR signaling [95]. Both pathways result in the downstream elevation of cyclic AMP (cAMP) levels and the cAMP dependent activation of kinases, e.g. protein kinase A (PKA) or calmodulin-dependent protein kinase (CAMK), which phosphorylate cAMP response element binding proteins (CREB). CREBs belong to a family of transcription factors that, upon phosphorylation, induce target gene expression by binding to cAMP response elements (CRE) [93], [95]. Additionally, Ca^{2+} and Ras activation dependent MAP kinase (MAPK) pathways have been described to converge on the transcriptional induction of CRE and serum response elements (SRE), another enhancer element of immediate early genes [93]. Ultimately, light induced activation of clock gene transcription in the SCN results in time-of-day dependent phase responses, thereby entraining the SCN to environmental Zeitgeber cycles [96] (for details see 1.3). Besides the RHT, other afferent projections to the SCN, e.g. from the thalamus or the arousal centers, have been proposed as pathways of non-photic entrainment but not many details are known so far.

Regarding its efferent projections, shell and core region of the SCN differ in their neuronal connectivity, gene and neuropeptide expression profiles, as well as their response to external light information. Thus, these regions constitute functionally distinct compartments within the SCN [80], [97]–[99]. Predominant neuronal populations of shell and core region are arginine vasopressin (AVP) and vasoactive intestinal polypeptide (VIP) neurons, respectively [100]. Gamma-aminobutyric acid (GABA) or glutamate expressing neurons are common for both regions [101]. Despite their different molecular makeup, shell and core oscillators synchronize with each other. Intercellular coupling between neuronal oscillators is achieved via exchange of secreted neurotransmitters, e.g. AVP, VIP, GABA, gastrin-releasing peptide (GRP), or via gap junctions [102] (for details see 1.4). It has been shown that SCN core and shell innervate the same target structures of surrounding brain regions, which then project to other neuronal or endocrine tissues that pass on SCN derived time information to the rest of the body [80], [103], [104]. “SCN splitting” experiments have demonstrated that exposure to non 24 hour light-dark conditions results in desynchronization and anti-phasic oscillations of distinct SCN regions, as well as in aberrant rest-activity and hormonal cycles [105]–[113]. Moreover, in 2015 Evans et al. showed that even though the SCN shell can maintain phase relationships of peripheral tissue clocks by itself, synchronization of SCN regions is important for high amplitude rhythmicity within the SCN, as well as in non-SCN tissues [103].

These findings suggest that the SCN acts as orchestrator of peripheral tissue oscillations and enhances rhythmicity of autonomous peripheral clocks. Thus, ultimately the SCN may not be a master pacemaker in a strict sense. It is not required to drive circadian oscillations of peripheral tissue clocks. But it appears to be required for the establishment of stable phase relationships among body clocks, high-amplitude rhythms of peripheral oscillators, as well as for the entrainment to the light-dark cycle. SCN dependent synchronization of the periphery can be achieved by various pathways, including direct neuronal or hormonal innervation of target tissues, indirect behavioral control (regulation of rest-activity or feeding-fasting cycles), or core body temperature variations [10] (for details see 1.3). Therefore, the SCN is still accepted as superior unit of mammalian timekeeping, even though the peripheral oscillators exhibit cell-autonomous and self-sustained rhythmicity.

1.2.3 Peripheral clocks, slave oscillators?

Today we know that mammals possess virtually as many circadian oscillators as cells in the body and most peripheral tissues have been shown to exhibit cell-autonomous circadian rhythmicity [35]. Even on the molecular level 3-10% of genes have been found to be rhythmically expressed in peripheral tissues [42], [114]–[116]. Nevertheless, as mentioned above, peripheral circadian clocks are often described as mere slave oscillators of the central pacemaker.

A breakthrough in studying peripheral circadian clocks was made in 1998, when Balsalobre et al. discovered mRNA oscillations in cultured rat fibroblasts that could be induced independently of SCN derived signals [38]. Their finding suggested that the underlying molecular components driving peripheral and central circadian oscillations are basically the same (for details see 1.2), supporting the idea of an evolutionary conserved design principle of all circadian clocks. Later is was discovered that, despite conservation of the core clock machinery, rhythmic gene/protein expression profiles and metabolic outputs are regulated in a tissue-specific fashion [81], [115], [117]. Thus, spatiotemporal separation of chemically or functionally incompatible processes, as well as coordination of rhythmic biological processes with their external demands must play an important role for peripheral clocks. For example, timing of catabolic processes at the time of feeding and anabolic processes at the time of rest, can provide advantages for an organism's energy homeostasis. Best described physiological functions regulated by peripheral circadian clocks include xenobiotic detoxification [118], carbohydrate [119]–[121] and lipid homeostasis [122], [123], blood-pressure and heart-rate regulation, as well as renal urine production [124].

The reason peripheral circadian clocks have been described as slave oscillators of the SCN is that SCN lesion experiments resulted in behavioral arrhythmicity and gradual dampening or even loss of circadian gene expression in peripheral tissues [41], [125], [126]. However, such gene expression studies require population sampling of arrhythmic animals housed under constant conditions. Therefore, it remained unclear whether failure to detect robust peripheral rhythms resulted from cross-sectional time series sampling of "unentrained" animals or indeed from a loss of circadian gene expression. In 2004, the Takahashi group development of a transgenic mouse model expressing a PER2::LUC fusion protein, which allowed to track bioluminescence oscillations of peripheral tissues from individual animals over time [35]. They

demonstrated that SCN lesion does not abolish circadian rhythmicity of peripheral tissue explants ex vivo but that the phases of distinct body clocks are no longer coherent [35]. Additionally, other groups showed that cultured fibroblasts and hepatocytes, as in vitro model of peripheral circadian oscillators, sustain cell-autonomous circadian rhythmicity in culture [47], [48], [89]. Nevertheless, also the latter results may have been confounded by explanation or culture procedures, which may act as synchronization signals for peripheral circadian oscillators. Thus, additional evidence from in vivo studies of peripheral circadian clocks in SCN lesion animals was necessary to further validate autonomy of peripheral circadian clocks. In 2012, Tahara et al. used IVIS imaging to record bioluminescence rhythms of peripheral clocks from individual animals [90]. However, since IVIS imaging only allows for snap-shot images of anesthetized animals at different timepoints, it was the Schibler group that first recorded peripheral oscillations in real-time from living animals [36]. Both groups demonstrated, that oscillations of individual peripheral tissues are maintained in SCN lesioned, arrhythmic animals housed under constant conditions. But as reported before, in vivo phases of peripheral tissue clocks started to drift apart upon SCN lesion [90]. These findings suggested that peripheral clocks, just like the SCN, are networks of cell-autonomous and self-sustained circadian oscillators. Nevertheless, despite their autonomous circadian rhythmicity, peripheral clocks require SCN derived or exogenous entrainment signals for their temporal coordination.

The SCN controls phasing of peripheral clocks via innervations from the autonomous nervous system [127], [128], rhythmic hormone signals, e.g. from pineal and adrenal gland [129]–[133], body temperature fluctuations [58], [82], or via rest-activity and feeding-fasting cycles [134] (for details see 1.3). In addition to these SCN dependent pathways, cultured cells and explanted tissues can be synchronized by a multitude of Zeitgeber signals [124]. Moreover, restricted feeding regimes and ambient temperature cycles have been demonstrated to entrain peripheral clocks, but not the SCN, in vivo [82], [85], [135]. This suggests that entrainment signals of peripheral clocks can be manifold and may act in a tissue-specific fashion. However, while such entrainment signals are important for the establishment of intertissue phase relationships, they appear not to be required for the maintenance of peripheral circadian oscillations per se. Thus, if peripheral clocks are able to maintain tissue rhythmicity in the absence of SCN derived or external Zeitgebers [36], [90], intratissue

synchrony among single cell oscillators must be maintained by alternative mechanisms. In contrast to the SCN, for which mechanism and functional relevance of intercellular coupling have been described, mechanisms of coupling among peripheral oscillators are poorly understood (for details see 1.4). Even though, peripheral clocks have been demonstrated to oscillate autonomously and in a self-sustained manner from single cell to tissue level, it remains debated whether or not maintenance of intratissue phase coherence is driven by systemic or environmental entrainment signals, intercellular coupling signals, or a combination of those. Computational modeling of single cell in vitro bioluminescence recordings has yielded indications of weak intercellular coupling in peripheral clock networks [89], [136]. However, other studies have reported lack of interoscillator synchronization in co-culture experiments of peripheral circadian oscillators [47], [137].

Thus, as for the SCN, peripheral clocks may not be defined as slave oscillators in a strict sense. They appear capable of generating self-sustained oscillations on cellular and tissue level independently of the SCN or extrinsic Zeitgebers. Nevertheless, entrainment signals from the SCN or the environment appear to be required for the maintenance of intertissue phase relationships among, as well as the enhancement of intratissue synchrony within peripheral circadian clocks.

1.2.4 The molecular clock machinery in mammals

Already in the 1930s, Erwin Bünning reported the inheritance of circadian period in plants [13]. However, it was not until almost 50 years later, that the basic components of the molecular clock machinery started to be discovered in *Drosophila*. Despite cyanobacteria and erythrocytes, which do not required a transcriptional machinery to generate circadian oscillations [50], [138], circadian clocks of most living organism follow the same molecular design principle: transcriptional-translational feedback loops (TTFL) generate circadian oscillations by self-sustained, temporally regulated cycles of clock gene expression in combination with time delayed repression or activation of these genes by their own protein products (Figure 1-4).

Circadian TTFLs are generated by a defined set of genes, the so-called clock genes, which contribute to different interlocked feedback loops generating circadian

oscillations in a tissue-specific fashion [81]. Components of the “core feedback loop” are *Clock, Bmal1* (also called *Arntl*), *Period1/2/3*, and *Cry1/2.* Following translation CLOCK and BMAL1 form basic helix-loop-helix (bHLH) transcription factor complexes that induces the expression of their target genes *Period1/2/3* and *Cry1/2* by binding to E-box enhancer elements in their promoter regions [139]. After a defined time delay, necessary to establish ~24 hour oscillations, PER and CRY protein products relocate to the nucleus where they suppress CLOCK/BMAL1 transcriptional activity either by direct or by indirect interaction [140], [141]. During the first half of a circadian cycle CLOCK/BMAL1 transcriptional activity is increasing until the accumulation of PER and CRY proteins results in the formation of repressive complexes. Depending on the half-lives of PER/CRY complex components, transcriptional repression is progressively relieved throughout the second half of a circadian cycle and until CLOCK/BMAL1 activity is restored, leading to the initiation of a new cycle [142], [143]. Post-translational modifications, most importantly phosphorylation and ubiquitination, have been described to regulate the activity and degradation of PER and CRY proteins [142]. CLOCK/BMAL1 heterodimers also regulate the E-box driven expression of *Nr1d1/2* (also called *Rev-erba/b*), *Rora/b*, and *Dbp* [10], [142], [144], which serve to fine-tune oscillations generated by the core loop. The nuclear receptors REV-ERBα/β and RORα/β regulate *Bmal1* transcription by competitive binding to its RevDR2 and RORE enhancer elements and ensure nearly anti-phasic expression of *Bmal1* and *Per1/2/3* [145], [146]. *Nr1d1/2 and Rora/b* driven feedback on *Bmal1* transcription is often referred to as “stabilizing feedback loop”. While the core loop (*Bmal1, Clock, Per, Cry*) is essential for the generation of circadian oscillations per se, the stabilizing loop seems to be important for the temporally organized expression of core loop components and with that for the regulation of circadian phase and period. Indeed, it has been shown that REV-ERBα knock-out mice, with regard to their locomotor activity, display shortened rhythms, larger period diversity, as well as increased and accelerated phase responses to light pulses during the second half of the night [145]–[147]. Expression of NFIL3 (also called E4BP4) is regulated by competitive action of REV-ERBs and RORs on their respective enhancer elements in the *Nfil3* promoter [148]. The proline and acidic amino acid-rich basic leucine zipper (PAR bZip) transcription factor DBP induces, while its anti-phasic bZip transcription factor NFIL3 suppresses D-box dependent gene transcription [148]. Just like REV-ERBα/β and RORα/β nuclear receptors, DBP and NFIL3 transcription factors compete for their D-

box binding sites [148], thereby regulating the expression of D-box target genes *Nr1d1/2*, *Rora/b,* and *Per1/2/3* [149]. Thus, based on their interconnection with core and stabilizing loops, DBP and NFIL3 transcriptional activity forms a third and so-called "accessory feedback loop". Due to their antagonist transcriptional activity and anti-phasic expression, it has been suggested that the accessory loop is important for the generation of high amplitude circadian oscillations [148], [150].

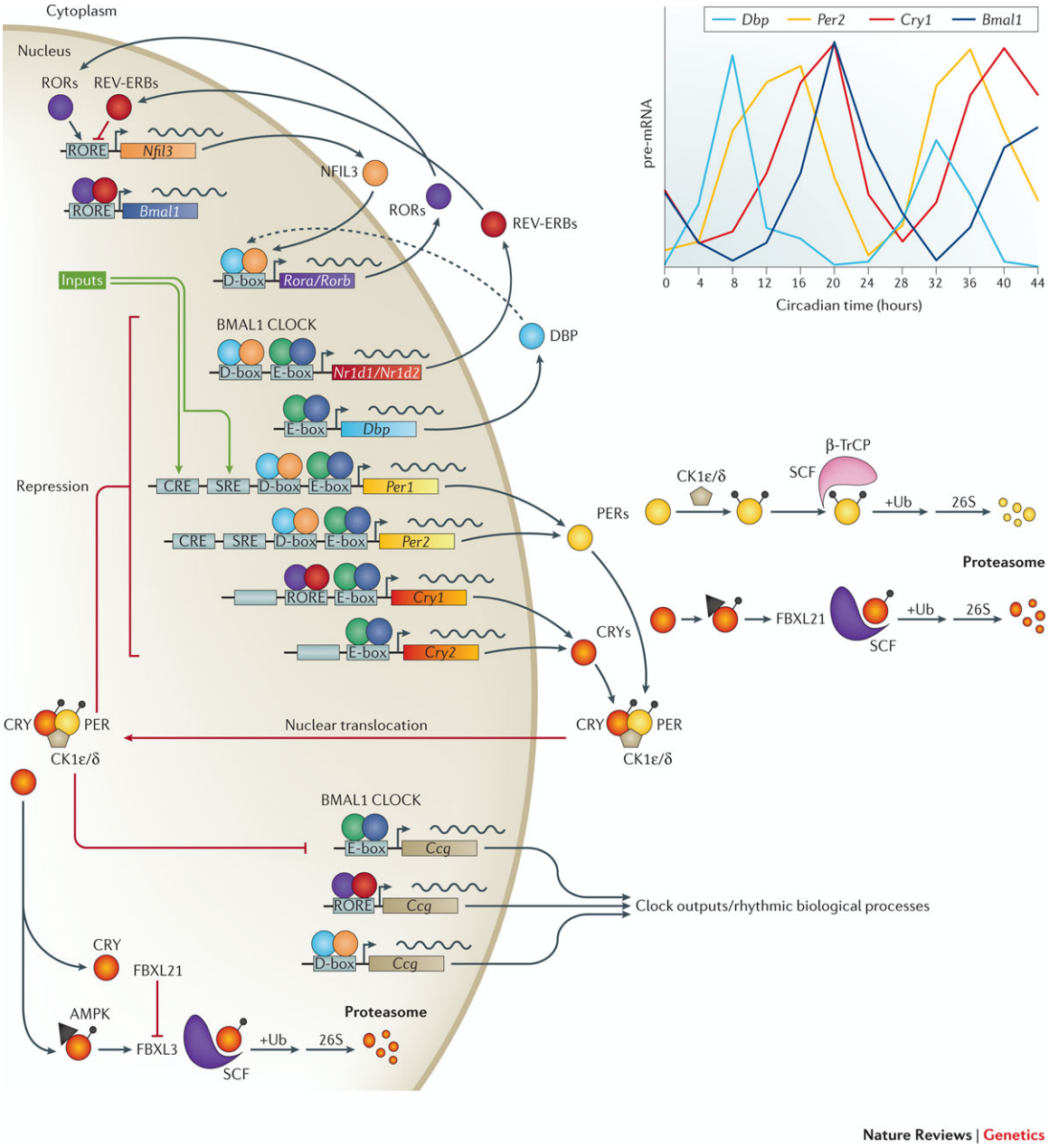

Figure 1-4: The mammalian core clock network

The transcription factors CLOCK and BMAL1 drive the E-box dependent expression of target proteins, including *Pers, Crys, Rev-erbs (Nr1d1/2), Rors, Dbp* (E-box sites not shown for all genes, but see [142], [144]). In the core feedback loop PER and CRY protein products form complexes and suppress their own transcription by inhibition of the CLOCK/BMAL1 heterodimers. The stability of PER and CRY

proteins is regulated by casein kinase 1 and E3 ubiquitin ligase pathways. In a stabilizing feedback loop, the nuclear receptors REV-ERBα/β (encoded by *Nr1d1*/2) and the retinoic acid-related orphan receptors RORα/β (encoded by *Rora/b*), competitively suppress and activate *Bmal1* transcription, by binding to its RevDR2 and RORE promoter elements. A third, accessory, feedback loop is generated by *Nifl3*, regulated by REV-ERBα/β and RORα/β, and *Dbp*, which competitively regulate the expression of a number of clock genes via binding to their D-box promoter elements. These three interlocked TTFLs constitute the mammalian circadian oscillator, with clock genes being expressed in specific relation to each other (see graph at the top right). Expression of rhythmic output genes, so-called clock-controlled genes (CCG), is regulated by the three TTFLs via binding to their respective enhancer elements in promoters of the CCGs. (AMPK = 5'AMP-activated protein kinase, CK1 = casein kinase 1, CRE = cAMP response element, FBX = F-box protein, SCF = SKP1-cullin-F-box protein, SRE = serum response element, Ub = ubiquitin). (adapted from [143])

Activation and repression of distinct clock-controlled promoter elements has been shown to be very important for the regulation of amplitude and transcriptional delay times required for the generation of ~24 hour oscillations [150]. Moreover, timing and order of regulation of these clock-controlled elements seems to be critical for the phase of circadian oscillations: E-boxes, RevDR2, and RORE sites follow a repressor-precedes-activator pattern, while D-boxes follow a repressor-antiphasic-to-activator pattern [151]. The temporal coordination of cis-regulatory DNA elements by interlocked TTFLs, appears to be an inherent design principle of mammalian circadian clocks and ensures both, robustness of circadian rhythms despite variations in gene expression levels, as well as plasticity with regard to the phases of gene expression. Moreover, TTFL dependent transcriptional regulation is not restricted to clock genes, but also appears at promoter sites of so-called clock-controlled genes (CCG). Thereby, circadian oscillations of 3-10% of mammalian transcripts are generated in a tissue-specific manner [41]–[46], [81].

1.3 Entrainment of mammalian circadian clocks

According to Didier Gonze (2011) "[entrainment is] the synchronization of an oscillator to a periodic signal of the environment [(Zeitgeber)], adjusting its phase to fit conditions of the environment" [152]. With respect to mammalian circadian clocks, entrainment is usually described as phase adaptation of the internal circadian rhythm to the

environmental light-dark cycle. However, also other periodically reoccurring signals, such as temperature, rest-activity, or feeding-fasting cycles, can serve as Zeitgebers.

1.3.1 Entrainment from a theoretical perspective

Both, extrinsic Zeitgebers and internal rhythmic processes can be subjected to large variations resulting from seasonal differences in light-dark and temperature cycles, physical activity, food availability and mealtimes, illness, menstrual or other hormonal cycles, and many more. Especially today, modern living conditions are accompanied by challenges of our circadian timing system due to artificial lighting, shift work, and travel across time zones. Thus, how can the circadian system ensure precise rhythmicity, while at the same time allowing enough plasticity to adapt to such variations?

Already in 1977, Halberg et al. compared entrainment to frequency relationships between interacting oscillators [153]. In agreement with this, the so-called range of entrainment has been defined as permissible range of Zeitgeber periods to which a circadian oscillator can still entrain [154]. Moreover, within a given range of entrainment the rhythmic Zeitgeber and the entrained oscillator attain fixed phase relationships, called phase of entrainment (ψ). Theoretical models predict that the phase of entrainment depends on the mismatch between free-running period (τ) of the entrained oscillator and the Zeitgeber period *T*, as well as on the ratio between Zeitgeber strength and oscillator amplitude (Figure 1-5 A,B) [57], [155]–[157]. Moreover, the phase of entrainment has been shown to follow a “180° rule”, i.e. ψ can attain values of +6 hours and -6 hours within any given range of entrainment [155], [156]. Additionally, Abraham et al. (2010) reported that entrainment range depends on the rigidity of an oscillator, i.e. its amplitude relaxation rate after perturbation (Figure 1-5 B,C) [57]. Thus, based on these relationships it can be deduced that strong oscillators (high amplitude) have narrow ranges of entrainment and display high sensitivity of ψ for relatively weak Zeitgebers and small differences in intrinsic and Zeitgeber period. For weak oscillators (low amplitude) however, the opposite is true. Or in other words, for an equally strong Zeitgeber weak oscillators are expected to tolerate much larger period mismatches than strong oscillators during entrainment [155].

With respect to the initial question, theoretical predictions imply that circadian oscillators are able to balance clock precision and plasticity by tuning phase and range

of entrainment. Moreover, assuming that tissue clocks differ in their oscillatory strength or robustness, distinct responses to entrainment signals can be explained. For example, Abraham et al. (2010) demonstrated that intercellular coupling, using SCN as model of strongly and lung as model of weakly coupled oscillators, influences entrainment range by making oscillator networks more rigid and enhancing network amplitudes [57], [157].

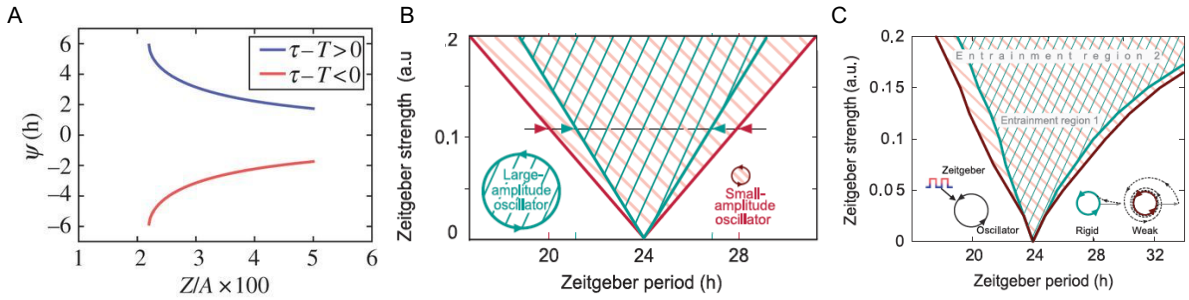

Figure 1-5: Theoretical concepts of entrainment

(A) Phase of entrainment (ψ) attains values between ±6 hours and depends on Zeitgeber strength relative to oscillator amplitude, as well as on the mismatch between intrinsic period (τ) and Zeitgeber period (T). (B) Schematic representation of entrainment range (Arnold tongue), which depends on Zeitgeber period (T) and Zeitgeber strength. Small amplitude oscillators exhibit broader range of entrainment than large amplitude oscillators. (C) Entrainment region of a Poincaré oscillator (radius = 1) as function of Zeitgeber period (T) and Zeitgeber strength. The entrainment range is broader for weak oscillators with low relaxation rates than for strong oscillators with high relaxation rates. (adapted from [57], [156])

1.3.2 Entrainment to the light-dark cycle

As described above (see 1.2) photic information is perceived by visual and nonvisual photoreceptors of the retina and passed on to the SCN via the retinohypothalamic tract (RHT). However, since the circadian system responds to photic signals of much higher intensities and durations than the visual system [158], [159], as well as despite visual blindness (loss of rod and cone photoreceptors) [160], [161], entrainment stimuli seem to differ from photic information conveying visual light perception. Melanopsin expressing intrinsically photosensitive retinal ganglion cells (ipRGC) have shown to project to the SCN, the intergeniculate leaflet (IGL), and the olivary pretectal nucleus (OPN) [162]. However, neither loss of rods and cones, nor of ipRGCs photoreceptors alone [163] abolishes circadian entrainment to light, indicating that all of these cell

types are involved in passing on photic information to the SCN. Nevertheless, the importance of the RHT for circadian entrainment has been demonstrated by lesion and electrical stimulation experiments [164], [165]. Innervation of SCN core neurons by efferent RHT projections has been shown to result in the induction of the core clock genes *Per1/2*, as well as phase resetting of the SCN clock (for details see 1.2). Daily resetting of the SCN is transmitted to peripheral circadian clocks in order to entrain the entire organism to the environmental light-dark cycle. Interestingly, light induced phase resetting by transcriptional activation is almost immediate in SCN core neurons, while changes in shell neurons follow gradually, generating “phase waves” during SCN entrainment [166].

Historically, two concepts of (photic) entrainment have been developed: (i) non-parametric entrainment due to daily phase shifts induced by light-dark transitions, as well as (ii) parametric entrainment due to de- or acceleration of the circadian clock period induced by sustained light exposure [167]. Nevertheless, ultimately changes of the circadian period will result in phase changes of the circadian cycle. Therefore, both, parametric and non-parametric entrainment describe how phase changes serve to adapt the free-running circadian period to the Zeitgeber period and establish phase coherence between internal and external cycles. Non-parametric entrainment can be described by so-called phase response curves (PRC), defined by times at which single Zeitgeber pulses induce phase delays, phase advances, or no phase change (also referred to as “dead-zone”). Parametric entrainment on the other hand is described by velocity response curves (VRC), which can be estimated from the PRC [22]. Today, phase response curves exist for a multitude of Zeitgebers in various species, model organisms, tissues or even cell lines (PRC Atlas: https://as.vanderbilt.edu/johnsonlab/prcatlas/). PRCs are graphical representations of phase shifts in response to Zeitgeber stimuli as a function of when the stimulus was given (can be circadian time, Zeitgeber time or similar) (Figure 1-6). Thus, they are defined by unique shapes and amplitudes that help to deduce information about temporal gating of the Zeitgeber responses, i.e. how oscillators respond to the same signal at different times of the day, as well as about underlying mechanisms of phase adjustments. Photic PRCs are commonly characterized by phase shifts during the subjective night (CT12-24), i.e. the part of the circadian cycle under constant conditions, which corresponds to night in the light-dark cycle [168]. Oppositely, non-

photic PRCs are often characterized by phase shifts during the subjective day (CT0-12), i.e. the part of the circadian cycle under constant conditions, which corresponds to day in the light-dark cycle. For example, responses to forced activity cycles or social interaction elicit such non-photic PRC profiles [169]. In addition to the kind of Zeitgeber, PRCs can be distinguished by the magnitude of phase shifts induced by a Zeitgeber stimulus. While type-0 PRCs are characterized by large phase responses (≥ 12 hours) resulting in abrupt switches between delaying and advancing shifts (the “break point”), type-1 PRCs are characterized by smaller phase shifts (< 6 hours) and gradual transitions between delays and advances (Figure 1-6) [170]. An alternative way of plotting phase responses to Zeitgeber stimuli are so-called phase transition curves (PTC), a plot of circadian phase prior to a stimulus versus circadian phase following a stimulus. Thus, type-0 and type-1 PRCs are derived from the slopes of such PTCs: if a Zeitgeber always resets the oscillator to the same phase, the slope of the PTC will be zero; it will be around 1 if the stimulus shifts the oscillator by a certain amount and in a time-dependent manner [171]. Whether type-0 or type-1 phase responses are induced usually depends on the strength of the Zeitgeber stimulus but can also be influenced by intercellular coupling among single cell oscillators within a network. Consistent with theoretical concepts of entrainment, intercellular coupling has been shown to regulate Zeitgeber responses by altering oscillator amplitudes, as well as amplitude relaxation rates [57], [172].

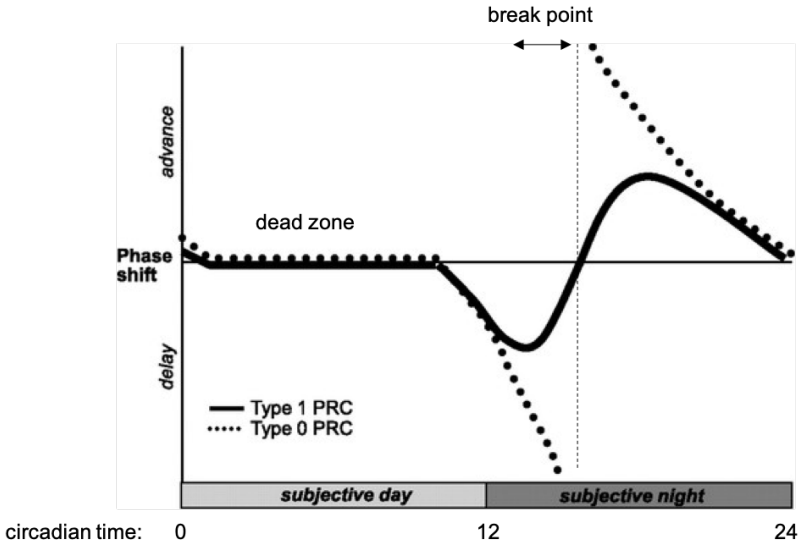

Figure 1-6: Types of phase response curves (PRCs)

In type-1 PRCs (solid line) small phase responses are occurring during the subjective night: phase delays at the early and phase advances at the late subjective night gradually transition from one to

another. Type-0 PRCs (dashed line) are characterized by large phase responses leading to a point of break point between phase delaying and phase advancing portion. Times at which no phase changes in response to a stimulus are occurring are referred to as dead zone and occur during the subjective day for photic PRCs. (adapted from [96])

Photic phase responses in mammals

For the mammalian circadian system light is the most dominant external Zeitgeber. Phase responses to light stimuli are characterized by type-1 photic PRCs. As described above (see 1.2), *Per1 and Per2* induction appear to be the underlying mechanism of photic phase adjustment. Therefore, *Per1/2* phase of expression has been related to the magnitude of light induced phase changes. Indeed, this is true for nocturnal rodents [96]. During the subjective day *Per1/2* expression is high, resulting in a dead-zone of light induced phase shifts of locomotor activity rhythms. During the early subjective night *Per1/2* expression is declining, resulting in phase delays. During the late subjective night *Per1/2* expression is inclining again, resulting in phase advances (Figure 1-5). Interestingly, even though diurnal mammals display a reversal in their activity pattern, phase responses to light stimuli resembles that of nocturnal mammals with regard to clock gene expression and locomotor activity [173]–[175]. Even today it is not clear which mechanisms, downstream of photic resetting, regulate the switch from nocturnality to diurnality but differences at the level of SCN output pathways have been suggested [176]–[178].

In mammals, immediate early induction of *Per1* expression by light stimulation and phase shifts of locomotor activity have been shown to correlate, with rapid (~0.5-1 hour) and strong responses at CT12-CT20 (subjective night) [179]. In the case of *Per2*, response to photic stimuli is more variable, with slower increases (~1.5-3 hours) in gene expression after light pulses given between CT12-CT16 (early subjective night) [94], [180]. Expression of *Per3*, a third *Period* homologue, has been shown to remain unaltered in response to light pulses during the subjective night [181]. Due to the distinct transcriptional responses of *Per1* and *Per2* to light stimuli, it has been proposed that *Per1* functions as primary target of photic entrainment in the SCN, while *Per2* induction may be mediated by secondarily effects, e.g. transcriptional activity of the immediate early expressed genes *c-Fos* and *c-Jun* [94], [180]. Additionally, lack of *Per3* induction by photic stimuli has strengthened the idea that the three *Period* homologues fulfill tissue-specific functions in Zeitgeber induced phase resetting and circadian time keeping [181], [182]. Moreover, even though time-of-day differences in

Per1 and Per2 expression have been associated with dualistic responses (advance versus delay) of the SCN to light pulses during the subjective day and the subjective night, precise mechanisms remain unclear. Induction of other clock components, e.g. *Clock* at CT10 [183], spatiotemporal patterns of synchronization between light-sensing SCN core SCN and shell neurons [166], as well as “gating” of light responsiveness in the SCN [184] have been proposed as alternative mechanism.

1.3.3 Entrainment of peripheral circadian clocks

Following photic entrainment of the SCN external timing information has to be passed on to peripheral circadian clocks in order to establish physiologically required phase relationships among tissue clocks. Thus, in order to entrain peripheral clocks to the light-dark cycle the SCN facilitates the following routes:

The autonomic nervous system
SCN derived sympathetic and parasympathetic projections innervate peripheral tissues, e.g. submandibular slavery glands and liver [185], and directly control their physiological functions, e.g. hepatic gluconeogenesis [186].

The hormonal system
Dominant entrainment signals for peripheral clocks are rhythms in glucocorticoids [131], which are controlled by the hypothalamus-pituitary-adrenal axis via the autonomic nervous system, rhythmic production of corticotropin releasing hormone (CRH) [187], or the adrenal clock itself [188]. Additionally, in vitro models of peripheral circadian oscillators have been shown to display type-0 PRCs in response to glucocorticoid signaling [47]. Thus, glucocorticoids are commonly used as synchronization agent in cell culture experiments. Comparable to phase changes in the SCN, glucocorticoid stimulation induces the expression of a number of core clock genes, including *Per1/2*, via transcriptional activation of glucocorticoid response elements (GRE) [120], [132], [133]. Interestingly, it has been shown that the SCN does not express glucocorticoid receptors [189], [190]. Thus, glucocorticoids have been suggested at serum factors, specifically mediating synchronization of peripheral oscillators. Indeed, it has been demonstrated that glucocorticoids reset circadian gene expression in peripheral tissues but not in the SCN [131].

Temperature rhythms

Mammals are homeothermic organisms, therefore the central pacemaker is rather robust to changes in ambient temperature [191]. Nevertheless, they do display rhythms in body temperature driven by the SCN. Such temperature cycles can serve as entrainment signals for a number of peripheral tissues as has been demonstrated by ex vivo experiments [58], [82]. Heat shock transcription factor 1 (HSF1), which activates transcriptional targets upon binding to heat shock enhancer elements (HSE), has been suggested as mediator of temperature driven entrainment. Indeed, inhibition of HSF1 has been shown to prevent temperature dependent phase resetting of peripheral tissues [58].

Behavioral rhythms (activity and feeding)

The SCN is involved in rhythmic coordination of behavioral processes, such as rest-activity and feeding-fasting cycles. In vivo, restricted feeding, as well as voluntary (wheel running) and forced (treadmill exercise) activity have been shown to entrain peripheral circadian clocks [135], [192]–[195]. Mechanisms of exercise induced phase responses are yet to be explored but the involvement of the hypothalamus-pituitary-adrenal axis and stress related glucocorticoid signaling have been suggested [196]. Likewise, mechanisms of how SCN derived feeding signals entrain peripheral circadian oscillators are poorly understood. Local metabolic changes in response to food intake constitute the most likely connection between circadian clock machinery and feeding rhythms. One the one hand, regulation of REV-ERBα/β and RORα/β nuclear receptors, as well as of glucocorticoid receptors has been suggested as feeding dependent input pathway to peripheral clocks [197], [198]. On the other hand, depending on the metabolic state of the cell, rhythmic components of the energy sensing machinery, e.g. adenosine monophosphate-activated protein kinase (AMPK) [199], and the redox system, e.g. nicotinamide dinucleotide and NAD-phosphate (NAD/NADP) [200], [201], have been proposed as feeding related regulators of circadian clocks. Interestingly, in addition to SCN derived feeding rhythm, so-called food anticipatory behavior exists independently of timing signals from the central pacemaker. This behavior has been shown to induce the reversal of locomotor activity rhythms when food is presented at times of inactivity (e.g. the subjective day for nocturnal rodents) and to persist despite food removal [202]. Underlying rhythmic

processes are often referred to as “food-entrainable-oscillator” (FEO), which may act as additional non-SCN pacemaker. Surprisingly, the FEO appears to bypass the core clock machinery as entrainment to feeding can be achieved even in *Bmal1* and *Per1/2* knock-out animals [203], [204]. Independent of their source, rhythmic feeding signals have been shown drive desynchronization between peripheral and the central clocks if presented in anti-phase to the SCN rhythm [85], [205]. Moreover, rhythmic feeding is able to entrain behavioral, temperature, and peripheral clock rhythmicity in SCN lesioned animals [135], [206], [207]. Thus, food entrainment of peripheral clocks seems to be an exception since it does not necessarily require SCN outputs but can be driven by an additional pacemaker, the FEO, which may even overrule SCN derived timing signals.

1.4 Intercellular coupling

Circadian clocks are comprised of millions of single cell oscillators that must be synchronized with environmental cycles, other tissue clocks, as well as with each other to generate coherent behavioral and physiological rhythms. Synchronization on the system level predominantly depends on entrainment of the central clock to the external light-dark cycle, as well as subsequent entrainment of peripheral clocks to SCN derived signals. Synchronization at tissue or rather cellular level is less well understood. Nevertheless, it is known that maintenance of synchronized tissue rhythms requires intercellular coupling among single cell oscillators. Without coupling the distribution of intrinsic circadian periods of heterogenous single cell oscillators would result in dephasing. Although mechanisms of intercellular coupling within the SCN have been described, it is still debated whether single cell oscillators in peripheral tissues are able to communicate circadian timing information and maintain phase coherent network oscillations at all.

1.4.1 Coupling from a theoretical perspective

Historically, networks of autonomous self-sustained oscillators have been classified into two distinct states: (i) desynchronized or incoherent (oscillators cycle independently of each other, with individual periods and phases) and (ii) synchronized

or coherent (oscillators cycle with locked or similar periods and phases) [208]. With regard to circadian systems, the concept of two oscillator states was expanded by Christoph Schmal et al. (2017). Authors describe the state of network oscillations as function of intercellular coupling strength between individual oscillators. Therefore, classification of network synchrony becomes gradual rather than binary and can be characterized by the distributions of the circadian parameters amplitude, phase, and period [172]. In this model three biologically relevant states (even though mixed states may exist) arise that can serve to explain experimentally observed behavior of circadian oscillators on single cell and population/network level:

(i) Uncoupled (incoherent): virtually no intercellular coupling, oscillators cycle independently with very broad phase/period distributions
(ii) Undercritically coupled: weak intercellular coupling, oscillators show some degree of phase coherence, frequency-locking, and amplitude expansion if a critical coupling threshold is reached
(iii) Overcritically coupled (coherent): strong intercellular coupling, complete synchronization of oscillators leading to network-wide frequency-locking and high amplitude rhythms, phase distributions may be become narrower in response to strong synchronizing signals

Moreover, since intercellular coupling is difficult to quantify in absolute numbers, it may be inferred from behavior of single cell oscillators within a population or from circadian parameters of the ensemble. Changes of parameters, which define circadian oscillations, in dependence of intercellular coupling are described below:

Phase synchronization

In the 1960s, Arthur Winfree introduced a model of self-sustained oscillator populations and their mutual interactions, incorporating a phase dependent “Influence Function” ($X(\phi)$), as well as a periodically varying “Sensitivity Function” ($Z(\phi)$) [209]. This model describes how each oscillator in a network exerts a phase dependent influence ($X(\phi)$) on all other oscillators, as well as how their resulting response is constrained by their sensitivity to this influence ($Z(\phi)$). Consistent with concepts of non-parametric entrainment, $X(\phi)$ and $Z(\phi)$ are assumed to determine de- or acceleration of oscillator period in a phase dependent fashion. This idea was picked up by Yoshiki Kuramoto in

the 1970s. He described that self-entrainment of oscillator populations is achieved when all mutual interactions X(ϕ) lead to increased oscillator synchrony. Thus, as a function of interoscillator coupling strength (k) and network period distribution, synchrony (or phase coherence) between oscillators is expected to induce progressive phase transition from incoherent to coherent network states once a critical coupling threshold is reached [210]–[212]. In coherent networks, oscillators with shorter free-running periods are expected to phase-lead, while oscillators with longer free-running periods are expected to phase-lack relative to the average phase of the network. This phenomenon is comparable with phase of entrainment (for details see 1.3) [155].

Period- (frequency-)locking

In line with the Kuramoto model, increased coupling strength is expected to result in the convergence of free-running periods of individual oscillators. Again, above a critical coupling threshold, oscillators will become “frequency-locked” to the population mean if their intrinsic periods are similar enough [172]. Additionally, if clusters of frequency-locked oscillators arise, they can exert “period-pulling” effects on the remaining oscillators until the entire network remains locked to the mean period (as for overcritical coupling). Ultimately, progressive frequency-locking will results in narrowing of the period distribution due to decreased period dispersion between oscillators until network-wide frequency-locking is achieved (overcritically coupled networks) [172]. The critical coupling threshold, which has to be reached to initiate frequency-locking of the network, depends on the spread of the free-running period distribution [172]. Whether or not coupling affects the mean period of a coupled network is not clear. Intuitively, period shortening with increased coupling strength appears plausible since amplitude resonance between coupled oscillators (see below) may promoter high frequency oscillations. However, for decoupled SCN neurons, i.e. upon knock-out of VIP or VPAC2 (see below), means of period distributions did not change compared to controls [53]. Moreover, theoretical models have reported both, no effect of coupling on the mean period, as well as shortening and lengthening of the mean period upon increased intercellular coupling strength [213], [214].

Amplitude expansion and relaxation

By definition resonance is described as “vibration of large amplitude in a mechanical or electrical system, caused by a relatively small periodic stimulus of the same or nearly

the same period as the natural vibration period of the system" [215]. For a network of oscillators, it can be interpreted as amplification of the amplitude of individual oscillators if their intrinsic frequency approaches the frequency of the population mean. In physics, this relationship is described by the so-called "Lorenztkurve" (or resonance curve), which predicts that resonance is maximized as the frequencies of a forcing and a forced oscillator approach each other. Thus, as a consequence of frequency-locking, coupling affects the amplitude of a network in such a way that increased coupling strength results in amplitude expansion by resonance effects [172]. Additionally, amplitude relaxation rate (λ) of the network, i.e. the return of the amplitude to its initial state following a perturbation, and intercellular coupling are interdependent entities. One the one hand, coupling renders oscillator networks more robust against deviations from the synchronized state [57], [157], [216], thereby making coupled networks more rigid (faster amplitude relaxation). On the other hand, amplitude relaxation rate of individual oscillators is inversely correlated with amplitude resonance [57], [172]. This means that rigid oscillators display almost no change in amplitude upon coupling, while non-rigid oscillators display relatively strong amplitude expansion. Additionally, amplitude relaxation rate, but not intrinsic amplitudes of individual oscillators affect the critical coupling threshold [57], [172]. This implies that increased amplitudes of single cell oscillators may increase the network amplitude independently of coupling dependent amplitude resonance effects.

Damping rates

Based on the inverse relationship between amplitude resonance and damping rate [217], damping of circadian oscillations (on network level) is a reflection of decreasing synchrony among individual oscillators. This is because a reduction of the network amplitude can be explained by increased dispersion of intrinsic oscillator frequencies or in other words: by decreased frequency-locking. Hence, logically increased coupling strength will result in decreased damping and vice versa.

Entrainment to Zeitgebers

As mentioned above (for details see 1.3), entrainment to a rhythmic Zeitgeber is characterized by the phase of entrainment (ψ) between intrinsic and extrinsic oscillations. The period mismatch (τ - T) between the free-running circadian clock period (τ) and the period of the extrinsic Zeitgeber (T) modulates the phase of

entrainment (ψ) [156]. Moreover, strength of an external Zeitgeber [155], [218], [219] relative to the amplitude of the endogenous oscillator [59], [220], [221] have been shown to impact the phase of entrainment. Thereby, these parameters govern the range of entrainment for which adaptation to a given Zeitgeber cycle is still possible. Since circadian parameters of oscillator networks, such as amplitude (based on resonance effects), amplitude relaxation rate, mean phase, and mean period, depend on oscillator synchrony, the concepts of entrainment and coupling are inherently interconnected. This idea was supported by Abraham et al. (2010), who pointed out that intercellular coupling, via changes of amplitude and amplitude relaxation rates, affects the response to entrainment signals, rendering more strongly coupled networks harder to entrain (smaller range of entrainment) and more robust against perturbation by Zeitgeber pulses [57]. Additionally, if frequency-locking results in altered network periods (even though this is still unclear), this may modify entrainment range due to altered relationships (τ - T).

1.4.2 Coupling in the central clock

Even though dispersed SCN neurons display consistent rhythmicity in electrical firing, gene expression, and secretion, they exhibit highly variable periods, leading to phase dispersion on the population level [37]. Thus, in order for the SCN to fulfill its task as pacemaker and entrain to the environmental light-dark cycle, individual neurons must couple with each other to oscillate synchronously (coherent phases/periods) [222], [223]. Both, synaptic communication by exchange of secreted neurotransmitters, e.g. GABA, AVP, GRP, VIP, and electrical coupling via gap junctions have been suggested as coupling mechanism in the SCN. Nevertheless, VIP dependent synaptic signaling is commonly accepted as major coupling pathway within the SCN. This assumption is based on studies, which demonstrated that (i) VIP is rhythmically secreted by SCN neurons [224] and induces time dependent phase shifts in vitro and in vivo. [225], [226], (ii) knock-out of *Vip* and its receptor *Vipr2* results in disruption of rhythmic behavior, gene expression, and electrical firing [53], [56], [227]–[229], as well as that (iii) administration of VIP receptor agonist or SCN grafts restore rhythmicity and synchrony in *Vip* knock-out models [53], [54]. VIP is produced by neurons in the ventral part of the SCN. Thus, following photic input, VIP expressing neurons in the SCN core transmit timing information either directly to their neighboring cells or, via synaptic

projections, to VPAC2 expressing neurons in the shell region (Figure 1-6) [230]. On the molecular level, VIP dependent coupling is very similar to light induced phase resetting. VIP receptor (VPAC2) is a G-protein coupled receptor that, upon ligand binding, induces the activation of adenylyl cyclase (AC). Intracellularly, AC activity leads to the production of cAMP (canonical pathway) or the release of Ca^{2+} (non-canonical pathway). Subsequently, this will result in the downstream activation of a number of protein kinases that impinge on the core clock machinery by inducing CREB driven *Per1/2* expression and *Period* dependent phase resetting (Figure 1-7) [231], [232]. VIP mediated coupling is dependent on the phase of rhythmic neurotransmitter signaling. In 2014, Ananthasubramaniam et al. computationally studied interneuron coupling in the SCN. They proposed that synchrony within the SCN can only be achieved when VIP acts in-phase with activators of the core clock machinery inducing *Per* expression during the early subjective day [233]. This is likely due to the fact that VIP acts as activator of *Per* expression itself. Moreover, while rhythmic VPAC2 expression appeared to be important for amplitude and entrainment range of the SCN, it did not affect interneuron coupling [233].

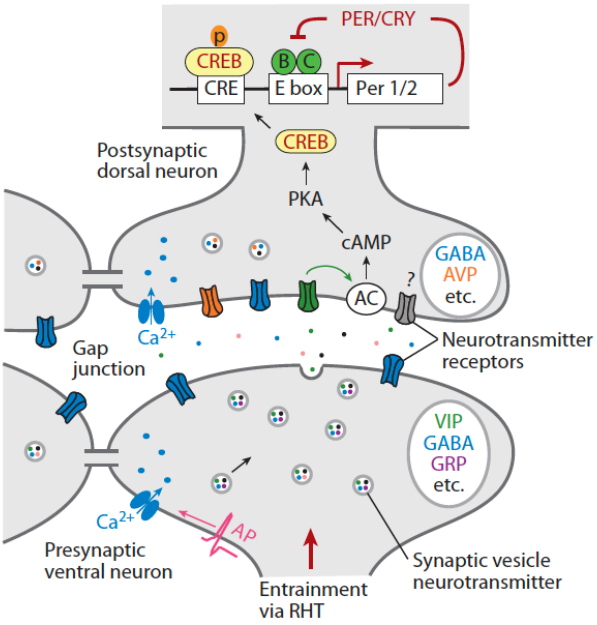

Figure 1-7: Coupling in the SCN

Schematic representation of intercellular signaling mechanisms in the SCN. Photic entrainment results in action potentials (AP) arriving at synaptic terminals of SCN core neurons, triggering the release of GABA, VIP, or GRP. During coupling, VIP binds to its postsynaptic VPAC2 receptors of shell neurons. This results in the elevation of intracellular Ca^{2+} and cAMP levels, activation of protein kinase A (PKA), phosphorylation of CREB, as well as induction of *Per1/2* expression and subsequent phase changes of

neuronal oscillators. Additionally, adjacent neurons may also couple via gap junctions. (adapted from [234])

In addition to VIP, other neurotransmitters, e.g. AVP, GRP and GABA, as well as gap junctions have been described to modulate coupling in the SCN. Like VIP, AVP is rhythmically transcribed and appears to maintain intercellular coupling in the SCN when VIP is absent [54], [235]. Moreover, knock-out of AVP receptor has been shown to result in period lengthening of activity rhythms in mice, as well as in altered entrainment behavior [55], [236]. Similar results were reported for casein kinase 1 and *Bmal1* knock-out in AVP expressing shell neurons [237], [238], suggesting that AVP signaling is involved in period regulation, as well as intercellular coupling in the SCN. GRP is expressed by SCN core neurons and acts as inducer of *Per* expression with phase shifting patterns comparable to VIP [239]. GABA is produced by neurons throughout the SCN and has been supposed to be important for long-distance phase information exchange between SCN core and shell region during entrainment. It can act as both, excitatory and inhibitory neurotransmitter [240]. To what extend gap junctions contribute to SCN synchronization is still debated. However, electrically coupled neurons have been shown to display synchronous firing activity and transgenic animals lacking gap junction protein connexin-36 (Cx36) were found to display weakened locomotor activity rhythms [241].

1.4.3 Coupling in peripheral clocks

Existence and mechanisms of coupling among peripheral circadian oscillators are still under debate. Even though single cell models of peripheral circadian oscillators display persistent cell-autonomous rhythmicity in vitro [47], [48], [89], rhythms of peripheral oscillator networks (on cellular or tissue level) have been shown to partially or completely dampen if deprived of rhythmic SCN derived or external signals [38], [39], [41], [125], [126]. This suggested that peripheral circadian oscillators are able to sustain cell-autonomous oscillations but do not couple to maintain synchronized network rhythmicity. However, in 2004 Yoo et al. demonstrated that, comparable to the SCN, peripheral tissues are able to maintain persistent circadian rhythmicity for up to 20 days ex vivo [35]. This finding, for the first time, indicated that single cell oscillators within peripheral tissue remain synchronized and are able to sustain coherent network

rhythmicity independently of the SCN or external Zeitgeber cycles. This hypothesis was further supported by studies showing that rhythmicity of peripheral tissues in SCN lesioned animals housed under constant conditions, is maintained for at least seven days in vivo (even though with reduced amplitudes) [36], [90]. Additionally, computational modeling approaches have yielded indications of undercritical coupling among peripheral oscillators in vitro [89], [136]. Guenthner et al. (2014) showed that clusters of neighboring hepatocytes display smaller period/phase variation than distant cells, as well as that phase dispersion in hepatocyte cultures is reduced compared to those predicted for incoherent networks [89]. Rougemont et al. (2006) reported that fibroblasts are induce phase shifts in neighboring oscillators, which could lead to synchronization if phase effects would be enhanced or if frequency dispersion among oscillators would be reduced. Moreover, in 2013 Noguchi et al. showed that rhythmicity of single fibroblasts depends on culture density, as well as that low amplitudes of sparsely cultured fibroblasts can be rescued by conditioned medium from other fibroblasts [61]. This suggested that secreted signaling molecules promote synchronous high amplitude rhythms on the population level and that peripheral oscillators may communicate via paracrine pathways. However, as mentioned before, in vitro studies are prone to perturbations by experimental handling and peripheral oscillators, in vitro and ex vivo, may be synchronized by a multitude of signals (for review see [242]). Thus, it should be mentioned that also contradicting evidence, speaking against intercellular peripheral coupling, exists. For example, Welsh et al. (2004) reported that populations of fibroblasts exhibit substantial variations in single cell periods and that neighboring cells do not display phase coherence [48]. Additionally, based on *Per1*:*Bmal1* expression ratios within peripheral tissues of individual animals, Guo et al. (2006) claimed to have demonstrated desynchronization of cellular oscillators within peripheral organs of SCN lesioned hamsters [243]. Moreover, Noguchi et al. (2012) and Nagoshi et al. (2004) have reported a lack of intercellular synchronization upon co-culture experiments of peripheral oscillator models [47], [137]. However, despite these in vitro studies, in vivo experiments have yielded convincing evidence supporting the idea of intercellular coupling among peripheral circadian oscillators. Tahara et al. (2012) and Saini et al. (2013), by in vivo recordings of peripheral tissue clocks in SCN lesion animals housed under constant conditions, have demonstrated that peripheral tissue rhythms are maintained independently of SCN-derived or environmental Zeitgeber signals. Nevertheless, even

under these conditions, it cannot be excluded that rhythmic feedback from other non-SCN body clocks was involved in the maintenance of the observed peripheral tissue oscillations. Recent publications have reported that tissue-specific clock knock-in in otherwise clock-less animals is sufficient to partially rescue tissue rhythmicity under light-dark cycles but not under constant conditions [244], [245]. This suggests that peripheral tissue oscillators require light-dark cycles or additional rhythmic input from other body clocks to maintain synchronized tissue rhythmicity. However, tissue oscillations (in otherwise clock-less animals) were assessed by population sampling under constant conditions. Thus, as discussed above, this may have deceived authors to believe peripheral oscillators within tissue clocks were desynchronized, while really individual arrhythmic animals were out of phase with each other.

After all, research on coupling within peripheral circadian clocks remains inconclusive and molecular mechanisms, as well as functional relevance are completely unknown. Nevertheless, due to the intertwined relationship between intercellular coupling and entrainment (see above), it appears likely that peripheral coupling plays an important role for the response of peripheral clocks to incoming Zeitgeber signals and thereby the temporal coordination of rhythmic organ functions. Under natural conditions, when the SCN is intact, intercellular coupling in the periphery may constitute an essential mechanism for regulating the balance between peripheral clock precision and plasticity in response to intrinsic, as well as extrinsic Zeitgeber signals.

1.5 Circadian alignment and physiology

Entrainment enables circadian clock systems to anticipate and adapt to reoccurring environmental changes by daily alignment of endogenous and exogenous rhythms. Under normal conditions photic timing information, received by the SCN, is passed on to the periphery in order to establish stable phase relationships among various tissue clocks and phase align their physiological outputs with external requirements. SCN lesion has been shown to result in behavioral arrhythmicity and phase dispersion of peripheral tissue clocks [33], [35]. In addition to the photic cues, non-photic entrainment signals can be integrated in a tissue-specific manner and may induce desynchrony between peripheral circadian clocks and the SCN if occurring in

dissonance with the light-dark cycle, e.g. feeding-fasting, sleep-wake, rest-activity, and temperature cycles [82], [85], [111].

Moreover, body clocks have been found to regulate transcriptional programs of clock-controlled genes (CCG) with little overlap between tissues [44], [46], [81], [246]. Thus, expression of these tissue-specific CCGs must be coordinated systemically to generate coherent circadian rhythms on the level of the organism. For example, it has been demonstrated that disruption of liver clocks, in otherwise wildtype animals, results in the loss of a majority of rhythmic hepatic transcripts leading to aberrant systemic glucose homeostasis and metabolic disruption [247]. Therefore, it appears that the circadian system must maintain a delicate balance between external or SCN driven synchronization and tissue-specific regulation of circadian organ functions in order to guarantee the correct temporal coordination of physiological processes in accordance with rhythmic environmental demands (Figure 1-8).

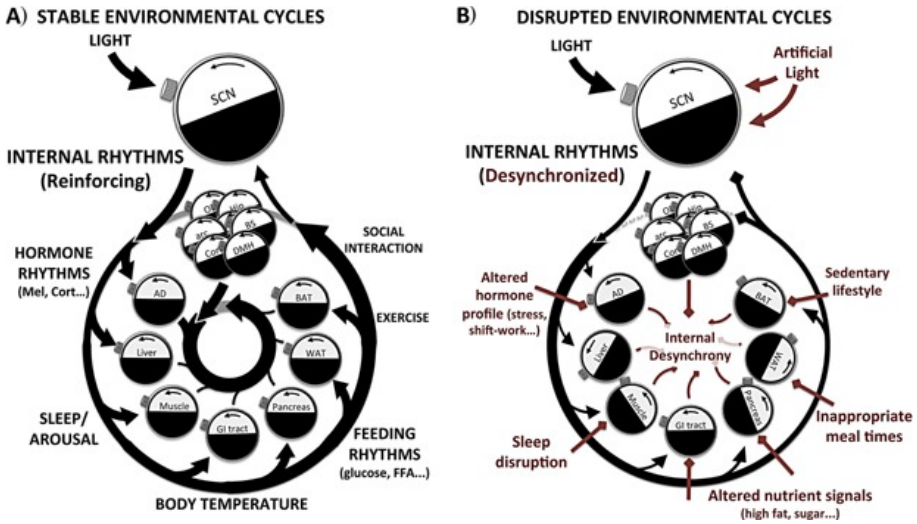

Figure 1-8: States of circadian (de)synchrony

(A) Aligned circadian clocks exists in a state of resonance between internal rhythms, environmental cycles, and behavior: the SCN is synchronized by the daily light-dark cycle and transmits timing information to the rest of the body via direct neuronal projections or the regulation of rhythmic hormone release, body temperature, and feeding. Subordinate clocks are entrained by the SCN but may consolidate system-level synchrony by rhythmic physiology and production of secreted/humoral factors (B) Disrupted or falsely timed external and internal cycles can induce disruption of the circadian system by constant (mistimed) phase resetting leading to internal desynchrony. This prevents the anticipation of rhythmic environmental changes, enables only passive responsiveness or induces complete misalignment of endogenous and exogenous rhythms. (adapted from [248])

1.5.1 The synchronized state: circadian physiology

In healthy organisms, phase relationships between exogenous Zeitgeber and endogenous circadian cycles, as well as among individual tissue clocks are stable, resulting in mutual reinforcement [248]. Phase coherence is achieved by daily phase resetting of the SCN via the light-dark cycle, converting external to central timing information. This time information is further transmitted to other body clocks either via direct neuronal projections or indirect regulation of physiological processes that impinge on the core clock machinery. Tissue-specific regulation of rhythmic biological functions has been shown take place on the level of genes, transcripts [41], [249]–[251], proteins [252]–[254], and metabolites [255]–[258]. Thus, in order to drive the temporal coordination of diverse organ functions in such a way that they align with external demands and reinforce synchronized rhythmicity on the system-level, synchronizing signals must arrive at their target sites during the right time of the circadian cycle (Figure 1-8 A) [86]. One example for complex feedback regulations of the circadian system are glucose homeostasis and hunger regulation [119], [259]–[262]. Involved hormone rhythms are driven by feeding-fasting cycles, generated by the SCN or the FEO, or by cellular oscillators in liver, pancreas, and adipose tissue themselves. Therefore, the same signals serve as input signals to tissue clocks, while at the same time functioning as feedback signals among body clocks to give information about the metabolic state of the organism. As a result of such feedback regulations, as well as of fluctuating environmental conditions, the circadian system has to be able to differentially integrate timing information coming from the external environment, the central pacemaker, and other tissue clocks. How body clocks are able to distinguish between origin, nature, and strength of the input signals, as well as how they are able to respond in a time- and tissue-specific manner to established synchronized physiological outputs remains elusive. Some studies suggest that tissue and phase specificity is achieved on the transcript level through distinct sets of circadian enhancer elements [263], histone modification [264], [265], chromatin landscape [266], or alternative TTFL usage [81]. Additionally, post-translational regulations or metabolic and redox states of the cell have been suggested to be involved in the generation and maintenance of tissue-specific oscillations and functions [267], [268].

1.5.2 The desynchronize state: circadian pathology

Modern lifestyle is commonly associated with behavior leading to the disruption of the synchronized circadian state, e.g. artificial lighting, use of electronic devices, shift work, long distance travel, social responsibilities, abnormal mealtimes, and food excess. As a consequence, external Zeitgeber or SCN derived synchronization signals are transmitted to the circadian system at times when they do not induce phase alignment but rather phase dispersion between internal and external or among internal clocks. Consequently, “circadian misalignment” is expected to result in non-resonating feedback regulations, which further contribute to the incoherence of rhythmic physiological processes, temporal instability of the circadian system (Figure 1-8 B), as well as development of associated pathologies [248]. For example, studies with clock deficient animals have shown that disruption of the circadian system results in serious health issues including metabolic disruption [122], [269], [270], cardiovascular disease [271], [272], obesity [273], premature aging [274], as well as cancer [275]. Moreover, while resonating endogenous and exogenous cycles appear to provide a selective advantage [276], discrepancy between the two has been associated with reduced survival in lower organisms [277], [278]. Also for humans, it has been shown that forced desynchrony protocols (keeping subjects in artificially short or long days resulting in non-resonating endogenous and behavioral cycles) lead to cognitive, cardiac and metabolic malfunctions [279]–[283], as well as alterations of the rhythmic transcriptome [284]. Underlying mechanisms of pathologies associated with circadian misalignment are suggested to derive from altered circadian oscillations on transcript [285], protein [286], and metabolite level [287], [288]. Moreover, disruption of VIP dependent coupling in the SCN has been demonstrated to impact entrainment to external Zeitgeber cycles (on behavioral and peripheral clock level) [53], [289], [290], suggesting that intercellular coupling constitutes and additional layer of system-level synchronization of the mammalian circadian system. Additionally, since tissue clocks regulate circadian processes in a tissue-specific manner, it has been suggested that circadian desynchrony results in organ-specific pathologies [291]. Therefore, it is possible that also intercellular coupling among peripheral circadian oscillators plays an important role for entrainment of peripheral tissue clocks, as well as the temporal coordination of tissue-specific circadian physiology.

1.6 Secretory pathway

Secretion is the movement of biological material between membrane separated cellular compartments or from within the cell to the extracellular space. Specifically, the secretory pathway describes vesicle mediated anterograde and retrograde traffic of proteins between the endoplasmic reticulum (site of protein production), Golgi complex (protein sorting, storage and modification), cell membrane (secretion or membrane expression of proteins), and lysosomes (degradation of proteins) [292]. About one third of the cellular proteome is subjected to trafficking through the secretory pathway. Moreover, exchange of signaling molecules, as well as the secretion of extracellular matrix (ECM) components are regulated by the secretory pathway and play important roles for normal biological tissue function, intercellular signaling, as well as tissue repair and regeneration.

1.6.1 Secretory pathway and circadian clocks

Secretion of neurotransmitters is indispensable for interneuron coupling in the SCN [102], as well as for the temporal regulation of systemic clock input and output pathways. In contrast to the SCN, the extent to which the secretory pathway is involved in intercellular coupling among single cell oscillators within peripheral tissues has yet to be studied. In 2017, S. Jäschke investigated the contribution of vesicular protein transport to normal circadian rhythmicity, as well as to intercellular communication among U-2 OS cells as model of peripheral circadian oscillators. His findings suggested that (i) secretory pathway is required for normal circadian rhythmicity since genetic and pharmacological manipulation resulted in aberrant circadian rhythms, (ii) circadian period and amplitude dependent on culture density, as well as that (iii) conditioned medium modulates circadian dynamics [293]. Similarly, Noguchi et al. (2013) reported that paracrine communication among fibroblasts enhances circadian rhythmicity of cellular oscillators [61].

Circadian clocks have been demonstrated to control rhythmic protein expression, including many secreted proteins [252], [253], [294]. Interestingly, of the 10-20% rhythmic proteins identified in liver and SCN not all could be associated with rhythmic expression of their respective mRNA [267], [295], suggesting that post-translational modifications are involved in the regulation of the circadian proteome [254]. Moreover,

circadian clocks have been described to control rhythmic secretion of proteins and endocrine factors [296], as well as to play a critical role for tissue homeostasis via the rhythmic regulation of secretory pathway and extracellular matrix components [297]. For example, disruption of the circadian clock machinery has been demonstrated to result in aberrant fibrous connective tissue formation [297], [298], indicating that rhythmic secretory pathway plays an important role for secreted proteins expression.

1.6.2 TGF-β family

The transforming growth factor β (TGF-β) family of ligands consists of a large number of secreted signaling molecules, which are structurally related and are involved in a multitude of biological functions regulated in a context dependent manner. Overall, the TGF-β family comprises 33 (known) members including three isoforms of TGF-β, nodal, myostatin (also called GDF8), anti-Müllerian hormone (AMH), as well as several isoforms of activin/inhibin, bone morphogenic protein (BMP), lefty, and growth differentiation factor (GDF) [299]. However, even though the number of TGF-β family ligands is numerous, they all signal through a limited number (12 in mammals) of dual specificity serine/threonine and tyrosine kinase receptors [300]. These receptors are classified as type I anaplastic lymphoma kinase (ALK) or type II receptors that induce downstream signaling in a ligand-specific fashion [301]. Common to all TGF-β family members is that they are encoded by large precursor polypeptides composed of a N-terminal signal peptide, a large pro-segment, and the C-terminal TGF-β family monomer polypeptide. While the monomer polypeptide, which encodes the active form of mature family members, is highly conserved, the pro-segment can vary largely in length and in sequence [302]. Thus, evolutionary relatedness of TGF-β family ligands can be determined based on their structural features and receptor specificity (Figure 1-9). In the case of TGF-β1/2/3 the pro-segment is referred to as latency associated peptide (LAP) that, upon secretion, remains non-covalently associated with dimers of the C-terminal polypeptide and prevents receptor binding. In addition to TGF-β, some but not all TGF-β family members remain associated with their pro-segments, e.g. BMP4/7/9/10, GDF5/11/8, and AMH. However, the functional role of this association is only well-described for TGF-β [303]. The three mammalian TGF-β isoforms are highly conserved in protein sequence. They encode an integrin recognition motif (RGD) in

the LAP segment (involved in the release of active TGF-β), a furin convertase motif (RXXR) following the pro-segment (mediating cleavage before secretion), as well as nine cysteine residues in the active segment (forming intra- and intermolecular disulfide bonds) [299].

Nomenclature of TGF-β family members is derived from their originally assigned functions but may be somewhat misleading. While TGF-β1/2/3 were initially shown to stimulate cell growth, it is now known that they can actually function as both, inhibitors and activators of proliferation, depending on the biological context. Additionally, they are involved in a number of other physiological processes, including angiogenesis, immune function, differentiation and migration [299], [303]. BMP, GDF, and myostatin, which were primarily associated with skeletal morphogenesis, muscle growth and differentiation, are often classified based on structural similarity even though their biological functions are not well-described [299].

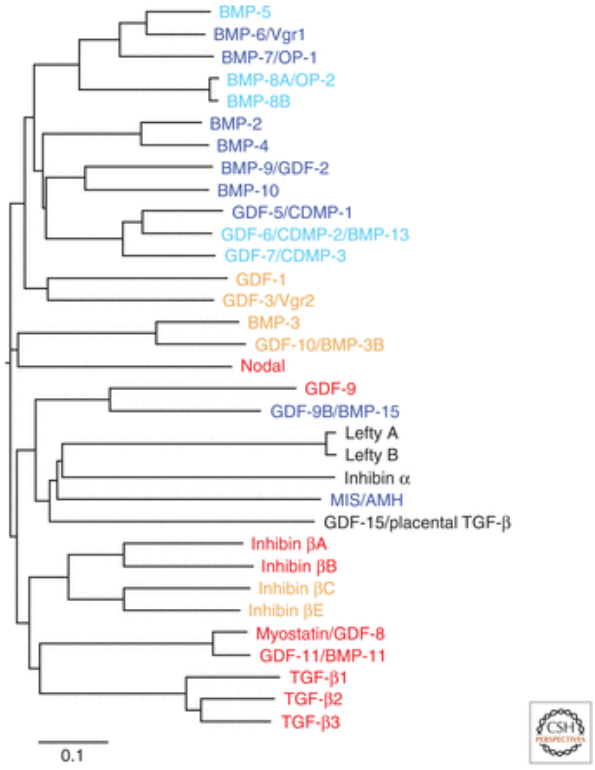

Figure 1-9: Phylogenetic tree of the 33 (human) TGF-β family polypeptides

Phylogenetic tree of the human TGF-β family members clustered based on similarity of their amino acid sequences. Ligands activating activin- and TGF-β-receptors or BMP-receptors are shown in red and in blue, respectively (or in orange and light blue, if they are likely to signal through these receptors). Bone morphogenetic protein (BMP); osteogenic protein (OP); growth and differentiation factor (GDF); cartilage-derived morphogenetic protein (CDMP); Müllerian-inhibiting substance/anti-Müllerian hormone (MIS/AMH); transforming growth factor β (TGF-β). (adapted from [299])

1.6.3 TGF-β secretion and signaling

TGF-β production, secretion, distribution, and activation are part of a complex signaling pathway (Figure 1-10). As described above, TGF-β1/2/3 are synthesized as large precursor proteins including the LAP pro-segment, which is cleaved off by furin convertases in the Golgi apparatus following proper folding and dimerization. As special feature of the TGF-β secretory pathway, LAP remains non-covalently bound to pre-mature TGF-β dimers upon secretion, forming the so-called small latent complex (SLC). Additionally, the SLC is bound by latent TGF-β binding proteins (LTBP1/3/4) extracellularly or intercellularly, forming the large latent complex (LLC) consisting of one LTBP bound to two latent TGF-β monomers [304]. While information about the molecular size of TGF-β complexes are rather variable, active TGF-β is often described as 12.5 kD monomer and 25 kD dimer, monomeric latent TGF-β as 45-65 kD complex, and LLC as 200-260 kD complex (information from various antibody suppliers).
Even though non-covalent association of LAP and mature TGF-β is sufficient to prevent TGF-β signaling, covalent binding to LTBPs, via disulfide bridges, regulates latent TGF-β storage, distribution and release from the extracellular matrix (ECM) [303]. Indeed, transgenic mice expressing a mutant version of TGF-β, unable to form LLC, display reduced levels of active TGF-β, suggesting that LLC formation is crucial for release of the active form and its biological function [305]. How exactly the liberation of active TGF-β from the latent complex is achieved, is not understood in detail. Proteases, e.g. plasmin and matrix metalloproteases (MMP2/9), reactive oxygen species (ROS), as well as physical conditions like heat, and acidic pH (~pH 3.0) have been found to act as releasers of active TGF-β in vitro [306]–[309]. However, in vivo, integrin ($\alpha_v\beta_6$ or $\alpha_v\beta_8$) binding to the RGD motif in LAP via LTBP-integrin-cytoskeleton association has been suggested to be most important for the release of active TGF-β, mediated by tensile forces or recruitment of ECM proteases [310]–[312]. Indeed, transgenic animals depleted of the integrin subunits β_6/β_8 display pathological changes similar to mice lacking TGF-β1/2/3 [310]. In addition to the relevance of latent complexes as mediators of active TGF-β release, it has been suggested that LAP and LTPB isoform selection may be involved in biological context dependent regulation of TGF-β activity [313], i.e. levels of active TGF-β may be regulated by LTBP isoform

dependent ECM deposition and/or the susceptibility of LAP isoforms to a given release mechanism.

In addition to the three TGF-β isoforms, also three TGF-β receptors exist that can be found in many mammalian tissues but with variable in gene and protein expression levels [314]. While TGF-β type III receptors lack a kinase domain for the intracellular transmission of TGF-β derived signals, they may act as co-receptors for type I and type II receptors regulating ligand availability [315], [316]. TGF-β type I (also ALK5) and TGF-β type II receptors act as transmembrane kinase receptors, which, in their unbound form, exist as monomeric, heterodimeric, or homodimeric complexes that associate into heterotetramers upon ligand binding [317], [318]. Depending on the TGF-β isoform, formation of receptor-ligand complex can occur in a stepwise or immediate fashion. TGF-β1 binds with high affinity to type II receptors, initiating the recruitment of ALK5, while TGF-β2 binds directly to preformed receptor tetramers [301]. Ultimately, ligand-receptor interaction results in the auto-phosphorylation of the TGF-β type II receptor [319], [320], which is not sufficient to activate downstream signaling components but is required for the subsequent phosphorylation and activation of the cytoplasmic kinase domain of type I receptors [319], [320]. Consequently, phosphorylation of type I receptors results in the direct serine dependent activation of SMAD proteins, classified into receptor activated SMAD1/2/3/5/8 (R-SMADs), co-regulator SMAD4 (co-SMADs), and inhibitory SMAD6/7 (I-SMADs). Activation of R-SMADs provides an additional mechanism for regulating specificity with regard to the TGF-β family, since isoform activation is controlled in a ligand-receptor dependent fashion [301]. Canonical TGF-β type I/type II receptor signaling leads to the activation of SMAD2/3. These activated R-SMADs dissociate from the receptor and bind SMAD4, forming a complex that will be shuttled into the nucleus where it interacts with various co-activator/-suppressor proteins or transcription factors to regulate the expression of target genes [321]. For example, interaction between the conserved SMAD mad homology 1 (MH1) domain with the transcriptional activators and nuclear adaptor proteins p300 and CREB binding protein (CBP) has been described in vitro and in vivo [322]–[324]. Besides SMAD mediated signaling, TGF-β receptors have been described to be involved in a number of non-canonical kinase pathways through interaction with and phosphorylation of alternative adapter proteins [325]. Non-canonical pathways include RhoA, NF-κB, ERK1/2, JNK,

and MAPK signaling pathways [326]. Fine-tuning of TGF-β receptor signaling is mediated by a variety of mechanisms including sumoylation and co-receptor dependent promotion of SMAD activation, interaction with regulatory membrane and/or cytoplasmic proteins, miRNA mediated suppression, ubiquitylation dependent degradation, as well as feedback regulations and endocytosis [301]. Especially SMAD7, whose expression is induced either directly or indirectly by TGF-β receptor signaling, has been described to play a crucial role in the feedback regulation of receptor activity. Recruitment of SMAD7 to the cytoplasmic receptor kinase domain has been shown to result in dephosphorylation, ubiquitination, and degradation of type I/type II receptor complexes [327]–[330]. In addition to the regulated termination of receptor signaling, targets promoting storage and release of active TGF-β, e.g. integrins, MMP2/9, and ECM components, as well as targets enhancing TGF-β signaling, e.g. contractile protein α-smooth muscle actin (α-SMA) and connective tissue growth factor (CTGF), are transcriptionally upregulated by type I/type II receptor signaling, generating important positive feedback loops [331].

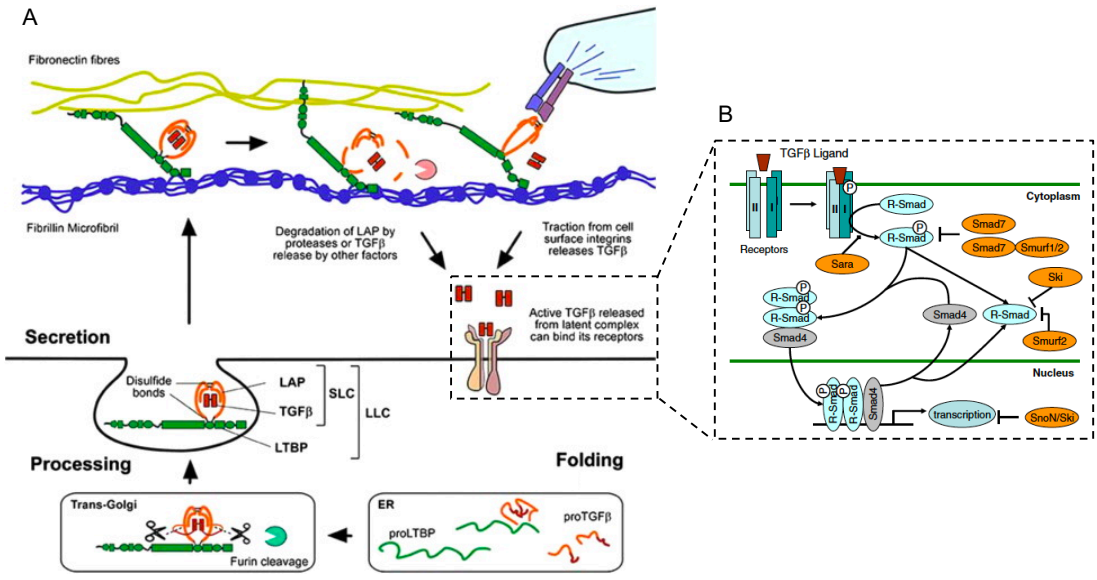

Figure 1-10: TGF-β secretion and signaling

(A) TGF-β is synthesized as precursor protein including the LAP pro-segment, which is cleaved by furin convertase in the Golgi apparatus. Pre-mature TGF-β is either secreted as SLC and associates with LTBPs extracellularly or is secreted as LLC. The LLC associates with fibrous extracellular matrix components where TGF-β is held in its latent form. Release of active TGF-β can be achieved by different routes including protease activity or integrin mediated tensile force. Transforming growth factor beta (TGF-β), latent TGF-β binding protein (LTBP), latency associated peptide (LAP), small latent complex

(SLC), large latent complex (LLC). (adapted from [332]). (B) Active TGF-β binds to its receptors and induces auto-phosphorylation. Subsequently, a signaling cascade involving R-SMADs, co-regulatory SMADs, and inhibitory SMADs is activated. SMAD activity is further regulated by receptor anchor proteins (SARA), ubiquitin ligases (SMURF1/2), or additional co-regulators (SnoN/SKI). Ultimately activated SMAD4/R-SMAD complexes translocate to the nucleus where they regulate the transcription of target genes. Receptor activated SMAD (R-SMAD), SMAD anchor for receptor activation (SARA), Mothers against decapentaplegic homolog (SMAD), SMAD-specific E3 ubiquitin ligase (SMURF), SKI like proto-oncogene (SnoN), SIK proto-oncogene (SKI). (adapted from [333])

TGF-β secretion and signaling underlies tightly regulated mechanisms and is involved in a variety of reciprocally regulated (patho-) physiological processes, such as proliferation and differentiation, tissue regeneration and inflammation, cell growth and transformation, cell survival and apoptosis, as well as fibrosis, epithelial-mesenchymal transition and metastasis. How exactly TGF-β function is controlled is still poorly understood but probably depends on the biological context in which signaling is induced.

1.6.4 TGF-β and circadian clocks

Only limited information about the connection between the circadian clock and TGF-β signaling is available. Nevertheless, studies have yielded indications for CLOCK/BMAL1 transcriptional regulation of TGF-β pathway genes, including *Tgfb1/2*, *Tgfbr2* and *Smad3*, via their E-box enhancer elements [334]–[336]. Authors further suggested a functional role of circadian clock mediated TGF-β expression for the regulation of brown adipocyte development, lung fibrogenesis, and tubulointerstitial fibrosis. Rhythmic or diurnal expression of TGF-β has been demonstrated in SCN and fibroblasts [335], [337]. Moreover, *Smad3* expression has been shown to be regulated by CLOCK/BMAL1 and in a circadian fashion in adipocytes, fibroblasts, mesenchymal stem cells, and mouse liver [334], [338]. Diurnal TGF-β signaling activity, as predicted by phosphorylation of SMAD3, has been detected in the SCN paraventricular nucleus [337]. In addition to its clock dependent transcriptional regulation, TGF-β has been shown to regulate circadian dynamics by phase shifting circadian oscillations in vitro and in vivo [339]. Moreover, a study in zebrafish demonstrated that transcription and expression of TGF-β signaling pathway components (*Smad3, Smad7, TGF-β1*) are rhythmically regulated by the circadian clock, as well as that disruption and stimulation

of TGF-β signaling results in alteration of both, molecular and behavioral circadian oscillations [340].

1.7 Aim of the study

Intercellular coupling among peripheral circadian oscillators is a highly controversial topic in chronobiological research. Evidence speaking for peripheral coupling in vitro and in vivo exists but is debated. Nevertheless, studies have suggested that paracrine communication among peripheral circadian oscillators plays an important role for normal circadian dynamics on single cell and population level [61], [293]. Moreover, peripheral circadian oscillations have been found to persist independently of SCN-derived or rhythmic environmental signals in vitro and in vivo [35], [36], [47], [48], [90]. However, neither molecular mechanisms nor functional relevance of peripheral coupling have been investigated so far.

In this thesis, the main hypothesis, we aimed to test, was that peripheral circadian oscillators couple with each other via the exchange of paracrine signaling molecules, which promote phase alignment, as well as interoscillator synchronization. We decided to use U-2 OS cells as a model for peripheral circadian oscillators because this cell line is well-described and commonly used in chronobiological research. Moreover, to our knowledge no coupling studies have been performed in U-2 OS cells, for which reason we hoped to provide additional evidence speaking for intercellular coupling in yet another model system of peripheral circadian clocks. Most importantly, the aim of this study was to investigate whether peripheral circadian oscillators couple intercellularly, as well as by which molecular mechanisms this coupling is achieved. Specifically, we wanted to test (i) whether peripheral circadian oscillators couple with each other via paracrine communication pathways, (ii) how this paracrine communication affects circadian dynamics on the phenotypic and the molecular level, (iii) which secreted molecules meditate observed effects, as well as (iv) which paracrine signaling pathways are required for intercellular coupling among peripheral circadian oscillators.

Intercellular coupling is tightly connected with entrainment and responsiveness to Zeitgeber stimuli [57], [156]. The prevalence of human disease associated with circadian misalignment is constantly increasing. Therefore, the results of this study may contribute to a better understanding of how peripheral body clocks regulate tissue-specific circadian physiology in adaptation to SCN derived or external Zeitgeber signals, as well as how they contribute to resonating circadian rhythmicity on the system level.

2 Materials and Methods

2.1 Materials

2.1.1 Animal strains

All animals were bred at the animal facility of the Charité University Medicine Berlin ("Forschungseinrichtung für experimentelle Medizin" FEM). Prior to the experiment the animals were transferred to the experimental animal facility and either prepared for isolation of primary hepatocytes or sacrificed for explanation of peripheral tissues (for details see 2.2).

Mouse strain	Source
C57BL/6J	FEM, Charité University Medicine Berlin
B6.129S6-Per2^{tm1Jt}/J (also called mPer2^{Luciferase} or PER2::LUC)	FEM, Charité University Medicine Berlin

2.1.2 Mammalian cell lines and primary cells

2.1.2.1 U-2 OS cells

U-2 OS cells were provided as kind gift of AG Hagemeier, Charité University Medicine Berlin, Germany and were originally purchased from the American Type Culture Collection (ATCC).

Organism:	*Homo Sapiens*, human
Tissue:	bone
Disease:	osteosarcoma
Origin:	15-year-old Caucasian female
Morphology:	epithelial
Special feature:	chromosomally highly altered
Growth properties:	adherent, contact inhibited growth
Culture conditions:	complete culture medium, 37°C, 5% CO_2
Subcultivation ratio:	1:5 – 1:7, two to three times a week

2.1.2.2 U-2 OS *Bmal1*:Luc cells

U-2 OS cells expressing a stably integrated pABhygro_*Bmal1*:Luc plasmid. Cell lines was generated in-house by clonal selection and expansion of U-2 OS cells transduced with pABhygro_*Bmal1*:Luc encoding lentivirus.

2.1.2.3 U-2 OS *Bmal1*:Luc *CRY2*$^{-/-}$ and *TNPO1*$^{-/-}$ knock-out cells

Knock-out cell lines were generated in-house by S. Korge and T. Börding using the CRISPR/Cas9 gene depletion method [341], [342].

2.1.2.4 U-2 OS *Per2*:Luc, 7xCRE:Luc, 7xmutCRE:Luc, and 7xSRE:Luc cells

U-2 OS cells were transduced with lentivirus containing pLenti6_*Per2*:Luc, pLenti6_7xCRE:Luc, pLenti6_7xmutCRE:Luc, or pLenti6_7xSRE:Luc expression plasmids. Antibiotic selection but no clonal selection was performed. Therefore, the reporter plasmids remained transiently integrated with variable copy numbers. U-2 OS reporter cells were used for up to two months until a new batch was transduced.

2.1.2.5 HEK293 cells

HEK293 cells were purchased from the American Type Culture Collection (ATCC).

Organism:	*Homo Sapiens*, human
Tissue:	embryonic kidney
Disease:	-
Origin:	fetus
Morphology:	epithelial
Special feature:	hypotriploid
Growth properties:	adherent
Culture conditions:	complete culture medium, 37°C, 5% CO_2
Subcultivation ratio:	1:6 – 1:10, two to three times a week

2.1.2.6 HEK293T cells

HEK293T cells were purchased from the American Type Culture Collection (ATCC).

Organism:	*Homo Sapiens*, human
Tissue:	embryonic kidney
Disease:	-
Origin:	fetus
Morphology:	epithelial
Special feature:	hypotriploid, contains the SV40 T-antigen
Growth properties:	adherent
Culture conditions:	complete culture medium, 37°C, 5% CO_2
Subcultivation ratio:	1:10 – 1:12, two to three times a week

2.1.2.7 R-spondin1 cells

Cultrex® R-spondin1 expressing HEK293T cells were purchased from Trevigen.

Organism:	*Homo Sapiens*, human
Tissue:	embryonic kidney
Disease:	-
Origin:	fetus
Morphology:	epithelial
Special feature:	secrete RSPO1
Growth properties:	adherent
Culture conditions (undifferentiated):	complete culture medium, 37°C, 5% CO_2
Subcultivation ratio:	1:10 – 1:12, two to three times a week

2.1.2.8 HCT116 cells

HCT116 cells were purchased from the American Type Culture Collection (ATCC).

Organism:	*Homo Sapiens*, human

Tissue:	colon
Disease:	colorectal carcinoma
Origin:	adult male
Morphology:	epithelial
Special feature:	tumorigenic, produces carcinoembryonic antigen and keratin
Growth properties:	adherent
Culture conditions:	complete culture medium, 37°C, 5% CO_2
Subcultivation ratio:	1:10 – 1:12, two to three times a week

2.1.2.9 C2C12 cells

C2C12 cells were provided as kind gift of AG Bass, Northwestern University Illinoise, United States of America. Original supplier is unknown.

Organism:	*Mus Musculus*, mouse
Tissue:	muscle
Disease:	-
Origin:	C3H strain
Morphology:	myoblast
Special feature:	differentiates rapidly forming contractile myotubes and producing muscle specific protein
Growth properties:	adherent
Culture conditions:	complete culture medium, 37°C, 5% CO_2
Subcultivation ratio:	1:10 – 1:12, two to three times a week

2.1.2.10 NIH3T3 cells

NIH3T3 cells were provided as kind gift of AG Schibler, University of Geneva, Switzerland. Original supplier is unknown.

Organism:	*Mus Musculus*, mouse
Tissue:	embryo

Disease:	-
Origin:	embryo, NIH/Swiss strain
Morphology:	fibroblast
Special feature:	-
Growth properties:	adherent
Culture conditions:	complete culture medium, 37°C, 5% CO_2
Subcultivation ratio:	1:10 – 1:12, two to three times a week

2.1.2.11 Wnt-3A cells

Wnt-3A cells were purchased from the American Type Culture Collection (ATCC).

Organism:	*Mus Musculus*, mouse
Tissue:	subcutaneous connective tissue
Disease:	-
Origin:	C3H/An strain
Morphology:	fibroblast
Special feature:	secrete WNT3A
Growth properties:	adherent
Culture conditions:	complete culture medium, 37°C, 5% CO_2
Subcultivation ratio:	1:10 – 1:12, two to three times a week

2.1.2.12 Mouse primary hepatocytes

Primary hepatocytes were prepared from mouse livers as described in methods (for details see 2.2)

Organism:	*Mus Musculus*, mouse
Tissue:	liver
Disease:	-
Origin:	adult, C57BL/6J strain
Morphology:	hepatocytes
Special feature:	express hepatocyte markers
Growth properties:	adherent

Culture conditions:	complete culture medium, 37°C, 5% CO_2, rat tail collagen type 1 coated plates
Subcultivation ratio:	-

2.1.2.13 Mouse liver organoids/hepanoids

Liver organoids/hepanoids were generated from mouse livers, maintained and differentiated in vitro as described in methods (for details see 2.2)

Organism:	*Mus Musculus*, mouse
Tissue:	liver
Disease:	-
Origin:	adult, B6.129S6-Per2^{tm1Jt}/J strain
Morphology:	organoid
Special feature:	derived from hepatic duct adult stem cells that self-organize into liver buds and can be differentiated into hepatocyte-like cell structures (hepanoids)
Growth properties:	adherent, in basement matrix
Culture conditions (undifferentiated):	mouse liver expansion medium, embedded in Matrigel
Culture conditions (differentiated):	mouse liver differentiation medium, embedded in Matrigel
Subcultivation ratio (undifferentiated):	1:10 – 1:12, two to three times a week
Subcultivation ratio (differentiated):	-

2.1.3 Bacterial cell lines

Bacterial strain	Source	Genotype
E. coli DH10β	Invitrogen	F– mcrA Δ(mrr-hsdRMS-mcrBC) Φ80lacZΔM15 ΔlacX74 recA1 endA1 araD139 Δ(ara leu) 7697

2.1.4 Culture media

Medium	Composition
Complete culture medium:	DMEM high glucose
	10% v/v fetal bovine serum (FBS)
	1X penicillin/streptomycin
	25 mM HEPES-buffer
Mouse liver basal medium:	Advanced DMEM/F-12
	1X GlutaMAX
	1X penicillin/streptomycin
	10 mM HEPES-buffer
Mouse liver wash medium:	DMEM high glucose GlutaMAX pyruvate
	1% v/v FBS
	1X penicillin/streptomycin
Mouse liver expansion medium:	Mouse liver basal medium
	1X B-27 supplement
	1 mM N-Acteylcisteinamide
	5% v/v Rspo1-condititioned medium
	10 mM Nicotinamide
	10 nM recombinant human Leu-Gastrin I
	50 ng/mL recombinant mouse EGF
	100 ng/mL recombinant human FGF10
	50 ng/mL recombinant human HGF
Mouse liver isolation medium:	Mouse liver expansion medium
	25 ng/mL rh Noggin
	30% v/v Wnt-3a conditioned medium
Mouse liver differentiation medium	Mouse liver basal medium
	1X B-27 supplement
	1 mM N-acteylcisteinamide
	10 nM recombinant human Leu-Gastrin I
	50 ng/mL recombinant mouse EGF
	100 ng/mL recombinant human FGF10
	50 nM A83-01
	10 µM DAPT

Serum-free culture medium:	DMEM high glucose 1X penicillin/streptomycin 25 mM HEPES-buffer
Reporter medium:	DMEM high glucose phenol red-free 1X penicillin/streptomycin 250 µM D-Luciferin
Freezing medium:	90% v/v FBS 10% v/v dimethyl sulfoxide (DMSO)
LB-Medium:	10 g NaCl 10 g Bactotryptone 5 g yeast extract 12.5 g agar 1 L aq. dest., autoclaved

2.1.5 Vectors

Vector	Description	Source
pLenti6_*Per2*:Luc	mouse *Per2* promoter region (-3309 - +105) in frame with luciferase sequence in lentiviral vector backbone	In-house, N. Tuvia
pLenti6_7xCRE:Luc	seven repeats of the cAMP-response element (CRE) upstream of a minimal promoter (TAGAGGGTATATAATGG AAGCTCGACTTCCAG) in frame with luciferase sequence in lentiviral vector backbone	In-house, N. Tuvia
pUC57_7xmutCRE	seven repeats of mutated CRE (TGACGTCA → TTAAACCA) in pUC57 cloning vector	Synthesized BioBasic Inc
pLenti6_7xmutCRE:Luc	seven repeats of the mutated CRE upstream of a minimal promoter in frame with luciferase sequence in lentiviral vector backbone	In-house, A. Finger

pStarprom_7xSRE:Luc	seven repeats of the serum response factor response element (SRE) upstream of a minimal promoter in frame with luciferase sequence in lentiviral vector backbone	AG Schibler, University of Geneva, Switzerland
pGIPZ_shRNA	RNAi mediated knock-down vectors encoding shRNA sequences targeting a human gene of interest in frame with the green fluorescent protein (GFP) sequence and under the control of a CMV promoter	GIPZ Whole Genome Library, Horizon Discovery
pABhygro_*Bmal1*:Luc	0.9kb mouse *Bmal1* promoter fragment in frame with luciferase sequence in lentiviral vector backbone	In-house, A. Grudziecki
psPAX	Lentiviral packaging plasmid	Addgene #12260
pMD2G	Lentiviral packaging plasmid	Addgene #12259

2.1.6 Antibodies

Target	Source	Supplier	Catalog number
TGF-β1/2/3 clone 1D11, (human, mouse)	mouse IgG_1, monoclonal	Thermo Fisher Scientific	15583482
IgG_1 isotype control kappa clone #11711	mouse IgG_1, monoclonal	R & D Systems	MAB002

2.1.7 Enzymes

Enzyme	Supplier	Catalog number
ApaI	New England Biolabs	R0114S
Collagenase type I	Worthington Biochemical	LS004197
Collagenase D	Roche	11088858001

Dispase	Sigma-Aldrich	42613-33-2
DNase I	Sigma-Aldrich	DN25-10MG
M-MLV reverse transcriptase	Thermo Fisher Scientific	28025013
NheI-HF	New England Biolabs	R0131L
RNase A	Thermo Fisher Scientific	12091021
Trypsin/EDTA	Lonza-Biozym	882
T4 DNA ligase	New England Biolabs	M0202 S

2.1.8 Buffers and solutions

Buffer	Composition or Supplier
Advanced DMEM/F-12	Life Technologies, cat# 12634-028
Bicinchonic acid (BCA) assay solution A	2% (w/v) Na_2CO_3
	1% (w/v) BCA-Na_2
	0.95% (w/v) $NaHCO_3$
	0.4% (w/v) NaOH
	0.16% (w/v) Na_2-tartrat
	Solved in aq. dest; pH 11.25
Bicinchonic acid (BCA) assay solution B	4% (w/v) $CuSO_4$ x 5 H_2O
10X CutSmart buffer	New England Biolabs, cat# B7204S
Coomassie staining solution	0.1% (w/v) Coomassie Brilliant Blue R-250
	40% (v/v) ethanol
	10% (v/v) acetic acid
Digestion buffer	50 mL 1X HBSS
	5000 U collagenase type I
DMEM, high glucose, HEPES, phenolred-free	Life technologies, cat# 21063029
DMEM, high glucose	Life technologies, cat# 41965039
1X EBSS without $CaCl_2$/$MgCl_2$	Gibco, cat# 14155048
100 mM EGTA	3.8 g EGTA
	Solved in 20 mL aq. dest, pH 11
	Bring to 100. mL aq. dest, pH 8.0
	Dissolve in 150. mL aq. dest

5X First Strand Buffer	250 mM Tris-HCl (pH 8.3) 375 mM KCl 15 mM Magnesium Chloride (supplied with M-MLV reverse transcriptase, Thermo Fisher Scientific, cat# 28025013)
1X HBSS phenol-red free	Biochrom, cat# L2035
1 M HEPES buffer	50 mM HEPES 140 mM NaCl 1 mM Na_2HPO4_2 Solved in aq. dest; pH 7.0, sterile filtered
Ketamin/Xylazin	80 mg/mL Ketavet in 0.9% NaCl 1.2% Rompun in 0.9% NaCl
LB-Agar	10 g NaCl 10 g Bactotryptone 5 g yeast extract 1 L aq. dest, autoclaved
Mouse liver digestion solution	0.125 mg/mL collagenase D 0.125 mg/mL dispase 0.1 mg/mL DNase I Mouse liver wash medium
4X NuPAGE™ LDS Sample Buffer	Thermo Fisher Scientific, cat# NP0007
20X NuPAGE™ MES SDS Running Buffer	Thermo Fisher Scientific, cat# NP0002
Opti-MEM	Life Technologies, cat# 31985047
Penicillin/streptomycin (10000U/mL)	Thermo Fisher Scientific, cat# 15140122
Perfusion buffer	500 mL 1X EBSS without $CaCl_2/MgCl_2$ 5 mL 50 mM EGTA
10X Phosphate buffered saline (PBS)	1.37 M NaCl 27 mM KCl 100 mM Na_2HPO_4 10 mM NaH_2PO_4 Solved in aq. dest, pH 7.2, autoclaved
1X Tris-EDTA buffer (TE)	Promega, cat# V6231

50X Tris-acetate-ETDA buffer (TAE)	2 M tris-base 50 mM EDTA 1 M 100% acetic acid Solved in aq. dest, pH 8.5

2.1.9 Reagents

Reagent	Supplier	Catalog #
Agarose	BD	3252375
Ampicillin	Carl Roth	K029.2
Ammonium sulfate	Sigma-Aldrich	A4418
A-83-01	Tocris	2939/10
β-mercaptoethanol	Carl Roth	4227.1
B-27 Supplement (50X)	Life Technologies	12587010
Blasticidine	Life technologies	R210-01
Bovine serum albumin (BSA)	Sigma-Aldrich	A7030
Corning® Matrigel® Matrix	Corning	354277
Coomassie Brilliant Blue R-250 Dye	Thermo Fisher Scientific	20278
Cultrex® reduced growth factor basement membrane matrix	Trevigen	3433-001-01
DAPT	Sigma-Aldrich	D5942-5MG
Dexamethasone (1 mM stock in EtOH)	Sigma-Aldrich	D4902
Dimethyl sulfoxide (DMSO)	AppliChem	A3672
Dithiothreitol (100 mM)	Thermo Fisher Scientific	28025013
D-Luciferin (25 mM stock in DMEM phenolred-free)	P.J.K	102112
dNTP mix (10 mM stock)	Thermo Fisher Scientific	611352
Easycoll separating solution	Biochrom	L2035
Fetal bovine serum (FBS)	Thermo Fisher Scientific	10106-169
HPLC water	Carl Roth	A511.2
Ketavet	Pfizer	PZN 3151811
Lipofectamin2000©	Thermo Fisher Scientific	11668019

LY2109761	Cayman Chemical	15409
N-Acteylcisteinamide	Sigma-Aldrich	A0737
Nicotinamide	Sigma-Aldrich	N0636-100G
6X Orange Loading Dye	Thermo Fisher Scientific	R0631
Protein G PLUS agarose	Santa Cruz	Sc-2002
Protamine sulfate	Sigma-Aldrich	P3369
Puromycin	Sigma-Aldrich	P9620
Recombinant human FGF10	Peptrotech	100-26
Recombinant human HGF	Peptrotech	100-39
Recombinant human TGF-β1/2/3	Abcam	ab50036/ab84070/ ab217402
Recombinant human Noggin	Peptrotech	120-10C
Recombinant human Leu^{15}-Gastrin I	Sigma-Aldrich	G9145-0.1MG
Recombinant mouse EGF	Life Technologies	PMG8043
RedSafe™	iNtRON Biotechnology DR	21141
RiboLock RNase Inhibitor	Thermo Fisher Scientific	EO0381
Rompun	Bayer	PZN 1320422
Tryptan blue	Sigma-Aldrich	T8154
1 kb DNA ladder	New England Biolabs	N3231
10X CutSmart Buffer	New England Biolabs	B7204S
10X T4 DNA Ligase Buffer	Thermo Fisher Scientific	B0202S
Zeozin	Thermo Fisher Scientific	R25005

2.1.10 Kits

Kit	Supplier	Catalog #
CalPhos™ Mammalian Transfection Kit	Clontech Laboratories	631312
Maxima™ SYBR Green qPCR Master Mix	Thermo Fisher Scientific	K0223
MycoAlert Detection Kit	Lonza-Biozym	LT07-418

NucleoSpin® Plasmid	Macherey Nagel GmbH & CoKG	740588.250
NucleoSpin® Gel and PCR Clean-up	Macherey Nagel GmbH & CoKG	740609.250
PureLink RNA Mini Kit	Thermo Fisher Scientific	12183025
T4 DNA Ligase Kit	Thermo Fisher Scientific	EL0011

2.1.11 Primers and Oligos

2.1.11.1 Quantitative real-time polymerase chain reaction (qRT-PCR)

Primers were ordered from Qiagen as pre-mixed QuantiTect primer assay or self-designed using Primer-BLAST and SnapGene and ordered from Eurofins MWG. All primer stocks were prepared as 1:1 mixture of forward and reverse primer at 100 µM.

Primer name	Sequence (5' → 3') or Supplier
hGapdh_fw	TGCACCACCAACTGCTTAGC
hGadpdh_rv	ACAGTCTTCTGGGTGGCAGTG
hArntl	QT00011844
hClock	QT00054481
hCry1	QT00025067
hCry2	QT00168868
hDbp	QT00055755
hNr1d1	QT00000413
hNr1d2	QT00008897
hPer1	QT00069265
hPer2_fw	CACCAAATTGTTTGTTCCAGG
hPer2_rv	AACCGAATGGGAGAATAGTCG
hPer3	QT00097713

2.1.11.2 Sequencing primers

Sequencing primers were self-designed using SnapGene and ordered from Eurofins MWG.

Primer name	Sequence (5' → 3')
2059 pLenti6_upstream ClaI	GAAGGAATAGAAGAAGAAGG
2068 pLenti6_upstream ClaII	CATTATCGTTTCAGACCCAC

2.1.11.3 Reverse transcriptase oligos

Oligo name	Supplier, Catalog #
Random hexamers	Thermo Fisher Scientific, #N8080127

2.1.12 Special equipment

Product	Supplier	Catalog #
Amicon® Ultra-15 Centrifugal Filters (3-100 kD)	Merck	UFC90
Amicon® Ultra-0.5 Centrifugal Filters (3 kD)	Merck	UFC500396
Falcon™ Cell Strainers (70 µm)	Fisher Scientific	08-771-2
Corning® BioCoat™ Collagen I-coated Flasks	Corning	354487
Cryogenic vials (2 mL/5 mL)	VWR International	66008-728/66008-732
Dow Corning high vacuum grease	Sigma-Aldrich	Z273554-1EA
Filtropur S 0.45	Sarstedt	83.1826
Hard-Shell® 96-well PCR plates	Bio-Rad Laboratories	HSP9601B
Milicell® Organotypic Inserts	Merck	PICMORG50
MultiSCREEN®HTS	Merck	MSFBN6B50
Nalgene® Vacuum Filtration System 0.2 µm	VWR	513-1221
Nunc™ Delta 35x10-mm dishes	Thermo Fisher Scientific	153066
Nunc™ Delta 100x17-mm dishes	Thermo Fisher Scientific	150350
Nunc™ F96 MicroWell™ plate, white	Thermo Fisher Scientific	136102

NuPAGE™ 4-12% Bis-Tris Midi Protein Gels	Thermo Fisher Scientific	WG1402BOX
Parafilm M	Sigma-Aldrich	P6543-1EA
96-well non-treated V-bottom Microplate	Costar/Corning	EW-01728-80
TopCount seals X100 Clearseal Diamond	Thermo Fisher	AB-0812

2.1.13 (Electronic) devices

Equipment	Description	Supplier
Agarose gel chambers		Febikon
ALPS 50™	Manual heat sealer	Thermo Fisher Scientific
CanoScan LiDE 400	Scanner	Canon
CFX96	Quantitative real-time PCR cycler	Bio-Rad Laboratories
ChemoCam Imager 3.2	Imaging station	Intas
Centrifuges (5810R, 5424R, 5415D)		Eppendorf
Consort E143	Electrophoresis power supply	Sigma-Aldrich
GFL 3032	Shaking incubator	GFL
Hera cell (150, 150i)	incubator	Thermo Fisher Scientific
Herasafe (S1)/Herasafe KS class II (S2)	Biosafety cabinet	Thermo Fisher Scientific
Infinite F200 pro	Microplate reader	Tecan
LumiCycle	Rotating luminometer	Actimetrics
LumiBoxen	Single box luminometer	Actimetrics
McIlwain Tissue Chopper TC752		Campden Instruments Ltd.
NanoDrop 2000c	Determination of DNA/ RNA/protein concentration	Thermo Fisher Scientific
Neubauer chamber	Cell counting chamber	Karl Hecht GmbH & CoKG

Orion II	Microplate luminometer	Berthold Ditection Systems
Lab pH meter into Lab® pH7110	pH meter	WTW
Liquidator™ 96	96-well multipipette	Steinbrenner
Pipettes (1-1000 µL)		Eppendorf
Pipettes, multichannel (5-300 µL)		Eppendorf
Rotating wheel		Labor-Brand
Standard power pack P25	Electrophoresis power supply	Biometra
Tabletop centrifuge		NeoLab
Temperature boxes	Temperature control units for LumiBoxen	In-house
Thriller®	Thermal shaker	VWR
TopCount	96-well plate luminometer	PerkinElmer
Unitwist RT	Rocking table shaker	UniEquip
Uno thermal cycler	PCR cycler	VWR
UV trans illuminator	UV imager	Konrad Benda
Vortex Genie 2	Vortexer	Scientific Industries Inc.
Xcell SureLock™ Mini-Cell	Electrophoresis system	Thermo Fisher Scientific

2.1.14 Databases, software and distributions

Software	Supplier/Source
anaconda3	Open source, Anaconda Inc.
CFX Manager	Bio-Rad Laboratories
ChronoStar	In-house, S. Lorenz & B. Maier
Circa DB – circadian expression profiles data base	http://circadb.hogeneschlab.org
DESeq2	Open source, Love et al. 2014
Ensemble genome browser	https://www.ensembl.org/index.html
FastQC	Open source, Babraham Bioinformatics
featureCounts (Subread)	Open source, Walter & Eliza Hall

GraphPad PRISM	GraphPad Software Inc.
GOrilla	Online software, Multi Knowledge Project http://cbl-gorilla.cs.technion.ac.il
Human Protein Atlas	https://www.proteinatlas.org
ImageJ	Open source
Jumo Imago	JUMO GmbH & CoKG
Leica Application Suite	Leica
LumyCycle, LabView	Actimetrics
Matlab	The MathWorks Inc.
Microsoft Office	Microsoft
MobaXterm	Open source, Mobatek
MultiQC	Open source, Phil Ewels
NCBI gene	https://www.ncbi.nlm.nih.gov/gene
NCBI primer blast	https://www.ncbi.nlm.nih.gov/tools/primer-blast/
PhotoNGraph	In-house
Python	Open source, Python Software Foundation
Primer-BLAST	Open source, National Center for Biotechnology Information, U.S. National Library of Medicine
QoRTs	Open source, Stephen Hartley
R/Rstudio	Open source, Rstudio Inc.
RseQC	Open source, Liguo Wang
SAMtools	Open source, Li et al. 2004 & 2009
Simplicity	Berthold Detection Systems
SnapGene	GSL Biotech LLC
STAR	Open source, Dobin et al. 2012
Subread	Open source, Walter & Eliza Hall
TopCount Observer	Perkin Elmer
UCSC tools (Kent Utils)	Open source, James Kent
Uniprot	https://www.uniprot.org

2.1.15 Company register

Company	Location
Abcam	Cambridge, UK
Actimetrics	Wilmette, USA
Addgene	Cambridge, USA
Agilent Technologies	Santa Clara, USA
Ansell	Iselin, USA
AppliChem GmbH	Darmstadt, Germany
Bayer	Leverkusen, Germany
Becton Dickison (BD)	Franklin Lakes, USA
Berthold Detection Systems	Pforzheim, Germany
BioBasic Inc.	Markham Ontario, Canada
BioCat	Heidelberg, Germany
Biometra	Göttingen, Germany
Bio-Rad Laboratories	Hercules, USA
Biozym Scientific GmbH	Hessisch Olendorf, Germany
Cayman Chemical	Ann Arbor, USA
Campden Instruments Ltd.	Loughborough, UK
Carl Roth	Karlsruhe, Germany
Cell Signaling	Leiden, Netherlands
Clontech Laboratories (Takara Nio Inc.)	Kusatu, Japan
Corning Life Sciences	Tewksbury, USA
Costar (Corning®)	Tewksbury, USA
Diversifieldbiotech	Massachusetts, USA
Eppendorf	Enfield, USA
Eurofins MWG Operon	Ebersberg, Germany
Febikon	Wermelskirchen, Germany
Fermentas GmbH	Leon, USA
Fluka	Buchs, Switzerland
GE Healthcare Dharmacon Inc.	Lafayette, USA
GFL	Burgwedel, Germany
Gibco (Thermo Fisher Scientific)	Darmstadt, Germany
Horizon Discovery	Waterbeach, UK

Illumnia	San Diego, USA
Intas	Ahmedabad, India
iNtRON Biotechnology DR	Burlington, USA
Invitrogen (Thermo Fisher Scientific)	Darmstadt, Germany
Karl Hecht GmbH & CoKG	Sondheim, Germany
Konrad Benda	Wiesloch, Germany
Labor Brand	Gießen, Germany
Life Technologies	Carlsbad, USA
Lonza-Biozym	Basel, Switzerland
Macherey Nagel GmbH & CoKG	Düren, Germany
Merck	Darmstadt, Germany
Microsynth AG Seqlab	Göttingen, Germany
Miltenyi Biotec GmbH	Teterow, Germany
NeoLab	Heidelberg, Germany
New England Biolabs (NEB)	Ipswich, USA
Olympus	Hamburg, Germany
Open Biosystems	Huntsville, USA
PAA Laboratories GmbH	Cölbe, Germany
Peqlab Biotechnologie GmbH	Erlangen, Germany
Peptrotech	Hamburg, Germany
PerkinElmer	Rodgan, Germany
Pfizer	New York, USA
Promega	Madison, USA
P.J.K	Kleinblittersdorf, Germany
Qiagen	Venlo, Netherlands
R & D Systems	Wiesbaden, Germany
Roche	Mannheim, Germany
SantaCruz Biotechnology	Dallas, USA
Sarstedt	Nümbrecht, Germany
Schleicher and Schuell	Munich, Germany
Scientific Industries, Inc.	Bohemia, USA
Sigma-Aldrich	St. Louis, USA
Serva	Heidelberg, Germany
Steinbrenner Laborsysteme	Wiesenbach, Germany

Tecan	Männedorf, Switzerland
Thermo Fischer Scientific	Darmstadt, Germany
Tocris	Bristol, UK
Trevingen	Helgerman, USA
VWR International GmbH	Darmstadt, Germany
Worthington Biochemical	Lakewood, USA
WTW (Xylem Analytics)	Weilheim, Germany

2.2 Methods

2.2.1 Animal based procedures

2.2.1.1 Primary mouse hepatocyte isolation

Isolation of primary hepatocytes was performed in collaboration with the Schupp laboratory at the Charité Berlin (Institute of Pharmacology) and as described in [343]. In brief livers of anesthetized (80mg/kg Ketamin, 12mg/kg Xylazin) male C57BL/6J mice were perfused with perfusion buffer, followed by digestion buffer containing 5000 units collagenase type I. After filtration and separation by Percoll gradients, cells were seeded in collagen-coated T-175 cm^2 flasks in 25 mL complete culture medium. Cells were cultured under standard tissue culture conditions.

2.2.1.2 Organotypic slice cultures of peripheral tissue explants

$Per2^{tm1Jt}$/J (also called $mPer2^{Luciferase}$ or PER2::LUC) male or female mice were anesthetized by isoflurane and euthanized by cervical dislocation. Organs were explanted and placed in cold 1X PBS. Heart, lung, and kidney were explanted as intact organs, muscle samples were excised from hind limbs of the animals. Organs were cut into 2-3 mm flat pieces with forceps and scissors, as well as further chopped into slices of 300-500 µm thickness using a McIlwain tissue chopper. Slices were cultured directly in 35-mm dishes with 2 mL/dish complete culture medium and under standard tissue culture conditions.

2.2.1.3 Liver organoid generation and maintenance

Isolation of adult liver duct stem cells, as well as generation and maintenance of liver organoids was performed as described in [344]. In brief livers of euthanized B6.129S6-Per2^{tm1Jt}/J (mPer2^{Luciferase}) male or female mice were explanted, and liver ducts isolated by collagenase digest as follows: tissue was minced, rinsed with mouse liver wash medium and incubated with mouse liver digestion solution for 45 mins up to 4 hours at 37°C (until ductal structures appeared). Digestion was stopped by addition of cold mouse liver wash medium, suspension was filtered through a 70 µm Nylon cell strainer and spun 5 mins at 200xG, 8°C. The pellet was washed twice in cold mouse liver wash medium and re-suspended in basement matrix for seeding in pre-warmed 24-well plates. Basement matrix was solidified at 37°C for 1 hour and droplet was overlaid with pre-warmed 500 µL/well mouse liver isolation medium. After 3-4 days mouse liver isolation medium was replaced by mouse liver expansion medium (without Wnt-3A conditioned medium and rh Noggin) and cells were cultured under standard tissue culture conditions until organoids became visible. Liver organoids were grown for 10-15 days following isolation. Basement matrix was removed, and organoids dissociated in single cells by centrifugation (5 mins, 150xG, 8°C) and washing in mouse liver basal medium. Subsequently, the pellet was re-suspended in basement matrix for seeding in pre-warmed 24-well plates, matrix was solidified at 37°C for 1hour and droplet was overlaid with 500µL/well mouse liver expansion medium. Organoids were maintained by this procedure and splitting ratios of 1:6-1:8 once or twice a week.

2.2.1.4 Liver organoid differentiation

Differentiation of mouse liver organoids into mouse liver hepanoids was performed as described in [344]. In brief organoids were expanded as described above, cells seeded in basement matrix into 35-mm dishes and cultured in 1.5 mL/dish mouse liver expansion medium for 3-5 days (until organoids became visible). To initiate differentiation mouse liver expansion medium was replaced by 1 mL/dish mouse liver differentiation medium and exchanged daily with fresh medium for up to 9 days. From day 13-15 following initiation, 1 mL/dish fresh mouse liver differentiation medium supplemented with 3 µM dexamethasone was added daily.

2.2.2 Cell culture procedures

2.2.2.1 Freezing and thawing of mammalian cells

Cells were grown to 90% confluence and detached by incubation with trypsin/EDTA for 10mins at 37°C. Enzymatic reaction was stopped by addition of complete culture medium and cells were mixed thoroughly by pipetting. The cell suspension was pelleted by centrifugation for (6 mins, 300xG, 8°C). Pellets were re-suspended in freezing medium to reach a concentration of 1-2 $x10^6$ cells/mL. The cell suspension was aliquoted in 2 mL cryogenic vials (1mL per vial) and slowly cooled down to -80°C in an isopropanol bath before transferal to liquid nitrogen tanks. Thawing was performed by rapid thawing of cryogenic vials in a 37°C water bath. Cell suspensions were seeded in an appropriate culture format in complete culture medium and incubate under standard tissue culture conditions (37°C, 5% CO_2, humid atmosphere) overnight. The next day, cells were supplemented with fresh complete culture medium and cultivated further as described below.

2.2.2.2 Cultivation and passaging of mammalian cells

Mammalian cells were maintained in culture for 2-3 months before new aliquots were thawed. Established cultures were maintained in complete culture medium under standard tissue culture conditions. Commonly, cells were passaged 2-3 times a week at 80-90% confluence. For passaging cells were washed once with 1X PBS and detached by incubation with trypsin/EDTA for 10mins at 37°C. Enzymatic reaction was stopped by addition of complete culture medium and cells were mixed thoroughly by pipetting. Subcultivation was performed according to ratios indicated above. Upon 1-2 days in culture, as well as before disposal 1mL supernatant was harvested and cultures tested for mycoplasma contamination using the luciferase-based MycoAlert detection kit according to the manufacturer's instructions.

2.2.2.3 Cell counting and seeding

To determine the concentration of cell suspensions, 10 µL of the suspension were mixed with 10µL trypan blue. Subsequently, 10µL of the 1:1 mixture were applied to a

Neubauer counting chamber and cells were counted in all four big squares. The concentration was determined by the following equation (Equation 2):

$$x = \frac{n}{2} * 10.000 \quad (2)$$

x = concentration [cells/mL]
n = cell count in 4 big squares

To seed desired numbers of cells in a volume of choice (e.g. Table 2-1), the concentration of the suspension was adjusted either by centrifugation (6mins, 300xG, 8°C) and re-suspension or by direct dilution. Following seeding, complete culture medium was added to the cells to reach required culture volumes (Table 2-1) and cells were incubated under standard tissue culture conditions until desired confluence was reached (usually 1-2 days).

Table 2-1: Cell culture numbers

Format	Desired density (confluence)	Cells at seeding	Seeding volume	Total culture volume
96-well	dense (90%)	2.0 x10^4	50 µL	100-150 µL
6-well	dense (90%)	3.0 x10^5	1 mL	2 mL
6-well	sparse (20%)	0.2-0.3 x10^5	1 mL	2 mL
35-mm dish	dense (90%)	3.0 x10^5	1 mL	2 mL
35-mm dish	sparse (20%)	0.2-0.4 x10^5	1 mL	2 mL
T-75 flask	dense (90%)	2.5-3.0 x10^6	5 mL	10-12 mL
T-175 flask	dense (90%)	5.0-6.0 x10^6	5 mL	20-25 mL

2.2.2.4 Synchronization

1 mM dexamethasone stock was prepared in ethanol and store at -20°C. If not stated otherwise, *Bmal1*:Luc and *Per2*:Luc reporter cells, spheroids, as well as PER2::LUC tissue explants or hepanoids were synchronized with 1 µM dexamethasone (final concentration). Cells were incubated 20-40 minutes under standard tissue culture conditions. Following incubation, cells and explants were twice with cold 1X PBS and

once with serum-free culture medium. Spheroids and hepanoids were washed once with pre-warmed 1X PBS and once with serum-free medium to not disrupt their basement matrix.

2.2.3 Bacterial cell based procedures

2.2.3.1 Transformation and expansion of bacterial cells

Competent bacterial cells were transformed with 10-50 ng plasmid DNA by heat-shock procedure as follows. Bacterial cells were thawed on ice and split into 50 µL aliquots. Pre-cooled plasmid DNA was gently mixed with the competent cells by pipetting and the transformation reaction was incubated for 30 mins on ice. Following the incubation, cells were heat-shocked at 42°C for 30-60 seconds and incubated for 5-10 mins on ice. 500-800 µL of pre-warmed (37°C) antibiotic-free LB medium was added to the transformation reaction and cells were incubate for 1-2 hours at 37°C in a thermal shaker (300-500 rpm). The transformation reaction was shortly spun down to pellet cells and 80% of the supernatant was removed. The pellet was re-suspended in the remaining supernatant and the suspension used to streak LB agar plates containing the appropriate selection antibiotic. Plates were incubated at 37°C overnight to grow bacterial colonies. To amplify and verify plasmid DNA, single colonies of transformed cells were picked (with sterile toothpicks) from LB agar plates and used to inoculate 5 mL LB medium containing the appropriate selection antibiotic. If cryogenic stocks of bacterial colonies harboring the verified plasmid DNA of interest were already available (see below), stocks were used directly to inoculate 5 mL LB medium containing the appropriate selection antibiotic. Bacterial cell cultures were grown at 37°C and 250rpm overnight.

2.2.3.2 Plasmid DNA preparation from bacterial cells

To isolate plasmid DNA from bacterial cells, cultures grown from single colonies or cryogenic stocks were spun down (10 mins, 3000xG, 4°C). Supernatant was discarded and DNA was prepared using the NucleoSpin® Plasmid DNA extraction kit according to the manufacturer's instructions. Plasmid DNA was eluted in 30-50 µL TE buffer,

concentration measured using the NanoDrop 2000c, and DNA was stored at -20°C. Verification of plasmid DNA was performed by restriction enzyme digest and sequencing and bacterial colonies harboring the confirmed plasmid DNA were prepared for storage as described below.

2.2.3.3 Storage of bacterial colonies

Single colonies of bacterial cells grown on LB agar plates containing the appropriate selection antibiotic were stored at 4°C for 4-8 weeks. For long-term storage of plasmid DNA, colonies of transformed bacterial cells were picked from LB agar plates and used to inoculate to 5 mL LB medium supplemented with the appropriate selection antibiotic. Cells were grown at 37°C and 250rpm overnight and 4.4 mL of the bacterial culture used to isolate and verify plasmid DNA as described above. If integrity and sequence of the plasmid DNA were confirmed, the remaining 600 µL of the bacterial culture were mixed with 600 µL glycerol in cryogenic vials and transferred to -80°C.

2.2.4 Imaging methods

2.2.4.1 Imaging of organotypic slice cultures, hepanoids, and spheroids

Explanted murine tissue slices and mouse liver hepanoids, expressing a PER2::LUC fusion protein, or spheroids grown from U-2 OS droplet cultures were synchronized as described. After washing, 35-mm dishes containing tissue slices and liver hepanoids were supplemented with 2 mL/dish reporter medium and sealed with grease and parafilm to avoid evaporation of the medium during recording. Dishes were transferred to LumiCycle or LumiBoxen and luciferase activity was continuously monitored (5-7 days) at 37°C and 5% CO_2.

2.2.4.2 Imaging of mammalian reporter cells

Unless stated otherwise, mammalian cells harboring a *Bmal1*:Luc or *Per2*:Luc circadian reporter were synchronized as described. Mammalian cells harboring a non-circadian reporter gene (7xCRE:Luc, 7xmutatedCRE:Luc, 7xSRE:Luc) were not

synchronized with dexamethasone but only washed twice with 1X PBS and once with serum-free culture medium. Cells were supplemented with reporter medium as follows: 100-150 µL/well for 96-well plates, 2 mL/dish for 35-mm dishes. 96-well plates were sealed with X100 Clearseal Diamond seals using the ALPS 50^{TM} heat sealer, 35-mm dishes were sealed with grease and parafilm. 96-well plates were imaged in the TopCount or Orion II at 37°C, 35-mm dishes were imaged in the LumiCycle or LumiBoxen at 37°C and 5% CO_2. Luciferase activity was continuously monitored (5-7 days).

2.2.5 Genetic and pharmacological perturbation of mammalian cells

2.2.5.1 Lentivirus production in HEK293T cells

Lentivirus production was performed according to the lab's standard operating procedures (Figure 6-8). In brief HEK293T cells were transfected with lentiviral packaging plasmids and lentiviral expression plasmid in a T-75 cm^2 format using the CalPhos^{TM} Mammalian Transfection Kit. Subsequently, lentivirus was harvested and prepared for transduction of target cells or storage at -80°C.

2.2.5.2 Lentivirus transduction and selection of mammalian cells

Mammalian cells were seeded to reach 30-50% confluence and lentivirus + 8µg/mL protamine sulfate was added directly to the ell suspension. Transduced cells were incubated overnight under standard tissue culture conditions. The next day lentivirus containing supernatant was replaced by complete culture medium. If lentiviral expression plasmids contained an antibiotic resistance element, transduced cells were selected for efficient plasmid integration by application of the appropriate antibiotic. Puromycin was used at a concentration of 10 µg/mL for 2-3 consecutive days, blasticidine at a concentration of 10 µg/mL for 7-8 consecutive days. If necessary cells were passaged as described.

2.2.5.3 RNAi screen

Lentiviral pGIPZ expression plasmids were prepared from an in-house short hairpin (sh) RNA glycerol library as follows: pGIPZ_shRNA containing E. coli were grown in overnight bacterial cultures with ampicillin (100 µg/mL) and zeozin (25 µg/mL). Plasmid DNA was purified from bacterial cells as described above. A prediluted 96-well sublibrary was prepared by dilution of pGIPZ_shRNA plasmid DNA to 0.14 µg/µL in ddH_2O. Plasmid DNA was stored at -20°C.

RNAi screens were performed according to the lab's standard operating procedures (Figure 6-9). In brief HEK293T cells were transfected with lentiviral packaging plasmids and lentiviral expression plasmid in a 96-well format using Lipofectamin2000©. Subsequently, lentivirus was harvested and prepared for transduction of target cells. For each experiment three 96-well plates of lentivirus producing HEK293T cells were prepared in parallel. One was used for the transduction of U-2 OS *Bmal1*:Luc reporter cells for the recording of bioluminescence oscillations following gene knock-down. Two were used for transduction of U-2 OS 7xCRE:Luc reporter cells for conditioned and control medium stimulation following gene knock-down.

2.2.5.4 Pharmacological perturbation of TGF-β signaling

LY2109761, a pharmacological inhibitor of TGF-β receptor was solved in 100% DMSO to generate a 1 mM stock solution that was stored at -20°C.

Dilution series

1000 to 0 µM pre-dilutions of the 1 mM stock were prepared in 100% DMSO by serial dilution and stored at -20°C. U-2 OS cells harboring a *Per2*:Luc or 7xCRE:Luc reporter gene were prepared for bioluminescence imaging in 96-well plates as described. Following the first cycle of bioluminescence oscillations, pre-dilutions were added 1:100 to supernatants of *Per2*:Luc reporter cells (1.5 µL in 150 µL). In the case of 7xCRE:Luc reporter cells, pre-dilutions were added 1:100 to 100X conditioned and control medium containing 250 µM D-luciferin. Following 24-72 hours of bioluminescence recording, reporter medium was aspirated from 7xCRE:Luc reporter cells and 30 µL/well 100X conditioned and control medium containing inhibitor pre-

dilutions and D-luciferin added to the cells. Cells were transferred back to the imaging device and luciferase activity continuously monitored.

Co-culture and temperature pulse experiments

1 mM LY210971 stock or 100% DMSO were added 1:200 to complete culture medium during seeding of U-2 OS *Bmal1*:Luc reporter cells or PER2::LUC tissue slices (5 µM and 0.5% final concentration, respectively). Cells and tissues slices were incubated in complete culture medium containing inhibitor or solvent overnight under standard tissue culture conditions. The next day cells and tissue slices were prepared for bioluminescence imaging in reporter medium containing 1:200 LY210971 or DMSO (5 µM and 0.5% final concentration, respectively). Luciferase activity was continuously monitored.

Phase shift experiments

1 mM LY210971 stock or 100% DMSO were added 1:200 to complete culture medium during seeding of U-2 OS *Bmal1*:Luc reporter cells (5 µM and 0.5% final concentration, respectively). Cells were incubated in complete culture medium containing inhibitor or solvent overnight under standard tissue culture conditions. The next day cells were prepared for bioluminescence imaging in reporter medium containing 1:200 LY210971 or DMSO (5 µM and 0.5% final concentration, respectively). Approximately 36 hours following synchronization (at the inferred trough of *PER2* expression) supernatants were aspirated and 50 µL/well (96-well format) conditioned or control medium containing 1:200 LY210971 or DMSO (5 µM and 0.5% final concentration, respectively) and 250 µM D-Luciferin added to cells. Cells were transferred back to the imaging device and luciferase activity was continuously monitored.

2.2.6 Stimulations

2.2.6.1 Conditioned and control medium stimulation (RT-qPCR and RNA sequencing)

U-2 OS cells were seeded in 6-well plates at 3.0 x10^5 cells/well (dense cultures) or at 0.3 x10^5 cells/well (sparse cultures). Plates were supplemented with 2 mL/well complete culture medium and incubated under standard tissue culture conditions

overnight. The next day cells were synchronized, supplemented with 2 mL/well serum-free culture medium and incubated for 16 hours under standard tissue culture conditions. Following incubation, supernatants were aspirated, and cells stimulated with 500 µL/well 60X conditioned or control medium for indicated incubation times (RT-qPCR) or 2 hours (RNA sequencing) under standard tissue culture conditions. Total RNA was isolated as described.

2.2.6.2 Conditioned and control medium stimulation (bioluminescence imaging)

Phase response curve

U-2 OS *Per2*:Luc reporter cells were prepared for bioluminescence imaging in 96-well plates as described. At the indicated times following synchronization supernatants were aspirated and 40 µL/well 60X conditioned or control medium containing 250 µM D-luciferin added to cells (excepted for unstimulated controls). Cells were transferred back to the imaging device and luciferase activity was continuously monitored.

Phase shifts

U-2 OS circadian reporter cells or PER2::LUC tissue slices were prepared for bioluminescence imaging as described above. At the inferred trough of *PER2/Per2* expression (usually 24-48 hours + 16 hours post-synchronization) supernatants were aspirated and 60-100X conditioned or control medium containing 250 µM D-luciferin added to cells or tissue slices as follows: 40 µL/well in 96-well format, 1 mL/dish in 35-mm format. Cells and slices were transferred back to the imaging device and luciferase activity was continuously monitored.

Enhancer element inductions (including stimulation with serum and forskolin)

U-2 OS 7xCRE:Luc, 7xmutCRE:Luc, or 7xSRE:Luc reporter cells were not synchronized but prepared for bioluminescence imaging in 96-well plates as described above. 24-72 hours following the start of recording, supernatants were aspirated and 20 µL/well 60-100X conditioned or control medium containing 250 µM D-luciferin or 20 µL/well reporter medium containing either 10% FBS, 10 µM forskolin or solvent control added to cells. Cells were transferred back to the imaging device and luciferase activity was continuously monitored.

2.2.6.3 Stimulation with chromatography fractions (bioluminescence imaging)

U-2 OS 7xCRE:Luc reporter cells were not synchronized but prepared for bioluminescence imaging in 96-well plates as described above. 24-72 hours following the start of recording, chromatography fractions were added 1:5 to supernatants of reporter cells (25 µL in 100 µL). Fractions from gel filtration chromatography were used directly for stimulations. Fractions from anion exchange chromatography were desalted prior to stimulation, using Amicon® Ultra-0.5 Centrifugal Filters (3 kD MWCO) according to the manufacturer's instructions. Cells were transferred back to the imaging device and luciferase activity was continuously monitored.

2.2.6.4 Stimulation with recombinant TGF-β

Lyophilized recombinant human TGF-β1, TGF-β2, and TGF-β3 were solved according to the manufacturer's instructions to generate 50 ng/mL (TGF-β1/3) or 200 ng/mL (TGF-β2) stock solutions.

Dose dependency (bioluminescence imaging)
50 to 0 ng/mL (TGF-β1/3) or 200 to 0 ng/mL (TGF-β2) pre-dilutions of the stock solutions were prepared in the respective solvents by serial dilution and stored at -20°C. U-2 OS 7xCRE:Luc reporter cells were not synchronized but prepared for bioluminescence imaging in 96-well plates as described. 24-72 hours following the start of recording pre-dilutions were added 1:10 to supernatants of reporter cells (10 µL in 100 µL). Cells were transferred back to the imaging device and luciferase activity was continuously monitored.

Clock gene expression (RT-qPCR)
U-2 OS cells were seeded into 6-well plates. Plates were supplemented with 2 mL/well complete culture medium and incubated under standard tissue culture conditions overnight. The next day cells were synchronized, supplemented with 2 mL/well serum-free culture medium and incubated for 16 hours under standard tissue culture conditions. Following incubation, supernatants were aspirated, and cells stimulated with a 2 hour pulse of 500 µL/well serum-free culture medium containing 1:10 TGF-β2

stock solution (20 ng/mL final concentration) or respective solvent control. Total RNA was isolated as described.

2.2.7 Special cell culture assays

2.2.7.1 Density dependence experiment

Bioluminescence imaging

U-2 OS cells harboring a *Per2*:Luc or *Bmal1*:Luc reporter gene were harvested as described. For each seeding density, concentration of the cell suspension was adjusted to allow for seeding of the indicated cell number in equal seeding volumes, i.e. 1 mL/35-mm dish or 1 mL/membrane insert. Membrane inserts were placed in empty 35-mm dishes. All dishes were supplemented with 2 mL/dish complete culture medium and incubated under standard tissue culture conditions overnight. Following incubation cells were prepared for bioluminescence imaging and luciferase activity was continuously monitored.

RT-qPCR, RNA sequencing

U-2 OS cells were seeded at dense (3.0 x10^5 cells/well) or sparse (0.3 x10^5 cells/well) culture density into 6-well dishes. Wells were supplemented with 2 mL/well complete culture medium and cells were incubated under standard tissue culture conditions overnight. Following incubation, cells were synchronized and supplemented with 2 mL/well serum-free culture medium. Cells were incubated for 18 hours under standard tissue culture conditions. Following incubation, RNA was isolated and RT-qPCR or RNA sequencing performed as described.

2.2.7.2 Phase-pulling experiments

U-2 OS cells harboring a *Per2*:Luc reporter gene and U-2 OS non-reporter cells were passaged into two T-75 cm^2 flasks each. Upon confluence cells were separated into “early” and “late” cells (one flask per cell line and timepoint), which were prepared for co-culture experiments 6 hours apart. At both timepoints, U-2 OS reporter and non-reporter cells were harvested and counted as described. Synchronization was

performed in solution by adding 1 µM Dexamethasone and incubating in a 37°C water bath for 30 minutes. For each co-culture ratio, concentrations of the cell suspensions were adjusted in serum-free culture medium to allow for seeding of the indicated cell numbers in equal seeding volumes, i.e. 100 µL/35-mm dish as indicated below (Table 2-2). "Early" cells were supplemented with 2 mL/dish reporter medium and incubated for 6 hours under standard tissue culture conditions. "Late" cells were prepared 6 hours later by the same procedure and were carefully added to 35-mm dishes containing the "early" cells, i.e. 100 µL/dish and as indicated below (Table 2-2). This way low-density U-2 OS *Per2*:Luc reporter cell were co-seeded with increasing numbers of 6 hour phase advanced or phase delayed non-reporter cells, while keeping the absolute culture density constant (total of 3.3 x10^5 cells/dish at seeding). 35-mm dishes were transferred to the LumiCycle and luciferase activity was continuously monitored.

Table 2-2: Seeding numbers of phase-pulling experiments

Early *Per2*:Luc	Early non-reporter	Late non-reporter*	Late *Per2*:Luc	Late non-reporter	Early non-reporter**
0.3 x10^5	0.0 x10^5	3.0 x10^5	0.3 x10^5	0.0 x10^5	3.0 x10^5
0.3 x10^5	0.5 x10^5	2.5 x10^5	0.3 x10^5	0.5 x10^5	2.5 x10^5
0.3 x10^5	1.0 x10^5	2.0 x10^5	0.3 x10^5	1.0 x10^5	2.0 x10^5
0.3 x10^5	1.5 x10^5	1.5 x10^5	0.3 x10^5	1.5 x10^5	1.5 x10^5
0.3 x10^5	2.0 x10^5	1.0 x10^5	0.3 x10^5	2.0 x10^5	1.0 x10^5
0.3 x10^5	2.5 x10^5	0.5 x10^5	0.3 x10^5	2.5 x10^5	0.5 x10^5
0.3 x10^5	3.0 x10^5	0.0 x10^5	0.3 x10^5	3.0 x10^5	0.0 x10^5

*6 hour phase delayed non-reporter cells relative to co-cultured early U-2 OS *Per2*:Luc reporter and non-reporter cells

**6 hour phase advanced non-reporter cells relative to co-cultured late U-2 OS *Per2*:Luc reporter and non-reporter cells

2.2.7.3 Period-pulling experiments

U-2 OS wildtype, *CRY2*$^{-/-}$, and *TNPO1*$^{-/-}$ knock-out cells harboring a circadian *Bmal1*:Luc reporter gene, as well as U-2 OS wildtype non-reporter cells were harvested as described. Concentrations of the cell suspensions were adjusted in complete culture medium to 3.0 x10^6 cells/mL. Mixed suspensions were prepared by mixing *Bmal1*:Luc reporter (either wildtype, *CRY2*$^{-/-}$ or *TNPO1*$^{-/-}$ knock-out) and non-reporter (wildtype) cells in a 1:5 ratio. Subsequently, 20-30 10 µL droplets (3.0 x10^3

cells/droplet) of pure reporter or mixed reporter:non-reporter cell suspensions were seeded on inverted lids of sterile 100-mm petri dishes. Dishes were supplemented with 10 mL/dish 1X PBS to prevent evaporation of droplets and lids were placed on the dish. Hanging drops were incubated under standard tissue culture conditions for 5-7 days. This way spheroids were generated by gravity dependent cell aggregate formation and 3-dimensional outgrowth. Spheroids were harvested by pipetting and transferred to a 15 mL sterile tube. Remaining supernatant was aspirated and spheroids were re-suspended in 50-100 µL Matrigel for seeding in pre-warmed 35-mm dishes. Basement matrix was solidified at 37°C for 1 hour and spheroids were supplemented 2mL/dish complete culture medium. Spheroids were incubated under standard tissue culture conditions overnight. Following incubation spheroids were synchronized and prepared for bioluminescence imaging as described. Luciferase activity was continuously monitored.

2.2.7.4 Amplitude and damping rescue experiments

U-2 OS cells harboring a *Bmal1*:Luc reporter gene and U-2 OS non-reporter cells were harvested as described. Sparse reporter cells (0.25 x10^5 cells/dish or insert) were seeded into 35-mm dishes or on 4.2 cm^2 membrane inserts. Membrane inserts were placed into empty 35-mm dishes. For each seeding density of non-reporter cells, concentration of the cell suspensions was adjusted to allow for seeding of the indicated cell number in equal seeding volumes, i.e.1 mL/35-mm dish. For direct co-cultures non-reporter cells were directly added to dishes containing reporter cells. For membrane separated co-cultures non-reporter cells were seeded into separate 35-mm dishes. Subsequently, all dishes were supplemented with 2 mL/dish complete culture medium and incubated under standard tissue culture conditions overnight. Following incubation cells were synchronized and prepared for bioluminescence imaging as described. Membrane inserts with reporter cells were transferred to dishes containing non-reporter cells. Ultimately, luciferase activity was continuously monitored.

2.2.7.5 Temperature pulse experiments

U-2 OS cells harboring a *Bmal1*:Luc reporter gene were seeded at dense (3.0x10^5 cells/dish) or sparse culture density (0.4 x10^5 cells/dish) into 35-mm dishes. Cells were

supplemented with 2 mL/dish complete culture medium containing 1:200 LY2109761 or DMSO (5 µM and 0.5% final concentration respectively) and incubated under standard tissue culture conditions overnight. Following incubation, cells were synchronized and supplemented with 2.5 mL/dish reporter medium containing 1:200 LY2109761 or DMSO (5 µM and 0.5% final concentration respectively). Temperature pulse experiments were performed in the LumiBoxen using Jumo Imago software (Table 2-3) in order to apply an 8 hour, 20°C temperature pulse at the inferred trough of *PER2* expression (anti-phasic to *Bmal1*:Luc expression).

Table 2-3: Temperature pulse protocol (Jumo Imago)

Density	Reagent	Pulse	No pulse control
Dense	DMSO	64 hours 37°C // 8 hours 20°C // hold 37°C	hold 37°C
Dense	LY2109761	70 hours 37°C // 8 hours 20°C // hold 37°C	hold 37°C
Sparse	DMSO	67 hours 37°C // 8 hours 20°C // hold 37°C	hold 37°C
Sparse	LY2109761	73 hours 37°C // 8 hours 20°C // hold 37°C	hold 37°C

2.2.8 RNA and DNA based procedures

2.2.8.1 Isolation of total RNA

6-wells plates were rinsed quickly with cold 1X PBS and 300 µL/well lysis buffer (supplied in PureLink RNA Mini Kit) + 1% β-mercaptoethanol was added to cells. Cells were either frozen at -80°C or kept on ice and processed directly. RNA isolation was performed using the PureLink RNA Mini Kit according to the manufacturer's instructions. An additional on-column DNase I treatment (15 minutes incubation) was performed as part of the first column wash. Purified RNA was eluted in 30-50 µL RNase-free water. Concentration and purity were determined using the NanoDrop 2000c. Eluted RNA was transferred to -20°C for short-term and to -80°C for long-term storage.

2.2.8.2 RNA and DNA concentration

Concentration and purity of DNA and RNA samples was determined using the NanoDrop 2000c according to the manufacturer's instructions.

2.2.8.3 Reverse transcription of whole cell RNA

0.5-2 µg RNA was prepared in 20 µL RNase-free water, mixed with 14.25 µL mastermix 1 (Table 2-4) and incubated for 5 minutes at 65°C to break secondary structures. Following incubation, samples were chilled on ice and 15.75 µL/sample mastermix 2 (Table 2-4) was added. cDNA synthesis was performed using the following PCR protocol: 10 minutes 25°C // 50 minutes 37°C // 15 minutes 70°C // hold at 10°C. cDNA was stored at 4°C overnight or at -20°C for long-term storage.

Table 2-4: Mastermix preparation for reverse transcription

Reagent	Mastermix 1 (µL/sample)	Mastermix 2 (µL/sample)
10 mM dNTP mix	1	-
20 µM random hexamers	5	-
ddH_2O	8.25	-
total:	14.25	-
40 U/µL RNase inhibitor	-	0.5
5X First strand buffer	-	10
0.1 M DTT	-	5
200 U/µL M-MLV reverse transcriptase	-	0.25
total:	-	15.75

2.2.8.4 Quantitative real-time polymerase chain reaction (qRT-PCR)

cDNA was diluted 1:10 in RNase-free water and stored at 4°C overnight or -20°C for long-term storage. For qRT-PCR 4 µL diluted cDNA was mixed with 5 µL SYBR Green and 1 µL primer mix per sample. Primers were either ordered as pre-mix from Qiagen

and used directly or self-designed as separate forward and reverse primers. Self-made primer mixes were prepared as follows: 30 µL 100 µM forward primer + 30 µL 100 µM reverse primer + 940 µL TE-Buffer. qRT-PCR was performed using the following protocol: 2 minutes 50°C // 10 minutes 95°C // 40x 15 seconds 95°C, 1 minute 60°C, plate read // end.

2.2.8.5 RNA sequencing

RNA sequencing was performed by the Genomics Core Facility of the Berlin Institute of Health (BIH). In brief, integrity of total RNA samples was assessed using the Agilent Bioanalyzer. NEBNext® Poly(A) mRNA Magnetic Isolation Module was used to enrich poly(A)+ mRNA, which was fragmented to app. 200 nt fragments (94°C, 15 minutes). NEBNext® Ultra™ RNA Library Prep Kit for Illumina® was used for cDNA synthesis and sequencing library preparation. Single read RNA sequencing was performed using the Illumnia NextSeq® 500/550 High Output Kit v2 (75 cycles).

2.2.9 Cloning of pLenti6_7xmutCRE:Luc

Cloning was performed in order to generate a lentiviral expression plasmid containing seven CRE elements of mutated sequence (TTAAACCA) upstream of a minimal promoter and in frame with the luciferase sequence. Therefore, the 7xmutCRE plus minimal promoter and 3' flanking sequence was designed analogous to the sequence contained in the pLenti6_7xCRE:Luc plasmid (except for the mutated CRE sites). A pUC57 cloning vector containing this sequence was acquired by gene synthesis (Bio Basic Inc.). The lyophilized pUC57_7xmutCRE gene synthesis product was eluted in 40 µL TE buffer and the concentration was determined using the NanoDrop 2000c.
The plasmid stock was either stored at -20°C or diluted 1:10 in TE buffer for bacterial transformation. pUC57_7xmutCRE DNA was prepared by transformation in competent bacterial cells as described. pLenti6_7xCRE:Luc plasmid DNA was prepared from a bacterial glycerol stock. Linearized 7xmutCRE insert (from the pUC57_7xmutCRE plasmid) and pLenti6_luciferase backbone (from the pLenti6_7xCRE:Luc plasmid) fragments were generated by restriction enzyme digest and subsequent preparative gel electrophoresis as described below. Cloning of the 7xmutCRE insert into the pLenti6_luciferase backbone was achieved by DNA ligation and as described below.

Resulting pLenti6_7xmutCRE:Luc ligation products were transformed into competent cells and plasmid DNA was prepared from bacterial cells as described. Successful integration of the 7xmutCRE insert into the pLenti6_luciferase backbone was verified by restriction enzyme digest of the pLenti6_7xmutCRE:Luc ligation product and analytical gel electrophoresis. Additionally, Sanger sequencing was performed to check the 7xmutCRE insert sequence for the presence of mutations or deletions.

2.2.9.1 Restriction enzyme digest

Purified plasmid DNA was linearized by restriction enzyme digest with ApaI and NheI-HF as follows (Table 2-4):

Table 2-5: Restriction enzyme digest using ApaI and NheI-HF

Digestion mix reagents	PCR program
4 µg plasmid DNA (pUC57_7xmutCRE, pLenti6_7xCRE:Luc, or pLenti6_7xmutCRE:Luc) 5µL 10X CutSmart Buffer 50 U ApaI 20 U NheI-HF Up to 50 µL ddH_2O	60 minutes, 25°C 60 minutes 37°C 20 minutes 70°C hold at 10°C

2.2.9.2 Agarose gel electrophoresis

0.8-1% agarose solutions were prepared by solving agarose (BD) in 1X TAE buffer (% w/v) while boiling. 3 µL/100 mL of RedSafe™ nucleic acid staining solution were added to agarose solution. Agarose gels were prepared by polymerization of the agarose solution in a gel cast at RT for 30-60 minutes. Restriction enzyme digested plasmid DNA was diluted 1:6 in 6X Orange loading dye, loaded into gel pockets, and separated by size using agarose gel electrophoresis. Electrophoresis was run at 120 V for 45-90 minutes depending on the size of the target DNA fragments. A 1 kb DNA ladder was used as molecular size standard. The separated DNA was visualized by UV exposure using the ChemoCam Imager 3.2 (for analytical electrophoresis) or the UV trans illuminator (for preparative electrophoresis). For preparative electrophoresis target DNA fragments were isolated from the agarose gel as described below. For analytical

electrophoresis the resulting band pattern was compared to that of an in silico control digest (performed in SnapGene).

2.2.9.3 DNA purification from preparative agarose gels

Target DNA fragments were cut from the agarose gel with a scalpel and transferred to a 1.5 mL sterile tube. DNA purification was performed using the NucleoSpin® Gel and PCR Clean-up kit according to the manufacturer's instructions. The DNA was eluted in 20 µL 1X TE buffer and concentration measured using the NanoDrop 2000c.

2.2.9.4 DNA ligation

DNA ligation mix was prepared at a 1:5 molar ratio of backbone:insert as follows: insert DNA + plasmid DNA + 1 µL 10X ligation buffer + 1 µL 10X ATP + 1 µL (5 U) T4 DNA ligase (all supplied in the T4 DNA Ligase Kit). The ligation mix was incubated for 45 minutes at RT and transformed into, as well as prepared from competent cells as described.

2.2.9.5 DNA sequencing for clone verification

Plasmid DNA of bacterial clones verified by analytical gel electrophoresis was analyzed by sanger sequencing using the sequencing primers 2059 pLenti6_upstream ClaI and 2068 pLenti6_upstream ClaII. Sequencing reactions were prepared as follows: 12 µL 80 µg/µL purified plasmid DNA + 3 µL 10 pmol/µL sequencing primer. Sequencing was performed by Microsynth AG Seqlab. Overlap of the resulting sequence with an in silico cloned pLenti6_7xmutCRE:Luc plasmid was controlled using SnapGene.

2.2.10 Protein based methods

2.2.10.1 Conditioned and control medium preparation and storage

Mammalian cells lines were cultured in T-175 cm^2 flasks until 80-90% confluence was reached. Confluent cultures were washed twice with 1X PBS and once with serum-free culture medium. Cells were supplemented with 15mL/flask serum-free culture medium and incubated under standard tissue culture conditions for 12-24 hours. Following incubation, supernatant was harvested and cells passaged as described. Supernatants were spun (10mins, 3000xG, 4°C) to remove cell debris and filtered through 0.2 µm sterile Nalgene® vacuum filters. Subsequently, supernatants were concentrated 60-100-fold using Amicon® Ultra-15 centrifugal filters with 10 kD MWCO. Control medium was produced by the same procedure but using empty T-175 cm^2 culture flasks. Concentrated conditioned and control medium from different preparations was pooled in 15mL sterile tubes and stored at -80°C.

2.2.10.2 Chromatography

Gel filtration and anion exchange chromatographies of conditioned medium samples were performed by our collaboration partners at the Protein Purification and Analysis Unit of the Max Planck Institute for Infectious Biology (Berlin, GER). In brief, gel filtration chromatography of crude 1000X conditioned medium (500 µL input) was done using Superdex HR-200GL columns (GE Healthcare) with a fractionation rate of 500 µL/fraction. Elution was performed with 1X PBS. Anion exchange chromatographies of gel filtration chromatography pools (2.5 mL input each) was done using Poros HQ-20 columns (PerSeptive Biosystems) with a fractionation rate of 1 mL/fraction. Elution was performed in 20 mM Tris (pH 8.0) and 1 M NaCl gradient.

2.2.10.3 Determination of protein concentration (chromatography fractions)

Protein concentrations of chromatography fractions was determined by our collaboration partners at the Protein Purification and Analysis Unit of the Max Planck Institute for Infectious Biology (Berlin, GER). In brief, protein concentration of gel filtration chromatography fractions was determined by bicinchoninic acid (BCA) assay.

Protein content of anion exchange chromatography fractions was approximated by absorbance at 280 nm.

2.2.10.4 Mass spectrometry

Mass spectrometry of selected anion exchange chromatography fractions was performed by our collaboration partners at the Protein Purification and Analysis Unit of the Max Planck Institute for Infectious Biology (Berlin, GER). In brief, chromatography samples were prepared by reduction, alkylation, and tryptic digest. Desalting was performed with C18 tips (Pierce, binding capacity 8 µg) and samples were solubilized in 23 µL 2% acetonitrile (CAN) with 0.1% trifluoroacetic acid (TFA) (v/v). Peptide separation was done using the UltiMate 3000 HPLC system (Thermo Fisher Scientific) with Acclaim™ PepMap™ 100 C18 nano-trap (Thermo Fisher Scientific, 2% CAN/0.1% TFA solvent) and Acclaim PepMap RSLC (Thermo Fisher Scientific, 0.1% formic acid (FA) solvent A and 80% CAN/0.1% FA solvent B) columns. Electrospray ionization mass spectrometry was performed using the Thermo Scientific™ Q Exactive™ hybrid quadrupole-Orbitrap mass spectrometer. Detected peptides were analyzed as described below.

2.2.10.5 SDS polyacrylamide gel electrophoresis (PAGE)

Ready-to-use NuPAGE™ polyacrylamide gels and 1X NuPAGE™ MES SDS Running Buffer were used for SDS-PAGE. Fractionated 60X conditioned medium samples were diluted 1:4 in 4X NuPAGE™ LDS sample buffer containing 0.8% β-mercaptoethanol, boiled at 95°C for 10 minutes, and loaded into gel pockets. Gel was run at 200V for 60 minutes.

2.2.10.6 Coomassie staining of polyacrylamide gels

SDS-PAGE gels were rinsed twice with ddH_2O. Staining was performed by incubating gels in Coomassie staining solution at 4°C overnight on a rocking table. The next day the gel was destained with ddH_2O at RT on a rocking table until the desired background was achieved. Stained gels were imaged using the CanoScan LiDE 400 scanner.

2.2.10.7 Ammonium sulfate precipitation

Conditioned and control medium was prepared as described and split into 15 mL aliquots. $(NH_4)_2SO_4$ was added to aliquots to reach desired saturation (at 25°C) as follows: 0% (0 g), 10% (0.84 g), 20% (1.73 g), 30% (2.67 g), 40% (3.68 g), 50% (4.77 g), 60% (5.92 g), 70% (7.17 g). Samples were stirred for 4 hours to solve ammonium sulfate and then incubated at 4°C overnight. Following incubation, samples were centrifuged (45 minutes, 3000xG, 4°C) to pellet precipitates. Pellets were resolubilized in 7.5 mL serum-free culture medium (2-fold concentration) and then concentrated 37.5-fold (7.5 mL → 200 µL) across Amicon® Ultra-15 centrifugal filters with 10kD MWCO. Concentrated precipitates were store at -20°C.

2.2.10.8 Size fractionation and heat treatment

Conditioned and control medium were prepared as described and concentrated 60-fold using Amicon® Ultra-15 centrifugal filters with 3-100 kD MWCO. Flow throughs were collected and concentrated 60-fold using Amicon® Ultra-15 centrifugal filters with 3 kD MWCO. 60X concentrates or flow throughs were either used directly for stimulations or were boiled at 95°C for 10 minutes and used subsequently.

2.2.10.9 Immunoprecipitation and neutralization of TGF-β

100X conditioned and control medium was prepared as described and αTGF-β1/2/3 or IgG_1 isotype control (R & D Systems) was added for a final concentration of 10 µg/mL. Samples were incubated at 4°C on a rotating wheel overnight. Following incubation, samples were spun (5 minutes, 12.000xG, RT) and supernatants transferred to a fresh sterile tube. For neutralization experiments supernatants were store at -20°C, for immunodepletion experiments antibody pulldown of supernatants was performed using protein G PLUS agarose beads. Prior to pulldowns, beads were washed three times with serum-free culture medium by centrifugation (30 seconds, 12.000xG, RT). Pulldowns were performed with 20-30 µL protein G PLUS agarose beads per 1 µg antibody by overnight incubation at 4°C on a rotating wheel. Following incubation, samples were spun (3 minutes, 2.500xG, RT) and supernatants transferred to a fresh sterile tube. Supernatants were stored at -20°C or used for stimulations.

2.2.11 Data analysis

2.2.11.1 Quantification of transcript levels from RT-qPCR data

Raw RT-qPCR data was attained using the CFX Manager software. Quantification of transcript levels was done using the $2^{-\Delta Cq}$ method. Cycle quantification values (Cq) of target genes were normalized to housekeeping control (*GAPDH*) and resulting ΔCq values used to calculate relative expression ratios $2^{-\Delta Cq}$. Fold change expression ratios were determined by dividing the relative expression ratios of samples by that of their respective control.

2.2.11.2 Quality control, differential gene expression, and GO analysis of RNA sequencing data

Raw sequencing reads of Illumnia RNA sequencing were provided as FASTQ files by the BIH Genomics Core Facility. Quality control of raw reads, as well as read mapping and counting was performed in Python according to [345]–[347]. Ensemble Genome Reference Consortium human build 38 (GRCh38.all.fa) was used as reference genome with its respective annotation library (Homo_sampiens_GRCh38.93.gft). The genome index was generated, read files merged and raw reads aligned using STAR algorithm (as described in [345], [348]). STAR alignments were stored in SAM/BAM format and results were visualized in Rstudio (as described in [349]). Alignment success was controlled using the SAMtools (samtools view and samtools flagstat scripts), and RseQC (bam_stat script) Python based software packages according to the developer's instructions and [345]. Biases in read distributions, in silico calculated RIN (RNA Integrity Number), and similarity between replicate samples were assessed using the anaconda3 (read_distribution and tin scripts), as well as RseQC (geneBody_coverage script) Python based software packages according to the developer's instructions and [345]. Following successful quality assessment, read counting per gene was performed using the featureCounts script of the Python subread package according to [345]. Hits were called if overlaps (1 bp or more) were found between reads and a single genomic feature (no multiple overlaps allowed). Read normalization, correlation and differential gene expression analysis, as well as visualization of results was performed in Rstudio using the DESeq2 and associated packages according to the developer's instructions and [350]–[352]. Genes with less

than 10 read counts across samples were excluded from the differential gene expression analysis. Gene ontology analysis of differentially expressed genes was conducted with the web-based application GOrilla. Significantly regulated genes were provided as target and all expressed genes in U-2 OS cells as background list to determine enrichment of GO terms (biological function).

2.2.11.3 Analysis of raw bioluminescence counts

Raw bioluminescence signals were analyzed using the in-house developed software ChronoStar. Data was trend-eliminated by dividing raw counts by their 24 hour running average. Subsequently, a sinusoidal function (Equation 3) was fitted to the detrended data and circadian parameters were extracted.

$$x(t) = e^{-dt} * A * \cos(\omega t * 24 - \omega * \phi) \quad (3)$$

A = amplitude
d = damping constant
$\omega = 2\pi$/period [hs]
ϕ = phase [hs]
t = time [hs]

2.2.11.4 Determination of ∆phase and ∆period

Stimulation of U-2 OS *Bmal1*:Luc or *Per2*:Luc reporter cells or PER2::LUC murine tissue explants were performed as described. Raw time series were trimmed to start at the timepoint of stimulation and circadian parameters were extracted using ChronoStar. Phases were normalized to periods. Absolute phase differences between samples and their respective controls were determined and transformed into “circular ∆phase” values, i.e. to range between ±12 hours.

Determination of ∆period was done by analyzing raw time series in ChronoStar, extracting period values and calculating the absolute difference between periods of samples and their respective controls.

Phase-pulling experiments

Peak phases of the U-2 OS *Per2*:Luc reporter cells were determined for the first, second, and third circadian cycle of bioluminescence oscillations post-synchronization. To do so raw time series were trimmed to start 12 hours (first peak), 36 hours (second peak), or 60 hours (third peak) post-synchronization. Circadian parameters were determined in ChronoStar and phases were normalized to periods.

2.2.11.5 Determination of AUC and fold change AUC

Stimulation of U-2 OS 7xCRE:Luc, 7xmutCRE:Luc, or 7xSRE:Luc was performed as described. Raw time series were trimmed to start at the timepoint of stimulation and area under the curve was determined in GraphPad PRISM (baseline: 0 cps, peak threshold: < 10% of the distance form minimum to maximum cps). Fold AUC was determined by dividing AUC values of samples by their respective controls.

2.2.11.6 Dose-responses to pharmacological TGF-β receptor inhibitor

AUC of 7xCRE:Luc reporter cells following stimulation with conditioned or control medium containing TGF-β receptor inhibitor, as well as circadian parameters of *Per2*:Luc report cells following the addition of TGF-β receptor inhibitor were determined as described. Relative fold change AUC was determined as follows: relative AUCs were calculated by dividing sample AUCs by their respective solvent controls, i.e. 0.0 µM LY2109761 in conditioned or control medium, relative AUCs of conditioned medium were normalized to respective relative AUCs of control medium.

Relative amplitude and damping parameters were determined by dividing amplitude and damping parameters of by their respective solvent controls, i.e. 0.0 µM LY2109761. ∆period values were determined as described above and relative to solvent control, i.e. 0.0 µM LY2109761. EC_{50} values were determined in GraphPad PRISM by non-linear regression fitting of an asymmetric sigmoidal curve to relative fold change AUC, relative amplitude/damping, or ∆period values.

2.2.11.7 Calculation of % recovery and selection of active chromatography fractions

Percent recovery of conditioned medium activity following stimulation of U-2 OS 7xCRE:Luc reporter cells was determined as follows:

(i) "assay AUC" was determined in GraphPad PRSIM as described above (for 1:5 dilution of input or fractions in reporter medium)
(ii) "5-fold AUC" was calculated by extrapolating the assay AUC (based on a previously determined standard curve of a conditioned medium dilution series)
(iii) Total activity of input and chromatography fractions was calculated by multiplying the 5-fold AUC with the absolute input or fraction volume
(iv) % recovery was calculated by dividing total activity of the fractions by total activity of the input (multiplied by 100)

Active fractions were defined as those fractions with % recovery > mean ± SD % recovery of all fractions, as well as with protein content < mean protein content of all fractions (excluding negative absorbance values at 280 nm).

2.2.11.8 Identification of secreted protein hits

Identification of protein hits from peptide sequences was done by our collaboration partners at the Protein Purification and Analysis Unit of the Max Planck Institute for Infectious Biology (Berlin, GER). In brief, observed mass spectrometry spectra were compared to a contaminant, as well as the SwissProt (release 2018_11, taxonomy: homo sapiens) primary sequence databases. Following parameters were used during the Mascot search:

Table 2-6: Mascot search parameters

Type of search	MS/MS Ion search
Enzyme	Trypsin/P
Variable modification	Acetyl (Protein N-term), Carbamidomethyl (C), Gln → pyro-Glu (N-term Q), Oxidation (M)

Mass values	Monoisotopic
Protein mass	Unrestricted
Peptide mass tolerance	± 5 ppm
Fragment mass tolerance	± 0.03 D
Max missed cleavage	2
Instrument type	ESI-FTICR
FDR	1%

Resulting Mascot protein hits of active and inactive fractions were filtered for human secreted proteins predicted by MDSEC using Rstudio (human protein atlas: https://www.proteinatlas.org/search/protein_class:Secreted+proteins+predicted+by+MDSEC, accessed Feb 2019). Subsequently, secreted proteins hits identified in inactive fractions were removed from hits of the active fractions.

2.2.11.9 Statistical analysis

All statistical analyses were carried out in GraphPad PRISM.

3 Results

U-2 OS cells have been derived from a female osteosarcoma patient about 15 years ago. Like virtually all other known mammalian cell types they possess the canonical molecular clock machinery and oscillate autonomously on single cell level. This cell line was chosen as primary model of peripheral circadian oscillators due to its well-described circadian rhythmicity, extensive characterization in knock-down studies, as well as its origin from human tissue. Moreover, to our knowledge no coupling studies have been conducted in U-2 OS cells so far.

3.1 Circadian rhythms depend on culture density

As described above the SCN exhibits synchronized and robust tissue rhythmicity due to intercellular coupling of heterogenous single cell oscillators within the tissue network. Whether peripheral circadian oscillators couple with each other is still debated. However, Noguchi et al. (2013) demonstrated that primary fibroblasts display weakened circadian rhythmicity on single cell level when cultured at low-densities [61]. Moreover, rhythmicity could be enhanced by substitution of low-density cultures with conditioned medium from high-density cultures [61]. This suggested that peripheral circadian oscillators required secreted signals from other cells to express normal circadian rhythms.

Thus, to test whether circadian rhythmicity of U-2 OS cells, as peripheral oscillator model, displays dependency on culture density, oscillations of *Per2*:Luc circadian reporter cells were imaged at varying culture densities. Comparable to fibroblasts, U-2 OS oscillations (on population level) showed a reduction of amplitude and increased damping with decreasing cell density (Figure 3-1 A-C). Note that these results were replicated in two independent sets of experiments: (i) performing the same experiment by an independent researcher [293] and (ii) by culturing U-2 OS cells at decreasing densities on membrane inserts (Figure 6-1 A-C). Impaired circadian rhythmicity may be a consequence of weakened single cell rhythms (as shown in [61]), desynchronization among single cell oscillators, or both. Nevertheless, according to theoretical concepts of intercellular coupling, decreased network amplitudes and

increased damping may be explained by dephasing and non-resonating single cell oscillators within incoherent networks (for details see 1.4).

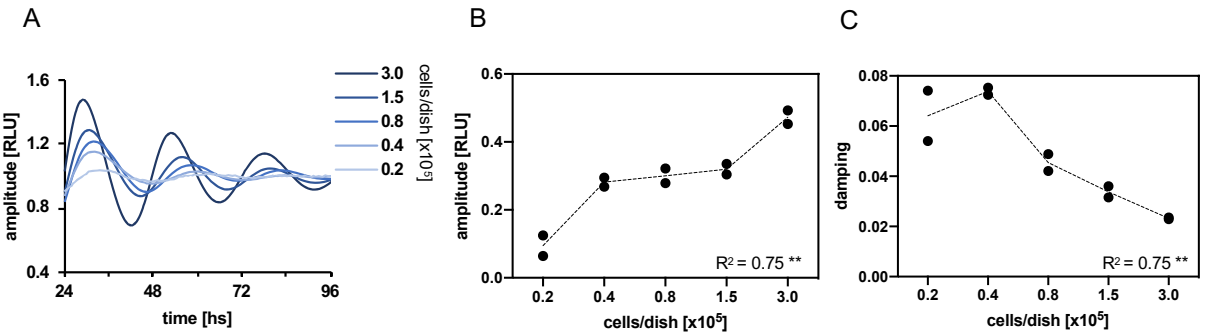

Figure 3-1: U-2 OS circadian rhythmicity depends on culture density

To assess effects of culture density on circadian dynamics, U-2 OS cells harboring a *Per2*:Luc reporter gene were seeded into 35-mm culture dishes in increasing densities, synchronized, and luciferase activity was continuously monitored. **(A)** Detrended time series of a representative culture density experiment. **(B,C)** Quantification of amplitudes (B) and damping (C) of circadian oscillations (n=1 repeat experiment with 2 technical replicates, individual values and connecting line displayed, linear regression test: **p<0.01).

To further test whether impaired circadian rhythmicity is reflected on the molecular level, expression levels of core clock genes were determined for sparse (0.3 x10^5 cells/35-mm dish) and dense (3.0 x10^5 cells/35-mm dish) cultures of U-2 OS cells. Consistent with weakened rhythms of U-2 OS *Per2*:Luc reporter cells, low-culture density resulted in reduced transcript levels of most of the core clock genes (Figure 3-2 A). This may indicate that low culture density and lack of contact to adjacent oscillators results in increased transcriptional repression or lack of transcriptional activation of the molecular core clock machinery. Yagita et al. (2010) reported that the emergence of circadian rhythmicity during cellular differentiation depends on threshold expression levels of certain core clock components driving functional molecular TTFLs [353]. Thus, assuming that reduced expression of core clocks genes is directly related to weakened rhythmicity, findings may suggest that peripheral circadian oscillators require signals from neighboring cells to enhance circadian rhythmicity on both, molecular and phenotypic level.

To gain a better understanding of how culture density dependent changes may be related to global transcriptional regulation, culture density dependent changes to the

U-2 OS transcriptome were assessed by RNA sequencing and differential gene expression (DGE) analysis. Indeed, on a global level culture density could be associated with specific gene expression profiles of dense and sparse cultures (Figure 3-2 B). In contrast to the core clock machinery, no trend towards significant transcriptional suppression was observed globally. Up- and downregulated transcripts were distributed equally (Figure 3-2 C), i.e. 47% of transcripts with padj < 0.01 displayed log2-fold changes > 0 and 53% Log2FC < 0. Moreover, gene expression changes of core clock genes resembled those detected by RT-qPCR (Figure 3-2 A), displaying transcriptional suppression of most of the core clock genes (Figure 3-2 C). Gene ontology (GO) analysis showed that DGE profiles of sparse versus densely cultured U-2 OS cells are associated with distinct biological functions. Significantly downregulated transcripts were associated with extracellular matrix (ECM) structure and extracellular signaling activity, significantly upregulated transcripts with nucleic acid binding and regulation (Figure 3-2 D). The top 20 differentially regulated transcripts (sparse versus dense cultures) reflected these global changes (Figure 3-2 E,F). Downregulated transcripts included a large number of genes involved in ECM remodeling and function, e.g. extracellular peptidases/proteases (*MMP7, KLK3, CFI*) and enzymes (*PPBP, ENPP3*), as well as filament (*KRT71, MYL10*) and glycoproteins (*CHI3L1, PRB1/2*). Upregulated transcripts included mainly long noncoding RNAs, which have been described as regulators of gene expression by controlling chromatin landscape, transcription, RNA turnover, as well as translational and post-translational processes in the cytoplasm [354]. RNA sequencing results may suggest that reducing culture density and thereby proximity to neighboring cells drives peripheral oscillators into a desynchronized state, characterized by reduced responsiveness to extracellular (paracrine) signals, as well as of increased cellular replication. This is in agreement with published studies, showing that peripheral oscillators require paracrine signals from adjacent cells to maintain normal circadian rhythmicity [61], as well as that increased cell division reduces coherence among single cell oscillators [355].

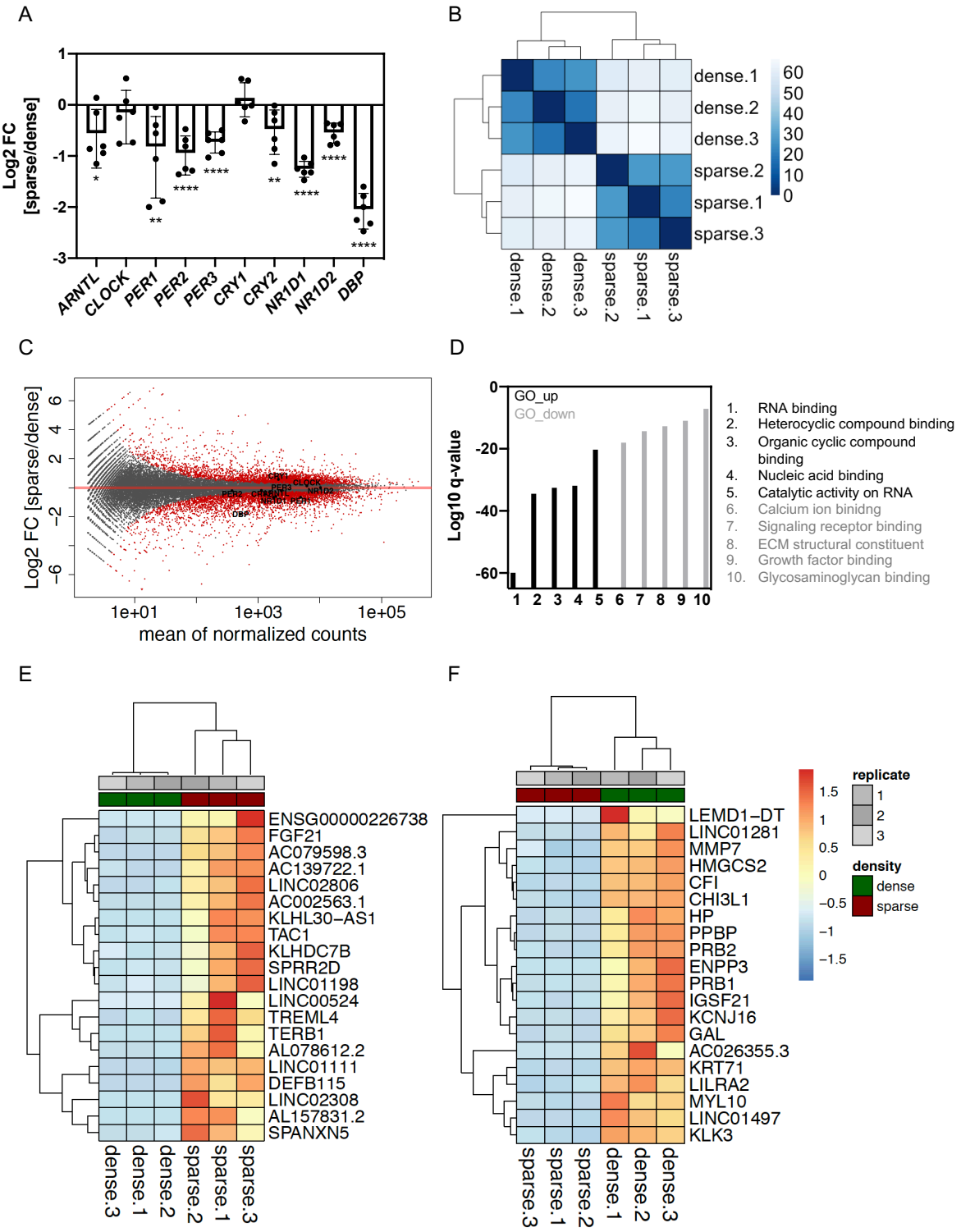

Figure 3-2: U-2 OS transcriptional profiles depend on culture density

To investigate density dependent transcriptional changes, U-2 OS cells were seeded at high (3.0 x10^5 cells/well) or low (0.3 x10^5 cells/well) culture density into 6-well plates, synchronized, and RNA was harvested 18 hours after synchronization. RT-qPCR, RNA sequencing (RNAseq) and bioinformatic analysis was performed as described. **(A)** Quantification of mRNA expression changes for sparse versus dense cultures determined by RT-qPCR (n=6 repeat experiments with 1-3 technical replicates each, measured in triplicates, normalized to *GAPDH*, mean ± SD, individual values displayed, Unpaired tow-tailed student's t-test against H_0: Log2FC=1: *p<0.05, **p<0.01, ****p<0.0001). **(B)** Euclidean

distance clustering of rlog-transformed RNAseq read counts (all RNAseq data are from n=3 repeat experiments with 1 technical replicate each). **(C)** Magnitude Average (MA)-plot of log2-transformed expression changes for sparse versus dense cultures, expression changes of core clock genes analyzed in (A) are highlighted in black (red dots=padj<0.01). **(D)** Top 5 GO terms (biological function) associated with significantly (padj<0.01) up- or downregulated transcripts tested against all expressed genes **(E,F)** Histograms of top 20 up- (E) and downregulated (F) transcripts in sparse versus densely cultured cells with padj<0.01 (Euclidean distance clustering of log2-transformed expression changes).

Overall, weakened rhythmicity, as well as transcriptional suppression of the core clock machinery and of genes associated with intercellular signaling activity in sparse cultures indicate that proximity to and communication among neighboring oscillators is able to enhance circadian rhythms. We suspect that amplitude increases and reduced damping are a reflection of both, strengthened single cell rhythmicity and enhanced network synchrony due to intercellular coupling.

3.2 Peripheral circadian oscillators (weakly) couple

Amplitude reduction, increased damping, as well as downregulation of core clock genes may be a consequence of impaired single cell rhythmicity, of network desynchronization, or both. Thus, support the hypothesis that cell-cell communication promotes intercellular coupling, we investigated whether cultures of peripheral circadian oscillators are able to synchronize with each other.

Firstly, if peripheral circadian oscillators are coupled, they are expected to integrate time information from adjacent cells and to display phase convergence upon mixture with differently phased oscillators. To test this, U-2 OS cells were synchronized 6 hours apart and cultured together directly before the start of bioluminescence recording. The experiment was conducted as described in methods. In brief, co-culture was performed with a population of *Per2*:Luc circadian reporter cells and a population of phase different non-reporter cells, in order to specifically track phase changes of the reporter cell population under co-culture conditions. To test whether phase convergence is dependent on the relative ratios between these two populations, reporter cells were kept constant at low density, while non-reporter cells were added in increasing numbers. However, to be able to separate effects of culture density and coupling, total

cell numbers were kept constant across all experimental conditions (3.3 x10^5 cells/35-mm dish) by “filling up” the co-culture with U-2 OS non-reporter cells, “phase equal” to the *Per2*:Luc population.

During the first circadian cycle, the phase of the reporter cell population was clearly pulled towards the phase of the non-reporter cells in a density dependent manner (Figure 3-3 A-D), suggesting that oscillator populations couple with each other to establish coherent network oscillations. Bidirectionality of phase convergence was observed, i.e. depending on the phase of the non-reporter cell population, reporter cells were pulled either towards earlier or later phases (Figure 3-3 A-D). This may further suggest that intercellular coupling depends on the exchange of rhythmic coupling signals, conveying time information about the phase of oscillation of individual single cell oscillators. As expected, an ~6 hour phase difference was observed for cells synchronized 6 hours apart, as indicated by the phase of circadian reporter cells under the 0 x10^5 co-cultured cell condition (13.4 hours versus 19.3 hours) (Figure 3-3 B,D). However, observed phase-pulling effects were smaller than would be expected for a completely synchronized population of 6 hour phase different oscillators. Based on the weighted phase average of the co-cultured populations, global mean field coupling was expected to result in ~5 hour phase changes of the reporter cell population upon largest co-culture ratios (1:11 reporter:non-reporter). During the first circadian cycle however, an approximate +1.4 hour advance and -2.4 hour delay was observed for reporter cells co-cultured with the highest number of phase advanced and phase delayed non-reporter cells, respectively (Figure 3-3 A-D). Moreover, phase-pulling effects appeared to be transient since they decreased during successive circadian cycles (Figure 6-2 A-H). Interestingly, phase delays were found to be more pronounced, as well as more stable (Figure 3-3 A,B and Figure 6-2 A-D) than phase advances (Figure 3-3 C,D and Figure 6-2 E-H). Therefore, results suggest that peripheral circadian oscillators display weak intercellular coupling resulting in partial or transient phase-synchronization of the network. Moreover, peripheral circadian oscillators seem to be more resistant against coupling induced phase advances than delays.

Secondly, if peripheral circadian oscillators are able to couple, they are expected to frequency-lock and display period-pulling upon co-culture of oscillator populations with distinct circadian periods. To test this, co-cultured experiments were performed as described in methods. In brief, 3-dimensional cell spheroids were grown from mixed

cultures of wildtype (24.9 hour period), *CRY2*$^{-/-}$ knock-out (27.7 hour period), or *TNPO1*$^{-/-}$ knock-out (23.8 hour period) U-2 OS *Bmal1*:Luc reporter cells with wildtype non-reporter cells (expected period ~24.9 hours). Period changes upon co-culture were compared to periods of spheroids grown from pure cultures of the respective circadian reporter cell lines. Spheroid culture rather than normal of 2-dimensional culture was performed to maximize the number of cellular connections within these 3-dimensional structures. Moreover, mixed spheroids were generated from a 1:5 ratio of reporter:non-reporter cells to enhance pulling effects by the non-reporter cell population, while still being able to detect bioluminescence signals from the mutant reporter cells.

The period of *CRY2*$^{-/-}$ knock-out reporter cells was shortened (Figure 3-3 E,G,H), while that of *TNPO1*$^{-/-}$ knock-out reporter cells was lengthened (Figure 3-3 F,G,H) upon co-culture with wildtype non-reporter cells. Mixed spheroids of wildtype reporter cells with wildtype non-reporter cells showed virtually no period changes (Figure 3-3 G,H). Again, bidirectionally of period-pulling effects was observed, meaning that long periods of *CRY2*$^{-/-}$ knock-out cells were shortened and short periods of *TNPO1*$^{-/-}$ knock-out lengthened upon co-culture with wildtype period non-reporter cells. This suggests that peripheral circadian frequency-lock via intercellular coupling, as well as that information about the oscillatory state of the coupled oscillators is exchanged. Based on the weighted period averages of the mutant reporter and wildtype non-reporter populations (1:5 ratio), a ~130 minute shortening of *CRY2*$^{-/-}$ and ~50 minute lengthening *TNPO1*$^{-/-}$ mutant periods was expected. However, both, *TNPO1*$^{-/-}$ and *CRY2*$^{-/-}$ mixed spheroids display period changes of approximately 40 minutes, i.e. shortening and lengthening of the reporter cell period, respectively (Figure 3-3 G,H). Thus, while synchronization of single cell oscillators within *TNPO1*$^{-/-}$ mixed spheroids appeared to be complete, that of single cell oscillators within *CRY2*$^{-/-}$ mixed spheroids appear to be partial again. Consistent with entrainment concepts, this may suggest that the ability of peripheral circadian oscillators to frequency-lock and to establish synchronized rhythms depends on coupling strength and permissible period differences between single cell oscillators. While wildtype and *TNPO1*$^{-/-}$ knock-out cells displayed absolute period differences of 1.1 hours, periods of wildtype and *CRY2*$^{-/-}$ knock-out cells differed by almost 3 hours. Thus, findings further suggest that intercellular coupling among peripheral circadian oscillators is weak and only sufficient to synchronize oscillators with Δperiod of ~1 hour. Note that bidirectional period

changes were only observed for 3-D spheroid but not for conventional 2-D cultures (data not shown), suggesting that complexity of cellular microenvironments is related to intercellular coupling strength.

Overall, observed phase- and period-pulling effects support the hypothesis that peripheral circadian oscillators couple intercellularly, as well as that this coupling is weak compared to coupling within the SCN. Moreover, findings may suggest that stronger intercellular coupling is required to achieve frequency-locking than is required to achieve phase-locking, as well as that complex 3-D tissue-like microenvironments enhance intercellular coupling strength.

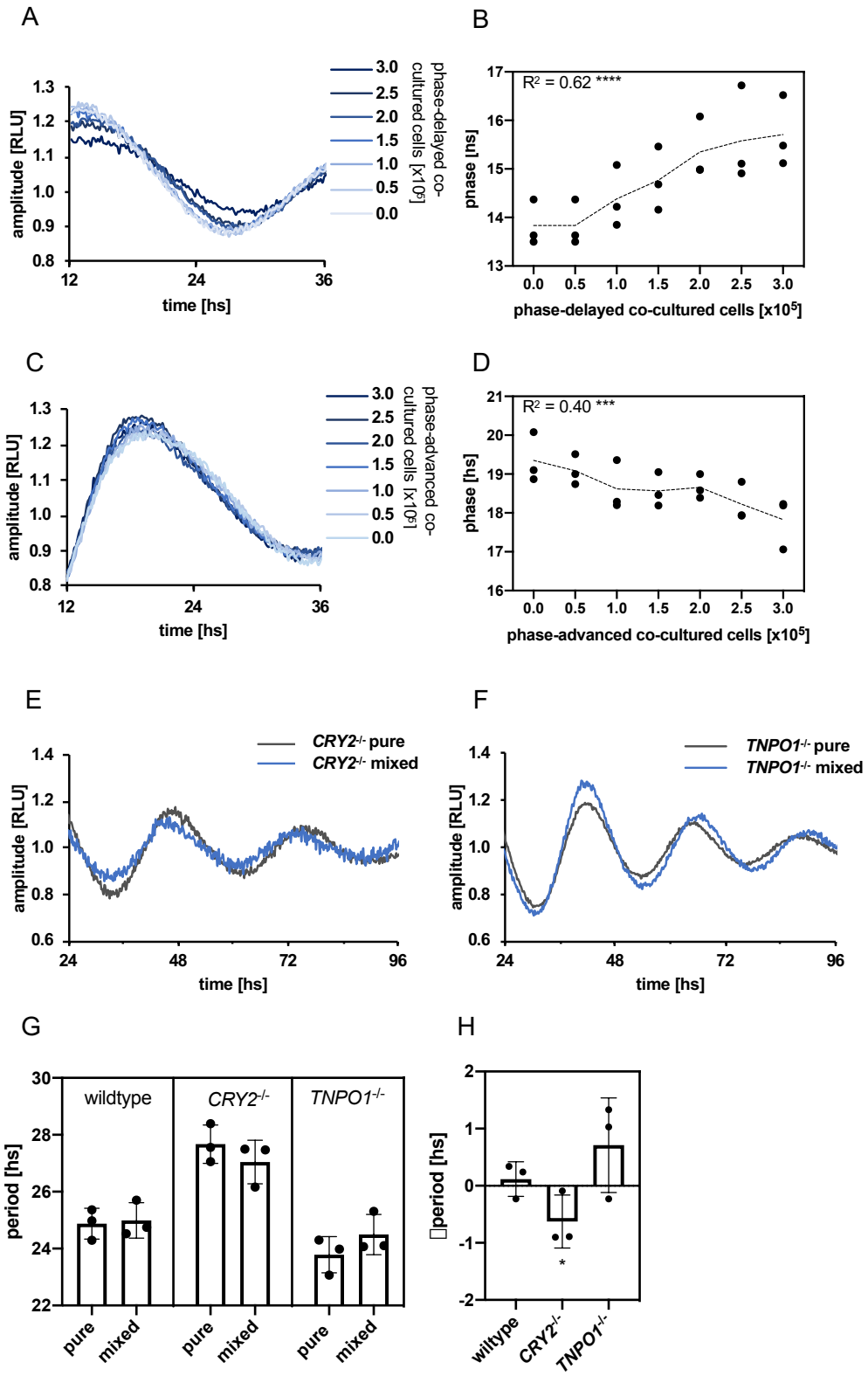

Figure 3-3: Co-cultured populations of U-2 OS cells display weak intercellular coupling with respect to phase and period

Co-culture experiments of distinct U-2 OS cell populations were performed to determine whether or not peripheral circadian oscillators are able to phase- and frequency-lock with each other. **(A-D)** Phase-

pulling experiments were performed as described. In brief U-2 OS cells harboring a *Per2*:Luc reporter gene were seeded at low density (0.3 x10^5 cells/dish) together with increasing numbers of phase advanced or -delayed non-reporter cells into 35-mm dishes. Luciferase activity was continuously monitored. **(A,C)** Detrended time series of a representative phase-pulling experiment (first circadian cycle). **(B)** Quantification of phases during the first cycle of bioluminescence oscillations of reporter cells co-cultured with 6 hour phase delayed (and phase equal) non-reporter cells (n=3 repeat experiments with 3 technical replicates each, individual values and connecting line displayed, linear regression test: ****p<0.0001). **(D)** Quantification of phases during the first cycle of bioluminescence oscillations of reporter cells co-cultured with 6 hour phase advanced (and phase equal) non-reporter cells (n=3 repeat experiments with 3 technical replicates each, individual values and connecting line displayed, linear regression test: ***p<0.001). **(E-H)** Period-pulling experiments were performed as described. In brief U-2 OS *CRY2*$^{-/-}$ or *TNPO1*$^{-/-}$ knock-out cells harboring a *Bmal1*:Luc reporter gene were grown to spheroids with (1:5 ratio) or without wildtype non-reporter cells. **(E,F)** Detrended time series of a representative period-pulling experiment. **(G)** Quantification of circadian periods of U-2 OS spheroids generated either from pure reporter cell cultures or from 1:5 mixtures of reporter and non-reporter cells (n=3 repeat experiments with 2 technical replicates each, mean ± SD, individual values displayed). **(H)** Quantification of the respective period changes of mixed versus pure spheroids (n=3 repeat experiments with 2 technical replicates each, mean ± SD, individual values displayed, Unpaired one-tailed student's t-test against wildtype group: *p<0.05).

Thirdly, if peripheral circadian oscillators are able to couple, network amplitudes are expected to increase due to resonance effects and damping is expected to decrease due to reduced desynchronization among single cell oscillators. To test this, low-density, low-amplitude, and highly damped U-2 OS *Bmal1*:Luc reporter cells (0.3 x10^5 cells/35-mm dish) were co-cultured with increasing numbers of non-reporter cells. In contrast to culture density experiments with varying numbers of reporter cells, this approach allowed us to track changes in circadian dynamics of a constant reporter cell population, while varying the number of non-report cells. Thereby, magnitude effects on amplitude and damping parameters can be excluded.

Both, low amplitudes and high damping of the sparse reporter cell population could be rescued by co-culture with non-reporter cells in a density dependent manner (Figure 3-4 A-C). Note that this result was replicated by an independent researcher , however only if peripheral circadian oscillators were exhibiting intact secretory pathways [293]. This supports the hypothesis that peripheral circadian oscillators couple with each other by the exchange of secreted signaling molecules.

Thus, to further test whether amplitude expansion and reduction of damping are dependent on direct cell-cell contact or whether exchange of diffusible factors is sufficient, co-cultures of low-density U-2 OS *Bmal1*:Luc reporter cells with increasing

numbers of non-reporter cells was performed using membrane inserts. These inserts facilitate a physical separation of the reporter and the non-reporter cell populations within one culture dish, thereby only allowing for the exchange of diffusible factors (> 500 kD based on 0.4 µm pore size) across relatively large distances.
Despite a lack of direct cell-cell contact, increases in amplitude and decreases in damping were still observed under co-culture conditions (Figure 3-4 D-F), suggesting that paracrine molecules are sufficient to promote synchronization of peripheral circadian oscillators. Interestingly, even though a linear correlation of amplitude and damping with cell density was not detected (for the tested range of densities), relative rescue effects of amplitudes and damping were more pronounced for membrane separated than for direct co-cultures. This means, across all numbers of co-cultured cells, membrane separated non-reporter cells induced larger changes in amplitude and damping parameters than directly co-culture non-reporter cells (Figure 3-4 B,C and Figure 3-4 E,F). Assuming that these effects are indeed due to difference in intercellular coupling, rather than due to experimental variation, this may suggest that lack of direct cell-cell contact enhances the susceptibility of low-density, low-amplitude, highly damped circadian reporter cells to paracrine coupling signals of the non-reporter cell population.

Overall, results indicate that peripheral circadian oscillators indeed couple with each other to generate synchronized circadian network rhythmicity. In agreement with theoretical models, coupling on the population level was inferred by (i) phase-synchronization (or phase-pulling), (ii) frequency-locking (or period-pulling), (iii) amplitude resonance (increased network amplitudes), and (iv) reduced desynchronization (decreased network damping) of peripheral circadian oscillators ensembles. Consistent with findings from Jäschke's and Noguchi et al. (2004) [61], [293], results suggest that paracrine communication pathways play an important role for interoscillator coupling. Moreover, in agreement with published studies [62], [89], observed intercellular coupling appears to be weak (undercritical), leading only to partial network synchronization.

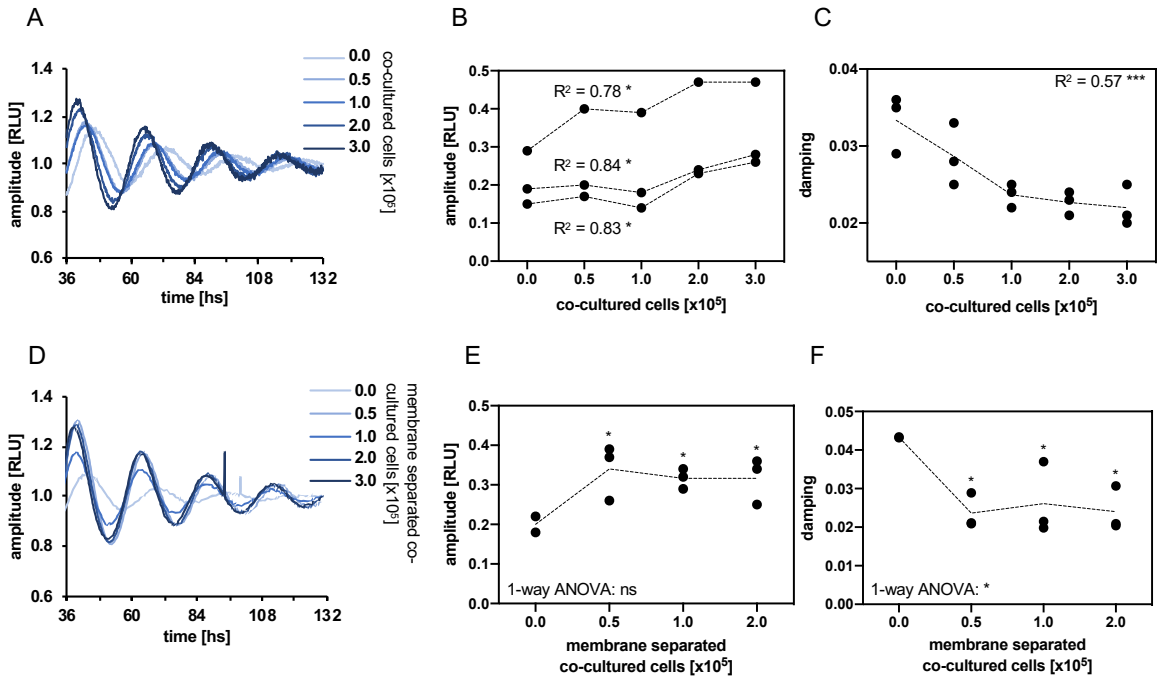

Figure 3-4: Co-cultured populations of U-2 OS cells display weak intercellular coupling with respect to amplitude and damping

Sparse U-2 OS *Bmal1*:Luc reporter cells (0.3 x10^5 cells/35-mm dish or 0.3 x10^5 cells/4.2 cm^2 insert) were co-cultured with increasing numbers of non-reporter cells in 35-mm dishes to determine whether or not intercellular coupling results in amplitude resonance and decreased damping. Direct and membrane separated co-culture experiments were performed as described. **(A)** Detrended time series of a representative direct co-culture experiment. **(B,C)** Quantification of amplitudes (B) and damping (C) of circadian oscillations of reporter cells upon direct co-culture (n=3 repeat experiment with 2 technical replicates each, individual connected values or individual values and connecting line displayed, linear regression test: *p<0.05, ***p<0.001). **(D)** Detrended time series of a representative membrane separated co-culture experiment. **(E,F)** Quantification of amplitudes (E) and damping (F) of circadian oscillations of reporter cells upon membrane separated co-culture (n=3 repeat experiment with 2 technical replicates each, individual values and connecting line displayed, One-way ANOVA with uncorrected Fisher's LSD post-hoc test against the 0.0 x10^5 co-cultured cells group: *p<0.05).

3.3 Paracrine factors modulate circadian dynamics and induce specific transcriptional profiles

Circadian clock and secretory pathway regulation have been demonstrated to be intertwined processes. On the one hand functional secretory pathway plays an important role for normal circadian rhythms [293], on the other hand circadian clocks

control the rhythmic secretion and expression of secretory pathway components [297]. Additionally, Noguchi's et al. (2013) and our findings indicated that diffusible factors contribute to robust rhythmicity and intercellular coupling within peripheral oscillator networks (see above and [61]). Thus, we hypothesized that peripheral circadian oscillators secrete factors, which carry time information to adjacent cells and may promote network synchronization.

To determine the extent and temporal profile of phase shifts in response to secreted factors, a phase response curve (PRC) for conditioned (CM) and control medium was established (Figure 3-5 A), assuming that CM contains all molecules secreted by U-2 OS cells.

Both, conditioned and control medium induced time-of-stimulation dependent phase responses of U-2 OS *Per2*:Luc reporter cells (Figure 3-5 A), suggesting that the stimulation procedure itself, e.g. due to changes in temperature/osmolarity/pH or removal of factors contained in the supernatants of imaged cells, modulates circadian dynamics. Therefore, phases responses specific for CM, and its secreted components, were considered those relative to control medium (Figure 3-5 B,C). Interestingly, times at which reporter cells exhibited strongest phase delays in response to CM stimulation (14-18 hours post-synchronization) coincided with the trough of *PER* (or *Per* in non-human models) expression, inferred from the trough of *Per2*:Luc expression (Figure 3-5 B,C). Thus, similar to photic PRCs in mammals, inducing phase delays or advances depending on *Per1/2* expression levels, CM may shift circadian dynamics by modulating *Per* gene expression.

To further test whether phase delays at the trough of *PER* expression are U-2 OS-specific or if they are conserved across different models of peripheral circadian clocks, CM was either produced from human and murine cell lines and used to stimulated U-2 OS reporter cells, or produced from U-2 OS cells and used to stimulate tissue explants and hepanoids (differentiated liver organoids) derived from PER2::LUC mice. Except for NIH3T3 fibroblasts, CM generated from various cellular models of human and murine peripheral oscillators induced phase delays of *Per2*:Luc oscillations between 3.5-8 hours (Figure 3-5 D,E). Moreover, U-2 OS CM induced phase delays of PER2::LUC rhythms between 1.5-7 hours in a tissue-specific fashion (Figure 3-5 F,G and Figure 6-3 A). Results suggest that communication via secreted factors is a conserved feature of mammalian peripheral circadian clocks, as well as that phase

responses may be temporally gated by endogenous *PER/Per* expression. However, the magnitude of induced phase responses may be influenced by species, tissue, and/or model-system dependent factors.

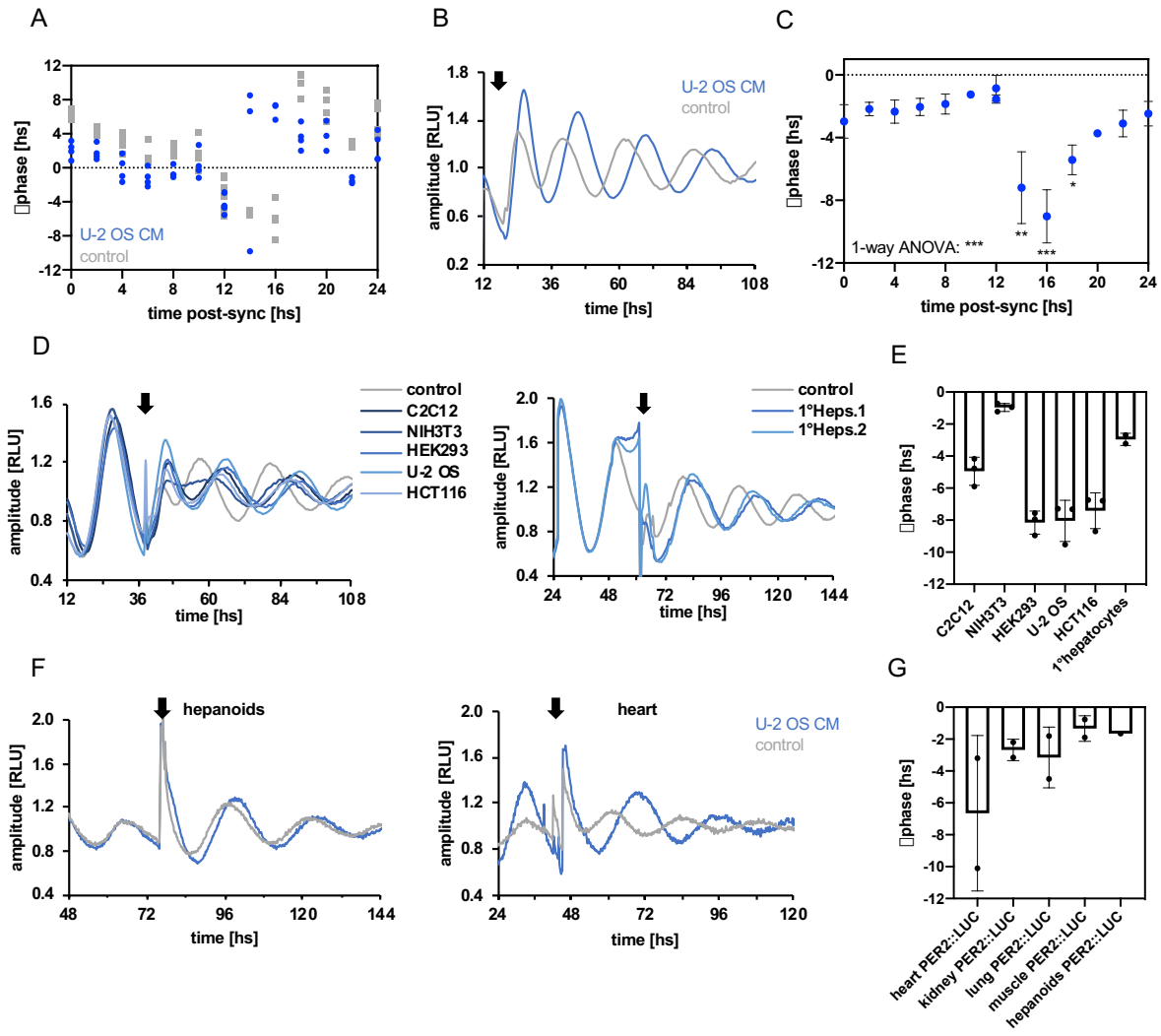

Figure 3-5: Factors secreted by peripheral circadian oscillators phase shift circadian rhythms

Mammalian reporter cells, tissue explants, or hepanoids were stimulated with conditioned and control medium to test whether secreted signaling molecules can act as Zeitgebers for peripheral circadian oscillators. CM and control medium were generated and stimulations performed as described. **(A)** Phase response curve (PRC) of U-2 OS *Per2*:Luc reporter cells upon CM and control medium stimulation relative to unstimulated control (n=1 repeat experiment with 2-4 technical replicates, individual values displayed). **(B)** Detrended time series of a representative experiment upon stimulation of U-2 OS reporter cells 16 hours post-synchronization. **(C)** Phase response curve (PRC) of U-2 OS *Per2*:Luc reporter cells upon CM stimulation relative to control medium (n=2 repeat experiments with 3-4 technical replicates each, mean ± SD, One-way ANOVA with Dunett's multiple comparison test against H_0: Δphase=0: *p<0.05, **p<0.01, ***p<0.001). **(D)** Detrended time series of a representative experiment upon stimulation of U-2 OS *Per2*:Luc with cell line CM at the inferred trough of *PER* expression. **(E)**

Quantification of phase shifts induced by cell line CM relative to control medium (immortalized cell lines: n=4 repeat experiments with 3 technical replicates each, primary cells: n=2 repeat experiments with 3 technical replicates each, mean ± SD, individual values displayed). **(F)** Detrended time series of a representative experiment upon stimulation of murine PER2::LUC tissue explants or hepanoids with U-2 OS CM at the inferred trough of *PER* expression. **(G)** Quantification of phase shifts induced by U-2 OS CM relative to control medium (explants: n=2 repeat experiment with 3-4 technical replicates each, hepanoids: n=1 repeat experiment with 4 technical replicates, mean ± SD, individual values displayed).

To further test the hypothesis that CM induced phase responses are mediated by transcriptional changes to the core clock machinery, especially via the induction of *PER/Per* gene expression, transcript levels of core clock genes were quantified following medium stimulation. Moreover, to gain a better understanding of the kinetics of conditioned medium activity, expression levels were assessed for increasing incubation times following stimulation 16 hours post-synchronization.
For all of the core clock genes analyzed, no differences in mRNA expression upon conditioned relative to control medium stimulation could be detected for incubation times ≤ 60 minutes (Figure 3-6 A). *PER2* expression was upregulated 2-4 hours following conditioned medium stimulation, E-box driven clock genes expression (*PER3*, *NR1D1/2*, *DBP,* and *CLOCK)* was downregulated 2-8 hours following CM stimulation (Figure 3-6 A). For *BMAL1* (*ARNTL*), *CRY1/2*, and *PER1* no significant changes in gene expression were observed upon stimulation with conditioned relative to control medium (Figure 6-3 B). Results suggest that conditioned medium, and its secreted components, induce phase shifts of circadian dynamics by modulating the molecular core clock machinery. Comparable to photic Zeitgeber and VIP coupling signals, secreted factors seem to induce the immediate early expression of *PER2* (rather than *PER1*). Moreover, due to the role *PER2* as repressor of CLOCK/BMAL1 heterodimers, slightly delayed suppression of the E-box driven clock genes *PER3*, *NR1D1/2*, *DBP,* and *CLOCK* may be a consequence of increased *PER2* levels.

Immediate early expression of *Per1/2* during photic entrainment or during VIP dependent coupling in the SCN is achieved via the transcriptional induction of cAMP response elements (CRE) in *Per* gene promoters. Even though CRE transcriptional activation usually drives the expression of immediate early genes within minutes, CRE dependent *Per2* responses to photic stimuli given between CT12-CT16 have been described to display slower response kinetics (~1.5-3 hours) [94], [180]. Moreover,

perturbations of intracellular Ca^{2+} and cAMP, upstream regulators of CRE activation, have been shown to result in alterations of circadian parameters such as amplitude, phase, and period [95]. Thus, CRE driven gene expression appears to constitute an important input pathway to mammalian circadian clocks, especially during entrainment and intercellular coupling. Interestingly, conditioned medium dependent phase responses and kinetics of *PER2* induction appeared to match the profile of CRE dependent input pathways described for the SCN. Thus, to test whether CRE sites also act as downstream targets in the response of peripheral circadian oscillators to secreted signals, a 7xCRE:Luc reporter gene was introduced into U-2 OS cells.

Conditioned medium stimulation of U-2 OS 7xCRE:Luc reporter cells resulted in an increase of luciferase signal, suggesting that CRE transcriptional activation indeed serves as input pathway of secreted factors to the molecular core clock machinery (Figure 3-6 B,C). As for phase shifts of *Per2*:Luc reporter cells, CRE induction was observed for conditioned medium generated from various human and murine cell lines (Figure 3-6 B,C). This further supports the hypothesis that communication via secreted factors, as well as underlying mechanisms are a conserved feature of mammalian peripheral circadian clocks.

However, in addition to CRE enhancer elements also serum-response elements (SRE) have been described to function as important binding sites of immediate early transcription factors, transmitting rhythmic systemic signals to peripheral circadian clocks [356]. Thus, to test whether response to conditioned medium requires functional CRE sites, as well as whether CM may act via the transcriptional induction of SRE enhancer elements, a 7xSRE:Luc and a mutated 7xCRE:Luc (TGACGTCA → TTAAACCA) reporter gene were introduced into U-2 OS cells.

Indeed, U-2 OS cells expressing a 7xSRE:Luc or a 7xmutCRE:Luc reporter gene displayed a significantly reduced responses to conditioned medium compared to 7xCRE:Luc reporter cells (Figure 3-6 D,E), suggesting that CM acts as specific activator of CRE mediated transcription. Functionality of the reporter gene constructs was confirmed by testing their responsiveness, or rather loss of responsiveness (in the case of the mutated CRE reporter), to their well-known activators (fetal bovine) serum and forskolin (Figure 6-3 C,D).

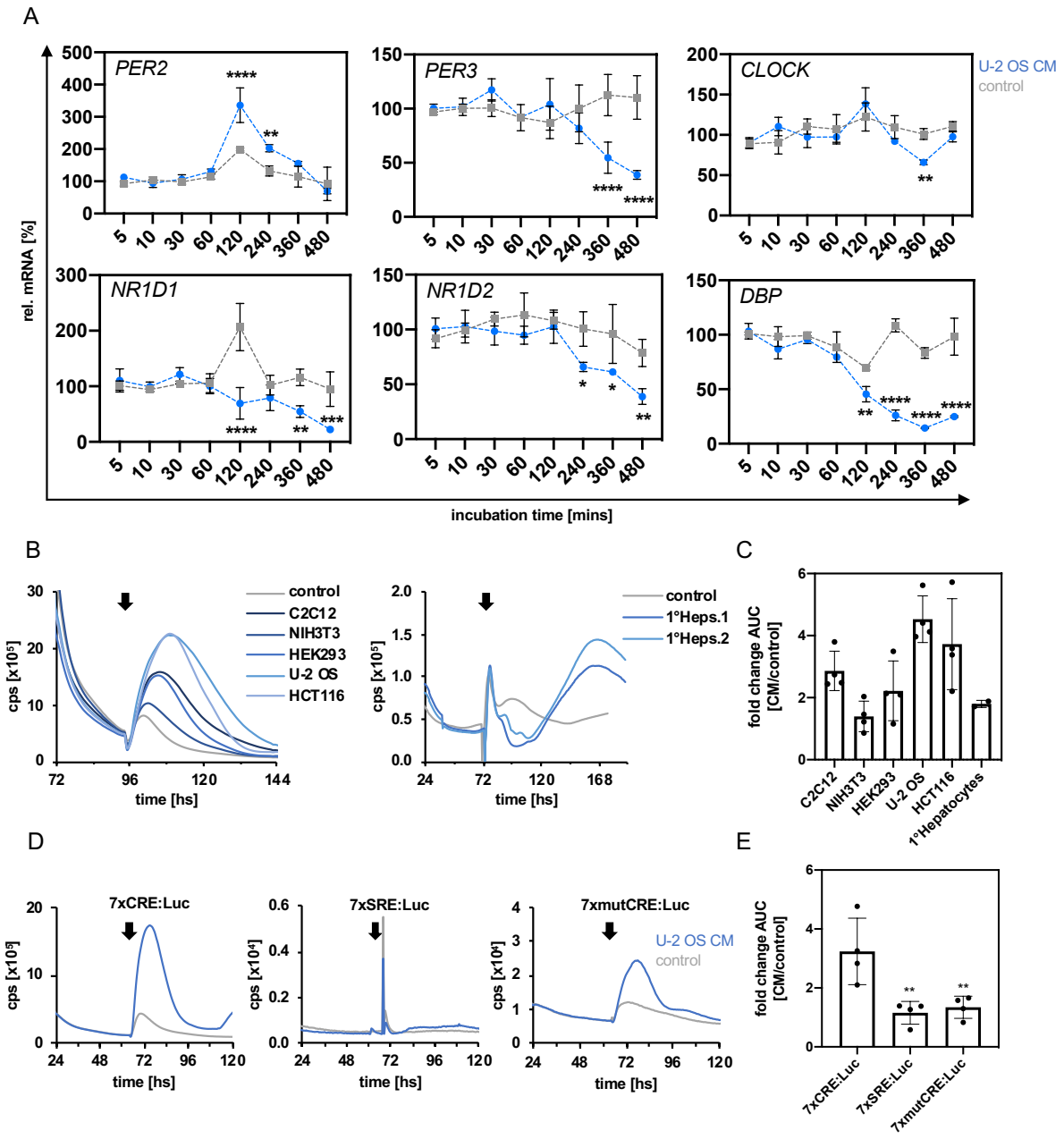

Figure 3-6: Factors secreted by peripheral circadian oscillators modulate clock gene expression and activate CRE enhancer elements

(A) Clock gene expression was assessed following conditioned and control medium stimulation in order to determine how secreted factors input to the molecular clock machinery. Conditioned and control medium were generated and used for stimulations as described. RNA was harvested after indicated incubation times following simulation 16 hours post-synchronization. RT-qPCR and area under the curve (AUC) analysis were performed as described. **(A)** Quantification of mRNA expression changes upon conditioned and control medium stimulations relative to unstimulated controls (n=3 repeat experiment with 3 technical replicates each, measured in triplicates, normalized to *GAPDH*, mean ± SD, One-way ANOVA with Dunett's multiple comparison test against control medium: *p<0.05, **p<0.01, ***p<0.001, ****p<0.0001). **(B-E)** Conditioned and control medium stimulation of U-2 OS 7xCRE:Luc, 7xmutCRE:Luc, and 7xSRE:Luc reporter cells was performed to test whether CRE enhancer elements

are required for CM responses. **(B)** Raw time series of a representative experiment upon stimulation of U-2 OS 7xCRE:Luc reporter cells with cell line CM. **(C)** Quantification of luciferase signal induced by CM relative to control medium (n=3-4 repeat experiment with 3-4 technical replicates each, mean ± SD, individual values displayed). **(D)** Raw time series of a representative experiment upon stimulation of U-2 OS 7xCRE:Luc, 7xSRE:Luc, and 7xmutCRE:Luc reporter cells with U-2 OS CM. **(E)** Quantification of luciferase signal induced by CM relative to control medium (n=4 repeat experiment with 3-4 technical replicates each, mean ± SD, individual values displayed, Unpaired one-tailed student's t-test against 7xCRE:Luc group: **p<0.01).

Assuming that paracrine signaling molecules within peripheral oscillator networks act as intercellular communication factors, we hypothesized that conditioned medium stimulation results in global transcriptomic changes that may help to identify underlying signaling pathways. To test this, RNA sequencing and differential gene expression analysis was performed for U-2 OS cells stimulated with conditioned or control medium 16 hours post-synchronization (2 hours incubation time). Both, dense and sparse cultures were used for this experiment in order to test for CM dependent responses independently of culture density, i.e. conditioned medium dependent transcriptional changes were quantified while controlling for density dependent changes. This appeared reasonable since principal component analysis showed that 56% of sample variance upon conditioned and control medium stimulation is explained by culture density (Figure 3-7 A).

CM stimulation induced specific gene expression profiles compared to control medium (Figure 3-7 A). A slight trend towards global transcriptional upregulation was observed (Figure 3-7 B) since 59% of transcripts with padj < 0 displayed Log2FC > 0 and 41% Log2FC < 0. Moreover, gene expression changes of core clock genes resembled those detected by RT-qPCR (Figure 3-6 A), displaying a clear transcriptional induction of *PER2* and suppression of *NR1D1/2* and *DBP* (Figure 3-7 B). Differently than before (Figure 3-2 D), gene ontology analysis did not yield distinct biological functions associated with transcriptional up- and downregulation upon conditioned medium stimulation (Figure 3-7 C). Both, transcriptional up- and downregulation were associated with DNA, RNA, and protein binding (Figure 3-7 C), suggesting that CM stimulation activates signaling pathways involved in the differential regulation of gene expression. For this reason, top 20 differentially regulated genes were sorted based on significance of transcriptional changes rather than based on magnitude of up- and downregulation (as in Figure 3-2 E,F). Interestingly, those transcripts most significantly altered upon CM stimulation included *EGR1* and *JUNB*, both encoding transcription

factors of immediate early genes known to regulate the circadian clock machinery in peripheral and central tissues [357], [358]. Moreover, many of the top 20 regulated transcripts were associated with cytokine and growth factor signaling (*EGR1, JUNB, TMEM88, BCL3, STAT3, WNT7B, TBX3, KDM6B, SKIL, LRRC32, ZC3H12A, ITK, CCL7*). Thus, RNA sequencing results may suggest that conditioned medium contains secreted growth factors regulating signaling pathways resulting in the downstream activation of immediate early transcription factors (TF), eventually including TFs targeting CRE enhancer elements.

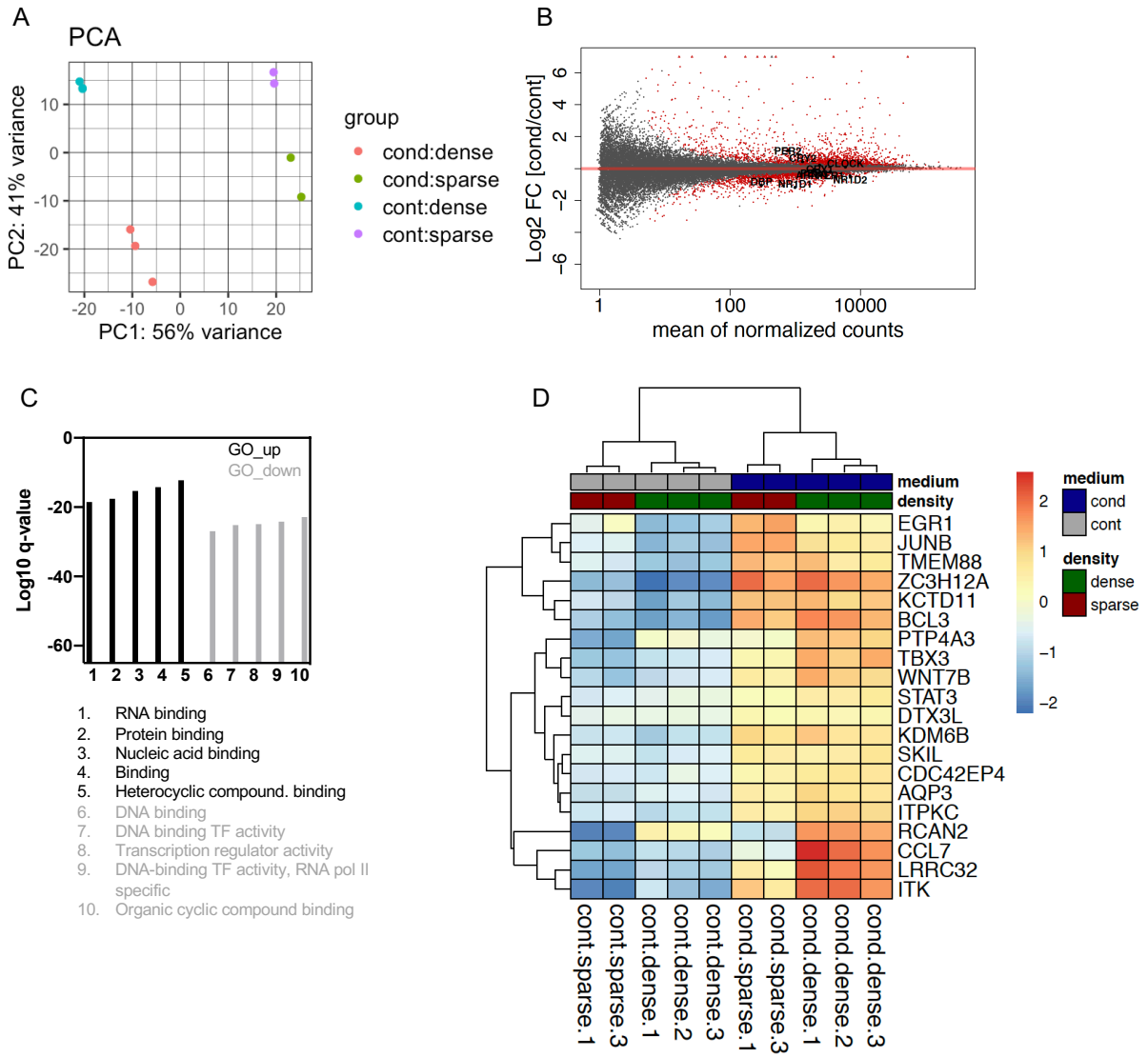

Figure 3-7: Factors secreted by peripheral circadian oscillators induce specific transcriptional profiles

To investigate conditioned medium dependent transcriptional changes, U-2 OS cells were seeded at high (3.0 x10^5 cells/well) or low (0.3 x10^5 cells/well) culture density into 6-well plates, synchronized, and stimulated with CM and control medium 16 hours post-synchronization. Following a 2 hour incubation

period RNA was harvested and RNA sequencing (RNAseq) and bioinformatic analysis performed as described. **(A)** Factor map of individual samples plotted across the principal components (PC) 1 and 2, cond=conditioned medium, cont=control medium. (RNAseq data from dense cultures are from n=3, RNAseq data from sparse cultures from n=2 repeat experiments with 1 technical replicate each). **(B)** Magnitude Average (MA)-plot of log2-transformed expression changes for conditioned versus control medium stimulation, expression changes of core clock genes analyzed in Figure 3-6 are highlighted in black (red dots=padj<0.01). **(C)** Top 5 GO terms (biological function) associated with significantly (padj<0.01) up- or downregulated transcripts tested against all expressed genes **(D)** Histograms of top 20 differentially regulated transcripts upon conditioned versus control medium stimulation with padj<0.01 (Euclidean distance clustering of log2-transformed expression changes).

Overall, results indicate that peripheral circadian oscillators secrete factors, which modulate circadian dynamics in a time dependent manner. This may serve as paracrine communication mechanism to exchange phase information and synchronize with adjacent oscillators. Moreover, secreted factors may belong to the family of growth factors, which induce temporally gated phase responses via the CRE driven transcriptional induction of *PER2/Per2* gene expression, as well as the subsequent suppression of E-box driven core clock genes. We suggest that this mechanism of interoscillator coupling may constitute a conserved mechanism across human and murine species, as well as across a number of peripheral tissues.

3.4 Secreted factors are proteins

Circadian clocks have been demonstrated to regulate the rhythmic expression of secretory pathway components, as well as the expression of many proteins, including those belonging to tissue-specific secretomes [294], [297]. Additionally, our results suggest that peripheral circadian oscillators communicate via the exchange of secreted signaling molecules. Moreover, by growth factor dependent transcriptional regulation appeared to be a potential mechanism of paracrine communication among peripheral circadian oscillators.

Thus, to test whether active conditioned medium components are likely to be (signaling) proteins, size fractionation in combination with heat treatment, as well as ammonium sulfate precipitation were performed. These experiments aimed to roughly

determine the molecular size and heat sensitivity of active factors, as well as to demonstrate that active factors can be recovered by a standard protein precipitation procedure. Induction of CRE driven luciferase expression was chosen as functional assay rather than phase shifts, or modulation of clock gene expression, due to its rapid, sensitive and reliable read out.

Ultrafiltration using size exclusion centrifugal filters with increasing molecular weight cut-offs (MWCO) showed that active CM factors are retained predominantly in the concentrates of columns with < 50 kD MWCO. For MWCO > 50 kD active factors were found also in the flow through (Figure 3-8 A-B). This may suggest that active CM components are larger than nucleic acid structures, e.g. miRNAs, or small peptides but likely smaller than extracellular vesicles, e.g. exosomes (~100 kD). However, since polyacrylamide gel electrophoresis of CM size fractions showed that filtration column cut-offs are imprecise (Figure 6-4 A,B), the actual size of active medium components should be determined by more sensitive methods. Additionally, regardless of the filter size used, heat treatment (90°C, 10 minutes) abolished CM medium activity of all concentrates and flow throughs tested, suggesting that activity of CM factors is denatured by heat (Figure 3-8 C-D). Thus, based on the molecular size and thermal instability of active medium components, it appeared likely that they belong to the protein class of biomolecules. To further validate that active CM components are proteins, one of the most common protein purification methods was performed. Salting out with ammonium sulfate preserves native protein structures, allowing for the subsequent assessment of precipitate activity. Moreover, while nucleic acids precipitate at low salt concentrations (≤ 30% $(NH_4)_2SO_4$), proteins are salted out only at higher concentrations [359], enabling the separation of these two molecule classes. As expected for proteinergic factors, active CM components started to precipitate at $(NH_4)_2SO_4$ saturations ≥ 30% and largest activity seemed to be recovered from resolubilized precipitates of ~50% ammonium sulfate (Figure 3-8 E-F). Again, these results support the hypothesis that peripheral circadian oscillators communicate by exchange of secreted signaling proteins.

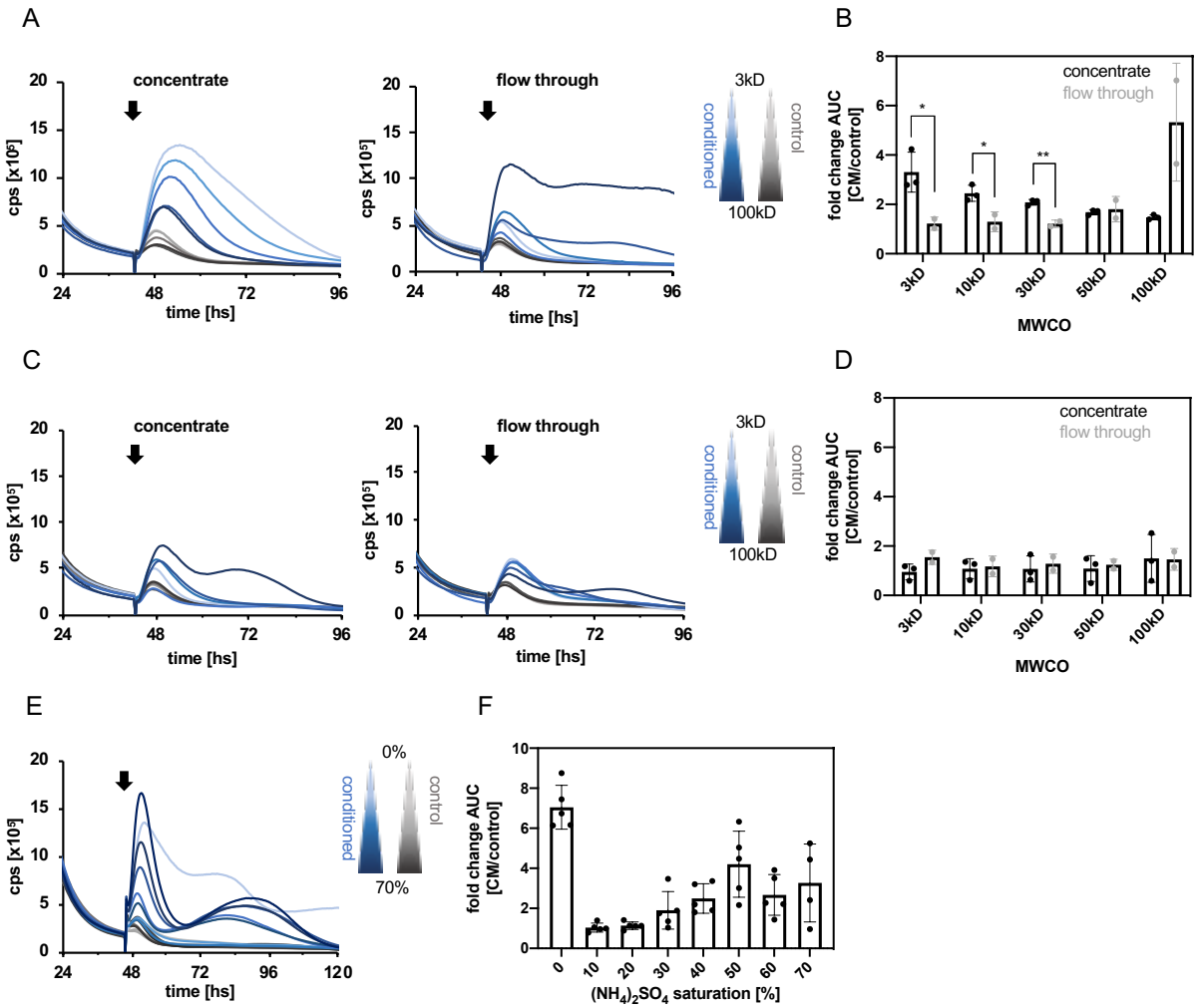

Figure 3-8: Active components in conditioned medium display characteristics of proteins

Size fractionation, heat treatment, and ammonium sulfate precipitation of conditioned and control medium was performed to test whether active CM components are proteins. All protein-based methods and stimulation of U-2 OS 7xCRE:Luc reporter cells were performed as described. **(A)** Raw time series of a representative experiment upon stimulation of 7xCRE:Luc reporter cells with conditioned or control medium size fractions. **(B)** Quantification of luciferase signal induced by CM relative to control medium (n=2-3 repeat experiment with 3 technical replicates each, mean ± SD, individual values displayed, Unpaired one-tailed student's t-test against respective concentrate group: *p<0.05, **p<0.01). **(C)** Raw time series of a representative experiment upon stimulation of 7xCRE:Luc reporter cells with size fractionated and heat treated conditioned and control medium. **(D)** Quantification of luciferase signal induced by CM relative to control medium (n=2-3 repeat experiment with 3 technical replicates each, mean ± SD, individual values displayed). **(E)** Raw time series of a representative experiment upon stimulation of 7xCRE:Luc reporter cells with resolubilized ammonium sulfate precipitates. **(F)** Quantification of luciferase signal induced by CM relative to control medium (n=4-5 repeat experiment with 3 technical replicates each, mean ± SD, individual values displayed).

Having gathered indications that active conditioned medium factors are proteins, their identity remained to be determined. However, in a complex mixture like conditioned medium those components modulating circadian dynamics are expected to be present in low abundance. Thus, a two-step chromatography was performed prior to mass spectrometry of conditioned medium in order to enrich active components (again with respect to CRE transcriptional activation). All chromatography and mass spectrometry (MS) experiments were performed in collaboration with our partners at the at the Protein Purification and Analysis Unit of the Max Planck Institute for Infectious Biology (Berlin, GER).

To separate active CM components by size, gel filtration chromatography was performed. In contrast to previous methods, gel filtration chromatography (Superdex HR-200GL column) allows for intermediate-resolution separation of proteins with a fractionation range between 10-600 kD [360]. The protein content of active fractions was determined to identify those with enriched activity compared to CM input, i.e. strong CRE induction and low protein content. Ultimately, 10 gel filtration chromatography fractions with enriched activity were identified and split into two so-called active CM pools (Figure 3-9 A). Unfortunately, due to the lack of a column size standard, determination of the absolute size of active factors was difficult. However, since active factors eluted early in the chromatography, i.e. they stayed mainly in the mobile phase, their size was estimated to lie within a rather high molecular weight range. To further fractionate and purify active CM components, CM pools were processed by anion exchange chromatography. Ion exchange chromatography fractionates inputs by reversible interactions of charged chromatography columns with charged proteins (based on their pH dependent surface charge). This method is commonly used for high-resolution purification of target proteins [361] but depends on elution of protein factors by a salt gradient (0-1M NaCl). Thus, to avoid salt effects during the 7xCRE:Luc activity assay, all anion exchange chromatography fractions were concentrated and desalted using centrifugal filters with a 3 kD MWCO. Again, the protein content of active fractions was determined to identify those with enriched activity compared to CM input. Both active pools of the initial gel filtration chromatography, showed similar overall activity profiles after anion exchange chromatography (Figure 3-9 B,C). Ultimately, five active fractions per pool with enriched activity were detected (Figure 3-9 B,C).

To identify proteins enriched in these active anion exchange chromatography fractions, as well as in two inactive fractions (as background control) ESI-MS/MS ion trap mass spectrometry was performed by our collaboration partners. Since previous results suggested that peripheral circadian oscillators communicate via paracrine pathways (see above and [61], [293]), resulting protein hits were filtered for human secreted proteins [362]. Those proteins contained in inactive background controls were considered impurities and removed from the list of active proteins, resulting in a limited number of secreted protein candidates (Figure 3-9 D-E). To further reduce the number of resulting hits, proteins were only considered potential “coupling factors” if they were present in at least 7 out of the 10 active fractions. Isoform specificity was disregarded because conventional mass spectrometry approaches often fail to clearly assign protein isoforms based on peptide information [363]. PSG (pregnancy-specific glycoprotein), SFRP (selected frizzled-related protein), SMOC (SPARC-related modular calcium binding protein), and TGFB (transforming growth factor beta) were identified as candidate coupling factors (Figure 3-9 D,E). Interestingly, except for PSGs, all candidate factors have been indicated in direct or ECM dependent cell-cell communication. However, only TGF-β signaling pathways has been described to interact with the circadian clock machinery [335], [339], [340].

Overall, findings indicate that active conditioned medium components are proteins. Moreover, consistent with previous results, indicating that secreted molecules mediate intercellular coupling, as well as due to its a priori role as paracrine signaling factor and known interaction with the circadian clock machinery, TGF-β appeared to be a likely candidate coupling factor.

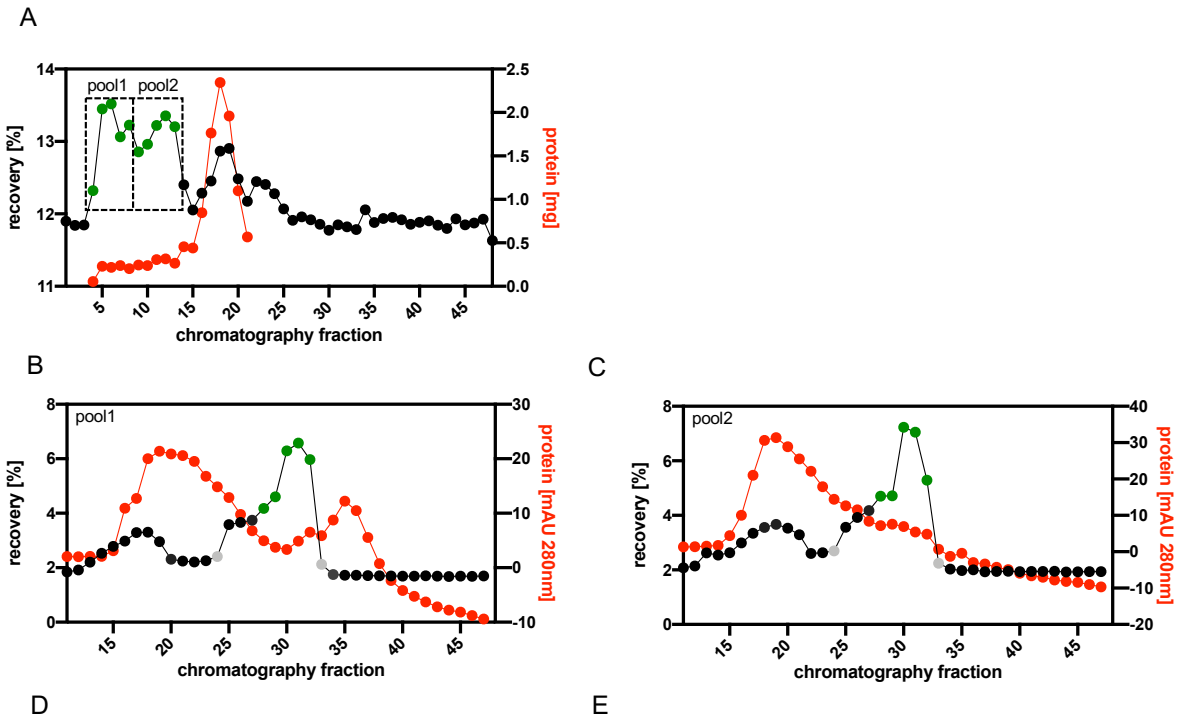

D

28	29	30	31	32
ACACB	ACACB	ACACB	AGK	CCBE1
AGK	CCBE1	CCBE1	HYOU1	CEP89
CEP89	CEP89	FGFR1	ITIH2	FGFR1
FGFR1	HEXB	FGFR2	TGFB2	FGFR2
FGFR2	PDGFD	FGFR3		FGFR3
FGFR3	PSG1	FGFR4		FGFR4
FGFR4	PSG3	FRAS1		FRAS1
HEXB	PSG4	PPT1		PDGFD
MYL1	PSG6	PSG1		PSG1
PSG1	SFRP1	PSG3		PSG3
PSG3	SMOC1	PSG4		PSG4
PSG4	TGFB2	PSG6		PSG6
PSG5		PSG7		PSG7
PSG6		PSG9		PSG9
PSG8		SFRP1		QSOX1
SFRP1		SMOC1		SAR1A
SMOC1		TGFB2		TGFB2
TGFB2				

E

28	29	30	31	32
CDHR1	APOM	APOM	APOM	APOM
CSN2	ATMIN	BCAM	CSN2	DAG1
CSN3	CDHR1	CSN3	LRP1	FRAS1
FSTL1	CSN3	DAG1	MMP3	L1CAM
HEXB	HEXB	HYOU1	PSG1	LRP1
HYOU1	HYOU1	LRP1	PSG3	LUM
PSMD1	MATR3	MMP3	PSG4	PSG1
RCN2	OS9	OS9	PSG6	PSG3
SFRP1	PSMD1	PSG3	PSG7	PSG4
SMOC1	RCN2	PSG4	PSG9	PSG6
TGFB2	SFRP1	RCN2	RCN2	RCN2
	SMOC1	SFRP1	SDC1	SDC1
	TGFB2	SMOC1	SEPT9	SMOC1
		TGFB2	SFRP1	TGFB2
			SMOC1	XYLT2
			TGFB2	
			TOR1B	

Figure 3-9: Active and secreted CM factors identified by chromatography and mass spectrometry

To identify active conditioned medium components, chromatography and mass spectrometry of CM was performed by our collaboration partners at the Max Planck Institute for Infectious Biology (Berlin, GER) as described. Fraction activity was determined by stimulation of U-2 OS 7xCRE:Luc cells and resulting protein hits filtered for components of the human secretome (as described in methods). **(A)** Quantification of recovered activity of gel filtration chromatography fractions relative to input, as well as of protein content (green=active fractions used for anion exchange chromatography, black=inactive fractions, red=protein content determined by BCA assay). **(B-C)** Quantification of recovered activity of anion exchange chromatography fractions relative to input, as well as of protein content (green=active fractions analyzed by MS, grey=inactive fractions analyzed by MS, black=inactive fractions, red=protein content approximated by absorption at 280 nm). **(D-E)** Active secreted protein hits identified in anion exchange chromatography fractions #28-32 of gel filtration chromatography pool1 (D) and pool2 (E) (red=hits common to at least 7 active fractions across pool1 and pool2).

3.5 Secreted TGF-β is important for normal circadian dynamics

Transforming growth factors beta (TGF-β1/2/3) are secreted growth factors driving the intracellular activation of SMAD transcription factors, which have been shown to regulate growth, proliferation, motility, and apoptosis [364]. TGF-β and SMAD transcription has been described to be regulated rhythmically by CLOCK/BMAL1 binding to their E-box enhancer elements (for details see 1.6). Moreover, TGF-β has been shown to feed back to the molecular clock machinery and to phase shift circadian rhythms in a time dependent manner [339].

Chromatography and mass spectrometry helped to identify TGF-β as one of the active CM factors. To test whether TGF-β is required for CRE driven luciferase expression in response to CM, U-2 OS 7xCRE:Luc reporter cells were stimulated with CM containing an αTGF-β1/2/3 antibody (neutralization), or CM immunodepleted of TGF-β. Both, neutralization and immunodepletion of TGF-β attenuated CM dependent CRE activation (Figure 3-10 A,B), indicating that TGF-β is indeed required for CM activity. To further test the role of TGF-β as active conditioned medium component, recombinant human TGF-β was used to activate CRE dependent transcription. Indeed, recombinant TGF-β induced CRE transcriptional activation in a dose dependent manner (Figure 3-10 E), strengthening its role as active CM component. Interestingly, compared to recombinant TGF-β1 and TGF-β2, CRE responses to TGF-β3 were weaker and not dose-dependent (Figure 3-10 C,D), suggesting that signaling pathways upstream of CRE activation show TGF-β isoform specificity.

If TGF-β, as active CM factor, also functions as interoscillator communication factor, it is predicted to phase shift circadian rhythms by modulating the expression of the molecular clock gene machinery. In 2008, Kon et al. demonstrated that TGF-β stimulation results in time dependent phase responses of rat fibroblasts [339]. To test whether described phase responses may be mediated by the immediate early induction of *PER2/Per2* expression, as observed for CM (Figure 3-6 A), U-2 OS cells were exposed to a 2 hour pulse of recombinant TGF-β 16 hours post-synchronization. Indeed, a significant increase in *PER2* transcript levels was observed upon TGF-β

stimulation (Figure 3-10 E), suggesting that TGF-β may mediate phase shifts of circadian rhythms by activating immediate early and CRE driven *PER2* expression.

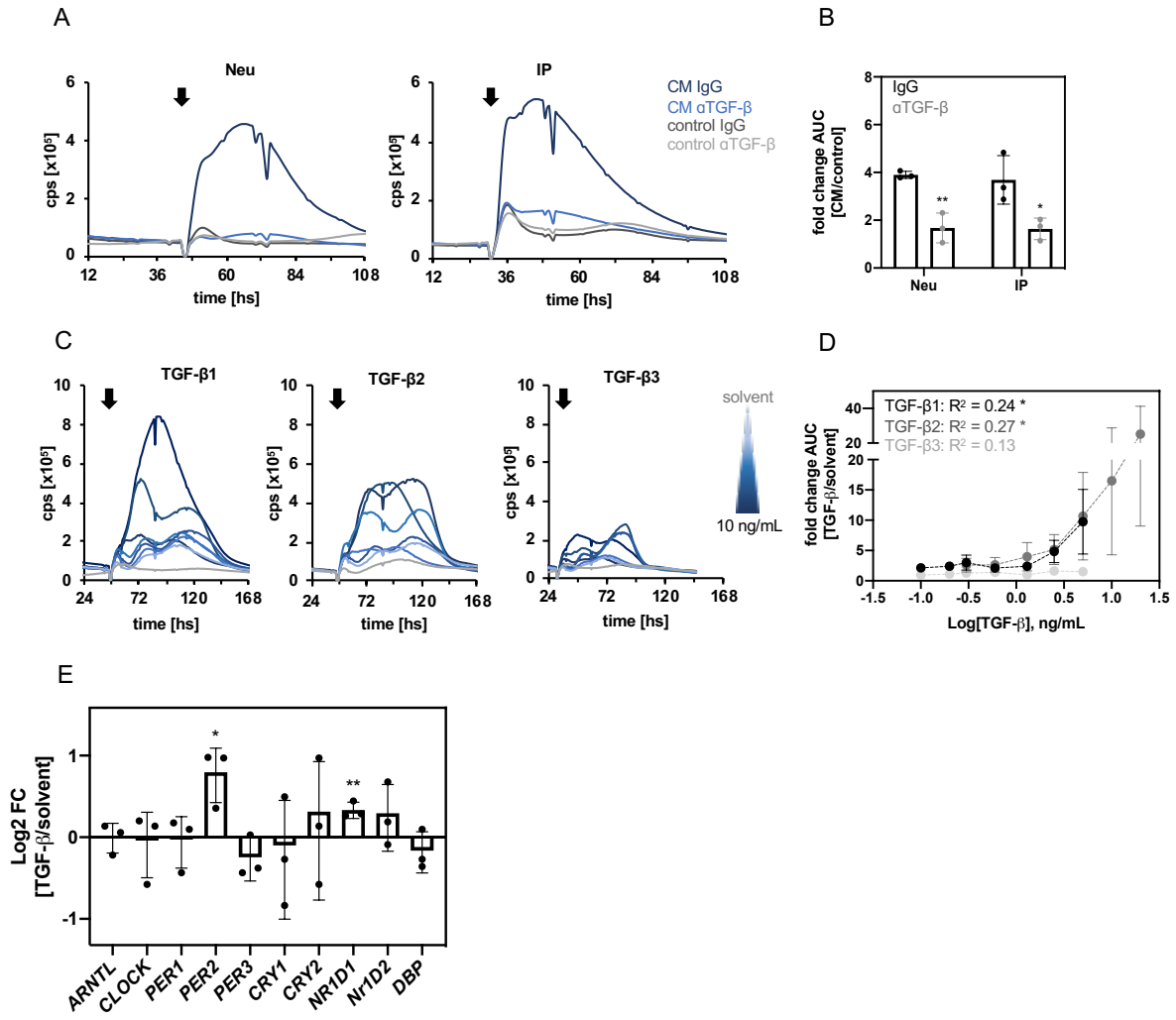

Figure 3-10: TGF-β acts as active CM factor with respect to CRE activation and *PER2* induction

To validate that TGF-β acts as active conditioned medium factor, depletion and stimulation experiments, as well as transcript analysis were performed in U-2 OS cells. **(A,B)** αTGF-β1/2/3 was used to neutralize or immunodeplete TGF-β from CM and U-2 OS 7xCRE:Luc reporter cells were stimulated as described. **(A)** Raw time series of a representative experiment upon stimulation of 7xCRE:Luc reporter cells with αTGF-β1/2/3 or IgG treated medium (Neu=neutralization, IP=immunodepletion by pull-down). **(B)** Quantification of luciferase signal induced by CM relative to control medium (n=3 repeat experiments with 3 technical replicates each, mean ± SD, individual values displayed, Unpaired one-tailed student's t-test against respective IgG group: *p<0.05, **p<0.01). **(C,D)** Dilution series of recombinant TGF-β1/2/3 was prepared in serum-free medium and used to stimulate U-2 OS cells expressing a 7xCRE:Luc reporter gene as described. **(C)** Raw time series of a representative experiment upon stimulation of 7xCRE:Luc reporter cells with recombinant TGF-β1/2/3. **(D)** Quantification of luciferase signal induced by TGF-β1/2/3 relative to solvent (n=3 repeat experiment with 3 technical replicates each, mean ± SD,

linear regression test: *p<0.05). **(E)** U-2 OS cells were stimulated with 20 ng/mL recombinant TGF-β2 16 hours post-synchronization (2 hour incubation time). RNA was harvested and transcript levels quantified as described. **(E)** Quantification of mRNA expression changes upon stimulation of U-2 OS cells with TGF-β2 relative to solvent (n=3 repeat experiment with 3 technical replicates each, measured in triplicates, normalized to *GAPDH*, mean ± SD, individual values displayed, Unpaired tow-tailed student's t-test against H_0: Log2FC=1: *p<0.05, **p<0.01).

If TGF-β and its associated signaling pathway are contributing to intercellular coupling among peripheral circadian oscillators via CRE dependent immediate early transcription of *PER2*, the following predictions can be made: (i) TGF-β signaling promotes robust circadian rhythmicity, i.e. high-amplitude and lowly damped oscillations, (ii) TGF-β signaling drives the transcriptional activation of CRE enhancer elements, and (iii) TGF-β signaling induces phase shifts of circadian rhythms. To test this, genetic and pharmacological perturbation experiments were performed.

Firstly, an RNA interference (RNAi) screen targeting extracellular, as well as intracellular components of the TGF-β signaling pathway was conducted. For each target gene, multiple (if available) short hairpin RNA (shRNA) constructs were chosen, which mediate gene silencing via RNAi dependent mechanisms following lentiviral delivery into U-2 OS reporter cells. Silencing of *SKI* (Ski oncogene), *SMAD4* (mothers against decapentaplegic homolog), and *TGFBR1* (TGF-β receptor type 1 or ALK5) resulted in significantly attenuated CRE responses upon conditioned medium activation for at least for one of the constructs tested (Figure 3-11 A,B). Oppositely, silencing of *ITGAV* (integrin αV) resulted in significantly increased CRE responses (Figure 3-11 A,B), likely by increasing the responsiveness to externally applied TGF-β when the release of active TGF-β from its endogenous latent pool is disturbed. Even though not significant, similar effects were observed for *LTPB1* (latent TGF-β binding protein), which is also required for the release of active TGF-β from its latent complexes. Moreover, silencing of all these genes resulted in decreased amplitudes and/or increased damping of U-2 OS *Bmal1*:Luc oscillations (Figure 3-11 C,D and Figure 6-5 A). Interestingly, a negative correlation between amplitude and damping was observed globally for knock-down of TGF-β signaling pathway components (Figure 3-11 C), which may imply that knock-downs resulting in reduced amplitudes also result in network desynchronization rather than changes of single cell oscillations.

While SKI and SMAD4 proteins are activated downstream of TGF-β receptor, constituting intracellular components of the canonical TGF-β signaling pathway, integrin αV and TGFBR1 (ALK5) are required for extracellular release and signaling of active TGF-β (for details see 1.6). Thus, results suggest that both, extracellular distribution of TGF-β and canonical TGF-β signaling play an important role for conditioned medium dependent activation of CRE driven transcription, as well as for normal circadian rhythmicity. The finding that silencing of *SKI, SMAD4, TGFBR1*, and *ITGAV* resulted in altered CRE activation, as well as reduced amplitudes and/or increased damping supports the hypothesis that paracrine coupling factors promote interoscillator synchronization via the downstream activation of CRE driven transcription (eventually of *PER2/Per2*).

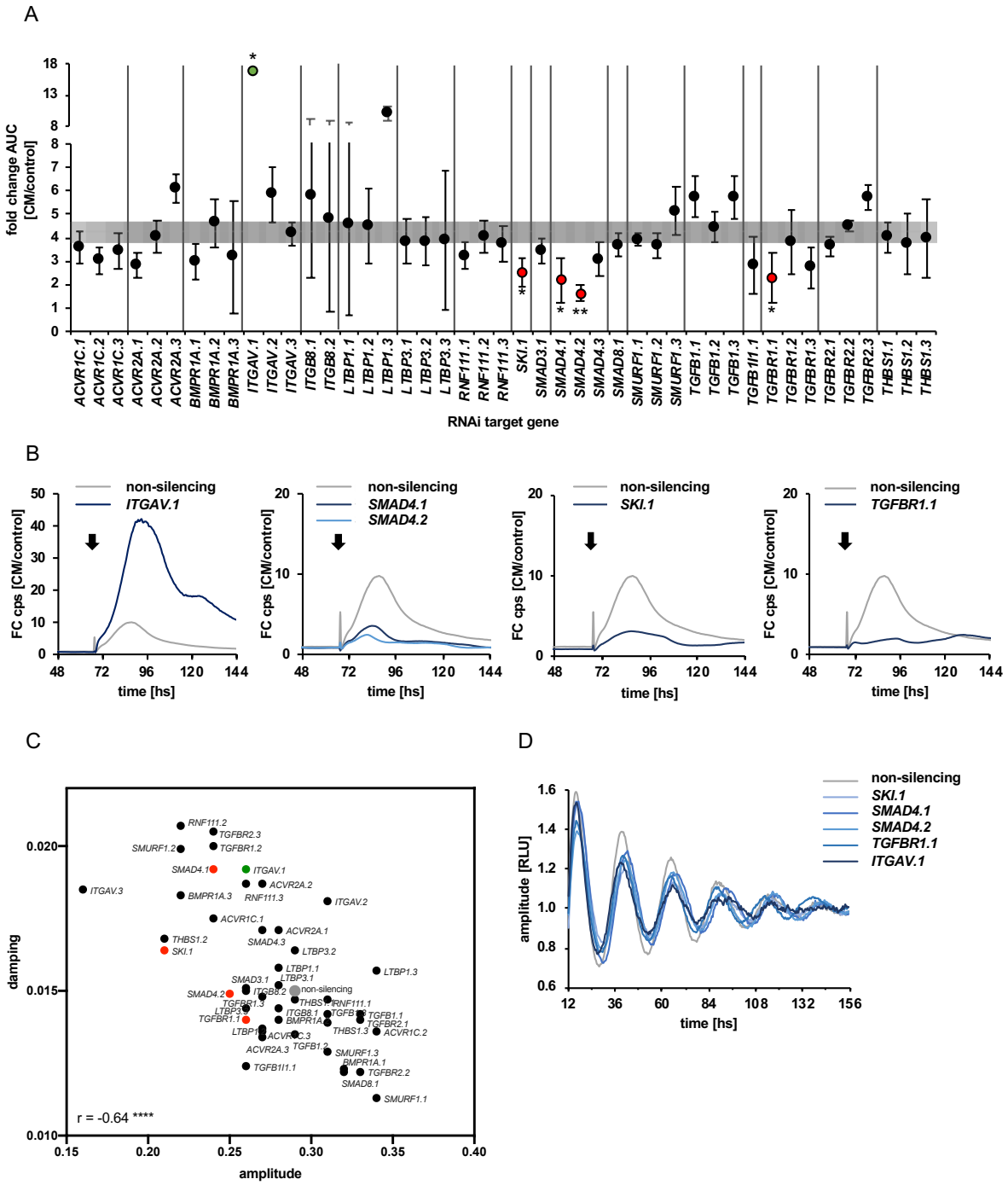

Figure 3-11: Genetic perturbation of TGF-β signaling alters CRE transcriptional activation and circadian dynamics

To test whether TGF-β signaling pathway is required for CRE transcriptional activation and coherent circadian dynamics, an RNAi knock-down screen of TGF-β signaling pathway components was performed in U-2 OS 7xCRE:Luc and *Bmal1*:Luc cells (as described in methods). 7xCRE:Luc reporter cells were stimulated with conditioned and control medium and fold change AUC quantified as described. *Bmal1*:Luc reporter cells were synchronized, and luciferase activity was continuously monitored. **(A)** Quantification of luciferase signal induced by CM relative to control medium upon knock-down of indicated genes, red=significantly attenuated CRE response to CM, green=significantly

enhanced CRE response to CM, grey shaded area=mean ± 2SD of non-silencing controls. (n=4 biological repeat experiments with 2 technical replicates per shRNA construct, mean ± SD, Multiple t-test against non-silencing group with Holm-Sidak multiple testing correction: *p<0.05, **p<0.01). **(B)** Normalized time series of a representative experiment upon conditioned and control medium stimulation of *ITGAV, SMAD4, SKI*, and *TGFBR1* 7xCRE:Luc knock-down cells. **(C)** Correlation plot of amplitude and damping parameters of *Bmal1*:Luc oscillations upon knock-down of indicated genes, red=significantly attenuated CRE response to CM, green=significantly enhanced CRE response to CM, grey=mean of non-silencing controls (as in (A)). (n=4 biological repeat experiments with 2 technical replicates per shRNA construct, means displayed, Pearson correlation test: ****p<0.0001). **(D)** Detrended time series of a representative experiment upon knock-down of *ITGAV, SMAD4, SKI*, and *TGFBR1* in *Bmal1*:Luc reporter cells.

Secondly, a selective small molecule inhibitor was used to block TGF-β type I/type II receptors. This inhibitor, called LY2109761, completely and specifically blocks the kinase domain of TGFBR1 (ALK5) and prevents the intracellular transmission of TGF-β signals [365]. Comparable to genetic perturbation, pharmacological inhibition of TGF-β signaling resulting in the attenuation of CM dependent CRE activation (Figure 3-12 A,B), as well as amplitude reduction and increased damping of U-2 OS *Per2*:Luc oscillations (Figure 3-12 C-E) in a dose-dependent manner. Again, this suggests that functional TGF-β signaling promotes robust network rhythmicity (high amplitudes, low damping), potentially by inducing interoscillator phase coherence via CRE transcriptional activation. Additionally, dose dependent period lengthening was observed upon TGF-β receptor inhibition (Figure 6-6 A), an effect that has been described before for sparse and presumably uncoupled networks, as well as upon perturbation of secretory pathway [293].

Based on calculated EC_{50} values, inhibition of TGF-β signaling appeared to more effectively block CRE transcriptional activation than to perturb circadian dynamics. We suspect that this may be a consequence of the complexity of circadian rhythm generation. While CRE activation is regulated directly downstream of TGF-β receptor activation, circadian oscillations are driven by complex transcriptional-translational feedback loops. Moreover, other than for CRE induction, intercellular coupling may render circadian rhythms more robust, thereby reducing LY2109761 efficacy.

Interestingly, significantly or a trend towards reduced amplitudes, increased dampening, and lengthened circadian periods upon pharmacological perturbation of TGF-β signaling was also observed for a number of peripheral tissue explants derived

from PER2::LUC mice (Figure 6-5 B-E). This may support the hypothesis that peripheral coupling via TGF-β signaling is conserved across species and tissues.

Thirdly, as mentioned above, TGF-β stimulation has been shown to phase shifts rat fibroblasts in a time dependent manner Kon et al. (2008) (Figure 4-1), suggesting that TGF-β may act as Zeitgeber for peripheral circadian oscillators. Thus, to test whether observed phase responses to conditioned medium (Figure 3-5) may be mediated by TGF-β, TGF-β receptor inhibitor was used to block TGF-β signaling pathway during CM stimulation of U-2 OS *Bmal1*:Luc circadian reporter cells. Again, stimulation was performed at the trough of *PER2* (inferred from the nearly anti-phasic *Bmal1*:Luc expression) because U-2 OS reporter cells had displayed strongest phase responses to conditioned medium at this time. Indeed, phase shifts in response to CM stimulation were significantly attenuated when TGF-β signaling was inhibited, suggesting that TGF-β acts as active CM medium factor, mediating phase responses of peripheral circadian oscillators.

Overall, consistent with theoretical models of decoupled oscillator networks, amplitudes were reduced, and damping was increased upon genetic and pharmacological perturbation of TGF-β signaling. This suggests that TGF-β promotes coupling among single cell peripheral oscillators, as well as coherent network rhythmicity. Moreover, TGF-β was identified as active conditioned medium factor mediating CRE activation and immediate early *PER2* expression. Additionally, genetic and pharmacological disruption of TGF-β signaling pathway was shown to interfere with the transcriptional activation of CRE sites, as well as phase responses to CM. This supports the hypothesis that TGF-β functions as paracrine signaling factor inducing phase synchronization among adjacent oscillators via the CRE driven immediate early induction of *PER2/Per2*. Moreover, based on the effect of TGF-β receptor inhibitor on circadian dynamics of peripheral tissue explants from PER2::LUC animals, it may be possible that the potential role of TGF-β as peripheral coupling factor is conserved across human and murine species, as well as across different peripheral tissues.

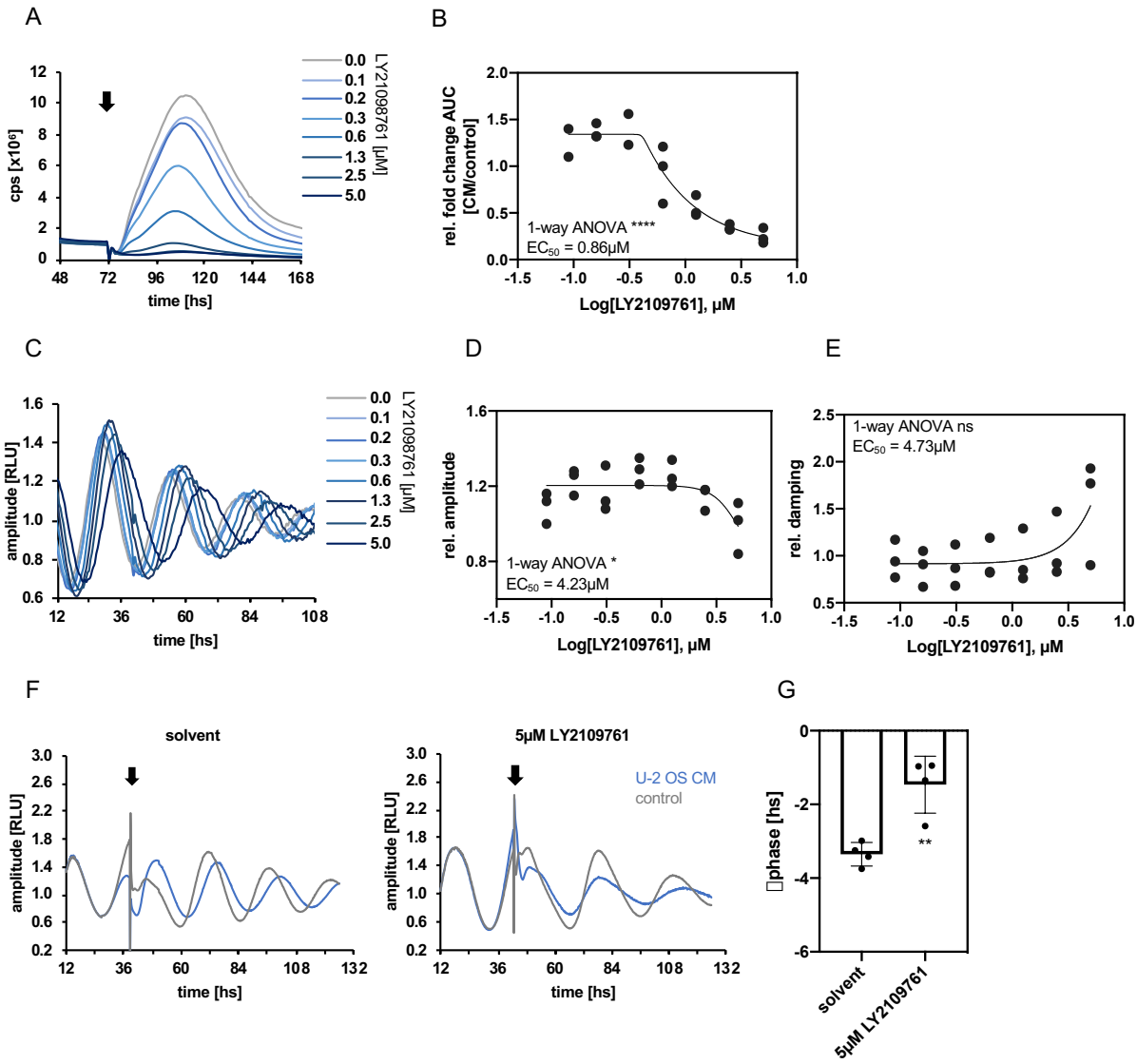

Figure 3-12: Pharmacological perturbation of TGF-β signaling alters CRE transcriptional activation, circadian dynamics, and phase responses to CM

To test whether TGF-β signaling pathway is required for CRE transcriptional activation, coherent circadian dynamics, as well as phase responses to CM, a pharmacological TGF-β receptor inhibitor (LY2109761) was used. LY2109761 dilution series and data analysis, as well as medium stimulations were performed as described. **(A)** Raw time series of a representative experiment of CM dependent CRE transcriptional activation upon increasing concentration of LY2109761. **(B)** Quantification of luciferase signal induced by CM relative to control medium following normalization to their respective solvent control (n=3 repeat experiments with 2-3 technical replicates each, individual values and asymmetric sigmoidal fit displayed, One-way ANOVA: ****p<0.0001 and non-linear regression fit of an asymmetric sigmoidal model). **(C)** Detrended time series of a representative experiment of *Per2*:Luc oscillations upon addition of increasing concentration of LY2109761. **(D,E)** Quantification of amplitudes (D) and damping (E) of circadian oscillations relative to the respective solvent control (n=3 repeat experiments with 3 technical replicates each, individual values and asymmetric sigmoidal fit displayed, One-way ANOVA: *p<0.05 and non-linear regression fit of an asymmetric sigmoidal model). **(F)**

Detrended time series of a representative experiment of CM dependent *Bmal1*:Luc phase shifts following inhibition of TGF-β receptor. **(G)** Quantification of phase shifts induced by CM relative to control medium with or without LY2109761 (n=4 repeat experiments with 6-8 technical replicates each, mean ± SD, individual values displayed, Unpaired one-tailed student's t-test against solvent group: **p<0.01).

3.6 TGF-β signaling pathway promotes intercellular coupling

Described findings suggested that peripheral circadian oscillators weakly couple with each other to establish (partially) synchronized networks rhythms. Moreover, TGF-β signaling pathway appeared to be involved in the maintenance of such synchronized network rhythms. In agreement with the Kuramoto model, progressive phase synchronization can result in transitions from incoherent to coherent (coupled) network states. Thus, we suggest that TGF-β may act as peripheral coupling factor mediating phase synchronization among single cell oscillators by the temporally gated induction of CRE enhancer element and immediate early expression of *PER2/Per2*.

Previous co-culture experiments of low-density, low-amplitude, highly damped U-2 OS reporter cells with increasing numbers of non-reporter cells showed that co-culture results in amplitude expansion and decreased damping of the reporter cell population in a density dependent manner (Figure 3-4). We assumed that amplitude increases, and damping decreases are due to intercellular coupling leading to amplitude resonance and decreased desynchronization of the co-cultured populations. To test whether of TGF-β signaling mediates these (coupling) effects, co-cultures were performed upon pharmacological inhibition of TGF-β receptor.

While solvent controls displayed density dependent increases in amplitudes of low-density U-2 OS *Bmal1*:Luc reporter cells (as seen in Figure 3-4), TGF-β receptor inhibition abolished density dependent amplitude expansion (Figure 3-13 A,B). This suggests that disruption of TGF-β signaling results in a reduction of intercellular coupling and thus attenuation of amplitude resonance effects among coupled (frequency-locked) oscillators. However, oppositely to expectations, TGF-β receptor inhibition resulted in larger absolute amplitudes, especially for low co-culture numbers (Figure 3-13 A,B). We suspect that amplitude increases are an artifact of dexamethasone synchronization prior to recording. Since TGF-β receptor inhibitor was

added to the co-cultures already during seeding (one day prior to recording), it appears likely that cells were already desynchronized when dexamethasone was applied. Consistent with theoretical predictions, reduced network synchrony enhances the susceptibility to Zeitgeber pulses [57], thereby leading to stronger dexamethasone responses when intercellular coupling is disturbed. This assumption is further supported by increased damping of *Bmal1*:Luc rhythms upon TGF-β receptor inhibition (Figure 3-13 A,C), suggesting that, following initial (dexamethasone) synchronization, disruption of TGF-β signaling results in even faster desynchronization of single cell oscillators within the co-cultured ensemble. Alternatively, absolute amplitude increases could be a consequence of stronger intercellular coupling upon perturbation of TGF-β signaling. This however is not consistent with previous observations and appears unlikely.

If TGF-β signaling promotes intercellular coupling and synchronized rhythmicity, it should render oscillator networks more robust against perturbation by Zeitgeber stimuli. Thus, as described above, oscillator ensembles are expected to respond to Zeitgeber pulses with larger phase shifts upon perturbation of TGF-β signaling. To test this U-2 OS *Bmal1*:Luc circadian reporter cells were subjected to a 20°C temperature pulse following pharmacological inhibition of TGF-β receptor. Indeed, compared to control, perturbation of TGF-β signaling resulted in much larger phase shifts of circadian oscillations following an 8 hour 20°C temperature pulse (Figure 3-13 D,E). This suggests that TGF-β signaling promotes intercellular coupling and thus robust networks rhythmicity. Interestingly however, reducing culture density alone did not increase susceptibility to the applied temperature pulse and strong phase responses were only observed upon additional TGF-β receptor inhibition (Figure 6-7 A,B). This result was unexpected because, consistent with previous findings, sparse oscillator networks were assumed to be less coupled and therefore more susceptible to perturbation by a Zeitgeber pulse. We suspect that, relative to residual intercellular coupling among sparsely cultured U-2 OS cells, the applied temperature pulse was only a weak Zeitgeber. Therefore, additional disruption of intercellular coupling by TGF-β receptor inhibition would be required to elicit temperature responses in both, dense and sparse peripheral oscillator networks. Additionally, timing of the temperature pulse may not have been optimal. Based on the conditioned medium PRC, the trough of *PER2* expression (inferred from nearly anti-phasic *Bmal1:Luc*

expression) was chosen as timepoint of the temperature pulse. Nevertheless, since temperature dependent phase resetting depends on other input routes than CM, e.g. via heat shock proteins binding to HSE sites, PRCs may differ. Thus, density effects on intercellular coupling and on responses to Zeitgeber stimuli may become more apparent at timepoints when temperature induced shifts are maximal.

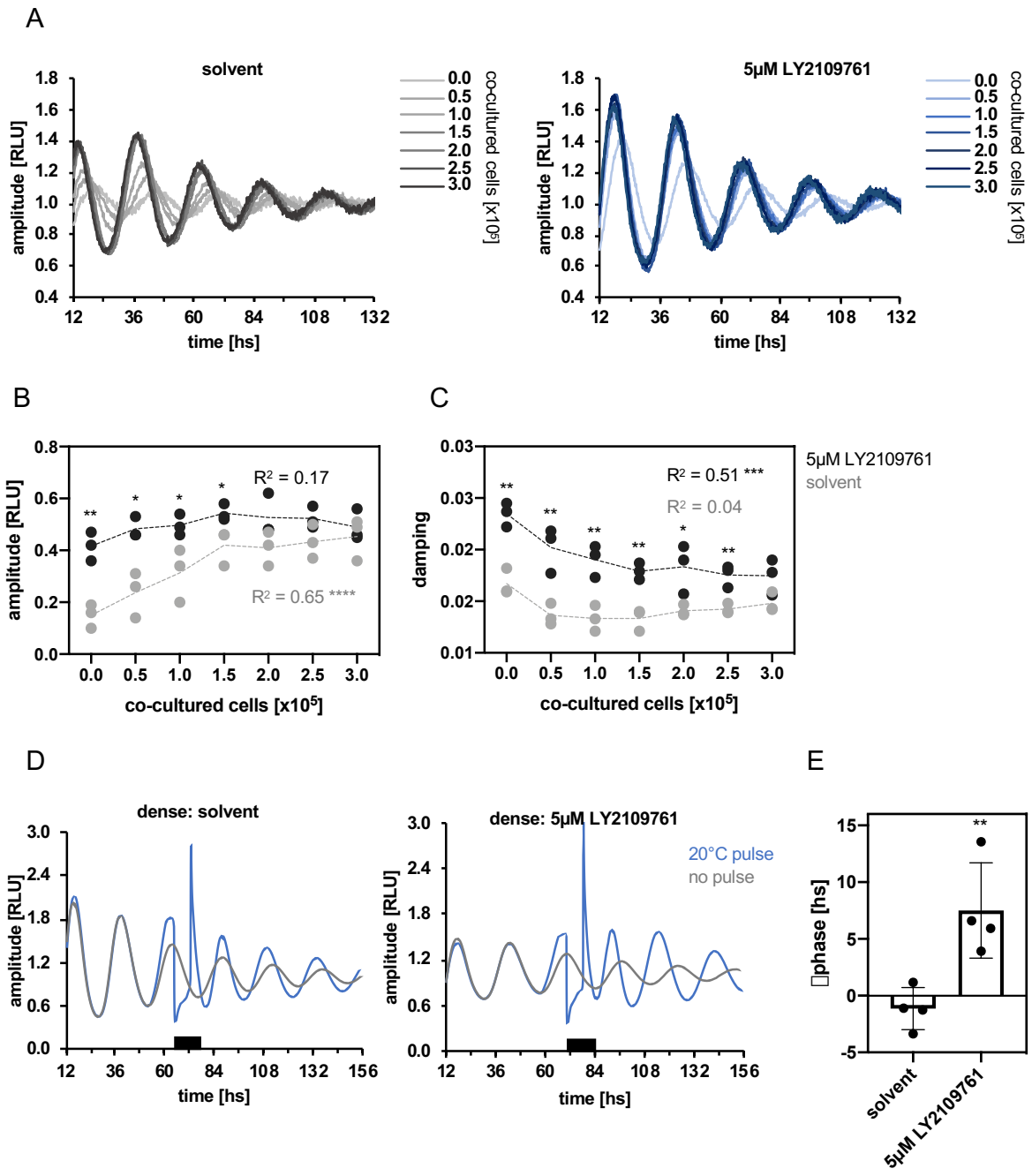

Figure 3-13: Pharmacological perturbation of TGF-β signaling attenuates intercellular coupling

TGF-β receptor inhibitor (LY2109761) was used to assess whether perturbation of TGF-β signaling attenuates intercellular coupling, as characterized by a lack of amplitude resonance, increased damping and increased susceptibility to perturbation by Zeitgeber pulses. **(A-C)** Co-cultures of sparse (0.3 x10^5

cells/dish) U-2 OS *Bmal1*:Luc reporter cells with increasing numbers of non-reporter cells were seeded into 35-mm dishes. TGF-β receptor inhibitor was applied during seeding and bioluminescence imaging. Co-cultures were synchronized, and luciferase activity continuously monitored. **(A)** Detrended time series of a representative co-culture experiment with or without TGF-β receptor inhibitor. **(B,C)** Quantification of amplitudes (B) and damping (E) of *Bmal1*:Luc oscillations under co-culture conditions and upon treatment with TGF-β receptor inhibitor or solvent control (n=3 repeat experiment with 2 technical replicates, individual values and connecting line displayed, linear regression test and Unpaired one-tailed student's t-test against respective solvent groups: *p<0.05, **p<0.01). **(D,E)** U-2 OS cells harboring a *Bmal1*:Luc reporter gene were seeded at high density (3.0 x10^5 cells/dish) into 35-mm dishes with or without TGF-β receptor inhibitor. An 8 hour, 20°C temperature pulse was applied at the inferred trough of *PER2* expression (nearly anti-phasic to *Bmal1*:Luc peak). **(D)** Detrended time series of a representative temperature pulse experiment with or without TGF-β receptor inhibitor. **(E)** Quantification of temperature induced phase shifts of *Bmal1*:Luc oscillations upon treatment with TGF-β receptor inhibitor or solvent control (n=4 repeat experiment with 2 technical replicates each, mean ± SD, individual values displayed, Unpaired one-tailed student's t-test against solvent group: **p<0.01).

Overall, these findings suggest that paracrine TGF-β signaling promotes robustness of circadian rhythmicity against perturbation by external Zeitgeber stimuli. Thereby, further supporting the role of TGF-β as potential intercellular coupling factor in peripheral oscillator networks.

4 Discussion

4.1 Peripheral coupling: state of the art

Mammalian circadian clocks are highly complex systems composed of molecular, cellular, tissue, and organismal oscillators. Coupling between oscillator entities occurs at every level of the circadian system. Multiple transcriptional-translational feedback loops are coupled to generate cell-autonomous and self-sustained circadian rhythm in gene expression [38], [40]. Cellular oscillators in the SCN are coupled to maintain synchronized, high amplitude, and robust rhythmicity of the tissue network [102], [366]–[368]. Peripheral tissue clocks are coupled to the SCN pacemaker to establish required phase-relationships between body clocks [35]. Moreover, weak coupling of rhythmic organism in social networks as been reported for mice, hamsters, flies and bees [369]–[373]. This multilayer clockwork guarantees the correct temporal organization of our endogenous rhythmic biological functions in constant exchange with rhythmic environmental and systemic Zeitgeber cues. Coupling promotes synchrony between individual oscillators at all levels of the mammalian circadian clock system and thus constitutes one if its integral features. Due to the inherent relationship between interoscillator coupling and circadian clock robustness (for details see 1.3 and 1.4), coupling largely influences entrainment behavior and response to Zeitgebers. Thus, very likely intercellular coupling on the level of tissue networks plays an important role for sustaining the right balance between temporal precision and plasticity of biological organ functions. However, while intercellular coupling in the SCN has been studied in detail, it remains highly debated whether or not oscillators within peripheral clock networks are able to couple with each other, how this coupling is achieved, and what its functional relevance may be.

Computational modeling of bioluminescence data from dispersed peripheral clock cells (i.e. primary fibroblasts and hepatocytes) yielded indications that peripheral oscillators display phase distributions in compliance with models of weakly coupled networks [62], [63]. However, both studies reported that the observed phase coupling was insufficient to synchronize oscillators, consistent with findings from co-culture experiments of fibroblasts and explanted tissues [47], [137]. In 2013, Noguchi et al. demonstrated that single cell rhythmicity of fibroblasts depends on cell density and exchange of paracrine

signals [61]. Additionally, evidence speaking for a functional connection between secretory pathway and circadian rhythms exists [293], [297]. Thus, published studies suggest that peripheral oscillators communicate via exchange of secreted (paracrine) factors to enhance circadian rhythmicity. Whether this intercellular communication serves to establish synchronized network rhythmicity remains disputed.

Intercellular coupling may be enhanced in vivo, where complex 3-dimensional microenvironments amplify cell-cell and cell-extracellular matrix interactions. In recent years the development of elaborated in vivo imaging techniques has enabled to study peripheral clock rhythms in living and SCN-lesioned animals. Experimental evidence suggests that peripheral circadian clocks, in vivo, are indeed able to sustain synchronized, yet low-amplitude, oscillations independently of the SCN or rhythmic external Zeitgebers, i.e. under constant housing conditions [36], [90]. To what extend these peripheral oscillations depend on other functional body clocks outside the SCN or rhythmic external signals of unknown source is not clear. Progress in addressing these questions has been made last year. Groups have investigating circadian rhythmicity on transcript, protein, and metabolite level in isolated peripheral clocks of animals, which harbor functional clocks only in the liver or in the skin [244], [245]. While both studies reported that reconstitution of liver/skin clocks in otherwise clock-less animals is sufficient to re-establish circadian tissue oscillations under light-dark cycles, rhythms were lost in constant conditions, i.e. constant darkness, ad libitum feeding, arrhythmic activity. The authors interpreted this as inability of isolated peripheral clocks to maintain synchronized rhythmicity independently of external Zeitgeber or other body clocks and thus as lack of intercellular coupling. However, failure to detect rhythmicity on transcript level in isolated peripheral clocks may have been a consequence of their experimental approach: cross-sectional time series sampling uses one or multiple animals per timepoint to determine rhythmicity of the population. Moreover, unpublished results from this year (personal communication, conference presentations) indicate that isolated peripheral circadian clocks, in vivo, are indeed able to sustain synchronized low-amplitude oscillations for long durations. Investigators reported that in vivo bioluminescence oscillations of livers in individual liver-only clock mice housed under constant conditions can be detected for up to 30 days.

Overall, intercellular coupling among peripheral circadian oscillators remains a controversial topic in chronobiological research. Existing evidence implies that even though peripheral oscillators communicate via paracrine pathways and weakly couple with each other, this may be insufficient to maintain globally synchronized network rhythmicity in vitro. In vivo, peripheral circadian clocks have been shown to maintain synchronized rhythmicity under constant conditions and independently of the SCN. However, whether this depends on intercellular coupling or on rhythmic input from other functional body clocks, as well as whether coupling in the periphery may be of relevance for circadian tissue functions remain open questions of the field.

4.2 Key findings discussed

This research project was aiming at elucidating molecular mechanisms of intercellular coupling among peripheral circadian oscillators (in vitro) to: (i) gather additional experimental evidence for coupling in peripheral clock networks, and (ii) discover peripheral coupling pathway(s) to provide a starting point for the targeted manipulation and functional characterization of coupling among peripheral oscillators in vitro and in vivo. We decided to use U-2 OS cells to study peripheral coupling because they constitute a well-characterized model system in chronobiology, represent an isolated peripheral oscillator network, as well as because this cell line has not been used for coupling studies before.

4.2.1 Peripheral circadian oscillators are coupled

In this study we present results showing that co-cultures of U-2 OS cells display characteristics of coupling on the population level: phase-pulling (Figure 3-3 A-D and Figure 6-2 A-H), frequency-pulling (Figure 3-3 E-H), amplitude expansion (Figure 3-4 A,B and Figure 3-4 D,E), and reduction of damping (Figure 3-4 A,C and Figure 3-4 D,F). In agreement with theoretical predictions [57], [156], [157], [172] this behavior supports the hypothesis that peripheral circadian oscillators couple intercellularly to establish synchronized network rhythmicity. Additionally, circadian rhythmicity of U-2 OS ensembles, with respect to amplitude and damping as well as clock gene expression levels were found to depend on culture density. Sparse U-2 OS cultures displayed reduced amplitudes (Figure 3-1 A,B and Figure 6-1 A,B), increased damping

(Figure 3-1 A,C and Figure 6-1 A,C), and transcriptional suppression of a number of core clock genes (Figure 3-2 A). These effects were accompanied by global transcriptomic changes in sparse versus densely cultured cells (Figure 3-2 B-F). While transcripts associated with DNA/RNA binding were upregulated, transcripts associated with ECM structure and extracellular signaling activity were downregulated (Figure 3-2 D-F). Together these results suggest that peripheral circadian oscillators require paracrine signals from neighboring cells in order to couple with each other and establish robust network rhythmicity at the genotypic and phenotypic level.

Cell density, circadian rhythmicity, and intercellular coupling

For coupled networks amplitudes are expected to increase due to resonance effects between phase- and frequency-locked oscillators [57], [172], [355]. Moreover, damping of oscillator ensembles is commonly accepted to result from desynchronization among heterogenous single cell oscillators, rather than from damping of cell-autonomous rhythms.

In agreement with Noguchi et al. (2013) [61], our findings show that high-amplitude and lowly damped rhythms of U-2 OS cells depend on cell density (Figure 3-1). On the population level, this may suggest that coupling results in amplitude resonance and decreased desynchronization between single cell oscillators. Nevertheless, we have to admit that population imaging cannot clearly distinguish between changes of cell intrinsic oscillations and desynchronization of the network. However, we suggest that both concepts may not be mutually exclusive. Co-dependency of single cell rhythmicity and network synchrony has been demonstrated for neurotransmitter dependent coupling in the SCN [374]. Noguchi et al. demonstrated that poor rhythmicity of sparse fibroblasts can be rescued by supplementing them with secreted factors (CM) from high-density cultures [61]. Moreover, emergence of circadian oscillations in differentiating cells has been related to the threshold level expression of core clock genes [353]. Similarly, our data shows that sparse culture of U-2 OS cells results in weakened ensemble rhythms, as well as in the transcriptional downregulation of clock genes (Figure 3-2 A). This may suggest that coupling promotes the intercellular feedback dependent induction of core clock genes, thereby strengthening rhythmicity of single cell oscillators, while at the same time promoting interoscillator synchrony. However, if this is true and single cell rhythmicity and oscillator synchrony are co-dependent, then intercellular coupling would be difficult to quantify even with the help

of single cell imaging. Targeted perturbation of intercellular coupling (based on the mechanism we are presenting here) could help to separate these two effects.

In 2016, Feeney et al. reported that extracellular luciferin concentration affects circadian amplitude and phase of luciferase reporter cells (fibroblasts) [375]. Thus, to exclude that observed amplitude/damping effects are a result of varying number of luciferase reporter cells (consuming different amounts of extracellular luciferin), amplitude and damping were also quantified under co-culture conditions. Again, density dependent amplitude expansion and reduced damping was observed, suggesting that the low-density reporter cells couple with the non-reporter cell population. In 2009, O'Neill et al. suggested that increased oscillator coherence in "mature" (dense) fibroblast cultures is a consequence of cell-cell contact dependent quiescence leading to a reduction of phase dispersion introduced by cell division [355]. However, our results suggest that intercellular coupling of U-2 OS cells is independent on direct cell-cell contact, since amplitude expansion and reduced damping were still be observed for physically separated co-cultures (Figure 4-3 D-F). This further supports the hypothesis that peripheral circadian oscillators couple via the exchange of paracrine signals [61], [293]. Moreover, as mentioned before, contact-less co-culture appeared to render sparse reporter cells even more sensitive to paracrine coupling signals of the non-reporter cell population. How exactly this may be achieved remains elusive but manufacturers of the membrane inserts claim that inserts promote formation of tissue-like cellular structure and function [376]. Thus, it could be speculated that low-density circadian reporter cells, cultured on membrane inserts, show improved ability to form extracellular microenvironments. Indeed, RNA sequencing results suggested that ECM structure and extracellular signaling may be related to the density dependence of circadian rhythms. Additionally, Yang et al. (2017) reported that ECM stiffness regulates circadian rhythmicity in a cell-type dependent fashion [377]. For epithelial cells (like U-2 OS cells) it was suggested that soft microenvironments, opposed to stiff plastic dishes, promote high-amplitude circadian rhythmicity [378]. Whether or not membrane inserts play a role for observed effects could be tested by performing co-culture with vertical rather than horizontal membrane inserts. This way reporter and non-reporter cells populations could be separated while co-culturing both populations on the same surface.

Phase- and frequency locking

In order for high-amplitude, lowly damped network rhythmicity to be maintained, single cell oscillators need to synchronize with each other. Otherwise differences in cell-intrinsic (free-running) circadian periods would results in desynchronization over time. Theoretical models of collective synchronization, developed by Winfree and Kuramoto [209], [211], [379], describe that synchronization depends on the average phase and phase coherence of individual oscillators within a network. Models further predict proportionality between phase coherence among oscillators and coupling strength of the network (for all-to-all coupling) [136], [216]. Thus, synchronization will take place when oscillators become coherent enough for the coupling strength to cross a threshold value, quick-starting phase-locking of oscillators and producing a rhythmic mean field [212]. As discussed before, intercellular feedback leading to enhanced clock gene expression may be one mechanism of raising coupling strength to a critical threshold values, initiating synchronization of single cell oscillators.

For the SCN it has been shown that, following transient perturbation of intercellular coupling, neuronal oscillators quickly re-synchronize and assume the same phase as before perturbation [367]. Gonze et al. (2005) [213] interpreted this behavior as “intrinsic property of [coupled oscillator] networks to assume conserved phase-relationships with the mean field” [213]. This implies that for co-cultures of two differently phased oscillator populations (one of them harboring a circadian reporter gene), phase drifts of the reporter cells towards the phase of the mean field should be observed. Additionally, it appears likely that the mean phase will depend on the relative rations between both oscillator populations. Our experimental data support this idea: 6 hour phase different non-reporter cells exerted density dependent phase-pulling effects on the low-density reporter cell population (Figure 3-3 A-D). Moreover, as expected for weak coupling, observed phase-pulling effects (+1.4 and -2.4 hours) were smaller than predicted (~5 hours) from the weighted average of the cellular populations and decayed over time (Figure 6-2). In agreement with Guenthner et al. (2014) [89] and Rougemont et al. (2007) [62], our results suggest that peripheral oscillators display weak (undercritical) coupling. This means that interoscillator synchronization will be achieved once a critical coupling strength is reached, as well as that oscillators may transition between coherent and incoherent network states (partial synchronization). Indeed, in contrast to Guenthner and Rougemont, who reported that intercellular

coupling among fibroblasts and hepatocytes does not result in oscillator synchronization, U-2 OS cells displayed at least partial network synchronization. We suspect that either U-2 OS cells are more strongly coupled than fibroblasts and hepatocytes per se, or that experimental conditions resulted in different intercellular coupling strength. For example, single cell imaging requires more sparsely cultured cells than population imaging, suggesting that coupling strength was reduced. Moreover, hepatocytes were cultured in collagen gel sandwiches, which may influence coupling due altered cell-cell and cell-ECM connectivity.

Interestingly, our findings also show that phase-pulling effects are bidirectional (Figure 3-3 A-D), suggesting that intercellular coupling enables the transmission of time information regarding the oscillatory state of neighboring cells. However, why reporter cells appeared to be more resistant to phase-pulling towards earlier phases remains unclear. In humans, light induced phase advances of melatonin and behavioral rhythms have been demonstrated to be more difficult than phase delays [380]–[383], likely because the average free-running period is > 24 hours, promoting delays. In 2005, Gonze et al. reported that intercellular coupling induces period lengthening of the mean field [213], which may explain why coupling promotes phase delays. However, other models have predicted different effects of coupling on the network period [214]. Moreover, transience of observed phase-pulling effects may be explained by mixed states of un- and coupled oscillators, which may arise from differences in coupling strength, e.g. due to period fluctuations modulating the critical coupling threshold over time (as described in [62], [136]).

According to Winfree and Strogatz, “transitions from uncoupled to coupled states will occur if coupling overcomes oscillator incoherence caused by large differences in intrinsic periods, setting a in motion a positive feedback between phase coherence and coupling” [209], [212]. Additionally, Gonze et al. (2005) reported that the permissible range of endogenous periods, for which intercellular coupling is still possible, depends on the coupling strength of the network [213]. Thus, in weakly coupled oscillators networks, small period differences should be overcome by intercellular coupling.

For co-cultures of period mutant reporter cells with wildtype non-reporter cells, we observed period changes of ± 40 minutes. Based on the weighted period averages, period lengthening effects were expected to lie within this range for *TNPO1*$^{-/-}$ knock-out cells (Δperiod 1.1 hours), while period shortening effects were expected to be larger

for CRY2$^{-/-}$ knock-out cells (Δperiod 2.8 hours). This result may support the hypothesis that intercellular coupling among peripheral circadian oscillators is weak, enabling global synchronization only within relatively small period ranges (~1 hour). Nevertheless, despite expectations of the magnitude, bidirectional frequency-pulling effects were observed upon co-culture, suggesting that (i) intercellular coupling depends on mutual information exchange between oscillators and (ii) that partial synchronization is still possible even for broader period ranges.

However, it should be mentioned that, in agreement with Noguchi et al. (2013) and Guenthner et al. (2014), we did not observe period-pulling effects under 2-dimensional co-culture conditions ([61], [89], own data not shown). Therefore, co-cultures of period-mutant and wildtype cells were grown as 3-D spheroids, which allows for increased interactions with adjacent cells and establishment of tissue-like extracellular microenvironments [384]–[386]. This may play an important role for peripheral coupling since cell-extracellular matrix interactions, based on cytoskeleton-integrin-ECM complexes, modulate intercellular communication. The ECM has been shown to regulate paracrine signaling due to the sequestration, concentration, mobilization, and distribution of signaling proteins, as well as the modulation of receptor-ligand interactions [387]. Moreover, as mentioned above, ECM stiffness has been demonstrated to regulate circadian clocks by raising clock gene expression levels and circadian amplitudes through integrin/focal adhesion dependent cell-ECM interactions [377]. Interestingly, mammary epithelial cells cultured in 3-D systems were found to oscillated with higher network amplitudes and more coherent phases than 2-D cultured cells [377], suggesting that 3-D conformation indeed promotes interoscillator coupling. Dynamics in cytoskeleton-integrin complexes have been suggested to link molecular clocks to the extracellular compartment via the regulation of SRF (serum response factor); an important immediate early transcription factor inducing *Per2* expression in peripheral tissues [356], [378]. Additionally, RNA sequencing further supported the hypothesis that cellular microenvironments contribute to intercellular coupling. Low-density cultures of U-2 OS cells displayed a downregulation of transcripts associated with extracellular signaling activity, as well as ECM remodeling and function. The top 20 differentially expressed genes included extracellular peptidases/proteases (MMP7, KLK3, CFI), enzymes (PPBP, ENPP3), filament proteins (KRT71, MYL10), and glycoproteins (CHI3L1, PRB1/2). Thus, it appears plausible that 3-D culture systems, due to the formation of complex cell-ECM-cell networks, enhance coupling strength in

peripheral oscillator ensembles and promote synchronization. Indeed, Bernard et al. (2007), reported that increased connectivity between interacting oscillators enhances synchronization in theoretical models of SCN coupling [374].

Overall, these results suggest that peripheral circadian oscillators weakly (undercritically) couple with each other to enhance single cell rhythmicity and generate partially synchronized network oscillations. Paracrine communication seems to be the major route of interoscillator coupling, which will also be supported by results discussed hereinafter. Moreover, formation of 3-D microenvironments appears to contribute to peripheral coupling, suggesting that interoscillator coupling within peripheral tissue clocks in vivo may be more pronounced than can be predicted from in vitro studies. Nevertheless, additional experiments should be performed to test this hypothesis. For example, coupling studies could be performed on different culture surfaces, e.g. dishes, membranes, or gelatinous protein mixtures (Matrigel, collagen etc.), in 3-D culture systems (organoids or spheroids), in combination with imaging methods quantifying ECM formation and turnover (fluorescent microscopy), or upon genetic manipulation of important ECM components.

Moreover, as for most coupling studies, one major question remains to be answered: do paracrine coupling signals have to be rhythmic? Theoretically both, rhythmic and constitutive signals may be able to induce synchronization of oscillators. Some computational models suggest that rhythmic coupling is required in order to drive individual (damped) oscillators, as well as rhythms of the synchronized network [213], [374]. Others propose that synchronization can result from phase changes in response to resetting signals or increases of coupling strength [98], [209], [388], [389]. Based on the bidirectionality of phase- and period-pulling effects, it appears likely that oscillator populations exchange time information about their oscillatory state. Thus, even though a constitutive signal may be able to promote initial synchronization (like a resetting signal), it seems implausible that it would enhance rhythmicity over time and induce bidirectional phase-/frequency-convergence. We suggest that intercellular coupling among peripheral oscillators depends on the exchange of rhythmic or at least diurnal coupling signals, which may be generated by rhythmic secretion, release, and/or activity of involved coupling factors. This way advanced oscillators may phase advance delayed oscillators and delayed oscillators may phase delay advanced oscillators in order to synchronize to a rhythmic mean field (as described in [389]).

4.2.2 Coupling is mediated by paracrine signaling factors

In this study we further demonstrate that factors secreted by U-2 OS cells are able to phase shift circadian oscillations in a time dependent manner (Figure 3-5 A-C), supporting the hypothesis that peripheral circadian oscillators couple via paracrine signaling pathways. Moreover, secreted signaling factors induced the immediate early expression of *PER2* and the subsequent downregulation of E-box driven clock genes (Figure 3-6 A), as well as the transcriptional activation of cAMP response elements (CRE) (Figure 3-6 B-E). Both, phase responses and activation of CRE enhancer elements were found to be conserved across murine and human species, as well as for a number of peripheral tissues (Figure 3-5 D-G and Figure 3-6 B,C). Therefore, we suggest that paracrine pathway dependent coupling among peripheral circadian oscillators may be a conserved mechanism. Additionally, RNA sequencing results indicated that factors secreted by peripheral circadian oscillators induce specific gene regulatory profiles (Figure 3-7 A-C). Based on the top 20 differentially expressed genes upon conditioned medium stimulation, growth factor signaling, and immediate early transcription factor activity appeared to play a role for paracrine communication among peripheral oscillators (Figure 3-7 D). Thus, similar to SCN coupling and in agreement with Ueda et al. (2002) [389], we suggest that peripheral coupling is achieved by the paracrine activity of secreted growth factors, resulting in the time dependent modulation of the molecular clock machinery and subsequent phase shifts.

Secreted (protein) factors modulate the molecular clock machinery

Conditioned medium (CM) is supernatant harvested from cultured cells and can be considered as tissue-specific secretome. It contains molecules secreted via canonical pathways, shed from the cell surface, or released from the intracellular space via non-classical secretory pathways or lysosomes/exosomes [390]. Previous studies have shown that secreted factors play an important role for normal circadian rhythmicity of single cells and populations [61], [293]. Moreover, circadian clocks have been demonstrated to regulate secretory pathway components in a rhythmic manner [297]. Within the SCN, secreted neurotransmitters are essential for intercellular coupling and network synchrony (for review see [391]).

Our results indicate that proximity to neighboring oscillators promotes intercellular coupling by exchange of diffusible factors (see above). Moreover, CM was found to act as Zeitgeber for peripheral circadian oscillators, inducing time-of-stimulation

dependent phase responses (Figure 3-5 A-C). This suggests that factors secreted by peripheral circadian oscillators convey time information to adjacent cells, promoting intercellular coupling by phase-synchronization (as described in [389]). Strongest phase responses to CM (14-18 hours post-synchronization) coincided with the trough of endogenous *PER2* expression, suggesting that phase changes are related to transcriptional rhythms of this gene (as reported in [392]).

Phase shifts of circadian rhythms are mediated by changes to the transcriptional translational feedback loops (TTFL) driving circadian oscillations. In the SCN immediate early expression of *Per2 is* induced 1.5-3 hours following light pulses perceived between CT12-CT16 [94], [180]. Similarly, immediate early induction of *PER2* (2-4 hours post-stimulation) was detected following CM stimulation of U-2 OS cells (Figure 3-6 A). Since *PER2* expression varies rhythmically throughout the day it is plausible that *PER2* dependent phase shifts are gated by this genes' endogenous expression levels. Moreover, due to its role as transcriptional suppressor in the core feedback loop, increases in *PER2 (Per2* in non-human species*)* expression are expected to result in phase delays of circadian rhythms. Therefore, prolonged *PER2* dependent repression of BMAL1/CLOCK activity may explain the slightly delayed reduction of E-box driven clock genes (Figure 3-6 A), as well as phase responses following CM stimulation (Figure 3-5 A-C) [140], [141]. Alternatively, *PER2* induction and E-box suppression may be mediated independently. For example, rapid induction of DEC1/2 activity has been described to suppress BMAL1/CLOCK transcription and induce phase delays at canonical (CACGTG) but not at non-canonical (CACGTT) E'-boxes, which are exclusively found in mouse *Per2* promoters [339], [393], [394]. However, since the human *PER2* gene appears to have both, canonical and non-canonical E-box enhancer elements (Figure 4-2), differential regulation via these promoter sites in U-2 OS cells appears unlikely. Thus, we suggest that peripheral oscillators couple via exchange of secreted factors, which induce temporally gated transcriptional activation of *PER2*/*Per2* leading to successive phase-synchronization. To test whether peripheral coupling factors indeed mediate phase shifts via *PER2*/*Per2* induction, CM stimulation could be performed upon silencing or depletion of this gene.

Moreover, phase delaying effects of CM stimulation at the trough of *PER2/Per2* expression were observed for murine and human cell lines, as well as peripheral tissue explants (Figure 3-5 D-G). Thus, we suggest that coupling or phase-synchronization by paracrine signals via the induction of *PER2/Per2* expression constitutes a

conserved mechanism across human and murine species and tissues. Nevertheless, magnitudes of such phase responses were variable. In agreement with published findings, showing that intercellular coupling among fibroblasts and hepatocyte does not lead to network synchronization [61], [62], [89], CM from NIH3T3 fibroblasts and hepatocytes induced only limited phase responses in U-2 OS reporter cells (Figure 3-5 D,E). This may support the hypothesis that for these cell types coupling via paracrine factors is very weak compared to other models of peripheral circadian oscillators, at least in vitro. Alternatively, these cells may facilitate other routes of intercellular communication or secrete coupling factors that U-2 OS cells are not responsive to. Additionally, peripheral tissue explants displayed smaller phase responses to CM than cellular models. We suspect that distinct culture (2-D versus 3-D) and luciferase reporter (gene versus protein) systems, have contributed to observed differences. But it cannot be excluded that magnitude effects are due to species-/tissue-specific variations in intercellular coupling. Therefore, we suggest that conservation of peripheral coupling mechanisms should be tested more vigorously. For example, coupling and phase shift experiments could be performed using different inter-/intraspecies/-tissue combinations or by targeting identified coupling pathways (see below) in different species/tissues in vitro and in vivo.

Non-canonical E-boxes (E'-boxes), D-boxes, cAMP response elements (CRE), glucocorticoid response elements (GRE), heat shock elements (HSE), and serum response elements (SRE) have been described as important enhancer elements regulating rhythmic and immediate early *Per2* (or *PER2* in humans) expression [150], [356], [395]–[397]. Especially, CRE and SRE enhancer sites have been suggested to transmit external and systemic input signals to peripheral clocks by regulating immediate early transcription of *Per2* [232], [356], [398]. Serum response transcription factors (SRF) bind SRE sites in response to systemic signals [356], while cAMP response element binding proteins and activating transcription factors (CREB, ATF) bind CRE sites in response to photic and to coupling signals (for review see [102]). Our results show that functional CRE but not SRE sites are required for transcriptional activation in response to CM stimulation (Figure 3-5 D,E). This may suggest that, similar to the SCN, CRE enhancer elements integrate paracrine signals from adjacent cells to modulate the molecular clock machinery in peripheral oscillators. Moreover, based on the known connection between CRE activation and *Period* gene induction,

we suggest that observed increases in *PER2* expression in response to conditioned medium may be mediated by the activation of its CRE promoter sites. Thus, CRE driven *PER2/Per2* expression may constitutes a signaling endpoint of interoscillator coupling among peripheral oscillators. As for phase shifts, CM dependent CRE activation appeared to be conserved across human and murine species (Figure 3-6 B,C), supporting the hypothesis that peripheral coupling may be mediated by a conserved mechanism in mammals. Consistent with phase effects, CM generated from NIH3T3 fibroblasts and hepatocytes displayed reduced activity with respect to CRE induction. This may further suggest that CRE induction and (*PER2/Per2* dependent) phase shifts are related, as well as that fibroblasts and hepatocytes may be less coupled compared to other cellular models of peripheral oscillators. However, as mentioned before, it is also possible that these cells facilitate other coupling routes or that U-2 OS cells are not responsive to paracrine signaling molecules secreted by these cells. Whether or not CRE promoter sites are indeed required for CM dependent *PER2/Per2* induction and phase responses could be tested by mutation/deletion of the genes' endogenous CRE promoter sites. If CRE driven *Period* expression is required for peripheral coupling, phase shifts in response to CM, as well as coupling effects under co-culture conditions are expected to be lost upon CRE mutation/deletion. Moreover, identified coupling factors may be tested for their ability to activate CRE sites, as well as to induce *PER2/Per2* expression and phase responses (see below). We admit that at this point of the study evidence for a direct connection between CRE activation and *PER2/Per2* induction is incomplete. Thus, additional experiments may help to identify a direct functional relationship. For example, RNA sequencing data could be screened for enrichment of CRE driven transcripts (including *PER2*) upon CM stimulation. Moreover, ChIP sequencing could show whether magnitude and temporal profiles of CRE transcription factor binding, e.g. CREB/ATF, to *PER2/Per2* CRE sites is enhanced or temporally shifted following CM stimulation.

Besides its feedback on the molecular core clock machinery, conditioned medium induced global gene expression changes associated with differential regulation of DNA/RNA binding and transcription factor activity (Figure 3-7 A-C). Certainly, differential gene regulation can be expected upon stimulation with secreted signaling molecules. Nevertheless, we were hoping to gain more information of the nature and signaling activity of paracrine coupling factors. Interestingly, PCA analysis suggested

that the responsive to CM is reduced in sparse cultures (since sparse conditioned and control medium stimulated samples grouped more closely together than those of dense cultures). This may support the hypothesis that peripheral coupling is strengthened in dense networks, e.g. due to the formation of complex microenvironments enhancing cellular connectivity. Indeed, secretion of fibrous ECM components and formation of cell-ECM complexes have been shown to be reduced in sparse cellular networks (Figure 3-2 D,F and [399]–[401]). Moreover, the top 20 significantly regulated transcripts included immediate early transcription factors known to regulate the circadian clock machinery (EGR1, JUNB) [357], [358], transcripts associated with growth factor signaling (e.g. EGR1, JUNB, TMEM88, BCL3, STAT3, WNT7B), especially mediators of the TGF-β signaling pathway (EGR1, JUNB, TBX3, STAT3, KDM6B, SKIL, LRRC32) [402]–[408], as well as transcripts involved in regulation of cell fate (e.g. PTP4A3, KCTD11, STAT3, TBX3, KDM6B) and immune response (e.g. ZC3H12A, STAT3, ITK, CCL7) (Figure 3-7 C,D). Interestingly, TGF-β signaling pathways had been demonstrated to regulate circadian clocks in zebrafish and mammalian model systems [335], [336], [339], [340], suggesting that it may constitute a potential coupling pathway within peripheral tissues.

Overall these results suggest that factors secreted by peripheral circadian oscillators act as paracrine signaling molecules to phase shift circadian oscillations in neighboring cells via the induction of CRE-driven and immediate early expression of *PER2*/Per2. In agreement with the Kuramoto model [212], [379], such paracrine communication dependent phase responses may lead to synchronization if phase changes result in large enough oscillator coherence for a critical coupling threshold to be reached. Moreover, temporal gating of phase responses, e.g. by rhythmic secretion/activity of paracrine signals or feedback regulated receptor expression, could explain how oscillators exchange time information bidirectionally to enhance network rhythmicity. Computational studies have shown that intercellular coupling in neuronal networks depends on extracellular rhythms of secreted coupling factors (neurotransmitters) that, in a time-of-day dependent manner, induce *Period* gene expression [213], [233]. However, to test whether comparable mechanisms, e.g. by rhythmic secretion of growth factors, mediate intercellular coupling in peripheral tissues, knowledge about involved coupling factors is necessary (see below).

4.2.3 TGF-β is a potential peripheral coupling factor

Based on RNA sequencing results, growth factor signaling, including TGF-β pathway, appeared to be a potential mechanism of intercellular coupling between peripheral circadian oscillators. Results presented here show that indeed active conditioned medium components are proteins (Figure 3-8 A-F), which can be enriched by chromatography (Figure 3-9 A-C). Moreover, mass spectrometry of active chromatography fractions helped to identify active conditioned medium components (Figure 3-9 D,E), of which TGF-β was shown to be required for activation of CRE driven gene expression (Figure 3-10 A-E) and to mediate *PER2* induction (Figure 3-10 F). Genetic and pharmacological perturbation of TGF-β signaling pathways demonstrated that TGF-β signaling is important for CRE transcriptional activity (Figure 3-11 A,B and Figure 3-12 A,B), robust circadian rhythms (Figure 3-11 C,D and Figure 3-12 C-E), as well as phase responses to CM (Figure 3-12F,G). Additionally, pharmacological inhibition of TGF-β receptor abolished density dependent amplitude expansion (Figure 3-13 A,B), increased damping of co-cultured U-2 OS cells (Figure 3-13 A,C), and led to increased susceptibility of U-2 OS ensembles to a temperature stimulus (Figure 3-13 D-F). Together these findings suggest that TGF-β signaling pathway acts as coupling pathway to promote intercellular coupling and synchrony among peripheral circadian oscillators.

TGF-β acts as active conditioned medium factor

Size fractionation, heat-treatment and ammonium sulfate precipitation supported the hypothesis that active CM factors are proteins (at least with respect to CRE activation). As expected, active CM factors (i) appeared to be of intermediate to large molecular size (average protein: ~30-50 kD [409]) (Figure 3-8 A,B), (ii) precipitated at $(NH_4)_2SO_4$ saturations ≥ 30% [359] (Figure 3-8 E,F), and (iii) were thermally instable (irreversible protein denaturation takes place at ≥ 80°C [410]) (Figure 3-8 C,D). Nevertheless, since up to 70% of transcripts may be belong to tissue-specific secretomes [411], conditioned medium is expected to constitute a complex mixture of secreted proteins. Thus, those protein factors mediating intercellular coupling among peripheral circadian oscillators are likely to be present in rather low abundance compared to factors involved in more general cellular functions. With the help of chromatography (performed by our collaboration partners at the Protein Purification and Analysis Unit

of the MPI Berlin), we were able to separate conditioned medium into fractions of distinct activity (Figure 3-9 A,C). Active fractions were defined as those showing enriched activity with respect to CRE transcriptional activation (as proxy for circadian clock response to paracrine molecules). CRE activation was used as read out because it allowed for quicker, more sensitive, and less variable screening of chromatography fractions compared to phase shifts or *PER2* induction. Additionally, proteins contained in these active fractions were identified by comparative mass spectrometry (Figure 3-9 D,E), again performed by our collaboration partners. Because previously discussed results had suggested that peripheral coupling factors are paracrine signaling molecules, mass spectrometry hits were filtered for secreted proteins [362]. By this approach, PSG (Pregnancy-Specific Glycoprotein), SFRP (Selected Frizzled-Related Protein), SMOC (SPARC-related Modular Calcium Binding Protein), and TGFB (Transforming Growth Factor Beta) were identified as candidate coupling factors secreted by peripheral circadian oscillators (Figure 3-9 D,E). PSGs are members of the carcinoembryonic antigen-related cell adhesion molecule (CEACAM) family, normally secreted by placental syncytioblasts. However, PSGs have also been described to be expressed in tumors and some epithelial cell types [412]. Besides their role in pregnancy, these proteins have been associated with immunomodulatory, angiogenic, and anti-platelet functions [413]–[416]. SFRPs are a family of proteins structurally related to Frizzled and were originally identified as antagonists of Wnt signaling pathway [417], [418]. Recently however, these proteins have been indicated as modulators of BMP signaling, tissue homeostasis, cell-cell signaling, and proteinase inhibition (for review see [419]). SMOCs are extracellular Ca^{2+} binding proteins that belong to the SPARC or BM-40 family (Secreted Protein Acidic and Rich in Cystein9) of secreted glycoproteins, which bind ECM components to regulate cell adhesion, proliferation and ECM turnover [420]. Especially SMOC1/2 have been described as basement membrane and ECM associated proteins involved in growth factor signaling and integrin binding [421]. TGFBs are growth factors belonging to the TGF-β family of ligands, which are involved in various biological processes including development, differentiation, cell cycle, migration, immune regulation, wound healing and many more (for details see 1.6 and [422]). Even though the majority of candidate factors appeared to be involved in direct or ECM dependent cell-cell communication, only TGF-β growth factors had been described to interact with the circadian clock machinery before [335], [339], [340]. Additionally, RNA sequencing data suggested that genes involved in TGF-

β signaling pathways are differentially regulated by CM (Figure 3-7 D) and immunodepletion and neutralization validated the role of TGF-β as active CM factor (Figure 3-10 A,B). Thus, based on these results, its connection to the clock machinery, as well as its described function as growth factor we hypothesized that TGF-β may act as paracrine signaling molecule promoting intercellular coupling among peripheral circadian oscillators.

TGF-β induces CRE driven transcription and mediates phase shifts

In 2008 Kon et al. demonstrated that TGF-β elicits time-of-day dependent phase responses in rat-1 fibroblasts [339] (Figure 4-1). Our results showed that perturbation of TGF-β signaling attenuates CM induced phase delays upon stimulation at the inferred trough of *PER2* expression (Figure 3-12 F,G). This supports the hypothesis that TGF-β acts as paracrine signaling factor mediating temporally gated phase responses among adjacent oscillators. As described above, such phase synchronization may induce transitions from incoherent to coherent network states [172], [212]. Nevertheless, whether TGF-β, as active CM component, functions as coupling factor mediating phase synchronization of peripheral oscillators via the immediate early induction of CRE driven *PER2/Per2* expression remained to be investigated.

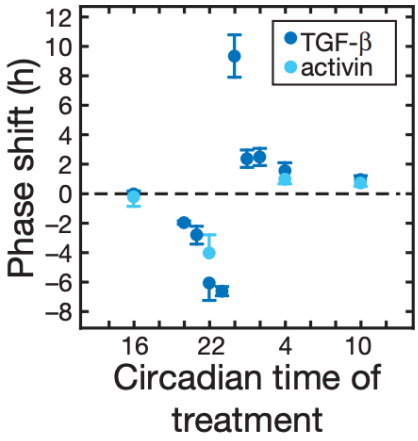

Figure 4-1: Phase response curve of TGF-β and activin

Rat-1 fibroblasts were synchronized with dexamethasone and stimulated by a 1 hour pulse of 2 ng/mL TGF-β1 or 20 ng/mL activin. Stimulation was performed at indicated circadian treatment times following the third cycle of bioluminescence rhythms. Phase shifts relative to solvent control are indicated. (adapted from [339])

Literature states that TGF-β activates SMAD proteins upon binding to its transmembrane receptors, inducing the downstream phosphorylation of receptor associated proteins (for details see 1.6 or [331]). Activated SMAD complexes translocate to the nucleus, where they act as transcription factors, binding either complete (GTCTAGAC), half-site (CAGA(CA)) or GC-rich Smad binding elements (SBE) [423], [424]. However, since SMADs bind their target sequences with low affinity, they commonly require additional transcription factors, co-activators and co-repressors as interaction partners to regulate target gene expression [423]. Among others, c-JUN, c-FOS, bHLH, and C/EBP (CCAAT/enhancer binding protein) transcription factors, as well as the co-regulators p300 (histone acetyltransferase), CBP (CREB binding protein), and ATF have been shown to form complexes with SMAD proteins and regulate the expression of target genes [425]–[431]. CRE driven gene expression is activated by CREB/ATF binding and phosphorylation dependent recruitment of the co-activator complex CBP/p300 [432], [433]. Indeed, it has been shown that synergistic binding of SMAD and AP-1 family transcription factors to their respective but adjacent DNA binding sites (SBE and AP-1 sites) is required for TGF-β dependent *c-Jun* expression [434]. Similarly, we hypothesize that synergistic binding of SMAD and CREB/ATF complexes to their respective enhancer elements (SBE and CRE sites) may enable TGF-β dependent *PER2/Per2* expression. Interestingly, sequence analysis showed that human *PER2*, as well as mouse and rat *Per2* promoters contain a number of half-site SBEs, some in close proximity to cAMP response elements (Figure 4-2 A). Indeed, immuno-depletion/neutralization experiments indicated that TGF-β in CM is required for CRE transcriptional activation (Figure 3-10 A-C), as well as that recombinant TGF-β induces CRE activation dose dependently (Figure 3-10 D,E). Consistent with *PER2/Per2* promoter analysis, seven SBE half sites were found to be located in direct proximity to each of the seven CRE sequences in the 7xCRE:Luc reporter construct (Figure 4-2 B). Thus, together with the finding that mutation of CRE sites in this reporter construct attenuates responsiveness to conditioned medium (Figure 3-6 D,E), these results suggest that TGF-β acts as upstream activator of CRE transcriptional activation, as well as that this may depend on synergistic activation of SBE and CRE enhancer elements.

Additionally, genetic and pharmacological perturbation experiments showed that functional TGF-β pathway is required for transcriptional activation of CRE sites (Figure 3-11 A,B and Figure 3-12 A,B). Knock-down of *ITGAV, SKI, SMAD4, and TGFBR1*

resulted in significant alteration of CM induced CRE activation (Figure 3-11 A,B). Moreover, pharmacological inhibition of TGF-β receptor resulted in a dose dependent reduction of CM dependent CRE activation (Figure 3-12 A,B). As described in the introduction, TGF-β ligands are synthesized and secreted as precursor proteins, as well as stored and distributed extracellularly in an inactive latent form. Active TGF-β is released from its latent complex by various mechanism, including proteolytic cleavage by protease or interaction with ECM proteins, most importantly with integrin αVβ6/8. Following the release of active TGF-β, it binds and activates its receptor complexes, which induce phosphorylation dependent activation of downstream mediators. SMAD activity is regulated by interaction with co-factors, such as SnoN (also called SKIL) and SKI, or ubiquitination by E3 Ub-ligases, such as RNF111 (also called Arkadia) and SMURFs (Figure 1-10) [435]. SMAD4 is required for nuclear shuttling and transcriptional activity of SMAD complexes at SBE sites in canonical TGF-β signaling, SKI is known as regulator of SMAD transcriptional activity. Thus, disruption of CRE activation upon knock-down of these genes may supports the hypothesis that induction of SBE and CRE enhancer elements is synergistically regulated in response to paracrine coupling factors. Moreover, as expected based on CRE activation by recombinant TGF-β (Figure 3-10 C,D), knock-down of *TGFBR1* resulted in significantly attenuated CRE activation, further suggesting that TGF-β acts as direct upstream activator of CRE driven transcription. Interestingly, knock-down of *ITGAV* resulted in a significant increase of CM dependent CRE activation, suggesting that disturbance of extracellular binding partners of latent TGF-β may alter the availability of active TGF-β forms, resulting in enhanced responsiveness to externally applied TGF-β.

Nevertheless, in order for CRE activation to translate into phase responses of peripheral circadian oscillators, it needs to alter expression of the core clock machinery. Indeed, consistent with CM stimulations (Figure 3-5), a 2 hour pulse of recombinant TGF-β, given at the trough of *PER2* expression (16 hours post-sync) resulted in significant upregulation of *PER2* (Figure 3-10 E). This may imply that TGF-β signaling drives the immediate early induction of *PER2/Per2* by activating CRE/SBE sites in the gene's promoter. In contrast to our findings, Kon et al. (2008) reported that phase shifts in response to TGF-β depend on the immediate early induction of *Dec1* and subsequent suppression of E-box driven clock genes [339]. Authors did not detect *Per2* induction 1 and 6 hours following a 1 hour pulse of TGF-β given at CT22 [339].

However, we also did not observe a significant upregulation of *PER2* ≤ 1 hour or ≥ 4 hours following conditioned medium stimulation (Figure 3-6 A), suggesting that differential results may be based on distinct measuring times. Moreover, in the same study, intraperitoneal injection of mice with TGF-β at CT24 induced significant elevation of *Per2* expression in a number of peripheral tissue 1.5-3 hours following injection [339]. Thus, we propose that TGF-β, via its canonical TGF-β/SMAD signaling pathways, acts as transcriptional activator of SBE and CRE enhancer elements contained in *PER2/Per2* promoters. This transcriptional activation may further promote immediate early expression of *PER2/Per2*, resulting in time-of-day dependent phase responses. Nevertheless, additional experiment should be performed to demonstrate a direct connection between TGF-β and SBE/CRE driven *PER2/Per2* expression. For example, ChIP sequencing with αSMAD, αCREB and/or αATF antibodies could show whether *PER2/Per2* promoter sequences are enriched following TGF-β stimulation. Proximity labeling techniques, e.g. APEX driven biotinylation, in combination with pull-downs of biotinylated proteins could help to elucidate whether SBE and CRE binding proteins co-localize in response to TGF-β signaling.

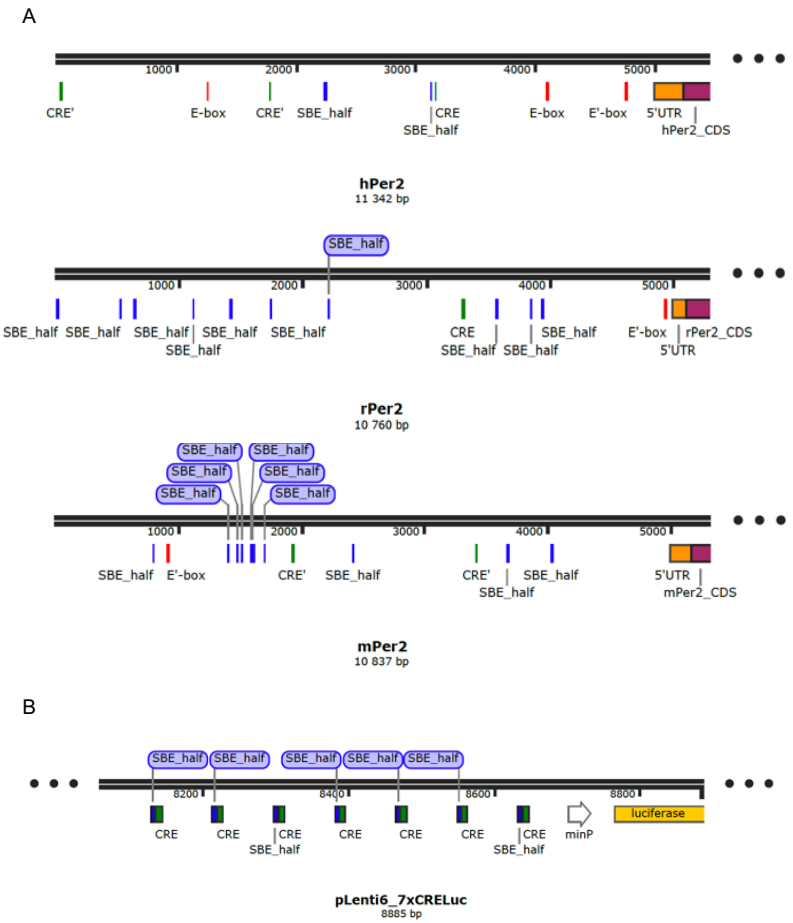

Figure 4-2: Enhancer elements in *Period* promoters and in the 7xCRE:Luc reporter construct

(A) Displayed are promoter sequence (5000 bp upstream of the *Per2* transcription start site), of the human, mouse, and rat *Per2* genes (curated. RefSeq entries NM_022817.2, NM_031678.1, NM_011066.3 respectively). (B) Displayed is the artificial promoter sequence (< 1000 bp upstream of the luciferase transcription start site) of the pLenti6_7xCRE:Luc reporter construct. Canonical E-box (CACGTG, red), non-canonical E'-box (CACGTT, red), canonical CRE (TGACGTCA, green), non-canonical CRE' (TGCCGTCA or TGAAGTCA, green), and half-site SBE (CAGACA, blue) sequences are indicated.

TGF-β is a potential peripheral coupling factor

Genetic and pharmacological perturbation of TGF-β signaling did not only resulted in altered CRE responses to conditioned medium but also disturbed circadian rhythmicity of U-2 OS ensembles. As discussed before, attenuated intercellular coupling is expected to result in decreased network amplitudes, due to reduced amplitude resonance, as well as in increased damping, due to faster desynchronization among single cell oscillators (for details see 1.4).

A negative correlation between amplitude and damping parameters could be observed globally upon RNAi mediated gene knock-downs (Figure 3-11 C), suggesting that perturbation of TGF-β pathway (at least for certain pathway components) promotes network desynchronization. Additionally, those genes leading to significantly altered CRE activation were also found to induce amplitude reduction and/or increased damping upon gene silencing (Figure 3-11 C,D and Figure 6-5 A). This may suggest that TGF-β dependent CRE activation and intercellular coupling are interconnected, eventually via the regulation of *PER2/Per2* dependent phase synchronization. This assumption was supported using a pharmacological TGF-β receptor inhibitor. The small molecule inhibitor LY2109761 blocks the kinase activity of TGF-β receptor complexes and prevents intracellular activation of SMAD proteins [365], [436]. Not only did pharmacological perturbation of TGF-β signaling result in dose dependent attenuation of CRE responses (Figure 3-12 A,B) but also in dose dependent amplitude decreases and damping increases. Moreover, TGF-β receptor inhibitor induced dose dependent period lengthening of circadian oscillations, an effect that had been previously observed for sparsely cultured cells, as well as upon disruption of the secretory pathway [293]. These findings further strengthen the hypothesis that TGF-β signaling is promoting intercellular coupling and synchronized circadian rhythmicity via the regulation of CRE driven transcription. Additionally, based on calculated EC_{50}

values, CRE transcriptional activation (EC_{50} = 0.86 µM) appeared to more sensitive to TGF-β receptor inhibition than changes in amplitude (EC_{50} = 4.23 µM) and damping (EC_{50} = 4.73 µM) parameters. We suspect that this effect may be a consequence of intercellular coupling, rendering oscillators networks more robust against perturbation [57], [157], which is not the case for direct transcriptional regulation. For example, it has been reported that intercellular coupling within the SCN is able to maintain network rhythmicity despite mutations of core clock genes in individual neuronal oscillators [60], [437].

Interestingly, pharmacological inhibition of TGF-β receptor also resulted in either significantly or a trend towards decreased amplitudes, increased damping, and lengthened periods in a number of murine peripheral tissues explants (Figure 6-6 B-E). Again, suggesting that the mechanism of paracrine signaling dependent coupling within peripheral oscillator networks is conserved, as well as that TGF-β may act as ubiquitous coupling factor across species and tissues. Indeed, similar effects of TGF-β receptor inhibition on circadian dynamics have even been reported for zebrafish [340]. Additionally, Kon et al. (2008) reported that intraperitoneal injection of TGF-β results in altered circadian phase of clock gene expression in mouse peripheral tissues [339]. Moreover, RNAi screen results imply that both, regulation of extracellular TGF-β availability, as well as intracellular regulation of TGF-β target gene expression play a role in TGF-β dependent coupling. With regard to the influence of culture density on intercellular coupling this may suggest that distribution of latent TGF-β, as well as release and signaling of active TGF-β is disturbed in low-density cultures. In fact reciprocal regulations of TGF-β and ECM dependent signaling processes have been described [303], [438], [439], suggesting that weakened circadian rhythms of sparse peripheral oscillator cultures may indeed be related to perturbed TGF-β signaling.

As discussed above, population imaging cannot clearly distinguish between population effects and changes to single cell oscillators upon perturbation of TGF-β signaling. Thus, we suggest that the role of TGF-β as peripheral coupling factor should be studied by single cell imaging to quantify phase distributions of peripheral circadian oscillators upon perturbation of TGF-β signaling. If TGF-β acts as coupling factor, disruption of TGF-β signaling is expected to result in faster phase dispersion among single cell oscillators. Moreover, due to increased reliability and decreased likelihood of off-target effects, we further suggest to study consequences of perturbed TGF-β

signaling in knock-out cells rather than by gene silencing or by using pharmacological inhibitors. Clonally selected knock-out clones could be generated by CRISPR/Cas9 mediated gene deletion, e.g. targeting *TGFBR1*.

For coupled oscillator networks, low amplitudes and high damping of low-density reporter cells are expected to be rescued density dependently upon co-culture with increasing numbers of non-reporter cells (Figure 3-4 A-C). Theoretically this can be explained by synchronization leading to amplitude resonance between phase- and frequency-locked oscillators (for details see 1.4.1). Perturbation of TGF-β signaling abolished density dependent amplitude resonance effects upon co-culture (Figure 3-13 A,B), suggesting that intercellular coupling may be disturbed. However, differently than expected for desynchronized networks [172], TGF-β receptor inhibition resulted in higher absolute amplitudes of the low-density reporter cell population, especially for low numbers of co-cultured cells (Figure 3-13 A,B). We suspect that increased amplitudes are an artifact of dexamethasone synchronization prior to the start of bioluminescence recording. According to Abraham et al. (2010) coupling strength is related to oscillator robustness, thereby determining responses to Zeitgeber stimuli and entrainment signals [57]. In agreement with this concept, dexamethasone is expected to act as stronger Zeitgeber for decoupled oscillator, supporting the idea that disturbed TGF-β signaling weakens intercellular coupling. Increased damping of low-density, co-cultured reporter cells upon TGF-β receptor inhibition (Figure 3-13 A,C) further strengths this assumption. It is plausible that stronger initial synchronization will result in increased damping of the ensemble rhythm if co-cultured oscillators are less coupled. Thus, we suggest that in future experiments TGF-β receptor inhibitor should only be added after dexamethasone synchronization, to avoid such artifacts when studying the role of TGF-β signaling for intercellular coupling.

The hypothesis that disturbed TGF-β signaling weakens intercellular coupling, rendering oscillator networks more susceptible to perturbation, was further validated by temperature pulse experiments. As expected for decoupled networks, TGF-β receptor inhibition resulted in large phase responses to external Zeitgeber pulses (Figure 3-13 D,E). Surprisingly, reducing culture density did not result in increased susceptibility the applied temperature pulse by itself (Figure 3-13F,G). Based on our and published results (Noguchi et al. (2013) [61]) we expected low-density cultures to display weakened rhythmicity, thereby making the ensemble less rigid against

perturbation. Nevertheless, we suspect that, even though weakened, intercellular coupling in sparse oscillator networks is still strong enough to resist phase perturbation by temperature pulse (8 hours, 20°C) given at the inferred trough of *PER2*. Only additional disruption of TGF-β signaling appears to reduce the coupling strength enough to render peripheral oscillator networks susceptible to temperature perturbation. Moreover, it is possible that temperature induced phase shifts of sparse cultures may become observable for stimulations times better suited for temperature dependent resetting, e.g. between CT8-CT15 as shown for fibroblasts [440]. Alternatively, yet unlikely due to described dexamethasone effects, TGF-β signaling may act as specific regulator of temperature input pathways to the molecular circadian clock. To exclude that observed phase responses are temperature specific, susceptibility to other Zeitgeber pulses upon perturbation of TGF-β signaling could be studied.

Overall, findings support the hypothesis that TGF-β acts as peripheral coupling factor promoting interoscillator synchronization and robustness of network oscillations. Mechanistically, TGF-β coupling may be mediated by temporally gated CRE driven and immediate early expression of *PER2/Per2* leading to phase-synchronization, as well as subsequent frequency-locking and amplitude resonance between autonomous single cell oscillators. Additionally, regulation of complex extracellular microenvironments by TGF-β, e.g. formation of cell-ECM interactions and regulation of ECM stiffness signals [441], [442], may contribute to paracrine communication between peripheral oscillators enhancing intercellular coupling.

4.3 Limitations and perspectives

Coupling in various model systems

U-2 OS cells constitute one of the most commonly used in vitro models in chronobiological research due to their (i) human origin, (ii) extensive characterization, (iii) easy handling, (iv) stable oscillations, and (v) susceptibility to genetic manipulations. Nevertheless, it has to be kept in mind that this cell line is derived from cancerous tissue with aberrant genetic material and behavior. Especially TGF-β

signaling is often deregulated in cancer, leading to altered signaling activity or responsiveness of tumor cells [443], [444].

Our findings suggest that that paracrine communication mechanisms are conserved across human and murine species, as well as across a number of peripheral tissues. Additionally, published studies in non-transformed human, murine, and even zebrafish model systems have yielded evidence of interactions between the molecular circadian clock machinery and TGF-β signaling pathway [335], [336], [339], [340]. Nevertheless, identification and functional role of TGF-β as paracrine signaling molecule and potential peripheral coupling factor based on the U-2 OS cell model should interpreted carefully until further validation. Nevertheless, despite drawbacks of in vitro culture systems, coupling constitutes an integral feature of cellular oscillators. Perturbation of coupling on the cellular level can affect the behavior of entire oscillator networks, e.g. its rhythmic biological functions [445], entrainment [57], or response to non-rhythmic signals [446]. Thus, even though cell-based systems constitute simplified and isolated models of complex in vivo phenomena, in vitro studies mark an important starting point for understanding molecular mechanisms of peripheral coupling.

As discussed, ex vivo 3-dimensional culture models seem to reflect in vivo tissue configurations and may provide new insights into coupling among peripheral circadian oscillators. Therefore, organoids derived from mammalian stem cells may be a good model for studying the role of TGF-β in peripheral coupling independently of its role in cancerous processes. In vivo, peripheral clocks have been shown to oscillate independently of the SCN, behavioral rhythms, external light-dark and feeding-fasting cycles [36]. However, whether or not tissues rhythms are maintained by intercellular coupling or by interaction with other peripheral tissue clocks needs to be elucidated. Neither in vitro nor ex vivo models can provide information about such complex processes. However, the role of TGF-β signaling for intercellular coupling within peripheral tissues, as well as for rhythmic organ functions can be studied in vivo. Newly developed mouse models [244], [245] and imaging techniques [36] allow for real-time recording of bioluminescence rhythms of isolated peripheral tissues, i.e. in otherwise clock-less animals. Thus, amplitude and damping parameters of free-running tissue rhythms, as well as response to Zeitgeber/entrainment signals with or without functional TGF-β signaling can be investigated in living animals. Moreover, functional consequences of disturbed TGF-β signaling in isolated peripheral clocks, as well as in

clocks receiving systemic and external Zeitgeber signals may be studied to elucidate the role of peripheral coupling for the temporal coordination of circadian tissue physiology.

Population versus single cell imaging

Population imaging, i.e. quantification of the average rhythm of cellular ensembles, for studying intercellular coupling constitutes one of the major limitations of this project. Circadian networks are composed of cell-autonomous single cell oscillators, which all cycle with their individual circadian parameters (period, phase, amplitude, damping). Thus, generally, intercellular coupling strength, which itself is difficult to quantify, is approximated by the distribution of circadian parameters of single cell oscillators. The widths of these distributions reflects the degree of synchronization within the network [172]. However, changes in amplitude, phase, and period distributions may also result from changes of cell-intrinsic oscillations independently of coupling. Therefore, population averages, as presented here, cannot clearly distinguish between changes of individual oscillators, changes of intercellular coupling between oscillators or a combination of both. Nevertheless, damping is commonly accepted to reflect desynchronization rather than damping of individual oscillators [48], [62], [447], [448]. Additionally, bidirectional phase-/period-pulling effects, as well as amplitude expansion upon physical separation of co-cultures are unlikely to arise simply from changes of single cell oscillators alone. Thus, even without single cell imaging, our data as whole strongly suggests that observed changes in circadian parameters depend on intercellular coupling or a combination of single cell changes and coupling.

In the context of cell division, precise separation between single cell and population-based effects may be of importance when studying intercellular coupling. O'Neill and Hastings (2008) suggest that desynchronization of fibroblasts is decreasing as cells mature because "phase-noise", introduced by cell division, decays [355]. Other studies have demonstrated unidirectional influence of cell cycle on circadian cycle resulting in period changes of circadian oscillations [47], [449], [450]. Considering that intercellular coupling is achieved by phase- and frequency-locking between oscillators, phase-/period-fluctuations introduced by cell division may lead to undetectable artifacts when studying coupling on the population level. However, as many in vitro models, U-2 OS cells exhibit contact inhibition under dense culture conditions. Thus, for most results

presented here, cell cycle effects can be neglected. Moreover, bioluminescence imaging was conducted using serum-free reporter medium in order to arrest also sparse cultures in G_0/G_1 phase and mimic in vivo situations of non-dividing resident tissue cells. TGF-β is known as cell cycle regulator, inducing G_1 arrest in most cell types, e.g. epithelial, hematopoietic and endothelial cells, but promoting growth of certain mesenchymal cells such as skin fibroblasts [336]. We have to admit that by population imaging we cannot exclude that TGF-β dependent cell cycle regulation impacts intercellular coupling. Especially pharmacological perturbation of TGF-β signaling may introduce growth effects that cannot be separated from coupling. Thus, even though we suggest that intact TGF-β signaling is promoting synchrony by peripheral oscillator coupling, we are aware that additional single cell recordings are necessary to strengthen our findings. For example, single cell imaging with dual reporter systems may enable to study phase dispersion of peripheral oscillators (as measure for coupling strength), as well as cell cycle progression upon perturbation of TGF-β signaling simultaneously. Alternatively, without a cell cycle reporter system, growth effects of TGF-β receptor inhibition could be controlled by quantifying cell number and/or cell covered surface area of times series data.

Technical and experimental limitations

RNA interference (RNAi) screens constitute an error prone technique. As for every high-throughput RNAi screen, short-hairpin RNA (shRNA) knock-down efficiencies could not be controlled by quantification of transcript and/or protein levels. Comparable lentivirus delivery-based gene silencing techniques often result in decreases of mRNA levels to < 25%. However, during a screen, it cannot be excluded that shRNA mediated silencing fails completely, that knock-down efficiencies are too low to disturb functionality of the targeted gene, or that off-target effects are introduced. Thus, as mentioned, results from RNAi based screens should be interpreted with care and the role of identified target genes should further be validated by more reliable genome editing approaches, e.g. CRISPR/Cas9 gene editing or generation of transgenic animal. So far generation of mutated/knock-out cells, such as SMAD4 or TGF-β receptor depleted U-2 OS cells, has not been done but should be attempted in the future. This would allow to study intercellular coupling without being dependent on pharmacological inhibitors, which are often accompanied by unspecific effects.

Differential gene expression (DGE) analysis and mass spectrometry are usually accompanied by technical constraints with regard to bioinformatical analysis of resulting datasets. While mass spectrometry may fail to detect very low abundant peptides in a complex mixture of proteins or to separate isoforms, DGE analysis may overestimate statistical relevance of expression changes of lowly expressed genes. Moreover, for both experimental approaches, transcripts and peptides have to present in available databases to be identified. We did the best to minimize these error sources by enriching active conditioned medium factors by chromatography prior to mass spectrometry, as well as by filtering and normalization of RNA sequencing data prior to DGE analysis (according to [350], [351], [451]). It appears unlikely, that for the human genome functional transcripts or peptides are not annotated.

The lack of evidence for a direct connection between TGF-β dependent CRE activation and modulation of the molecular clock machinery, as well as the observed phase responses constitutes an additional limitation of this project. Kon et al. (2008) have shown that TGF-β stimulation alters clock gene expression levels and elicits time-of-day dependent phase responses [339]. Moreover, it has been shown that rhythmic transcription factor binding to CRE sites in the *Period* promoter is important for oscillations of this gene and circadian rhythmicity in peripheral oscillator models [395]. Our results suggest that TGF-β signaling promotes synchronized and robust network oscillations. However, whether SBE/CRE-driven *PER2/Per2* induction constitutes the input pathway of TGF-β signals to the circadian clocks remains to be studied in detail. We suggest that coupling experiments in cells/tissues with mutated or depleted clock-relevant CRE sites in the endogenous *Period* gene promoter should be conducted. If TGF-β dependent CRE induction of *PER2/Per2* is required for intercellular coupling and/or phase responses these effects should be lost upon genetic manipulation. Additionally, whether TGF-β signaling induces CRE-driven *Period* transcription could be measured by ChIP sequencing using αSMAD/αCREB antibodies or proximity labeling of transcription factors present at *Per2* CRE site following TGF-β stimulation.

4.4 Conclusions

If TGF-β indeed functions as coupling factor in peripheral tissues, targeted manipulation of its signaling pathway will enable to answer many open questions in the field of chronobiology. Are peripheral circadian oscillators coupled? Is the mechanism conserved? What is the functional relevance of this coupling? How does peripheral coupling contribute to or protect from circadian misalignment?

Based on the results presented here we strongly believe that coupling among peripheral circadian oscillators exists and that it is mediated by paracrine communication of single cell oscillators within tissue networks. We have accumulated evidence that TGF-β functions as paracrine coupling factor in peripheral oscillator networks (Figure 4-3). We propose a mechanism by which cAMP response element driven, immediate early expression of *Per2 (*or *PER2* in human models*)* elicits temporally gated phase responses and phase-synchronization of neighboring oscillators (Figure 4-3). Subsequently, increased phase coherence may result in frequency-locking and amplitude resonance of synchronized oscillators. In agreement with theoretical models, this initial synchronization will increase the coupling strength of the network and recruit more and more oscillators into the synchronized pack [212]. Once a critical coupling threshold is reached the network transitions from the incoherent to the coupled state [172], [212]. For peripheral circadian oscillators intercellular coupling appears to be weak, at least in vitro, likely resulting in partial network synchronization. However, we suspect that peripheral coupling in vivo may be strengthened by more complex tissue microenvironments and formation of 3-dimensional cell-extracellular matrix interactions.

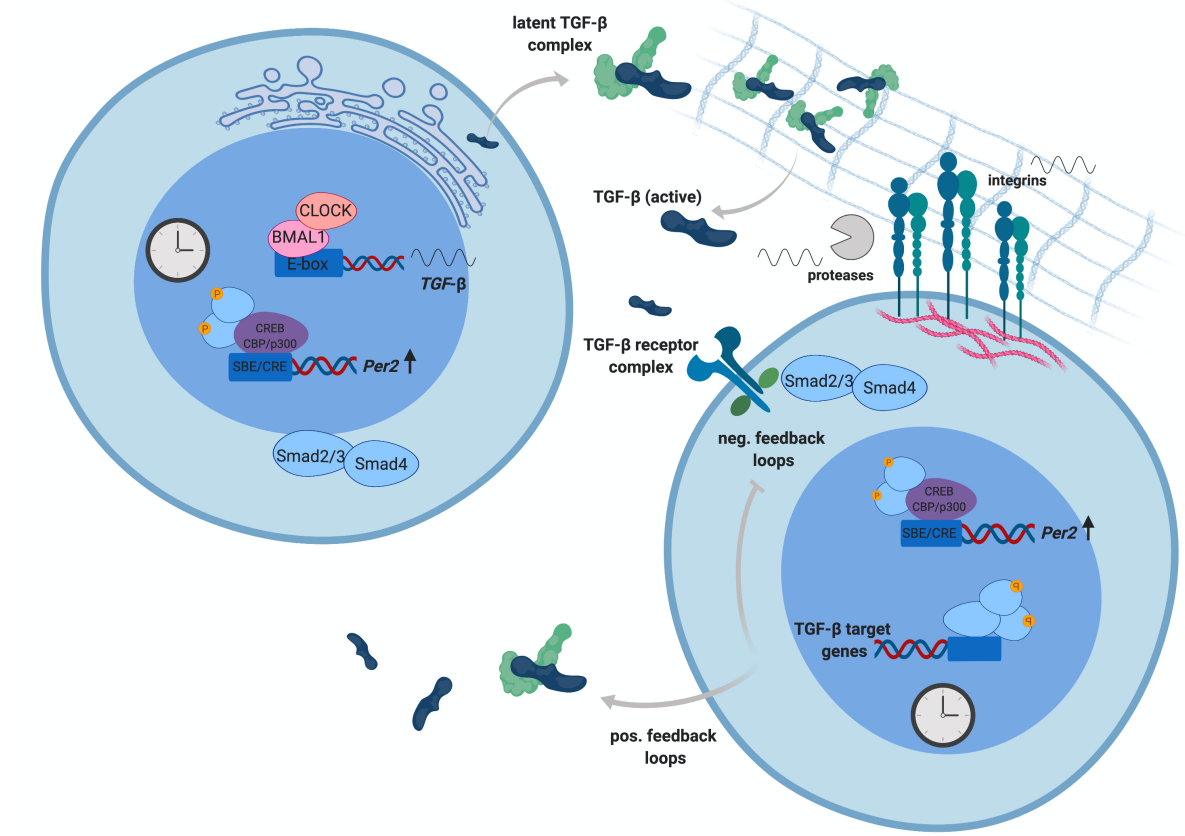

Figure 4-3: Model of TGF-β coupling among peripheral circadian oscillators

TGF-β transcription may be regulated rhythmically by BMAL1/CLOCK activity [335]. It gets secreted from peripheral circadian oscillators as inactive form and is distributed and stored in the extracellular matrix until its release is triggered by ECM components, including proteases and integrins. ECM components themselves may be produced and/or regulated rhythmically. Thus, active TGF-β may signal rhythmically via its TGF-β type I/type II receptor complexes resulting in intracellular activation and assembly of SMAD proteins, which translocate to the nucleus where they associate with additional transcriptional factors and/or transcriptional regulators. Binding of SMAD/CREB/CBP/p300 complex to SBE and CRE sites in the *Per2* promoter may result in the immediate early expression of *Per2* and respective phase responses of the receiving oscillator. Additionally, TGF-β signaling may result in feedback regulation of its own signaling pathway and extracellular availability further modulating intercellular TGF-β coupling among peripheral circadian oscillators. (TGF-β=Transforming Growth Factor beta, ECM=extracellular matrix, CREB=cAMP response element binding protein, CBP=CREB binding protein, p300=p300 histone acetyltransferase, CRE=cAMP response element, SBE=SMAD binding element, E-box=enhancer box, SMAD2/3 = R-SMADs, SMAD4 = Co-SMAD).

Known mechanisms of TGF-β secretion, ECM disposition, distribution, and activation support the idea that peripheral coupling is achieved by global mean field coupling and collective synchronization rather than by local effects. Latent TGF-β has been reported to have a half-life of > 100 minutes, while its active form is stable for 2-3 minutes [452].

Half-lives suggest that latent TGF-β may be distributed over a wide range of cells by simple diffusion before its activating results in the rapid induction of downstream signaling pathways. In agreement with Gonze et al. (2005) rapid diffusion relative to the 24 hour circadian cycle enables global synchronization of oscillators by rhythmic paracrine factors [213]. While TGF-β has been described to be under rhythmic control of BMAL1/CLOCK driven E-box transcription [334], [335], we are not aware of studies investigating rhythms in TGF-β secretion and/or activity. Nevertheless, functional secretory pathway has been demonstrated to play an important role for rhythmic secretion of ECM components, as well as for regulation of circadian rhythmicity [293], [297]. Thus, we suspect that rhythms in TGF-β signaling may be introduced by rhythmic production and secretion of latent TGF-β or rhythmic release of active of TGF-β (including rhythms in ECM components that promote the release). Rhythmic response to TGF-β, e.g. rhythmic expression of the receptor or SMADs [337], [338], as well as delayed feedback regulations of TGF-β signaling [331], [453]–[455] may contribute to coupling among peripheral oscillators (Figure 4-3). Computational models predict that rhythmic receptor expression can enhance amplitudes and modulate entrainment range of oscillator networks [233]. Additionally, duration and dose (molecules per cell) of TGF-β signals have been described to dictate dynamics of SMAD activity , receptor recycling, cellular responses and target gene expression [453], [454], [456]. Thus, all these regulatory layers may contribute to the fine-tuning of TGF-β dependent intercellular coupling in peripheral oscillator networks.

Alternatively, constant paracrine signals may promote spontaneous and rapid (phase-) synchronization, e.g. by sudden reduction of noisiness in the network or strong resetting signals. Whether or not this could explain bidirectionality of coupling as observed for co-culture experiments is unclear. We suggest that future studies of TGF-β dependent peripheral coupling may be supported by computational models to answer the following questions: Is peripheral coupling dependent on rhythmic coupling factors? Is synchronization achieved by global or local coupling? Do mutual feedback regulations in response to paracrine signals play a role or is unidirectional information transfer from one oscillator to the other is sufficient?

Lastly, we propose that intercellular coupling between peripheral circadian oscillators is of functional relevance in vivo. In the SCN, coupling maintains tissue rhythmicity despite variable or even aberrant single cell oscillations [52], [60], suggesting that it is

a major determinant of clock precision. Compared to central coupling, we and others ([61]–[63]) have demonstrated that peripheral coupling, at least in vitro, is weak. Moreover, SCN derived and rhythmic external signals have been shown to be indispensable for high-amplitude peripheral oscillations and the maintenance of normal phase relationships between tissue clocks [35], [85], [457]. However, due to its interconnection with oscillator robustness, entrainment, and response to Zeitgeber signals, coupling in peripheral tissue clocks likely plays a role for the temporal coordination of rhythmic organ functions. We suggest that, rather than governing precision and rigidity of tissue oscillations, peripheral coupling is required for fine-tuning responses of peripheral tissues to incoming Zeitgeber signals as it modulates robustness and plasticity of tissue clocks. The mammalian circadian system is exposed to a multitude of internal and external perturbations on a daily basis, e.g. mealtimes, physical activity, temperature changes, hormone levels, and humoral (metabolic) signals. Thus, with increasing evidence for an association between severe health consequences and chronic circadian disruption and/or misalignment, a better understanding of peripheral coupling and its relation to circadian tissue physiology may help to uncover sources and potential treatment options of “circadian diseases”.

Thus, to close with Jürgen Aschoffs' words: “the self-sustained circadian oscillator has to be taken into account. Its main properties seem to be the same in human beings as in all other organisms. We have to study them before we can discuss practical problems successfully. As always in science, a better understanding of the basic phenomena will be the first step toward a proper application in practice.” [1]

5 Bibliography

[1] J. Aschoff, “Circadian Rhythms in Man: A self-sustained oscillator with an inherent frequency underlies human 24-hour periodicity,” *Science (80-.).*, 1965.

[2] J. J. . De Mairan, “Observation Botanique,” *Hist. l’Academie R. des Sci.*, 1729.

[3] C. R. McClung, “Plant circadian rhythms,” *Plant Cell*. 2006.

[4] A.P. de Candolle, *Physiologie Végétale*. Paris: Béchet, 1832.

[5] C. H. Johnson, “Circadian rhythms: as time glows by in bacteria.,” *Nature*, 2004.

[6] J. Cha, M. Zhou, and Y. Liu, “Mechanism of the Neurospora circadian clock, a FREQUENCY-centric view,” *Biochemistry*, 2015.

[7] M. J. Gardner, K. E. Hubbard, C. T. Hotta, A. N. Dodd, and A. A. R. Webb, “How plants tell the time,” *Biochemical Journal*. 2006.

[8] P. Menegazzi, T. Yoshii, and C. Helfrich-Förster, “Laboratory versus nature: The two sides of the Drosophila circadian clock,” *J. Biol. Rhythms*, 2012.

[9] E. D. Buhr and J. S. Takahashi, “Molecular components of the mammalian circadian clock,” *Handb. Exp. Pharmacol.*, 2013.

[10] J. A. Mohawk, C. B. Green, and J. S. Takahashi, “Central and Peripheral Circadian Clocks in Mammals,” *Annu. Rev. Neurosci.*, 2012.

[11] L. Gaspar and S. A. Brown, “Measuring circadian clock function in human cells,” in *Methods in Enzymology*, 2015.

[12] S. N. Peirson, S. Haiford, and R. G. Foster, “The evolution of irradiance detection: Melanopsin and the non-visual opsins,” *Philosophical Transactions of the Royal Society B: Biological Sciences*. 2009.

[13] Bünning E., “Zur Kenntnis der erblichen Tagesperiodizität bei den Primärblättern von Phaseolus multiflorus,” *Jahrb Wiss Bot*, vol. 81, pp. 411–418, 1935.

[14] Bünning E., “Die endonome tagesrhythmik als grundlage der photoperiodischen reaktion,” *Ber Dtsch Bot Ges*, vol. 54, pp. 590–607, 1936.

[15] F. HALBERG, “Physiologic 24-hour periodicity; general and procedural considerations with reference to the adrenal cycle.,” *Int. Zeitschrift f??r Vitaminforschung. Beih.*, 1959.

[16] F. Halberg, Y. L. Tong, and E. A. Johnson, “Circadian System Phase — An Aspect of Temporal Morphology; Procedures and Illustrative Examples,” in *The Cellular Aspects of Biorhythms*, 1967.

[17] R. J. Konopka and S. Benzer, “Clock mutants of Drosophila melanogaster.,” *Proc. Natl. Acad. Sci. U. S. A.*, 1971.

[18] W. A. Zehring *et al.*, “P-element transformation with period locus DNA restores rhythmicity to mutant, arrhythmic drosophila melanogaster,” *Cell*, 1984.

[19] M. R. Ralph and M. Menaker, “A mutation of the circadian system in golden hamsters,” *Science (80-.).*, 1988.

[20] M. H. Vitaterna *et al.*, “Mutagenesis and mapping of a mouse gene, clock, essential for circadian behavior,” *Science (80-.).*, 1994.

[21] P. E. Hardin, J. C. Hall, and M. Rosbash, “Feedback of the Drosophila period gene product on circadian cycling of its messenger RNA levels,” *Nature*, 1990.

[22] S. Daan, “Colin Pittendrigh, Jurgen Aschoff, and the natural entrainment of circadian systems,” in *Journal of Biological Rhythms*, 2000.

[23] S. Daan and J. Aschoff, “The Entrainment of Circadian Systems,” 2001.

[24] R. Y. Moore and N. J. Lenn, “A retinohypothalamic projection in the rat,” *J. Comp. Neurol.*, 1972.

[25] C. P. Richter, “Sleep and activity: their relation to the 24-hour clock.,” *Res. Publ.*

Assoc. Res. Nerv. Ment. Dis., 1967.
[26] F. A. Jenner, “Biological Clocks in Medicine and Psychiatry. By Curt Paul Richter. Springfield, Illinois: Charles C. Thomas. 1965. Pp. 109.,” *Br. J. Psychiatry*, 1966.
[27] R. Y. Moore and V. B. Eichler, “Loss of a circadian adrenal corticosterone rhythm following suprachiasmatic lesions in the rat,” *Brain Res.*, 1972.
[28] F. K. Stephan and I. Zucker, “Circadian rhythms in drinking behavior and locomotor activity of rats are eliminated by hypothalamic lesions.,” *Proc. Natl. Acad. Sci. U. S. A.*, 1972.
[29] S. T. Inouye and H. Kawamura, “Persistence of circadian rhythmicity in a mammalian hypothalamic ‘island’ containing the suprachiasmatic nucleus,” *Proc. Natl. Acad. Sci. U. S. A.*, 1979.
[30] D. J. Green and R. Gillette, “Circadian rhythm of firing rate recorded from single cells in the rat suprachiasmatic brain slice,” *Brain Res.*, 1982.
[31] G. J. Moore and J. C. Rosenior, “Characterization of the ‘Giant Precursors’ (70–80K) of Vasopressin and Oxytocin in the Rat Hypothalamus,” *Prog. Brain Res.*, 1983.
[32] D. J. Earnest and C. D. Sladek, “Circadian rhythms of vasopressin release from individual rat suprachiasmatic explants in vitro,” *Brain Res.*, 1986.
[33] M. R. Ralph, R. G. Foster, F. C. Davis, and M. Menaker, “Transplanted suprachiasmatic nucleus determines circadian period,” *Science (80-.).*, 1990.
[34] T. Kondo *et al.*, “Circadian rhythms in prokaryotes: Luciferase as a reporter of circadian gene expression in cyanobacteria,” *Proc. Natl. Acad. Sci. U. S. A.*, 1993.
[35] S. H. Yoo *et al.*, “PERIOD2::LUCIFERASE real-time reporting of circadian dynamics reveals persistent circadian oscillations in mouse peripheral tissues,” *Proc. Natl. Acad. Sci. U. S. A.*, 2004.
[36] C. Saini *et al.*, “Real-time recording of circadian liver gene expression in freely moving mice reveals the phase-setting behavior of hepatocyte clocks,” *Genes Dev.*, 2013.
[37] D. K. Welsh, D. E. Logothetis, M. Meister, and S. M. Reppert, “Individual neurons dissociated from rat suprachiasmatic nucleus express independently phased circadian firing rhythms,” *Neuron*, 1995.
[38] A. Balsalobre, F. Damiola, and U. Schibler, “A serum shock induces circadian gene expression in mammalian tissue culture cells,” *Cell*, 1998.
[39] S. Yamazaki *et al.*, “Resetting central and peripheral circadian oscillators in transgenic rats,” *Science (80-.).*, 2000.
[40] K. Yagita, F. Tamanini, G. T. J. Van der Horst, and H. Okamura, “Molecular mechanisms of the biological clock in cultured fibroblasts,” *Science (80-.).*, 2001.
[41] R. A. Akhtar *et al.*, “Circadian cycling of the mouse liver transcriptome, as revealed by cDNA microarray, is driven by the suprachiasmatic nucleus,” *Curr. Biol.*, 2002.
[42] G. E. Duffield, J. D. Best, B. H. Meurers, A. Bittner, J. J. Loros, and J. C. Dunlap, “Circadian programs of transcriptional activation, signaling, and protein turnover revealed by microarray analysis of mammalian cells,” *Curr. Biol.*, 2002.
[43] B. H. Miller *et al.*, “Circadian and CLOCK-controlled regulation of the mouse transcriptome and cell proliferation,” *Proc. Natl. Acad. Sci. U. S. A.*, 2007.
[44] S. Panda *et al.*, “Coordinated transcription of key pathways in the mouse by the circadian clock,” *Cell*, 2002.
[45] M. Keller *et al.*, “A circadian clock in macrophages controls inflammatory immune responses,” *Proc. Natl. Acad. Sci. U. S. A.*, 2009.

[46] K. F. Storch *et al.*, “Extensive and divergent circadian gene expression in liver and heart,” *Nature*, 2002.
[47] E. Nagoshi, C. Saini, C. Bauer, T. Laroche, F. Naef, and U. Schibler, “Circadian gene expression in individual fibroblasts: Cell-autonomous and self-sustained oscillators pass time to daughter cells,” *Cell*, 2004.
[48] D. K. Welsh, S. H. Yoo, A. C. Liu, J. S. Takahashi, and S. A. Kay, “Bioluminescence imaging of individual fibroblasts reveals persistent, independently phased circadian rhythms of clock gene expression,” *Curr. Biol.*, 2004.
[49] M. Nakajima *et al.*, “Reconstitution of circadian oscillation of cyanobacterial KaiC phosphorylation in vitro,” *Science (80-.).*, 2005.
[50] J. S. O-Neill and A. B. Reddy, “Circadian clocks in human red blood cells,” *Nature*, 2011.
[51] R. Silver, J. LeSauter, P. A. Tresco, and M. N. Lehman, “A diffusible coupling signal from the transplanted suprachiasmatic nucleus controlling circadian locomotor rhythms,” *Nature*, 1996.
[52] E. D. Herzog, S. J. Aton, R. Numano, Y. Sakaki, and H. Tei, “Temporal Precision in the Mammalian Circadian System: A Reliable Clock from Less Reliable Neurons,” *J. Biol. Rhythms*, 2004.
[53] S. J. Aton, C. S. Colwell, A. J. Harmar, J. Waschek, and E. D. Herzog, “Vasoactive intestinal polypeptide mediates circadian rhythmicity and synchrony in mammalian clock neurons,” *Nat. Neurosci.*, 2005.
[54] E. S. Maywood, J. E. Chesham, J. A. O’Brien, and M. H. Hastings, “A diversity of paracrine signals sustains molecular circadian cycling in suprachiasmatic nucleus circuits,” *Proc. Natl. Acad. Sci. U. S. A.*, 2011.
[55] Y. Yamaguchi *et al.*, “Mice genetically deficient in vasopressin V1a and V1b receptors are resistant to jet lag,” *Science (80-.).*, 2013.
[56] A. J. Harmar *et al.*, “The VPAC2 receptor is essential for circadian function in the mouse suprachiasmatic nuclei,” *Cell*, 2002.
[57] U. Abraham, A. E. Granada, P. O. Westermark, M. Heine, A. Kramer, and H. Herzel, “Coupling governs entrainment range of circadian clocks,” *Mol. Syst. Biol.*, 2010.
[58] E. D. Buhr, S. H. Yoo, and J. S. Takahashi, “Temperature as a universal resetting cue for mammalian circadian oscillators,” *Science (80-.).*, 2010.
[59] M. H. Vitaterna *et al.*, “The mouse Clock mutation reduces circadian pacemaker amplitude and enhances efficacy of resetting stimuli and phase-response curve amplitude,” *Proc. Natl. Acad. Sci. U. S. A.*, 2006.
[60] A. C. Liu *et al.*, “Intercellular Coupling Confers Robustness against Mutations in the SCN Circadian Clock Network,” *Cell*, 2007.
[61] T. Noguchi, L. L. Wang, and D. K. Welsh, “Fibroblast PER2 circadian rhythmicity depends on cell density,” *J. Biol. Rhythms*, 2013.
[62] J. Rougemont and F. Naef, “Dynamical signatures of cellular fluctuations and oscillator stability in peripheral circadian clocks,” *Mol. Syst. Biol.*, 2007.
[63] C. J. Guenthner *et al.*, “Circadian rhythms of PER2::LUC in individual primary mouse hepatocytes and cultures,” *PLoS One*, 2014.
[64] “biological clock,” 2019. [Online]. Available: https://www.merriam-webster.com/dictionary/biological clock. [Accessed: 17-Jul-2019].
[65] D. J. Kuhlman SJ, Craig LM, “Introduction to Chronobiology.,” *Cold Spring Harb Perspect Biol*, vol. 10, no. 9, 2018.
[66] C. Darwin, *On the Origin of the Species*. 1859.
[67] K. M. Vaze, K. L. Nikhil, and V. K. Sharma, “Circadian rhythms: 4. Why do living

organisms have them?," *Resonance*, 2014.
[68] J. Richards and M. L. Gumz, "Mechanism of the circadian clock in physiology," *American Journal of Physiology - Regulatory Integrative and Comparative Physiology*. 2013.
[69] M. A. Woelfle, Y. Ouyang, K. Phanvijhitsiri, and C. H. Johnson, "The adaptive value of circadian clocks: An experimental assessment in cyanobacteria," *Curr. Biol.*, 2004.
[70] P. J. DeCoursey, J. K. Walker, and S. A. Smith, "A circadian pacemaker in free-living chipmunks: Essential for survival?," *J. Comp. Physiol. - A Sensory, Neural, Behav. Physiol.*, 2000.
[71] N. F. Ruby, J. Dark, H. C. Heller, and I. Zucker, "Ablation of suprachiasmatic nucleus alters timing of hibernation in ground squirrels," *Proc. Natl. Acad. Sci. U. S. A.*, 1996.
[72] P. J. DeCoursey, J. R. Krulas, G. Mele, and D. C. Holley, "Circadian performance of suprachiasmatic nuclei (SCN)-lesioned antelope ground squirrels in a desert enclosure," *Physiol. Behav.*, 1997.
[73] N. Park, S. Cheon, G. H. Son, S. Cho, and K. Kim, "Chronic circadian disturbance by a shortened light-dark cycle increases mortality," *Neurobiol. Aging*, 2012.
[74] J. Aschoff, "Tagesperiodik bei Mäusestämmen unter konstanten Umgebungsbedingungen," *Pflugers Arch. Gesamte Physiol. Menschen Tiere*, 1955.
[75] J. Aschoff and J. Meyer-Lohmann, "Angeborene 24-Stunden-Periodik beim Kücken," *Pflugers Arch. Gesamte Physiol. Menschen Tiere*, 1954.
[76] V. Sheeba, V. K. Sharma, M. K. Chandrashekaran, and A. Joshi, "Persistence of eclosion rhythm in Drosophila melanogaster after 600 generations in an aperiodic environment," *Naturwissenschaften*, 1999.
[77] M. N. Lehman, R. Silver, W. R. Gladstone, R. M. Kahn, M. Gibson, and E. L. Bittman, "Circadian rhythmicity restored by neural transplant. Immunocytochemical characterization of the graft and its integration with the host brain," *J. Neurosci.*, 1987.
[78] R. G. Foster, I. Provencio, D. Hudson, S. Fiske, W. De Grip, and M. Menaker, "Circadian photoreception in the retinally degenerate mouse (rd/rd)," *J. Comp. Physiol. A*, 1991.
[79] I. Provencio, I. R. Rodriguez, G. Jiang, W. P. Hayes, E. F. Moreira, and M. D. Rollag, "A novel human opsin in the inner retina," *J. Neurosci.*, 2000.
[80] E. E. Abrahamson and R. Y. Moore, "Suprachiasmatic nucleus in the mouse: Retinal innervation, intrinsic organization and efferent projections," *Brain Res.*, 2001.
[81] J. P. Pett, M. Kondoff, G. Bordyugov, A. Kramer, and H. Herzel, "Co-existing feedback loops generate tissue-specific circadian rhythms," *Life Sci. Alliance*, 2018.
[82] S. A. Brown, G. Zumbrunn, F. Fleury-Olela, N. Preitner, and U. Schibler, "Rhythms of mammalian body temperature can sustain peripheral circadian clocks," *Curr. Biol.*, 2002.
[83] H. Guo, J. M. K. Brewer, A. Champhekar, R. B. S. Harris, and E. L. Bittman, "Differential control of peripheral circadian rhythms by suprachiasmatic-dependent neural signals," *Proc. Natl. Acad. Sci. U. S. A.*, 2005.
[84] A. Ishida *et al.*, "Light activates the adrenal gland: Timing of gene expression and glucocorticoid release," *Cell Metab.*, 2005.
[85] F. Damiola, N. Le Minli, N. Preitner, B. Kornmann, F. Fleury-Olela, and U.

Schibler, “Restricted feeding uncouples circadian oscillators in peripheral tissues from the central pacemaker in the suprachiasmatic nucleus,” *Genes Dev.*, 2000.
[86] U. Albrecht, “Timing to Perfection: The Biology of Central and Peripheral Circadian Clocks,” *Neuron*. 2012.
[87] C. S. Pittendrigh, “Circadian rhythms and the circadian organization of living systems.,” *Cold Spring Harb. Symp. Quant. Biol.*, 1960.
[88] D. R. Weaver, “The Suprachiasmatic Nucleus: A 25-Year Retrospective,” *J. Biol. Rhythms*, 1998.
[89] C. J. Guenthner *et al.*, “Circadian rhythms of PER2::LUC in individual primary mouse hepatocytes and cultures,” *PLoS One*, 2014.
[90] Y. Tahara *et al.*, “In vivo monitoring of peripheral circadian clocks in the mouse,” *Curr. Biol.*, 2012.
[91] R. G. Foster, “Shedding light on the biological clock,” *Neuron*. 1998.
[92] H. D. Piggins and C. Guilding, “The neural circadian system of mammals,” *Essays Biochem.*, 2011.
[93] J. M. Kornhauser, K. E. Mayo, and J. S. Takahashi, “Light, immediate-early genes, and circadian rhythms,” *Behavior Genetics*. 1996.
[94] L. P. Shearman, M. J. Zylka, D. R. Weaver, L. F. Kolakowski, and S. M. Reppert, “Two period homologs: Circadian expression and photic regulation in the suprachiasmatic nuclei,” *Neuron*, 1997.
[95] J. S. O’Neill and A. B. Reddy, “The essential role of cAMP/Ca 2+ signalling in mammalian circadian timekeeping,” *Biochemical Society Transactions*. 2012.
[96] D. A. Golombek and R. E. Rosenstein, “Physiology of circadian entrainment,” *Physiological Reviews*. 2010.
[97] W. Nakamura, S. Yamazaki, N. N. Takasu, K. Mishima, and G. D. Block, “Differential response of Period 1 expression within the suprachiasmatic nucleus,” *J. Neurosci.*, 2005.
[98] M. C. Antle, D. K. Foley, N. C. Foley, and R. Silver, “Gates and oscillators: A network model of the brain clock,” *J. Biol. Rhythms*, 2003.
[99] A. Sumová and H. Illnerová, “Effect of photic stimuli disturbing overt circadian rhythms on the dorsomedial and ventrolateral SCN rhythmicity,” *Brain Res.*, 2005.
[100] L. P. Morin, “SCN organization reconsidered,” *Journal of Biological Rhythms*. 2007.
[101] L. N. Cui, E. Coderre, and L. P. Renaud, “Glutamate and GABA mediate suprachiasmatic nucleus inputs to spinal-projecting paraventricular neurons,” *Am. J. Physiol. - Regul. Integr. Comp. Physiol.*, 2001.
[102] D. K. Welsh, J. S. Takahashi, and S. A. Kay, “Suprachiasmatic Nucleus: Cell Autonomy and Network Properties,” *Annu. Rev. Physiol.*, 2010.
[103] J. A. Evans *et al.*, “Shell neurons of the master circadian clock coordinate the phase of tissue clocks throughout the brain and body,” *BMC Biol.*, 2015.
[104] C. S. Colwell, “Linking neural activity and molecular oscillations in the SCN,” *Nature Reviews Neuroscience*. 2011.
[105] H. Ohta, S. Yamazaki, and D. G. McMahon, “Constant light desynchronizes mammalian clock neurons,” *Nat. Neurosci.*, 2005.
[106] N. Inagaki, S. Honma, D. Ono, Y. Tanahashi, and K. I. Honma, “Separate oscillating cell groups in mouse suprachiasmatic nucleus couple photoperiodically to the onset and end of daily activity,” *Proc. Natl. Acad. Sci. U. S. A.*, 2007.
[107] J. A. Evans, T. L. Leise, O. Castanon-Cervantes, and A. J. Davidson, “Dynamic Interactions Mediated by Nonredundant Signaling Mechanisms Couple

Circadian Clock Neurons," *Neuron*, 2013.
[108] H. O. De la Iglesia, J. Meyer, J. Carpino A., and W. J. Schwartz, "Antiphase oscillation of the left and right suprachiasmatic nuclei," *Science (80-.).*, 2000.
[109] M. P. Butler, M. N. Rainbow, E. Rodriguez, S. M. Lyon, and R. Silver, "Twelve-hour days in the brain and behavior of split hamsters," *Eur. J. Neurosci.*, 2012.
[110] L. Yan, N. C. Foley, J. M. Bobula, L. J. Kriegsfeld, and R. Silver, "Two antiphase oscillations occur in each suprachiasmatic nucleus of behaviorally split hamsters," *J. Neurosci.*, 2005.
[111] C. Wotus *et al.*, "Forced Desynchrony Reveals Independent Contributions of Suprachiasmatic Oscillators to the Daily Plasma Corticosterone Rhythm in Male Rats," *PLoS One*, 2013.
[112] M. D. Schwartz *et al.*, "Dissociation of circadian and light inhibition of melatonin release through forced desynchronization in the rat," *Proc. Natl. Acad. Sci. U. S. A.*, 2009.
[113] B. L. Smarr, E. Morris, and H. O. De La Iglesia, "The dorsomedial suprachiasmatic nucleus times circadian expression of Kiss1 and the luteinizing hormone surge," *Endocrinology*, 2012.
[114] T. Yamamoto, Y. Nakahata, H. Soma, M. Akashi, T. Mamine, and T. Takumi, "Transcriptional oscillation of canonical clock genes in mouse peripheral tissues," *BMC Mol. Biol.*, 2004.
[115] R. Zhang, N. F. Lahens, H. I. Ballance, M. E. Hughes, and J. B. Hogenesch, "A circadian gene expression atlas in mammals: Implications for biology and medicine," *Proc. Natl. Acad. Sci. U. S. A.*, 2014.
[116] Y. Wang *et al.*, "A proteomics landscape of circadian clock in mouse liver," *Nat. Commun.*, 2018.
[117] J. Yan, H. Wang, Y. Liu, and C. Shao, "Analysis of gene regulatory networks in the mammalian circadian rhythm," *PLoS Comput. Biol.*, 2008.
[118] F. Gachon, F. F. Olela, O. Schaad, P. Descombes, and U. Schibler, "The circadian PAR-domain basic leucine zipper transcription factors DBP, TEF, and HLF modulate basal and inducible xenobiotic detoxification," *Cell Metab.*, 2006.
[119] K. A. Lamia, K. F. Storch, and C. J. Weitz, "Physiological significance of a peripheral tissue circadian clock," *Proc. Natl. Acad. Sci. U. S. A.*, 2008.
[120] A. Y. L. So, T. U. Bernal, M. L. Pillsbury, K. R. Yamamoto, and B. J. Feldman, "Glucocorticoid regulation of the circadian clock modulates glucose homeostasis," *Proc. Natl. Acad. Sci. U. S. A.*, 2009.
[121] B. Marcheva *et al.*, "Disruption of the clock components CLOCK and BMAL1 leads to hypoinsulinaemia and diabetes," *Nature*, 2010.
[122] F. W. Turek *et al.*, "Obesity and metabolic syndrome in circadian Clock mutant nice," *Science (80-.).*, 2005.
[123] G. Le Martelot *et al.*, "REV-ERBα participates in circadian SREBP signaling and bile acid homeostasis," *PLoS Biol.*, 2009.
[124] F. Gachon, E. Nagoshi, S. A. Brown, J. Ripperger, and U. Schibler, "The mammalian circadian timing sytem: From gene expression to physiology," *Chromosoma*. 2004.
[125] K. Sakamoto *et al.*, "Multitissue circadian expression of rat period homolog (rPer2) mRNA is governed by the mammalian circadian clock, the suprachiasmatic nucleus in the brain," *J. Biol. Chem.*, 1998.
[126] H. Terazono *et al.*, "Adrenergic regulation of clock gene expression in mouse liver," *Proc. Natl. Acad. Sci. U. S. A.*, 2003.
[127] C. Cailotto *et al.*, "The suprachiasmatic nucleus controls the daily variation of plasma glucose via the autonomic output to the liver: Are the clock genes

involved?," *Eur. J. Neurosci.*, 2005.
[128] A. Kalsbeek, J. J. Van Heerikhuize, J. Wortel, and R. M. Buijs, "A diurnal rhythm of stimulatory input to the hypothalamo-pituitary- adrenal system as revealed by timed intrahypothalamic administration of the vasopressin V1 antagonist," *J. Neurosci.*, 1996.
[129] A. Kalsbeek, R. van der Spek, J. Lei, E. Endert, R. M. Buijs, and E. Fliers, "Circadian rhythms in the hypothalamo-pituitary-adrenal (HPA) axis," *Molecular and Cellular Endocrinology*. 2012.
[130] M. Kaneko, K. Kaneko, J. Shinsako, and M. F. Dallman, "Adrenal sensitivity to adrenocorticotropin varies diurnally," *Endocrinology*, 1981.
[131] A. Balsalobre *et al.*, "Resetting of circadian time in peripheral tissues by glucocorticoid signaling," *Science (80-.).*, 2000.
[132] A. B. Reddy *et al.*, "Glucocorticoid signaling synchronizes the liver circadian transcriptome," *Hepatology*, 2007.
[133] T. Yamamoto *et al.*, "Acute physical stress elevates mouse Period1 mRNA expression in mouse peripheral tissues via a glucocorticoid-responsive element," *J. Biol. Chem.*, 2005.
[134] U. Schibler and E. F. M. A. H. D. F. S. E. J. W. van S. and R. M. B. A Kalsbeek, "Circadian time keeping: the daily ups and downs of genes, cells, and organisms BT - Progress in Brain Research," in *Progress in Brain Research*, 2006.
[135] R. Hara *et al.*, "Restricted feeding entrains liver clock without participation of the suprachiasmatic nucleus," *Genes to Cells*, 2001.
[136] J. Rougemont and F. Naef, "Collective synchronization in populations of globally coupled phase oscillators with drifting frequencies," *Phys. Rev. E - Stat. Nonlinear, Soft Matter Phys.*, 2006.
[137] T. Noguchi, M. Ikeda, Y. Ohmiya, and Y. Nakajima, "A dual-color luciferase assay system reveals circadian resetting of cultured fibroblasts by co-cultured adrenal glands," *PLoS One*, 2012.
[138] M. Ishiura *et al.*, "Expression of a gene cluster kaiABC as a circadian feedback process in cyanobacteria," *Science (80-.).*, 1998.
[139] N. Gekakis *et al.*, "Role of the CLOCK protein in the mammalian circadian mechanism," *Science (80-.).*, 1998.
[140] C. Lee, J. P. Etchegaray, F. R. A. Cagampang, A. S. I. Loudon, and S. M. Reppert, "Posttranslational mechanisms regulate the mammalian circadian clock," *Cell*, 2001.
[141] R. P. Aryal *et al.*, "Macromolecular Assemblies of the Mammalian Circadian Clock," *Mol. Cell*, 2017.
[142] M. Gallego and D. M. Virshup, "Post-translational modifications regulate the ticking of the circadian clock," *Nature Reviews Molecular Cell Biology*. 2007.
[143] J. S. Takahashi, "Transcriptional architecture of the mammalian circadian clock," *Nature Reviews Genetics*. 2017.
[144] J. A. Ripperger and U. Schibler, "Rhythmic CLOCK-BMAL1 binding to multiple E-box motifs drives circadian Dbp transcription and chromatin transitions," *Nat. Genet.*, 2006.
[145] N. Preitner *et al.*, "The orphan nuclear receptor REV-ERBα controls circadian transcription within the positive limb of the mammalian circadian oscillator," *Cell*, 2002.
[146] T. K. Sato *et al.*, "A functional genomics strategy reveals rora as a component of the mammalian circadian clock," *Neuron*, 2004.
[147] H. Cho *et al.*, "Regulation of circadian behaviour and metabolism by REV-ERB-α and REV-ERB-β," *Nature*, 2012.

[148] S. Mitsui, S. Yamaguchi, T. Matsuo, Y. Ishida, and H. Okamura, “Antagonistic role of E4BP4 and PAR proteins in the circadian oscillatory mechanism,” *Genes Dev.*, 2001.
[149] H. Yoshitane *et al.*, “Functional D-box sequences reset the circadian clock and drive mRNA rhythms,” *Commun. Biol.*, 2019.
[150] H. R. Ueda *et al.*, “System-level identification of transcriptional circuits underlying mammalian circadian clocks,” *Nat. Genet.*, 2005.
[151] M. Ukai-Tadenuma, T. Kasukawa, and H. R. Ueda, “Proof-by-synthesis of the transcriptional logic of mammalian circadian clocks,” *Nat. Cell Biol.*, 2008.
[152] D. Gonze, “Modeling circadian clocks: From equations to oscillations,” *Central European Journal of Biology*. 2011.
[153] F. Halberg, F. Carandente, G. Cornelissen, and G. S. Katinas, “Glossary of chronobiology,” *Chronobiologia*, 1977.
[154] C. S. Pittendrigh and S. Daan, “A functional analysis of circadian pacemakers in nocturnal rodents - IV. Entrainment: Pacemaker as clock,” *J. Comp. Physiol. ■ A*, 1976.
[155] A. E. Granada, G. Bordyugov, A. Kramer, and H. Herzel, “Human Chronotypes from a Theoretical Perspective,” *PLoS One*, 2013.
[156] G. Bordyugov *et al.*, “Tuning the phase of circadian entrainment,” *J. R. Soc. Interface*, 2015.
[157] G. Bordyugov, A. E. Granada, and H. Herzel, “How coupling determines the entrainment of circadian clocks,” *Eur. Phys. J. B*, 2011.
[158] J. S. Takahashi, P. J. Decoursey, L. Bauman, and M. Menaker, “Spectral sensitivity of a novel photoreceptive system mediating entrainment of mammalian circadian rhythms,” *Nature*, 1984.
[159] D. E. Nelson and J. S. Takahashi, “Sensitivity and integration in a visual pathway for circadian entrainment in the hamster (Mesocricetus auratus).,” *J. Physiol.*, 1991.
[160] A. D. Güler *et al.*, “Melanopsin cells are the principal conduits for rod-cone input to non-image-forming vision,” *Nature*, 2008.
[161] S. Panda *et al.*, “Melanopsin is required for non-image-forming photic responses in blind mice,” *Science (80-.).*, 2003.
[162] S. Hattar *et al.*, “Central projections of melanopsin-expressing retinal ganglion cells in the mouse,” *J. Comp. Neurol.*, 2006.
[163] S. Panda *et al.*, “Melanopsin (Opn4) requirement for normal light-induced circadian phase shifting,” *Science (80-.).*, 2002.
[164] R. F. Johnson, R. Y. Moore, and L. P. Morin, “Loss of entrainment and anatomical plasticity after lesions of the hamster retinohypothalamic tract,” *Brain Res.*, 1988.
[165] S. Shibata and R. Y. Moore, “Neuropeptide Y and optic chiasm stimulation of affect suprachiasmatic nucleus circadian function in vitro,” *Brain Res.*, 1993.
[166] A. M. Rosenwasser, “Entrainment of Circadian Rhythms by Light,” in *Encyclopedia of Neuroscience*, 2009.
[167] T. Roenneberg, R. Hut, S. Daan, and M. Merrow, “Entrainment concepts revisited,” *J. Biol. Rhythms*, 2010.
[168] S. Daan and C. S. Pittendrigh, “A Functional analysis of circadian pacemakers in nocturnal rodents - II. The variability of phase response curves,” *J. Comp. Physiol. ■ A*, 1976.
[169] N. Mrosovsky, S. G. Reebs, G. I. Honrado, and P. A. Salmon, “Behavioural entrainment of circadian rhythms,” *Experientia*. 1989.
[170] A. T. Winfree, “Phase control of neural pacemakers,” *Science (80-.).*, 1977.

[171] T. Roenneberg and M. Merrow, “Type 1 and Type 0 Resetting,” in *Encyclopedia of Neuroscience*, 2008.
[172] C. Schmal, E. D. Herzog, and H. Herzel, “Measuring Relative Coupling Strength in Circadian Systems,” *J. Biol. Rhythms*, 2018.
[173] I. Caldelas, V. J. Poirel, B. Sicard, P. Pévet, and E. Challet, “Circadian profile and photic regulation of clock genes in the suprachiasmatic nucleus of a diurnal mammal Arvicanthis ansorgei,” *Neuroscience*, 2003.
[174] T. M. Hoban and F. M. Sulzman, “Light effects on circadian timing system of a diurnal primate, the squirrel monkey,” *Am. J. Physiol. - Regul. Integr. Comp. Physiol.*, 1985.
[175] M. Mahoney, A. Bult, and L. Smale, “Phase response curve and light-induced fos expression in the suprachiasmatic nucleus and adjacent hypothalamus of Arvicanthis niloticus,” *J. Biol. Rhythms*, 2001.
[176] L. Smale, T. Lee, and A. A. Nunez, “Mammalian diurnality: Some facts and gaps,” *Journal of Biological Rhythms*. 2003.
[177] A. E. Fidler and E. Gwinner, “Comparative analysis of Avian BMAL1 and CLOCK protein sequences: A search for features associated with owl nocturnal behaviour,” in *Comparative Biochemistry and Physiology - B Biochemistry and Molecular Biology*, 2003.
[178] N. Mrosovsky and S. Hattar, “Diurnal mice (Mus musculus) and other examples of temporal niche switching,” *Journal of Comparative Physiology A: Neuroethology, Sensory, Neural, and Behavioral Physiology*. 2005.
[179] Y. Shigeyoshi *et al.*, “Light-induced resetting of a mammalian circadian clock is associated with rapid induction of the mPer1 transcript,” *Cell*, 1997.
[180] U. Albrecht, Z. S. Sun, G. Eichele, and C. C. Lee, “A differential response of two putative mammalian circadian regulators, mper1 and mper2, to light,” *Cell*, 1997.
[181] M. J. Zylka, L. P. Shearman, D. R. Weaver, and S. M. Reppert, “Three period homologs in mammals: Differential light responses in the suprachiasmatic circadian clock and oscillating transcripts outside of brain,” *Neuron*, 1998.
[182] J. S. Pendergast, K. D. Niswender, and S. Yamazaki, “Tissue-specific function of period3 in circadian rhythmicity,” *PLoS One*, 2012.
[183] H. Abe *et al.*, “Phase-dependent induction by light of rat Clock gene expression in the suprachiasmatic nucleus,” *Mol. Brain Res.*, 1999.
[184] J. H. Meijer and W. J. Schwartz, “In search of the pathways for light-induced pacemaker resetting in the suprachiasmatic nucleus,” *Journal of Biological Rhythms*. 2003.
[185] T. Ueyama *et al.*, “Suprachiasmatic nucleus: A central autonomic clock [1],” *Nature Neuroscience*. 1999.
[186] A. Kalsbeek, S. La Fleur, C. Van Heijningen, and R. M. Buijs, “Suprachiasmatic GABAergic inputs to the paraventricular nucleus control plasma glucose concentrations in the rat via sympathetic innervation of the liver,” *J. Neurosci.*, 2004.
[187] M. Kaneko, T. Hiroshige, J. Shinsako, and M. F. Dallman, “Diurnal changes in amplification of hormone rhythms in the adrenocortical system,” *Am. J. Physiol. - Regul. Integr. Comp. Physiol.*, 1980.
[188] H. Oster *et al.*, “The circadian rhythm of glucocorticoids is regulated by a gating mechanism residing in the adrenal cortical clock,” *Cell Metab.*, 2006.
[189] P. Rosenfeld, J. A. M. van Eekelen, S. Levine, and E. R. de Kloet, “Ontogeny of corticosteroid receptors in the brain,” *Cell. Mol. Neurobiol.*, 1993.
[190] P. Rosenfeld, J. A. M. Van Eekelen, S. Levine, and E. R. De Kloet, “Ontogeny of the Type 2 glucocorticoid receptor in discrete rat brain regions: an

immunocytochemical study," *Dev. Brain Res.*, 1988.
[191] R. Refinetti, "Entrainment of circadian rhythm by ambient temperature cycles in mice," *J. Biol. Rhythms*, 2010.
[192] Y. Tahara and S. Shibata, "Chrono-biology, chrono-pharmacology, and chrono-nutrition," *Journal of Pharmacological Sciences*. 2014.
[193] G. Wolff and K. A. Esser, "Scheduled exercise phase shifts the circadian clock in skeletal Muscle," *Med. Sci. Sports Exerc.*, 2012.
[194] A. M. Schroeder, D. Truong, D. H. Loh, M. C. Jordan, K. P. Roos, and C. S. Colwell, "Voluntary scheduled exercise alters diurnal rhythms of behaviour, physiology and gene expression in wild-type and vasoactive intestinal peptide-deficient mice," *J. Physiol.*, 2012.
[195] J. S. Pendergast, K. L. Branecky, R. Huang, K. D. Niswender, and S. Yamazaki, "Wheel-running activity modulates circadian organization and the daily rhythm of eating behavior," *Front. Psychol.*, 2014.
[196] H. Sasaki *et al.*, "Forced rather than voluntary exercise entrains peripheral clocks via a corticosterone/noradrenaline increase in PER2::LUC mice," *Sci. Rep.*, 2016.
[197] X. Yang *et al.*, "Nuclear Receptor Expression Links the Circadian Clock to Metabolism," *Cell*, 2006.
[198] C. Liu, S. Li, T. Liu, J. Borjigin, and J. D. Lin, "Transcriptional coactivator PGC-1α integrates the mammalian clock and energy metabolism," *Nature*, 2007.
[199] K. A. Lamia *et al.*, "AMPK regulates the circadian clock by cryptochrome phosphorylation and degradation," *Science (80-.).*, 2009.
[200] K. M. Ramsey *et al.*, "Circadian clock feedback cycle through NAMPT-Mediated NAD+ biosynthesis," *Science (80-.).*, 2009.
[201] J. Rutter, M. Reick, L. C. Wu, and S. L. McKnight, "Regulation of crock and NPAS2 DNA binding by the redox state of NAD cofactors," *Science (80-.).*, 2001.
[202] J. S. Pendergast and S. Yamazaki, "The Mysterious Food-Entrainable Oscillator: Insights from Mutant and Engineered Mouse Models," *Journal of Biological Rhythms*. 2018.
[203] J. S. Pendergast, W. Nakamura, R. C. Friday, F. Hatanaka, T. Takumi, and S. Yamazaki, "Robust food anticipatory activity in BMAL1-deficient mice," *PLoS One*, 2009.
[204] K. F. Storch and C. J. Weitz, "Daily rhythms of food-anticipatory behavioral activity do not require the known circadian clock," *Proc. Natl. Acad. Sci. U. S. A.*, 2009.
[205] P. Pezuk, J. A. Mohawk, T. Yoshikawa, M. T. Sellix, and M. Menaker, "Circadian organization is governed by extra-SCN pacemakers," *J. Biol. Rhythms*, 2010.
[206] F. K. Stephan, J. M. Swann, and C. L. Sisk, "Entrainment of circadian rhythms by feeding schedules in rats with suprachiasmatic lesions," *Behav. Neural Biol.*, 1979.
[207] D. T. Krieger, H. Hauser, and L. C. Krey, "Suprachiasmatic nuclear lesions do not abolish food-shifted circadian adrenal and temperature rhythmicity," *Science (80-.).*, 1977.
[208] Y. Kuramoto, *Chemical Oscillations, Waves and Turbulence.* 1983.
[209] A. T. Winfree, "Biological rhythms and the behavior of populations of coupled oscillators," *J. Theor. Biol.*, 1967.
[210] Y. Kuramoto, "Self-entrainment of a population of coupled non-linear oscillators," in *International Symposium on Mathematical Problems in Theoretical Physics*, 2005.
[211] Y. Kuramoto, "Self-entrainment of a population of coupled non-linear oscillators

BT - International Symposium on Mathematical Problems in Theoretical Physics," in *International Symposium on Mathematical Problems in Theoretical Physics*, 1975.
[212] S. H. Strogatz, "From Kuramoto to Crawford: Exploring the onset of synchronization in populations of coupled oscillators," *Phys. D Nonlinear Phenom.*, 2000.
[213] D. Gonze, S. Bernard, C. Waltermann, A. Kramer, and H. Herzel, "Spontaneous synchronization of coupled circadian oscillators," *Biophys. J.*, 2005.
[214] J. K. Kim, Z. P. Kilpatrick, M. R. Bennett, and K. Josić, "Molecular mechanisms that regulate the coupled period of the mammalian circadian clock," *Biophys. J.*, 2014.
[215] Merriam-Webster Inc., "Resonance," *The Merriam-Webster.com Dictionary*. [Online]. Available: https://www.merriam-webster.com/dictionary/resonance. [Accessed: 21-Jan-2020].
[216] A. S. Pikovsky, "On the interaction of strange attractors," *Zeitschrift für Phys. B Condens. Matter*, 1984.
[217] P. O. Westermark, D. K. Welsh, H. Okamura, and H. Herzel, "Quantification of circadian rhythms in single cells," *PLoS Comput. Biol.*, 2009.
[218] K. Hoffmann, "Zum Einfluß der Zeitgeberstärke auf die Phasenlage der synchronisierten circadianen Periodik," *Z. Vgl. Physiol.*, 1969.
[219] C. H. Johnson, J. A. Elliott, and R. Foster, "Entrainment of circadian programs," *Chronobiology International*. 2003.
[220] C. S. Pittendrigh, W. T. Kyner, and T. Takamura, "The Amplitude of Circadian Oscillations: Temperature Dependence, Latitudinal Clines, and the Photoperiodic Time Measurement," *J. Biol. Rhythms*, 1991.
[221] S. A. Brown *et al.*, "Molecular insights into human daily behavior," *Proc. Natl. Acad. Sci. U. S. A.*, 2008.
[222] S. Honma, T. Shirakawa, Y. Katsuno, M. Namihira, and K. I. Honma, "Circadian periods of single suprachiasmatic neurons in rats," *Neurosci. Lett.*, 1998.
[223] T. Shirakawa, S. Honma, Y. Katsuno, H. Oguchi, and K. I. Honma, "Synchronization of circadian firing rhythms in cultured rat suprachiasmatic neurons," *Eur. J. Neurosci.*, 2000.
[224] K. Shinohara, S. Honma, Y. Katsuno, H. Abe, and K. Honma, "Two distinct oscillators in the rat suprachiasmatic nucleus in vitro," *Proc. Natl. Acad. Sci. U. S. A.*, 1995.
[225] H. E. Reed, A. Meyer-Spasche, D. J. Cutler, C. W. Coen, and H. D. Piggins, "Vasoactive intestinal polypeptide (VIP) phase-shifts the rat suprachiasmatic nucleus clock in vitro," *Eur. J. Neurosci.*, 2001.
[226] J. R. Jones, M. C. Tackenberg, and D. G. Mcmahon, "Manipulating circadian clock neuron firing rate resets molecular circadian rhythms and behavior," *Nat. Neurosci.*, 2015.
[227] C. S. Colwell *et al.*, "Disrupted circadian rhythms in VIP- and PHI-deficient mice," *Am. J. Physiol. - Regul. Integr. Comp. Physiol.*, 2003.
[228] D. J. Cutler *et al.*, "The mouse VPAC2 receptor confers suprachiasmatic nuclei cellular rhythmicity and responsiveness to vasoactive intestinal polypeptide in vitro," *Eur. J. Neurosci.*, 2003.
[229] T. M. Brown, C. S. Colwell, J. A. Waschek, and H. D. Piggins, "Disrupted neuronal activity rhythms in the suprachiasmatic nuclei of vasoactive intestinal polypeptide-deficient mice," *J. Neurophysiol.*, 2007.
[230] I. Kalló *et al.*, "Transgenic approach reveals expression of the VPAC2 receptor in phenotypically defined neurons in the mouse suprachiasmatic nucleus and in

its efferent target sites," *Eur. J. Neurosci.*, 2004.
[231] C. Schomerus, E. Maronde, E. Laedtke, and H. W. Korf, "Vasoactive intestinal peptide (VIP) and pituitary adenylate cyclase-activating polypeptide (PACAP) induce phosphorylation of the transcription factor CREB in subpopulations of rat pinealocytes: Immunocytochemical and immunochemical evidence," *Cell Tissue Res.*, 1996.
[232] Z. Travnickova-Bendova, N. Cermakian, S. M. Reppert, and P. Sassone-Corsi, "Bimodal regulation of mPeriod promoters by CREB-dependent signaling and CLOCK/BMAL1 activity," *Proc. Natl. Acad. Sci. U. S. A.*, 2002.
[233] B. Ananthasubramaniam, E. D. Herzog, and H. Herzel, "Timing of Neuropeptide Coupling Determines Synchrony and Entrainment in the Mammalian Circadian Clock," *PLoS Comput. Biol.*, 2014.
[234] A. C. Liu, W. G. Lewis, and S. A. Kay, "Mammalian circadian signaling networks and therapeutic targets," *Nature Chemical Biology*. 2007.
[235] D. Ono, S. Honma, and K. ichi Honma, "Differential roles of AVP and VIP signaling in the postnatal changes of neural networks for coherent circadian rhythms in the SCN," *Sci. Adv.*, 2016.
[236] J. Da Li, K. J. Burton, C. Zhang, S. B. Hu, and Q. Y. Zhou, "Vasopressin receptor V1a regulates circadian rhythms of locomotor activity and expression of clock-controlled genes in the suprachiasmatic nuclei," *Am. J. Physiol. - Regul. Integr. Comp. Physiol.*, 2009.
[237] M. Mieda *et al.*, "Cellular clocks in AVP neurons of the scn are critical for interneuronal coupling regulating circadian behavior rhythm," *Neuron*, 2015.
[238] M. Mieda, H. Okamoto, and T. Sakurai, "Manipulating the Cellular Circadian Period of Arginine Vasopressin Neurons Alters the Behavioral Circadian Period," *Curr. Biol.*, 2016.
[239] A. J. McArthur, A. N. Coogan, S. Ajpru, D. Sugden, S. M. Biello, and H. D. Piggins, "Gastrin-releasing peptide phase-shifts suprachiasmatic nuclei neuronal rhythms in vitro," *J. Neurosci.*, 2000.
[240] H. Albus, M. J. Vansteensel, S. Michel, G. D. Block, and J. H. Meijer, "A GABAergic mechanism is necessary for coupling dissociable ventral and dorsal regional oscillators within the circadian clock," *Curr. Biol.*, 2005.
[241] M. A. Long, M. J. Jutras, B. W. Connors, and R. D. Burwell, "Electrical synapses coordinate activity in the suprachiasmatic nucleus," *Nat. Neurosci.*, 2005.
[242] M. Stratmann and U. Schibler, "Properties, entrainment, and physiological functions of mammalian peripheral oscillators," *Journal of Biological Rhythms*. 2006.
[243] H. Guo, J. M. K. Brewer, M. N. Lehman, and E. L. Bittman, "Suprachiasmatic regulation of circadian rhythms of gene expression in hamster peripheral organs: Effects of transplanting the pacemaker," *J. Neurosci.*, 2006.
[244] K. B. Koronowski *et al.*, "Defining the Independence of the Liver Circadian Clock," *Cell*, 2019.
[245] P. S. Welz *et al.*, "BMAL1-Driven Tissue Clocks Respond Independently to Light to Maintain Homeostasis," *Cell*, 2019.
[246] M. D. Ruben *et al.*, "A database of tissue-specific rhythmically expressed human genes has potential applications in circadian medicine," *Sci. Transl. Med.*, 2018.
[247] B. Kornmann, O. Schaad, H. Bujard, J. S. Takahashi, and U. Schibler, "System-driven and oscillator-dependent circadian transcription in mice with a conditionally active liver clock," *PLoS Biol.*, 2007.
[248] A. C. West and D. A. Bechtold, "The cost of circadian desynchrony: Evidence, insights and open questions," *BioEssays*, 2015.

[249] M. E. Hughes *et al.*, “Harmonics of circadian gene transcription in mammals,” *PLoS Genet.*, 2009.
[250] B. D. Harfmann, E. A. Schroder, and K. A. Esser, “Circadian rhythms, the molecular clock, and skeletal muscle,” *Journal of Biological Rhythms*. 2015.
[251] A. Shostak, J. Husse, and H. Oster, “Circadian regulation of adipose function,” *Adipocyte*, 2013.
[252] M. S. Robles and M. Mann, “Proteomic approaches in circadian biology,” *Handb. Exp. Pharmacol.*, 2013.
[253] M. S. Robles, J. Cox, and M. Mann, “In-Vivo Quantitative Proteomics Reveals a Key Contribution of Post-Transcriptional Mechanisms to the Circadian Regulation of Liver Metabolism,” *PLoS Genet.*, 2014.
[254] M. S. Robles, S. J. Humphrey, and M. Mann, “Phosphorylation Is a Central Mechanism for Circadian Control of Metabolism and Physiology,” *Cell Metab.*, 2017.
[255] K. Thurley *et al.*, “Principles for circadian orchestration of metabolic pathways,” *Proc. Natl. Acad. Sci. U. S. A.*, 2017.
[256] H. Wijnen and M. W. Young, “Interplay of Circadian Clocks and Metabolic Rhythms,” *Annu. Rev. Genet.*, 2006.
[257] R. Dallmann, A. U. Viola, L. Tarokh, C. Cajochen, and S. A. Brown, “The human circadian metabolome,” *Proc. Natl. Acad. Sci. U. S. A.*, 2012.
[258] Y. Adamovich, R. Aviram, and G. Asher, “The emerging roles of lipids in circadian control,” *Biochimica et Biophysica Acta - Molecular and Cell Biology of Lipids*. 2015.
[259] S. E. La Fleur, A. Kalsbeek, J. Wortel, and R. M. Buijs, “A suprachiasmatic nucleus generated rhythm in basal glucose concentrations,” *J. Neuroendocrinol.*, 1999.
[260] M. Ruiter, S. E. La Fleur, C. Van Heijningen, J. Van der Vliet, A. Kalsbeek, and R. M. Buijs, “The daily rhythm in plasma glucagon concentrations in the rat is modulated by the biological clock and by feeding behavior,” *Diabetes*, 2003.
[261] R. S. Ahima, D. Prabakaran, and J. S. Flier, “Postnatal leptin surge and regulation of circadian rhythm of leptin by feeding. Implications for energy homeostasis and neuroendocrine function,” *J. Clin. Invest.*, 1998.
[262] A. Kohsaka and J. Bass, “A sense of time: how molecular clocks organize metabolism,” *Trends in Endocrinology and Metabolism*. 2007.
[263] B. Fang *et al.*, “Circadian enhancers coordinate multiple phases of rhythmic gene transcription in vivo,” *Cell*, 2014.
[264] H. A. Duong and C. J. Weitz, “Temporal orchestration of repressive chromatin modifiers by circadian clock Period complexes,” *Nat. Struct. Mol. Biol.*, 2014.
[265] D. Feng *et al.*, “A circadian rhythm orchestrated by histone deacetylase 3 controls hepatic lipid metabolism,” *Science (80-.).*, 2011.
[266] N. Koike *et al.*, “Transcriptional architecture and chromatin landscape of the core circadian clock in mammals,” *Science (80-.).*, 2012.
[267] A. B. Reddy *et al.*, “Circadian Orchestration of the Hepatic Proteome,” *Curr. Biol.*, 2006.
[268] R. S. Edgar *et al.*, “Peroxiredoxins are conserved markers of circadian rhythms,” *Nature*, 2012.
[269] S. Yang *et al.*, “The role of mPer2 clock gene in glucocorticoid and feeding rhythms,” *Endocrinology*, 2009.
[270] J. Delezie *et al.*, “The nuclear receptor REV-ERBα is required for the daily balance of carbohydrate and lipid metabolism,” *FASEB J.*, 2012.
[271] S. S. Thosar, M. P. Butler, and S. A. Shea, “Role of the circadian system in

cardiovascular disease," *Journal of Clinical Investigation*. 2018.
[272] M. E. Young and M. S. Bray, "Potential role for peripheral circadian clock dyssynchrony in the pathogenesis of cardiovascular dysfunction," *Sleep Med.*, 2007.
[273] K. L. Eckel-Mahan *et al.*, "Reprogramming of the circadian clock by nutritional challenge," *Cell*, 2013.
[274] R. V. Kondratov, A. A. Kondratova, V. Y. Gorbacheva, O. V. Vykhovanets, and M. P. Antoch, "Early aging and age-related pathologies in mice deficient in BMAL1, the core component of the circadian clock," *Genes Dev.*, 2006.
[275] L. Fu, H. Pelicano, J. Liu, P. Huang, and C. C. Lee, "The circadian gene Period2 plays an important role in tumor suppression and DNA damage response in vivo," *Cell*, 2002.
[276] Y. Ouyang, C. R. Andersson, T. Kondo, S. S. Golden, and C. H. Johnson, "Resonating circadian clocks enhance fitness in cyanobacteria," *Proc. Natl. Acad. Sci. U. S. A.*, 1998.
[277] C. S. Pittendrigh and D. H. Minis, "Circadian systems: longevity as a function of circadian resonance in Drosophila melanogaster.," *Proc. Natl. Acad. Sci. U. S. A.*, 1972.
[278] J. ASCHOFF and U. V. SAINT PAUL, "Circadian rhythms in the blowfly, Phormia terraenovae: the period in constant light," *Physiol. Entomol.*, 1982.
[279] D. -J DIJK, J. F. DUFFY, and C. A. CZEISLER, "Circadian and sleep/wake dependent aspects of subjective alertness and cognitive performance," *J. Sleep Res.*, 1992.
[280] M. Litinski, F. A. J. L. Scheer, and S. A. Shea, "Influence of the Circadian System on Disease Severity," *Sleep Medicine Clinics*. 2009.
[281] R. Leproult, U. Holmbäck, and E. Van Cauter, "Circadian misalignment augments markers of insulin resistance and inflammation, independently of sleep loss," *Diabetes*, 2014.
[282] C. J. Morris, D. Aeschbach, and F. A. J. L. Scheer, "Circadian system, sleep and endocrinology," *Molecular and Cellular Endocrinology*. 2012.
[283] J. Qian, C. J. Morris, R. Caputo, M. Garaulet, and F. A. J. L. Scheer, "Ghrelin is impacted by the endogenous circadian system and by circadian misalignment in humans," *Int. J. Obes.*, 2019.
[284] S. N. Archer *et al.*, "Mistimed sleep disrupts circadian regulation of the human transcriptome," *Proc. Natl. Acad. Sci. U. S. A.*, 2014.
[285] L. Kervezee, M. Cuesta, N. Cermakian, and D. B. Boivin, "Simulated night shift work induces circadian misalignment of the human peripheral blood mononuclear cell transcriptome," *Proc. Natl. Acad. Sci. U. S. A.*, 2018.
[286] C. M. Depner, E. L. Melanson, A. W. McHill, and K. P. Wright, "Mistimed food intake and sleep alters 24-hour time-of-day patterns of the human plasma proteome," *Proc. Natl. Acad. Sci. U. S. A.*, 2018.
[287] G. F. Giskeødegård, S. K. Davies, V. L. Revell, H. Keun, and D. J. Skene, "Diurnal rhythms in the human urine metabolome during sleep and total sleep deprivation," *Sci. Rep.*, 2015.
[288] S. K. Davies *et al.*, "Effect of sleep deprivation on the human metabolome," *Proc. Natl. Acad. Sci. U. S. A.*, 2014.
[289] W. J. Sheward *et al.*, "Entrainment to feeding but not to light: Circadian phenotype of VPAC 2 receptor-null mice," *J. Neurosci.*, 2007.
[290] S. An *et al.*, "A neuropeptide speeds circadian entrainment by reducing intercellular synchrony," *Proc. Natl. Acad. Sci. U. S. A.*, 2013.
[291] J. Bass and M. A. Lazar, "Circadian time signatures of fitness and disease,"

Science. 2016.
[292] E. A. Lodish H, Berk A, Zipursky SL, “Overview of the Secretory Pathway.,” *Mol. Cell Biol.*, 2000.
[293] S. Jäschke, “The role of secretory pathway for the mammalian circadian clock,” Freie Universität Berlin, 2018.
[294] D. Mauvoisin *et al.*, “Circadian clock-dependent and -independent rhythmic proteomes implement distinct diurnal functions in mouse liver,” *Proc. Natl. Acad. Sci. U. S. A.*, 2014.
[295] M. J. Deery *et al.*, “Proteomic Analysis Reveals the Role of Synaptic Vesicle Cycling in Sustaining the Suprachiasmatic Circadian Clock,” *Curr. Biol.*, 2009.
[296] K. L. Gamble, R. Berry, S. J. Frank, and M. E. Young, “Circadian clock control of endocrine factors,” *Nature Reviews Endocrinology*. 2014.
[297] J. Chang *et al.*, “Circadian control of the secretory pathway maintains collagen homeostasis,” *Nat. Cell Biol.*, vol. 22, no. 1, pp. 74–86, 2020.
[298] C. Y. C. Yeung *et al.*, “Gremlin-2 is a BMP antagonist that is regulated by the circadian clock,” *Sci. Rep.*, 2014.
[299] M. Morikawa, R. Derynck, and K. Miyazono, “TGF- β and the TGF-β family: Context-dependent roles in cell and tissue physiology,” *Cold Spring Harbor Perspectives in Biology*. 2016.
[300] C. H. Heldin, B. Lu, R. Evans, and J. S. Gutkind, “Signals and receptors,” *Cold Spring Harb. Perspect. Biol.*, 2016.
[301] C. H. Heldin and A. Moustakas, “Signaling receptors for TGF-β family members,” *Cold Spring Harb. Perspect. Biol.*, 2016.
[302] R. Derynck *et al.*, “A new type of transforming growth factor-beta, TGF-beta 3.,” *EMBO J.*, 1988.
[303] M. Horiguchi, M. Ota, and D. B. Rifkin, “Matrix control of transforming growth factor-β function,” *J. Biochem.*, 2012.
[304] M. Shi *et al.*, “Latent TGF-β structure and activation,” *Nature*, 2011.
[305] K. Yoshinaga *et al.*, “Perturbation of transforming growth factor (TGF)-β1 association with latent TGF-β binding protein yields inflammation and tumors,” *Proc. Natl. Acad. Sci. U. S. A.*, 2008.
[306] D. A. Lawrence, R. Pircher, and P. Jullien, “Conversion of a high molecular weight latent β-TGF from chicken embryo fibroblasts into a low molecular weight active β-TGF under acidic conditions,” *Biochem. Biophys. Res. Commun.*, 1985.
[307] Q. Yu and I. Stamenkovic, “Cell surface-localized matrix metalloproteinase-9 proteolytically activates TGF-β and promotes tumor invasion and angiogenesis,” *Genes Dev.*, 2000.
[308] Y. Sato and D. B. Rifkin, “Inhibition of endothelial cell movement by pericytes and smooth muscle cells: Activation of a latent transforming growth factor-β1-like molecule by plasmin during co-culture,” *J. Cell Biol.*, 1989.
[309] M. H. Barcellos-Hoff and T. A. Dix, “Redox-mediated activation of latent transforming growth factor-beta 1.,” *Mol. Endocrinol.*, 1996.
[310] J. S. Munger *et al.*, “The Integrin ␣v␤6 Binds and Activates Latent TGF␤1: A Mechanism for Regulating Pulmonary Inflammation and Fibrosis,” *Cell*, 1999.
[311] D. Mu *et al.*, “The integrin αvβ8 mediates epithelial homeostasis through MT1-MMP-dependent activation of TGF-β1,” *J. Cell Biol.*, 2002.
[312] X. Dong *et al.*, “Force interacts with macromolecular structure in activation of TGF-β,” *Nature*, 2017.
[313] J. P. Annes, J. S. Munger, and D. B. Rifkin, “Making sense of latent TGFβ activation,” *Journal of Cell Science*. 2003.
[314] S. Cheifetz *et al.*, “The transforming growth factor-β system, a complex pattern

of cross-reactive ligands and receptors," *Cell*, 1987.
[315] F. López-Casillas, H. M. Payne, J. L. Andres, and J. Massagué, "Betaglycan can act as a dual modulator of TGF-β access to signaling receptors: Mapping of ligand binding and GAG attachment sites," *J. Cell Biol.*, 1994.
[316] J. Esparza-López, J. L. Montiel, M. M. Vilchis-Landeros, T. Okadome, K. Miyazono, and F. López-Casillas, "Ligand binding and functional properties of betaglycan, a co-receptor of the transforming growth factor-β superfamily. Specialized binding regions for transforming growth factor-β and inhibin A," *J. Biol. Chem.*, 2001.
[317] A. Moustakas, H. Y. Lin, Y. I. Henis, J. Plamondon, M. D. O'Connor-McCourt, and H. F. Lodish, "The transforming growth factor β receptors types I, II, and III form hetero-oligomeric complexes in the presence of ligand," *J. Biol. Chem.*, 1993.
[318] M. Ehrlich, O. Gutman, P. Knaus, and Y. I. Henis, "Oligomeric interactions of TGF-β and BMP receptors," *FEBS Letters*. 2012.
[319] S. Lawler *et al.*, "The type II transforming growth factor-β receptor autophosphorylates not only on serine and threonine but also on tyrosine residues," *J. Biol. Chem.*, 1997.
[320] K. Luo and H. F. Lodish, "Positive and negative regulation of type II TGF-β receptor signal transduction by autophosphorylation on multiple serine residues," *EMBO J.*, 1997.
[321] J. Massagué, J. Seoane, and D. Wotton, "Smad transcription factors," *Genes and Development*. 2005.
[322] X. H. Feng, Y. Zhang, R. Y. Wu, and R. Derynck, "The tumor suppressor Smad4/DPC4 and transcriptional adaptor CBP/p300 are coactivators for Smad3 in TGF-β-induced transcriptional activation," *Genes Dev.*, 1998.
[323] C. Pouponnot, L. Jayaraman, and J. Massagué, "Physical and functional interaction of SMADS and p300/CBP," *J. Biol. Chem.*, 1998.
[324] J. N. Topper *et al.*, "CREB binding protein is a required coactivator for Smad-dependent, transforming growth factor β transcriptional responses in endothelial cells," *Proc. Natl. Acad. Sci. U. S. A.*, 1998.
[325] A. Moustakas and C. H. Heldin, "Non-Smad TGF-β signals," *Journal of Cell Science*. 2005.
[326] Y. Shi and J. Massagué, "Mechanisms of TGF-β signaling from cell membrane to the nucleus," *Cell*. 2003.
[327] H. Hayashi *et al.*, "The MAD-related protein Smad7 associates with the TGFβ receptor and functions as an antagonist of TGFβ signaling," *Cell*, 1997.
[328] Y. Kamiya, K. Miyazono, and K. Miyazawa, "Smad7 inhibits transforming growth factor-β family type I receptors through two distinct modes of interaction," *J. Biol. Chem.*, 2010.
[329] P. Lönn *et al.*, "Transcriptional induction of salt-inducible kinase 1 by transforming growth factor β leads to negative regulation of type I receptor signaling in cooperation with the Smurf2 ubiquitin ligase," *J. Biol. Chem.*, 2012.
[330] X. Yan and Y. G. Chen, "Smad7: Not only a regulator, but also a cross-talk mediator of TGF-β signalling," *Biochemical Journal*. 2011.
[331] X. Yan, X. Xiong, and Y. G. Chen, "Feedback regulation of TGF-β signaling," *Acta Biochimica et Biophysica Sinica*. 2018.
[332] I. B. Robertson, M. Horiguchi, L. Zilberberg, B. Dabovic, K. Hadjiolova, and D. B. Rifkin, "Latent TGF-β-binding proteins," *Matrix Biology*. 2015.
[333] K. Wegner *et al.*, "Dynamics and feedback loops in the transforming growth factor β signaling pathway," *Biophys. Chem.*, 2012.

[334] D. Nam *et al.*, “The adipocyte clock controls brown adipogenesis through the TGF-β and BMP signaling pathways,” *J. Cell Sci.*, 2015.
[335] W. D. Chen *et al.*, “Circadian CLOCK mediates activation of transforming growth factor-β signaling and renal fibrosis through cyclooxygenase 2,” *Am. J. Pathol.*, 2015.
[336] C. Dong, R. Gongora, M. L. Sosulski, F. Luo, and C. G. Sanchez, “Regulation of transforming growth factor-beta1 (TGF-β1)-induced pro-fibrotic activities by circadian clock gene BMAL1,” *Respir. Res.*, 2016.
[337] A. L. Beynon, J. Thome, and A. N. Coogan, “Age and time of day influences on the expression of transforming growth factor-beta and phosphorylated SMAD3 in the mouse suprachiasmatic and paraventricular nuclei,” *Neuroimmunomodulation*, 2009.
[338] F. Sato *et al.*, “Smad3 and Snail show circadian expression in human gingival fibroblasts, human mesenchymal stem cell, and in mouse liver,” *Biochem. Biophys. Res. Commun.*, 2012.
[339] N. Kon, T. Hirota, T. Kawamoto, Y. Kato, T. Tsubota, and Y. Fukada, “Activation of TGF-β/activin signalling resets the circadian clock through rapid induction of Dec1 transcripts,” *Nat. Cell Biol.*, 2008.
[340] H. E. Sloin, G. Ruggiero, A. Rubinstein, S. S. Storz, N. S. Foulkes, and Y. Gothilf, “Interactions between the circadian clock and TGF-β signaling pathway in zebrafish,” *PLoS One*, 2018.
[341] T. Börding, A. N. Abdo, B. Maier, C. Gabriel, and A. Kramer, “Generation of human CrY1 and Cry2 knockout cells using duplex CRISPR/Cas9 technology,” *Front. Physiol.*, 2019.
[342] S. Korge *et al.*, “The non-classical nuclear import carrier Transportin 1 modulates circadian rhythms through its effect on PER1 nuclear localization,” *PLoS Genet.*, 2018.
[343] C. G. Wilson, M. Schupp, B. R. Burkhardt, J. Wu, R. A. Young, and B. A. Wolf, “Liver-specific overexpression of pancreatic-derived factor (PANDER) induces fasting hyperglycemia in mice,” *Endocrinology*, 2010.
[344] L. Broutier *et al.*, “Culture and establishment of self-renewing human and mouse adult liver and pancreas 3D organoids and their genetic manipulation,” *Nat. Protoc.*, 2016.
[345] F. Dundar, L. Skrabanek, and P. Zumbo, “Introduction to differential gene expression analysis using RNA-seq,” *Cornell Work.*, 2015.
[346] G. Chen, T. Shi, and L. Shi, “Characterizing and annotating the genome using RNA-seq data,” *Science China Life Sciences*. 2017.
[347] S. Zhao and B. Zhang, “A comprehensive evaluation of ensembl, RefSeq, and UCSC annotations in the context of RNA-seq read mapping and gene quantification,” *BMC Genomics*, 2015.
[348] A. Dobin, “STAR manual 2.5.1a,” Ithaca, NY, 2016.
[349] F. Dündar, “Visualizing the alignment stats of STAR using R,” Ithaca, NY, 2015.
[350] M. Love, S. Anders, and W. Huber, “Analyzing RNA-seq data with DESeq2,” *Bioconductor*, 2017.
[351] M. I. Love, W. Huber, and S. Anders, *Beginner’s guide to using the DESeq2 package.* 2014.
[352] M. I. Love, S. Anders, V. Kim, and W. Huber, “RNA-Seq workflow: gene-level exploratory analysis and differential expression [version 2; peer review: 2 approved],” *F1000Research*, 2016.
[353] K. Yagita *et al.*, “Development of the circadian oscillator during differentiation of mouse embryonic stem cells in vitro,” *Proc. Natl. Acad. Sci. U. S. A.*, 2010.

[354] R. W. Yao, Y. Wang, and L. L. Chen, “Cellular functions of long noncoding RNAs,” *Nature Cell Biology*. 2019.
[355] J. S. O’Neill and M. H. Hastings, “Increased coherence of circadian rhythms in mature fibroblast cultures,” *J. Biol. Rhythms*, 2008.
[356] A. Gerber, C. Esnault, G. Aubert, R. Treisman, F. Pralong, and U. Schibler, “Blood-borne circadian signal stimulates daily oscillations in actin dynamics and SRF activity,” *Cell*, 2013.
[357] W. Tao *et al.*, “EGR1 regulates hepatic clock gene amplitude by activating Per1 transcription,” *Sci. Rep.*, 2015.
[358] K. Edelstein, C. Beaulé, R. D’Abramo, and S. Amir, “Expression profiles of JunB and c-Fos proteins in the rat circadian system,” *Brain Res.*, 2000.
[359] P. Novák and V. Havlíček, “Protein Extraction and Precipitation,” in *Proteomic Profiling and Analytical Chemistry: The Crossroads: Second Edition*, 2016.
[360] GE Healthcare Dharmacon Inc., “Instruction 29027271 AH - Size exlusion chromatography columns,” 2018. [Online]. Available: https://cdn.gelifesciences.com/dmm3bwsv3/AssetStream.aspx?mediaformatid=10061&destinationid=10016&assetid=16443. [Accessed: 19-Nov-2019].
[361] GE Healthcare Dharmacon Inc., “Strategies for Protein Purification Handbook,” 2010. [Online]. Available: https://www.sigmaaldrich.com/content/dam/sigma-aldrich/docs/Sigma-Aldrich/General_Information/1/ge-strategies-for-protein-purification.pdf. [Accessed: 23-Nov-2019].
[362] Proteinatlas.org, “The Human Protein Atlas Search.” [Online]. Available: https://www.proteinatlas.org/search/sa_location:Intracellular+and+membrane%2CSecreted+-+unknown+location%2CSecreted+in+brain%2CSecreted+in+female+reproductive+system%2CSecreted+in+male+reproductive+system%2CSecreted+in+other+tissues%2CSecreted+to+blood%2C. [Accessed: 23-Nov-2019].
[363] J. D. Tipton, J. C. Tran, A. D. Catherman, D. R. Ahlf, K. R. Durbin, and N. L. Kelleher, “Analysis of intact protein isoforms by mass spectrometry,” *Journal of Biological Chemistry*. 2011.
[364] C. H. Heldin, M. Landström, and A. Moustakas, “Mechanism of TGF-β signaling to growth arrest, apoptosis, and epithelial-mesenchymal transition,” *Current Opinion in Cell Biology*. 2009.
[365] X. He, X. Guo, H. Zhang, X. Kong, F. Yang, and C. Zheng, “Mechanism of action and efficacy of LY2109761---a TGF-β receptor inhibitor, targeting tumor microenvironment in liver cancer after TACE,” *Oncotarget*, 2018.
[366] J. L. Bedont and S. Blackshaw, “Constructing the suprachiasmatic nucleus: A watchmaker’s perspective on the central clockworks,” *Frontiers in Systems Neuroscience*. 2015.
[367] S. Yamaguchi *et al.*, “Synchronization of Cellular Clocks in the Suprachiasmatic Nucleus,” *Science (80-.)*., 2003.
[368] E. D. Herzog, T. Hermanstyne, N. J. Smyllie, and M. H. Hastings, “Regulating the suprachiasmatic nucleus (SCN) circadian clockwork: Interplay between cell-autonomous and circuit-level mechanisms,” *Cold Spring Harb. Perspect. Biol.*, 2017.
[369] G. Bloch, E. D. Herzog, J. D. Levine, and W. J. Schwartz, “Socially synchronized circadian oscillators,” *Proceedings of the Royal Society B: Biological Sciences*. 2013.
[370] T. Fuchikawa, A. Eban-Rothschild, M. Nagari, Y. Shemesh, and G. Bloch, “Potent social synchronization can override photic entrainment of circadian rhythms,” *Nat. Commun.*, 2016.

[371] M. J. Paul, P. Indic, and W. J. Schwartz, “Social forces can impact the circadian clocks of cohabiting hamsters,” *Proc. R. Soc. B Biol. Sci.*, 2014.
[372] M. J. Paul, P. Indic, and W. J. Schwartz, “Social synchronization of circadian rhythmicity in female mice depends on the number of cohabiting animals,” *Biol. Lett.*, 2015.
[373] J. D. Levine, P. Funes, H. B. Dowse, and J. C. Hall, “Resetting the Circadian clock by social experience in Drosophila melanogaster,” *Science (80-.).*, 2002.
[374] S. Bernard, D. Gonze, B. Čajavec, H. Herzel, and A. Kramer, “Synchronization-induced rhythmicity of circadian oscillators in the suprachiasmatic nucleus,” *PLoS Comput. Biol.*, 2007.
[375] K. A. Feeney, M. Putker, M. Brancaccio, and J. S. O’Neill, “In-depth Characterization of Firefly Luciferase as a Reporter of Circadian Gene Expression in Mammalian Cells,” *J. Biol. Rhythms*, 2016.
[376] E. M. Corporation, “Millicell® Hanging and Standing Inserts,” in *Prepare. Grow. Analyze. Advanced cell culture systems for every challenge.*, Billerica, MA, USA, 2012.
[377] N. Yang *et al.*, “Cellular mechano-environment regulates the mammary circadian clock,” *Nat. Commun.*, 2017.
[378] C. H. Streuli and Q. J. Meng, “Influence of the extracellular matrix on cell-intrinsic circadian clocks,” *Journal of Cell Science*. 2019.
[379] Y. Kuramoto, “Lecture Notes in Physics,” *Int. Symp. Math. Probl. Theor. Phys.*, 1975.
[380] P. J. Mitchell, E. K. Hoese, L. Liu, L. F. Fogg, and C. I. Eastman, “Conflicting Bright Light Exposure during Night Shifts Impedes Circadian Adaptation,” *J. Biol. Rhythms*, 1997.
[381] C. I. Eastman and S. K. Martin, “How to use light and dark to produce circadian adaptation to night shift work,” *Annals of Medicine*. 1999.
[382] T. L. Shanahan, R. E. Kronauer, J. F. Duffy, G. H. Williams, and C. A. Czeisler, “Melatonin rhythm observed throughout a three-cycle bright-light stimulus designed to reset the human circadian pacemaker,” *J. Biol. Rhythms*, 1999.
[383] T. H. Monk, D. J. Buysse, J. Carrier, and D. J. Kupfer, “Inducing jet-lag in older people: Directional asymmetry,” *J. Sleep Res.*, 2000.
[384] F. Pampaloni, E. G. Reynaud, and E. H. K. Stelzer, “The third dimension bridges the gap between cell culture and live tissue,” *Nature Reviews Molecular Cell Biology*. 2007.
[385] L. G. Griffith and M. A. Swartz, “Capturing complex 3D tissue physiology in vitro,” *Nature Reviews Molecular Cell Biology*. 2006.
[386] J. Lee, M. J. Cuddihy, and N. A. Kotov, “Three-dimensional cell culture matrices: State of the art,” *Tissue Engineering - Part B: Reviews*. 2008.
[387] P. Müller and A. F. Schier, “Extracellular Movement of Signaling Molecules,” *Developmental Cell*. 2011.
[388] A. T. Winfree, “Oscillating systems: On emerging coherence,” *Science*. 2002.
[389] H. R. Ueda, K. Hirose, and M. Iino, “Intercellular coupling mechanism for synchronized and noise-resistant circadian oscillators,” *J. Theor. Biol.*, 2002.
[390] P. Dowling and M. Clynes, “Conditioned media from cell lines: A complementary model to clinical specimens for the discovery of disease-specific biomarkers,” *Proteomics*. 2011.
[391] M. Mieda, “The network mechanism of the central circadian pacemaker of the SCN: Do AVP neurons play a more critical role than expected?,” *Frontiers in Neuroscience*. 2019.
[392] S. R. Pulivarthy, N. Tanaka, D. K. Welsh, L. De Haro, I. M. Verma, and S. Panda,

"Reciprocity between phase shifts and amplitude changes in the mammalian circadian clock," *Proc. Natl. Acad. Sci. U. S. A.*, 2007.
[393] S. Honma *et al.*, "Dec1 and Dec2 are regulators of the mammalian molecular clock," *Nature*, 2002.
[394] A. Nakashima *et al.*, "DEC1 Modulates the Circadian Phase of Clock Gene Expression," *Mol. Cell. Biol.*, 2008.
[395] S. Koyanagi *et al.*, "cAMP-response Element (CRE)-mediated transcription by Activating Transcription Factor-4 (ATF4) is essential for circadian expression of the Period2 gene," *J. Biol. Chem.*, 2011.
[396] S. Cheon, N. Park, S. Cho, and K. Kim, "Glucocorticoid-mediated Period2 induction delays the phase of circadian rhythm," *Nucleic Acids Res.*, 2013.
[397] S. Chappuis *et al.*, "Role of the circadian clock gene Per2 in adaptation to cold temperature," *Mol. Metab.*, 2013.
[398] U. Schibler, "The 2008 Pittendrigh/Aschoff lecture: Peripheral phase coordination in the mammalian circadian timing system," *Journal of Biological Rhythms*. 2009.
[399] R. L. Mauck, S. L. Seyhan, G. A. Ateshian, and C. T. Hung, "Influence of seeding density and dynamic deformational loading on the developing structure/function relationships of chondrocyte-seeded agarose hydrogels," *Ann. Biomed. Eng.*, 2002.
[400] T. Y. Hui, K. M. C. Cheung, W. L. Cheung, D. Chan, and B. P. Chan, "In vitro chondrogenic differentiation of human mesenchymal stem cells in collagen microspheres: Influence of cell seeding density and collagen concentration," *Biomaterials*, 2008.
[401] A. Wolthuis, A. Boes, and J. Grand, "Cell density modulates growth, extracellular matrix, and protein synthesis of cultured rat mesangial cells," *Am. J. Pathol.*, 1993.
[402] F. Verrecchia, C. Tacheau, M. Schorpp-Kistner, P. Angel, and A. Mauviel, "Induction of the AP-1 members c-Jun and JunB by TGF-β/Smad suppresses early Smad-driven gene activation," *Oncogene*, 2001.
[403] S. J. Chen *et al.*, "The early-immediate gene EGR-1 is induced by transforming growth factor-β and mediates stimulation of collagen gene expression," *J. Biol. Chem.*, 2006.
[404] L. Y. Tang *et al.*, "Transforming growth factor-β (TGF-β) directly activates the JAK1-STAT3 axis to induce hepatic fibrosis in coordination with the SMAD pathway," *J. Biol. Chem.*, 2017.
[405] A. C. Tecalco-Cruz, M. Sosa-Garrocho, G. Vázquez-Victorio, L. Ortiz-García, E. Domínguez-Hüttinger, and M. Macías-Silva, "Transforming growth factor-β/SMAD target gene SKIL is negatively regulated by the transcriptional cofactor complex SNON-SMAD4," *J. Biol. Chem.*, 2012.
[406] J. P. Edwards, H. Fujii, A. X. Zhou, J. Creemers, D. Unutmaz, and E. M. Shevach, "Regulation of the Expression of GARP/Latent TGF-β1 Complexes on Mouse T Cells and Their Role in Regulatory T Cell and Th17 Differentiation," *J. Immunol.*, 2013.
[407] J. Li, M. S. Weinberg, L. Zerbini, and S. Prince, "The oncogenic TBX3 is a downstream target and mediator of the TGF-β1 signaling pathway," *Mol. Biol. Cell*, 2013.
[408] S. Ramadoss, X. Chen, and C. Y. Wang, "Histone demethylase KDM6B promotes epithelial-mesenchymal transition," *J. Biol. Chem.*, 2012.
[409] Integrated DNA Technologies, "Molecular Facts and Figures," 2011. [Online]. Available: https://sfvideo.blob.core.windows.net/sitefinity/docs/default-

source/biotech-basics/molecular-facts-and-figures.pdf?sfvrsn=4563407_4. [Accessed: 21-Dec-2019].
[410] Y. Matsuura *et al.*, “Thermodynamics of protein denaturation at temperatures over 100°C: CutA1 mutant proteins substituted with hydrophobic and charged residues,” *Sci. Rep.*, 2015.
[411] M. Uhlén *et al.*, “Tissue-based map of the human proteome,” *Science (80-.).*, 2015.
[412] A. Houston *et al.*, “Pregnancy-specific glycoprotein expression in normal gastrointestinal tract and in tumors detected with novel monoclonal antibodies,” *MAbs*, 2016.
[413] J. Wessells *et al.*, “Pregnancy specific glycoprotein 18 induces IL-10 expression in murine macrophages,” *Eur. J. Immunol.*, 2000.
[414] S. K. Snyder *et al.*, “Pregnancy-specific glycoproteins function as immunomodulators by inducing secretion of IL-10, IL-6 and TGF-β1 by human monocytes,” *Am. J. Reprod. Immunol.*, 2001.
[415] B. F. Bebo and G. S. Dveksler, “Evidence that pregnancy specific glycoproteins regulate T-cell function and inflammatory autoimmune disease during pregnancy,” *Current Drug Targets: Inflammation and Allergy*. 2005.
[416] L. Fialová, B. Kohoutová, Z. Pelísková, I. Malbohan, and L. Mikulíková, “Serum levels of trophoblast-specific beta-1-globulin (SP1) and alpha-1-fetoprotein (AFP) in pregnant women with rheumatoid arthritis,” *Cesk. Gynekol.*, 1991.
[417] L. Leyns, T. Bouwmeester, S. H. Kim, S. Piccolo, and E. M. De Robertis, “Frzb-1 is a secreted antagonist of Wnt signaling expressed in the Spemann organizer,” *Cell*, 1997.
[418] S. Wang, M. Krinks, K. Lin, F. P. Luyten, and M. Moos, “Frzb, a secreted protein expressed in the Spemann organizer, binds and inhibits Wnt-8,” *Cell*, 1997.
[419] P. Bovolenta, P. Esteve, J. M. Ruiz, E. Cisneros, and J. Lopez-Rios, “Beyond Wnt inhibition: New functions of secreted Frizzled-related proteins in development and disease,” *Journal of Cell Science*. 2008.
[420] K. Motamed, “SPARC (osteonectin/BM-40),” *Int. J. Biochem. Cell Biol.*, 1999.
[421] A. D. Bradshaw, “Diverse biological functions of the SPARC family of proteins,” *International Journal of Biochemistry and Cell Biology*. 2012.
[422] D. Chin, G. M. Boyle, P. G. Parsons, and W. B. Coman, “What is transforming growth factor-beta (TGF-β)?,” *British Journal of Plastic Surgery*. 2004.
[423] M. Morikawa, D. Koinuma, K. Miyazono, and C. H. Heldin, “Genome-wide mechanisms of Smad binding,” *Oncogene*. 2013.
[424] L. J. C. Jonk, S. Itoh, C. H. Heldin, P. Ten Dijke, and W. Kruijer, “Identification and functional characterization of a smad binding element (SBE) in the JunB promoter that acts as a transforming growth factor-β, activin, and bone morphogenetic protein-inducible enhancer,” *J. Biol. Chem.*, 1998.
[425] Y. Zhang, X. H. Feng, and R. Derynck, “Smad3 and Smad4 cooperate with c-Jun/c-Fos to mediate TGF-β-induced transcription,” *Nature*, 1998.
[426] H. Ikushima *et al.*, “An Id-like molecule, HHM, is a synexpression group-restricted regulator of TGF-β signalling,” *EMBO J.*, 2008.
[427] S. J. Yoon, A. E. Wills, E. Chuong, R. Gupta, and J. C. Baker, “HEB and E2A function as SMAD/FOXH1 cofactors,” *Genes Dev.*, 2011.
[428] R. R. Gomis, C. Alarcón, C. Nadal, C. Van Poznak, and J. Massagué, “C/EBPβ at the core of the TGFβ cytostatic response and its evasion in metastatic breast cancer cells,” *Cancer Cell*, 2006.
[429] A. Nishihara *et al.*, “Role of p300, a transcriptional coactivator, in signalling of TGF-β,” *Genes to Cells*, 1998.

[430] R. Janknecht, N. J. Wells, and T. Hunter, “TGF-β-stimulated cooperation of Smad proteins with the coactivators CBP/p300,” *Genes Dev.*, 1998.
[431] Y. Kang, C. R. Chen, and J. Massagué, “A self-enabling TGFβ response coupled to stress signaling: Smad engages stress response factor ATF3 for Id1 repression in epithelial cells,” *Mol. Cell*, 2003.
[432] B. Mayr and M. Montminy, “Transcriptional regulation by the phosphorylation-dependent factor creb,” *Nature Reviews Molecular Cell Biology*. 2001.
[433] X. Zhang *et al.*, “Genome-wide analysis of cAMP-response element binding protein occupancy, phosphorylation, and target gene activation in human tissues,” *Proc. Natl. Acad. Sci. U. S. A.*, 2005.
[434] C. Wong *et al.*, “Smad3-Smad4 and AP-1 Complexes Synergize in Transcriptional Activation of the c-Jun Promoter by Transforming Growth Factor β,” *Mol. Cell. Biol.*, 1999.
[435] A. Hata and Y. G. Chen, “TGF-β signaling from receptors to smads,” *Cold Spring Harb. Perspect. Biol.*, 2016.
[436] D. Melisi *et al.*, “LY2109761, a novel transforming growth factor β receptor type I and type II dual inhibitor, as a therapeutic approach to suppressing pancreatic cancer metastasis,” *Mol. Cancer Ther.*, 2008.
[437] I. T. Tokuda, D. Ono, S. Honma, K. I. Honma, and H. Herzel, “Coherency of circadian rhythms in the SCN is governed by the interplay of two coupling factors,” *PLoS Comput. Biol.*, 2018.
[438] J. H. Li, X. R. Huang, H. J. Zhu, R. Johnson, and H. Y. Lan, “Role of TGF-β signaling in extracellular matrix production under high glucose conditions,” *Kidney Int.*, 2003.
[439] N. Garamszegi *et al.*, “Extracellular matrix-induced transforming growth factor-B receptor signaling dynamics,” *Oncogene*, 2010.
[440] U. Abraham, J. K. Schlichting, A. Kramer, and H. Herzel, “Quantitative analysis of circadian single cell oscillations in response to temperature,” *PLoS One*, 2018.
[441] B. Hinz, “The extracellular matrix and transforming growth factor-β1: Tale of a strained relationship,” *Matrix Biology*. 2015.
[442] R. G. Wells and D. E. Discher, “Matrix elasticity, cytoskeletal tension, and TGF-β : The insoluble and soluble meet,” *Science Signaling*. 2008.
[443] S. Colak and P. ten Dijke, “Targeting TGF-β Signaling in Cancer,” *Trends in Cancer*. 2017.
[444] R. L. Elliott and G. C. Blobe, “Role of transforming growth factor beta in human cancer,” *Journal of Clinical Oncology*. 2005.
[445] D. A. Bechtold, T. M. Brown, S. M. Luckman, and H. D. Piggins, “Metabolic rhythm abnormalities in mice lacking VIP-VPAC2 signaling,” *Am. J. Physiol. - Regul. Integr. Comp. Physiol.*, 2008.
[446] A. Granada, R. M. Hennig, B. Ronacher, A. Kramer, and H. Herzel, “Chapter 1 Phase Response Curves. Elucidating the Dynamics of Coupled Oscillators,” *Methods in Enzymology*. 2009.
[447] T. J. Kobayashi, H. Ukai, and H. R. Ueda, “Desynchronization of noisy multi-cellular clocks underlies the population-level singularity behavior of mammalian circadian clock,” in *AIP Conference Proceedings*, 2007.
[448] H. Ukai *et al.*, “Melanopsin-dependent photo-perturbation reveals desynchronization underlying the singularity of mammalian circadian clocks,” *Nat. Cell Biol.*, 2007.
[449] J. Bieler, R. Cannavo, K. Gustafson, C. Gobet, D. Gatfield, and F. Naef, “Robust synchronization of coupled circadian and cell cycle oscillators in single mammalian cells,” *Mol. Syst. Biol.*, 2014.

[450] C. Droin, E. R. Paquet, and F. Naef, “Low-dimensional dynamics of two coupled biological oscillators,” *Nat. Phys.*, 2019.
[451] M. I. Love, W. Huber, and S. Anders, “Moderated estimation of fold change and dispersion for RNA-seq data with DESeq2,” *Genome Biol.*, 2014.
[452] L. M. Wakefield, T. S. Winokur, R. S. Hollands, K. Christopherson, A. D. Levinson, and M. B. Sporn, “Recombinant latent transforming growth factor β1 has a longer plasma half-life in rats than active transforming growth factor β1, and a different tissue distribution,” *J. Clin. Invest.*, 1990.
[453] Z. Zi, D. A. Chapnick, and X. Liu, “Dynamics of TGF-β/Smad signaling,” *FEBS Letters*. 2012.
[454] J. Wang *et al.*, “The Self-Limiting Dynamics of TGF-β Signaling In Silico and In Vitro, with Negative Feedback through PPM1A Upregulation,” *PLoS Comput. Biol.*, 2014.
[455] K. Miyazono, “Positive and negative regulation of TGF-β signaling,” *Journal of Cell Science*. 2000.
[456] P. Vizán, D. S. J. Miller, I. Gori, D. Das, B. Schmierer, and C. S. Hill, “Controlling long-term signaling: Receptor dynamics determine attenuation and refractory behavior of the TGF-β pathway,” *Sci. Signal.*, 2013.
[457] K. A. Stokkan, S. Yamazaki, H. Tei, Y. Sakaki, and M. Menaker, “Entrainment of the circadian clock in the liver by feeding,” *Science (80-.).*, 2001.

6 Appendix

Supplementary Figures

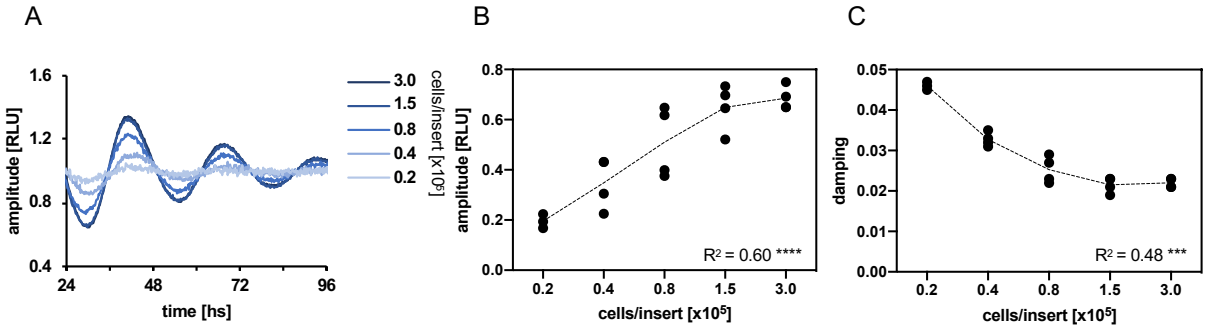

Figure 6-1: U-2 OS circadian rhythmicity depends on culture density

To assess effects of culture density on circadian dynamics, U-2 OS cells harboring a *Per2*:Luc reporter gene were seeded on membrane inserts (4.2 cm^2) in increasing densities. sells were synchronized, and luciferase activity was continuously monitored. **(A)** Detrended time series of a representative culture density experiment. **(B,C)** Quantification of amplitudes (B) and (C) damping of circadian oscillations (n=1 repeat experiment with 4 technical replicates, individual values and connecting line displayed, linear regression test: ***p<0.001, ****p<0.0001).

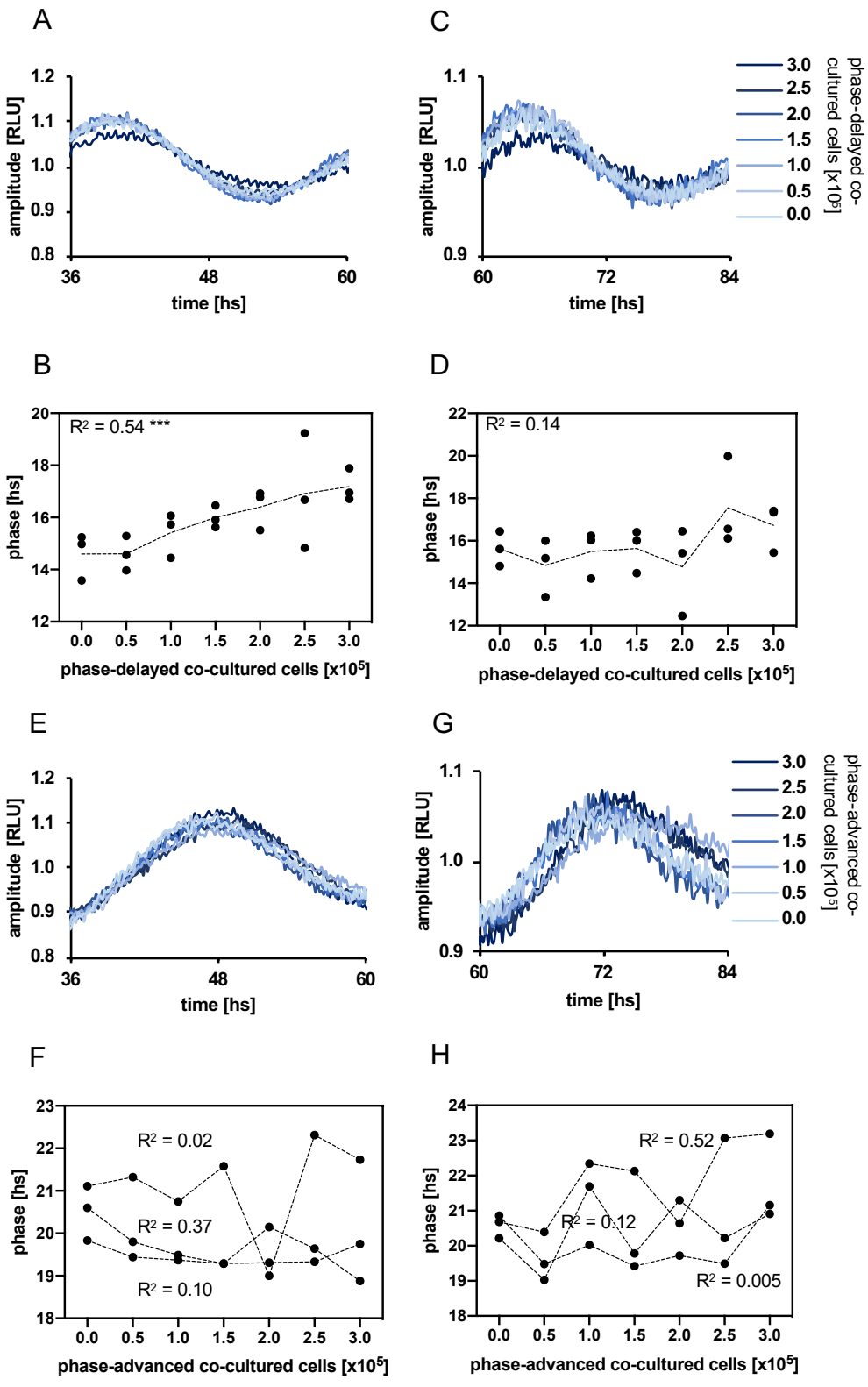

Figure 6-2: Co-cultured populations of U-2 OS cells display weak intercellular coupling with respect to phase

Co-culture experiments of distinct U-2 OS cell populations were performed to determine whether or not Phase-pulling experiments were performed as described. In brief U-2 OS cells harboring a *Per2*:Luc reporter gene were seeded at low density (0.3 x10^5 cells/dish) together with increasing numbers of

phase advanced or -delayed non-reporter cells into 35-mm dishes. Luciferase activity was continuously monitored. **(A,C)** Detrended time series of a representative phase-pulling experiment of co-cultures with phase delayed non-reporter cells (second (A) and third (C) circadian cycle). **(B,D)** Quantification of phases during the second (B) and third (D) cycle of bioluminescence oscillations for reporter cells co-cultured with 6 hour phase delayed (and phase equal) non-reporter cells (n=3 repeat experiments with 3 technical replicates each, individual values and connecting line displayed, linear regression test: ***$p<0.001$). **(E,G)** Detrended time series of a representative phase-pulling experiment of co-cultures with phase advanced non-reporter cells (second (E) and third (G) circadian cycle). **(F,H)** Quantification of phases during the second (F) and third (H) cycle of bioluminescence oscillations for reporter cells co-cultured with 6 hour phase advanced (and phase equal) non-reporter cells (n=3 repeat experiments with 3 technical replicates, individual connected values displayed, linear regression test).

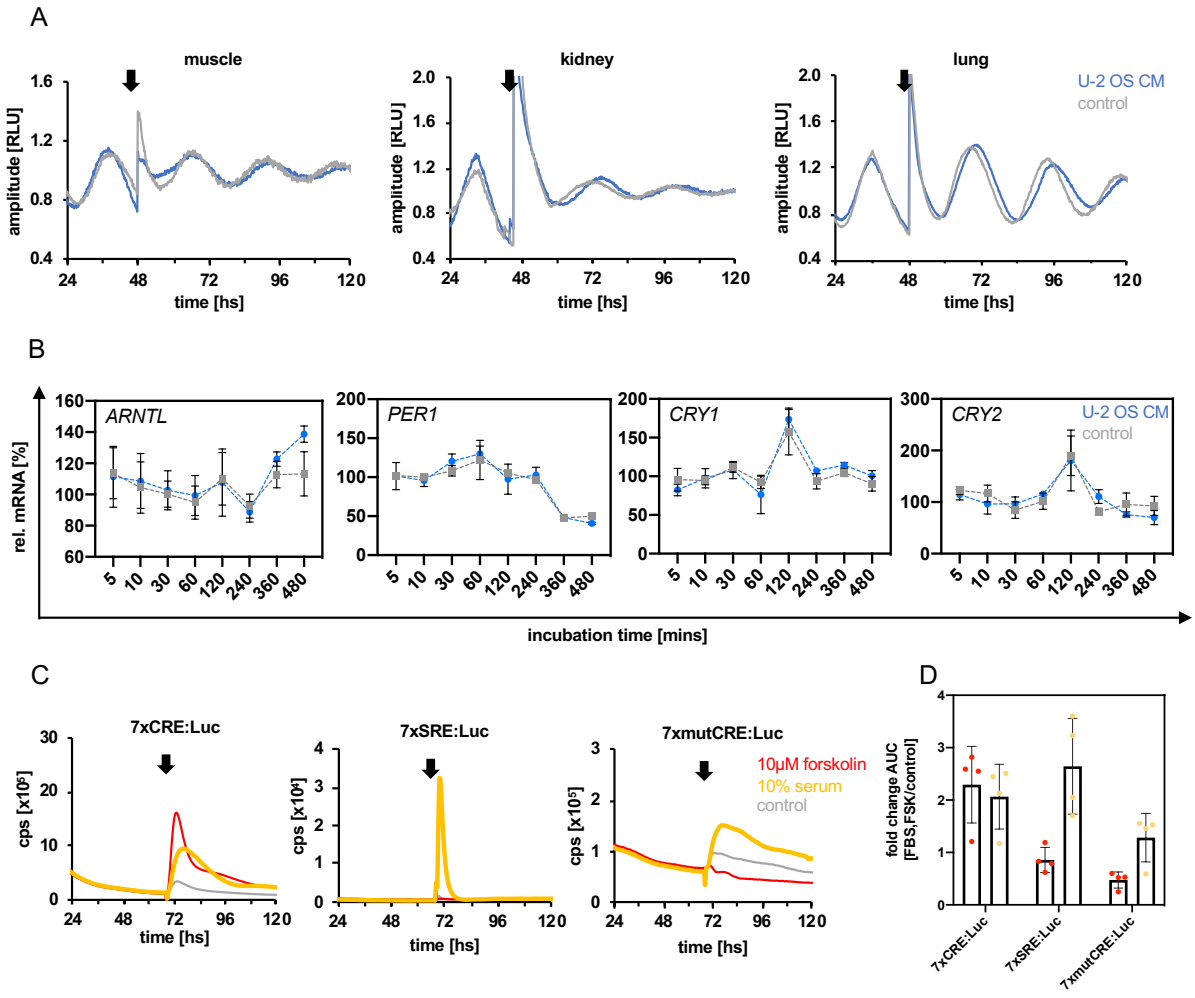

Figure 6-3: Factors secreted by peripheral circadian oscillators modulate circadian dynamics

(A,B) Mammalian reporter cells and tissue explants were stimulated with conditioned and control medium to test whether secreted signaling molecules can act as Zeitgebers for peripheral circadian oscillators and modulate clock gene expression. CM and control medium were generated and stimulations performed as described. RNA was harvested after indicated incubation times following simulation 16 hours post-synchronization. **(A)** Detrended time series of a representative experiment upon stimulation of murine PER2::LUC tissue explants at the inferred trough of *Per* expression. **(B)** Quantification of mRNA expression changes upon conditioned and control medium stimulations relative to unstimulated controls (n=3 repeat experiment with 3 technical replicates each, measured in triplicates, normalized to *GAPDH*, mean ± SD, One-way ANOVA with Dunett's multiple comparison test against control medium). **(C,D)** Serum and forskolin stimulation of U-2 OS 7xCRE:Luc, 7xmutCRE:Luc, and 7xSRE:Luc reporter cells was performed to test lentiviral reporter constructs are functional. **(C)** Detrended time series of a representative experiment upon stimulation of U-2 OS 7xCRE:Luc, 7xSRE:Luc, and 7xmutCRE:Luc reporter cells. **(D)** Quantification of luciferase signal induced by forskolin or 10% serum relative to control medium (n=4 repeat experiment with 3-4 technical replicates each, mean ± SD, individual values displayed).

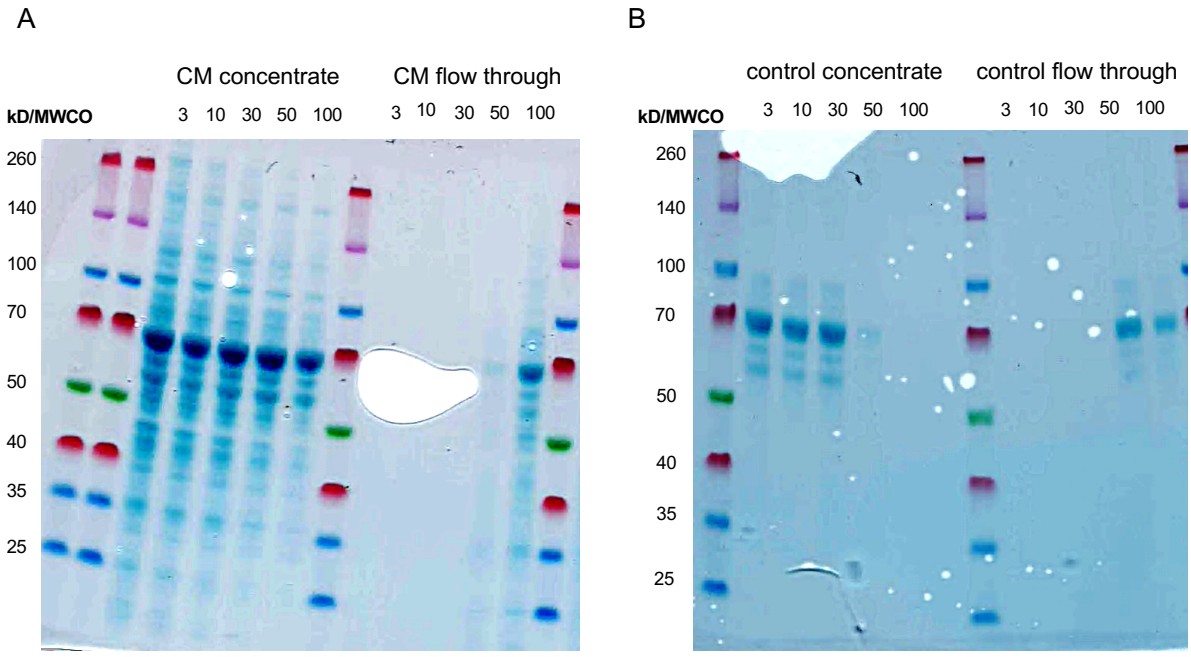

Figure 6-4: Protein content of size fractionated conditioned and control medium

Conditioned and control medium was size fractionated using ultrafiltration size exclusion columns with indicated molecular weight cut-offs (MWCO) to test activity of concentrates and flow throughs. SDS-PAGE and Coomassie staining of resulting size fractions was performed as described in methods. **(A)** Coomassie stained SDS-PAGE gel of conditioned medium concentrates and flow throughs. **(B)** Coomassie stained SDS-PAGE gel of control medium concentrates and flow throughs.

A

Mean	amplitude [RLU]	damping	period [hs]	phase [hs]	magnitude [cps]	SD	amplitude [RLU]	damping	period [hs]	phase [hs]	magnitude [cps]
non-silencing	0.29	0.015	24.48	14.23	10505.73	non-silencing	0.02	0.0004	0.21	0.97	142.13
ACVR1C.1	0.24	0.017	25.40	13.52	12298.11	*ACVR1C.1*	0.04	0.002	1.08	2.98	3981.90
ACVR1C.2	0.34	0.014	23.78	14.21	9104.95	*ACVR1C.2*	0.06	0.002	0.32	2.41	2244.74
ACVR1C.3	0.27	0.014	24.07	14.53	12364.53	*ACVR1C.3*	0.07	0.001	0.49	2.11	1936.30
ACVR2A.1	0.28	0.017	23.99	15.05	10139.11	*ACVR2A.1*	0.06	0.006	0.44	0.95	4742.77
ACVR2A.2	0.27	0.019	24.74	14.31	8078.55	*ACVR2A.2*	0.05	0.001	0.28	1.45	4494.62
ACVR2A.3	0.27	0.013	23.98	13.52	9246.48	*ACVR2A.3*	0.08	0.001	0.23	2.12	2310.84
BMPR1A.1	0.32	0.012	24.46	14.38	13709.51	*BMPR1A.1*	0.03	0.003	0.50	2.40	2056.98
BMPR1A.2	0.28	0.014	24.39	13.89	12129.14	*BMPR1A.2*	0.07	0.001	0.35	2.24	826.39
BMPR1A.3	0.22	0.018	24.19	14.30	13280.11	*BMPR1A.3*	0.05	0.004	0.29	2.25	4228.60
ITGAV.1	0.26	0.019	24.30	14.71	5881.78	*ITGAV.1*	0.07	0.003	0.20	2.17	2284.41
ITGAV.2	0.31	0.018	24.20	14.97	3971.54	*ITGAV.2*	0.10	0.007	0.48	1.99	1196.54
ITGAV.3	0.16	0.018	24.63	15.42	2794.40	*ITGAV.3*	0.06	0.006	0.59	2.22	1662.34
ITGB8.1	0.28	0.014	24.02	14.53	10649.17	*ITGB8.1*	0.08	0.003	0.70	2.10	2737.55
ITGB8.2	0.26	0.015	23.49	14.54	9891.53	*ITGB8.2*	0.05	0.001	0.50	2.50	884.04
LTBP1.1	0.28	0.016	24.60	14.41	10087.49	*LTBP1.1*	0.01	0.002	0.39	2.26	4878.45
LTBP1.2	0.27	0.014	24.31	14.43	8225.17	*LTBP1.2*	0.06	0.004	0.67	0.99	410.08
LTBP1.3	0.34	0.016	24.52	13.66	4753.92	*LTBP1.3*	0.05	0.000	0.67	2.35	1376.85
LTBP3.1	0.28	0.015	24.67	14.02	9404.50	*LTBP3.1*	0.05	0.001	1.25	2.33	588.11
LTBP3.2	0.29	0.016	24.54	13.52	11001.44	*LTBP3.2*	0.05	0.001	0.56	1.84	1998.68
LTBP3.3	0.26	0.014	23.93	15.53	8690.69	*LTBP3.3*	0.05	0.002	0.57	2.41	3641.47
RNF111.1	0.31	0.015	24.52	13.83	12901.26	*RNF111.1*	0.05	0.002	0.67	2.08	1326.77
RNF111.2	0.22	0.021	24.98	14.56	7309.30	*RNF111.2*	0.04	0.003	0.20	1.21	1474.46
RNF111.3	0.26	0.019	24.64	14.05	7598.30	*RNF111.3*	0.08	0.005	0.39	2.64	2127.78
SKI.1	0.21	0.016	24.81	15.27	11737.70	*SKI.1*	0.05	0.002	0.91	1.93	1279.03
SMAD3.1	0.26	0.015	24.59	14.74	9852.83	*SMAD3.1*	0.05	0.002	0.11	1.75	3430.43
SMAD4.1	0.24	0.019	25.13	14.51	7037.86	*SMAD4.1*	0.08	0.002	0.10	2.09	3749.24
SMAD4.2	0.25	0.015	25.08	13.99	11837.68	*SMAD4.2*	0.03	0.001	0.59	2.00	883.63
SMAD4.3	0.27	0.017	24.43	14.06	10497.28	*SMAD4.3*	0.04	0.003	0.11	1.83	1984.96
SMAD8.1	0.32	0.012	24.11	13.89	15850.60	*SMAD8.1*	0.03	0.001	0.26	1.82	739.54
SMURF1.1	0.34	0.011	23.84	14.57	7791.74	*SMURF1.1*	0.03	0.001	0.27	2.11	1160.00
SMURF1.2	0.22	0.020	25.00	14.84	6954.81	*SMURF1.2*	0.08	0.006	1.10	1.60	2640.26
SMURF1.3	0.31	0.013	24.10	14.19	8649.28	*SMURF1.3*	0.06	0.002	0.29	1.90	676.42
TGFB1.1	0.33	0.014	24.58	13.37	8119.14	*TGFB1.1*	0.06	0.003	0.79	2.07	706.61
TGFB1.2	0.29	0.014	24.39	14.25	12191.65	*TGFB1.2*	0.12	0.003	0.40	1.89	4329.14
TGFB1.3	0.31	0.014	24.43	14.61	7232.32	*TGFB1.3*	0.04	0.002	0.40	1.83	3202.59
TGFB1I1.1	0.26	0.012	24.61	14.79	13754.90	*TGFB1I1.1*	0.06	0.004	0.76	0.59	1581.87
TGFBR1.1	0.26	0.014	23.97	14.58	9379.85	*TGFBR1.1*	0.04	0.003	0.72	1.87	2360.65
TGFBR1.2	0.24	0.020	24.75	14.95	7506.25	*TGFBR1.2*	0.03	0.002	0.17	1.32	853.00
TGFBR1.3	0.27	0.015	24.29	14.45	9349.49	*TGFBR1.3*	0.04	0.003	0.93	2.76	3552.19
TGFBR2.1	0.33	0.014	24.27	13.83	9992.08	*TGFBR2.1*	0.05	0.002	0.31	2.27	1696.71
TGFBR2.2	0.33	0.012	23.68	14.24	8651.67	*TGFBR2.2*	0.06	0.002	0.37	2.15	1024.05
TGFBR2.3	0.24	0.021	24.71	14.21	10085.98	*TGFBR2.3*	0.05	0.005	0.79	2.12	666.92
THBS1.1	0.29	0.015	24.17	13.75	9657.45	*THBS1.1*	0.07	0.001	0.24	1.92	1086.95
THBS1.2	0.21	0.017	24.29	14.63	14649.56	*THBS1.2*	0.06	0.007	0.21	1.37	1498.57
THBS1.3	0.31	0.014	24.47	13.96	8155.75	*THBS1.3*	0.02	0.003	0.77	3.32	2706.62

Figure 6-5: Genetic perturbation of TGF-β signaling pathway alters circadian dynamics

To test whether TGF-β signaling pathway is required for coherent circadian dynamics, an RNAi knock-down screen of TGF-β signaling pathway components was performed in U-2 OS *Bmal1*:Luc cells (as described in methods). Cells were synchronized and luciferase activity was continuously monitored. **(A)** Quantification of circadian parameters of *Bmal1*:Luc oscillations upon knock-down of indicated genes, red shading=amplitude mean of knock-down < amplitude mean ± SD of non-silencing control or damping mean of knock-down > damping mean ± SD of non-silencing control. (n=4 biological repeat experiments with 2 technical replicates per shRNA construct, mean ± SD).

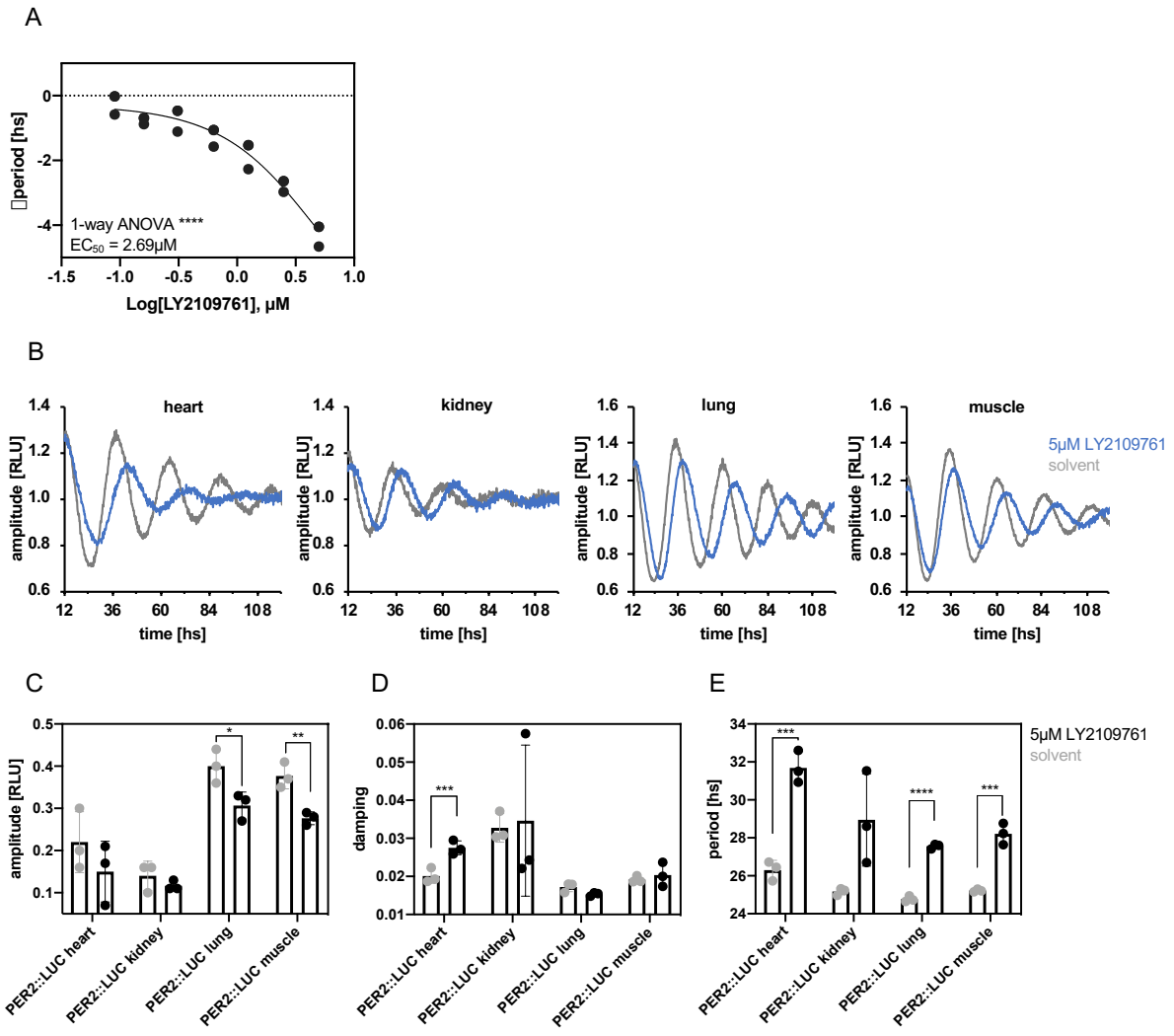

Figure 6-6: Pharmacological perturbation of TGF-β signaling pathway alters circadian dynamics

To test whether TGF-β signaling pathway is required for coherent circadian dynamics, a pharmacological TGF-β receptor inhibitor (LY2109761) was used. U-2 OS cells harboring a *Per2*:Luc reporter gene or peripheral tissue explants from PER2::LUC mice were subjected to TGF-β receptor inhibitor as described. **(A)** Quantification of period changes of *Per2*:Luc oscillations induced by increasing concentrations of LY2109761 relative to solvent control (n=3 repeat experiment with 3 technical replicates each, individual values and asymmetric sigmoidal fit displayed, One-way ANOVA: ****p<0.0001 and non-linear regression fit of an asymmetric sigmoidal model). **(B)** Detrended time series of a representative experiment of PER2::LUC tissue oscillations upon TGF-β receptor inhibition. **(C-E)** Quantification of amplitudes (C), damping (D), and periods (E) of PER2::LUC tissue oscillations upon treatment with TGF-β receptor inhibition or solvent control (n=3 repeat experiment with 1 technical replicate each, mean ± SD, individual values displayed, Unpaired two-tailed student's t-test against respective solvent group: *p<0.05, **p<0.01, ***p<0.001, ****p<0.0001).

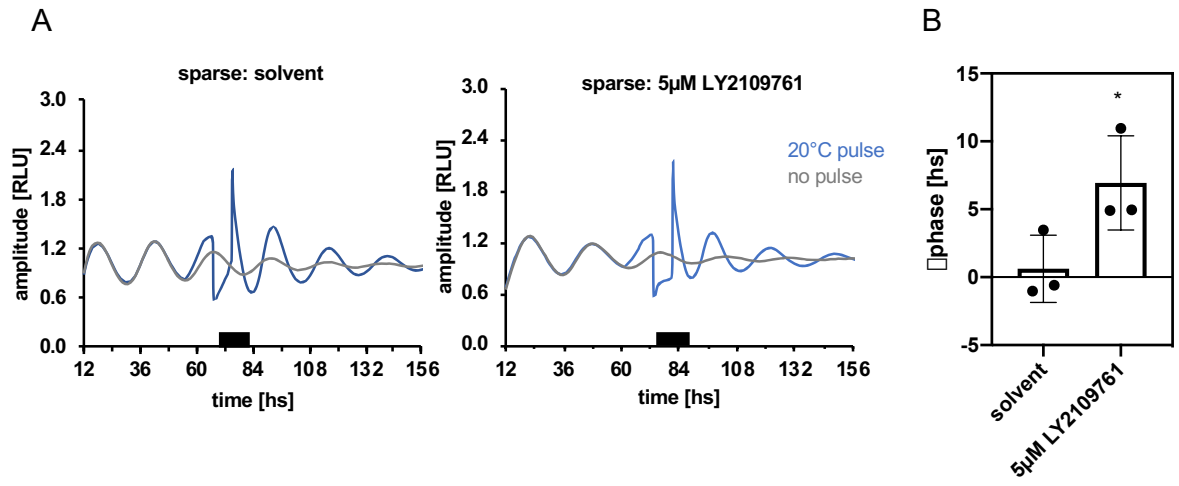

Figure 6-7: Pharmacological perturbation of TGF-β signaling attenuates intercellular coupling

TGF-β receptor inhibitor (LY2109761) was used to assess whether perturbation of TGF-β signaling attenuates intercellular coupling, as characterized by increased susceptibility to perturbation by Zeitgeber pulses. U-2 OS cells harboring a *Bmal1*:Luc reporter gene were seeded at low density (0.3 x10^5 cells/dish) into 35-mm dishes with or without TGF-β receptor inhibitor. An 8 hour, 20°C temperature pulse was applied at the inferred trough of *PER2* expression (nearly anti-phasic to *Bmal1*:Luc peak). **(A)** Detrended time series of a representative temperature pulse experiment with or without TGF-β receptor inhibitor. **(B)** Quantification of temperature induced phase shifts of *Bmal1*:Luc oscillations upon treatment with TGF-β receptor inhibitor or solvent control (n=3 repeat experiment with 2 technical replicates each, mean ± SD, individual values displayed, Unpaired one-tailed student's t-test against solvent group: *p<0.05).

Open Data

RNA sequencing, differential gene expression analysis, Mascot search hits, and reference list of secreted proteins can be found on the electronic version of the thesis in the HTMLreports folder.

RNA sequencing

Aligned RNA sequencing read counts: RNAseq_readcounts.html

Differential gene expression results (sparse versus dense culture density): DEG_sparseversusdense.html

Differential gene expression results (conditioned versus control medium, culture density corrected): DEG_condversuscont.html

Mass spectrometry

human secreted proteins predicted by MDSEC (human protein atlas, accessed Feb 2019): HPA_secretedproteins.html

Mascot search hits:

1. Pool1 active fractions: Mascot_pool1_active.html
2. Pool2 active fractions: Mascot_pool2_active.html
3. Pool1 inactive fractions: Mascot_pool1_inactive.html
4. Pool2 inactive fractions: Mascot_pool2_inactive.html

Standard Operating Procedures

Standard Operating Procedure
Lentivirus Production

Day 0

Seeding of HEK293T cells

Trypsinize an almost confluent 175cm^2 cell culture flask of HEK293T cells (culture time < 6 weeks) with Trypsin/EDTA for ~5 min at 37 °C.
Seed 3 (7) 175 cm^2 (75 cm^2) flasks with HEK293T cells in equal parts in 25 ml (12.5 ml) culture medium each. Adjust flask-size and number of flasks according to experimental requirements.

Day 1

Transfection of HEK293T cells with packaging plasmid and lentiviral vector

Replace culture medium of cells.
Prepare one 1.5 ml eppendorf tube (tube A) per transfection (flask):

- Add 17.5 µg (8.4 µg) of lentiviral expression plasmid, 12.5 µg (6 µg) psPAX and 7.5 µg (3.6 µg) pMD2G plasmid.
- Adjust volume to 1095 µl (526 µl) of plasmids with supplied H_2O (CalPhos™-Kit).
- Add 155 µl (74 µl) of supplied 2M Calcium solution (CalPhos™-Kit).

Prepare one 15ml tube (tube B) per transfection:

- Add 1250 µl (600 µl) 2xHBS (supplied with CalPhos™-Kit).

Mix both by carefully vortexing solution B while adding drop wise solution A.
Incubate the transfection solution for 20 min at RT.
Add 2.5 ml (1.2 ml) of each transfection solution to one 175 cm^2 (75 cm^2) flask.
Incubate over night at cell culture conditions.

Day 2, morning

Replace Culture Medium

Replace culture medium of HEK293T cells (from day 1). Handle with care because cells only loosely stick to the plastic.

Day 3, afternoon

Harvest lentiviral supernatant I

Pour supernatant into 50 ml tube and store on ice over night in fridge. Refill flask with 25 ml (12.5 ml) culture medium.

Day 4, morning

Harvest lentiviral supernatant II

Pour supernatant into corresponding 50 ml tube of day 3 and spin tube at maximal g-force (> 2000 x g) for 15 min to remove cell debris. Pass supernatant through an 0.45 µm filter.
Supernatant might either be used directly or frozen down to -80°C in working aliquots.

Figure 6-8: Standard operating procedure for lentivirus production

Standard Operating Procedure
RNAi Screen Multichannel

Day 0

Seed HEK293T cells.

HEK293T cells (culture time < 9 weeks) should have grown in log phase, trypsinized with Trypsin/EDTA (BIOCHROM AG #L2143) for ~5 min at 37 °C. One 175 cm^2 flask will give ~ 60 * 10^6 cells - about seven 96 well plates.
Seed 30*10^3 cells in 100 µl per well in culture media on clear 96 well plate (BD Falcon™, #35 3072), flat well tissue culture treated.

Day 1

Transfection of HEK293T cells with packaging plasmid and pGIPZ

Prepare a prediluted pGIPZ sublibrary in 96 format with ~ 0.14 µg/µl in HPLC H_2O. Prepare two 15 ml Tubes with 2.75 ml OptiMEM (GIBCO, #31985) each. Tube A ad 11 µg psPAX and 6.6 µg pMD2G plasmid. Tube B ad 55 µl Lipofectamin2000©, incubate for 5 min at RT.
Use multichannel pipette to pipette 25 µl of tube A onto 96 PCR V-bottom microtiter plate (Costar, #3363). Use multichannel pipette to transfer 1 µl of prediluted pGIPZ sublibrary in the same 96 well PCR microtiter plate. Seal with adhesive tape (Roth, #EN83.1) and mix well, spin down with ~400 x g (max. 2 x 4 plates per run). Use multichannel pipette to pipette 25 µl of tube B onto 96 well PCR microtiter plate. Seal with adhesive tape and mix well, spin down with ~400 x g. Incubate for 20 – 40 min at RT. Transfer transfection mix to 96 well microtiter plate with HEK293T cells (from day 0).

Day 2

Replace Culture Media

Take of supernatant from HEK293T cells (from day 1) with a NUNC™ Immuno-Washer™ (NUNC™, #470175), 9.5 mm comb depth, and replace with 150 µl fresh culture media. Handle with care because cells stick only loosely to the plastic.

Day 3

Reporter cell preparation

Prepare reporter cell line U-2OS BLH TD1 2K5 (culture time < 9 weeks) grown in log phase (one 175 cm2 flask gives cells for 3-4 plates). Trypsinize with trypsin/EDTA for ~ 5 min at 37 °C. Seed reporter cells (20 * 10^3/well) in 50 µl culture media plus 32 µg/ml protamine-sulfate (final concentration 8 µg/ml) on top of lentiviral supernatant in white 96 well plates.

Transfer supernatant

Transfer supernatant from HEK293T cells (from day 2) to MultiScreen® HTS filter plates (Milipore, #MSFBN6B50) which are placed on top of a white 96 well culture plate (NUNC, #136101). Filter supernatant onto culture plates by spinning at 3000 x g for 1 min. Measure the GFP expression of the HEK293T cells with the Infinite F200Pro™ Device (TECAN™).

Day 4

Replace culture media

Take of supernatant from reporter cell plate (from day 3) using the NUNC™ Immuno-Washer™ and replace with 150 µl fresh culture media plus puromycin (10 µg/ml).

Day 7

Start long term monitoring

Prepare 10 ml of culture media with 4 µM dexamethason (Sigma-Aldrich™, #D4902, solubilized in EtOH). Synchronize cells by adding 50 µl of dexamethason solution to reporter cell plate (from day 4), using a multichannel pipette. Incubate for 15 -30 min at at 37 °C, 5% CO_2. Wash reporter cell plate twice with 150 µl prewarmed PBS/well (with Immuno-Washer™). During the second wash with PBS on plate, measure the GFP expression of the U-2OS cells with the Infinite F200Pro™ Device (TECAN™). Finally ad 150µl reporter media per well to the plate and seal with Diamont Seal™ (Abgene™, #AB-0812) and the ALPS 50™ device (Abgene™) (2 times with 165 °C, 3 s each, rotating the plate for 180° in the horizontal plane). Start luminescence recording in TopCount™/LumiStar™/OrionII™.

Restart procedure with next pGIPZ sublibrary

Go to day 0 of this protocol to screen the next pGIPZ sublibrary.

Figure 6-9: Standard operating procedure for RNA interference screens

Vector maps

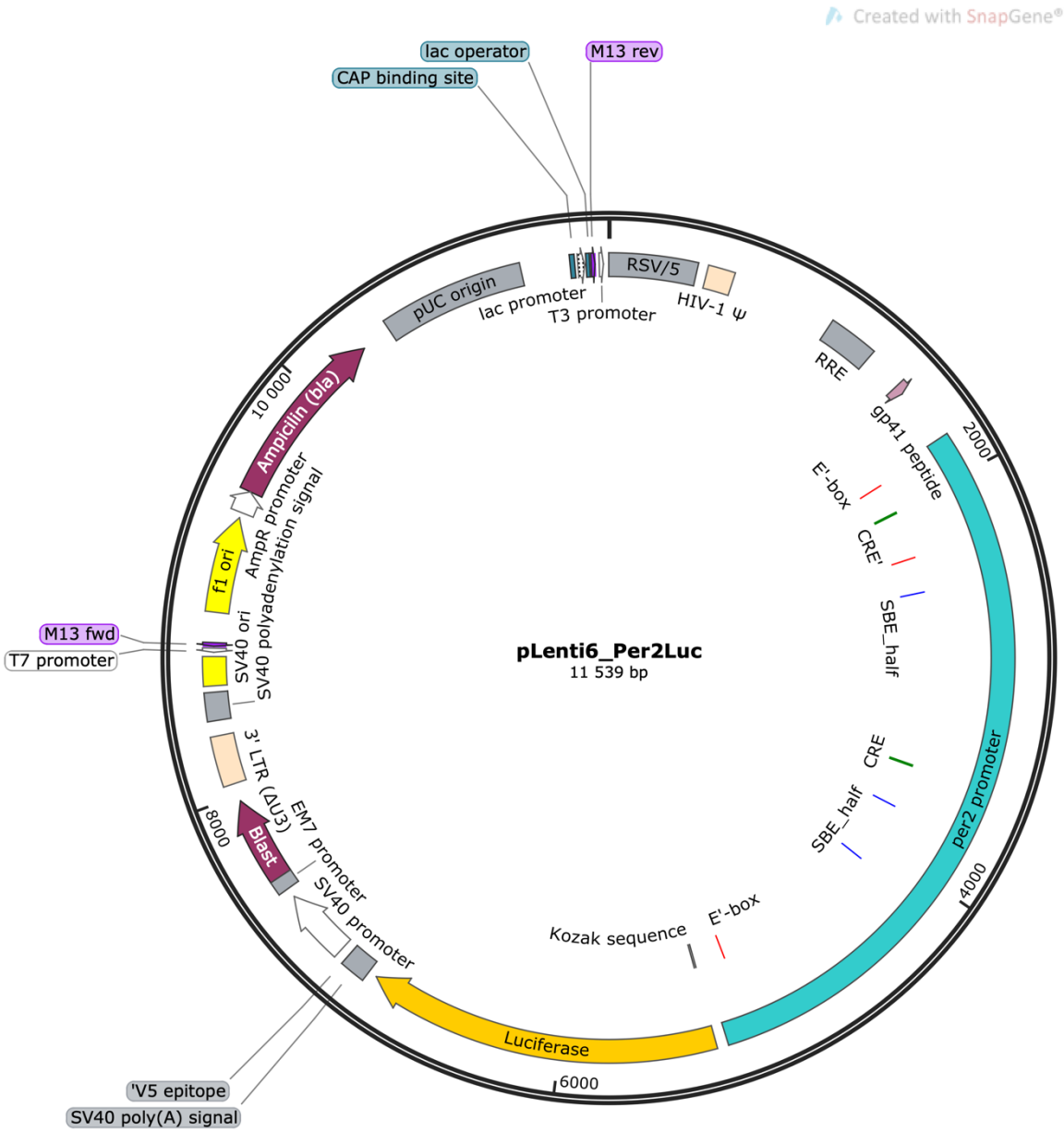

Figure 6-10: Vector map of pLenti6_Per2:Luc

Figure 6-11: Vector map pABhygro_Bmal1:Luc

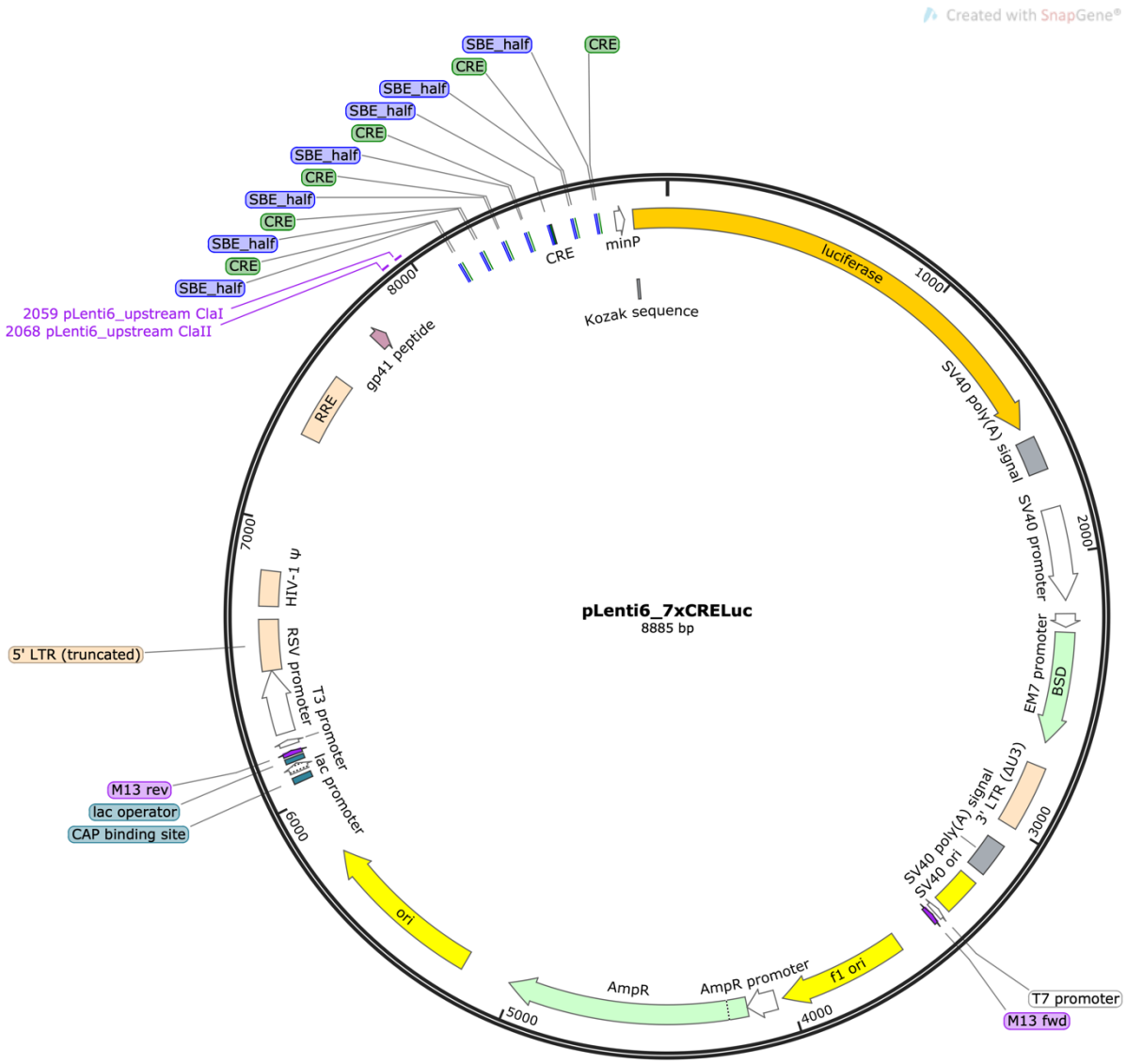

Figure 6-12: Vector map of pLenti6_7xCRE:Luc

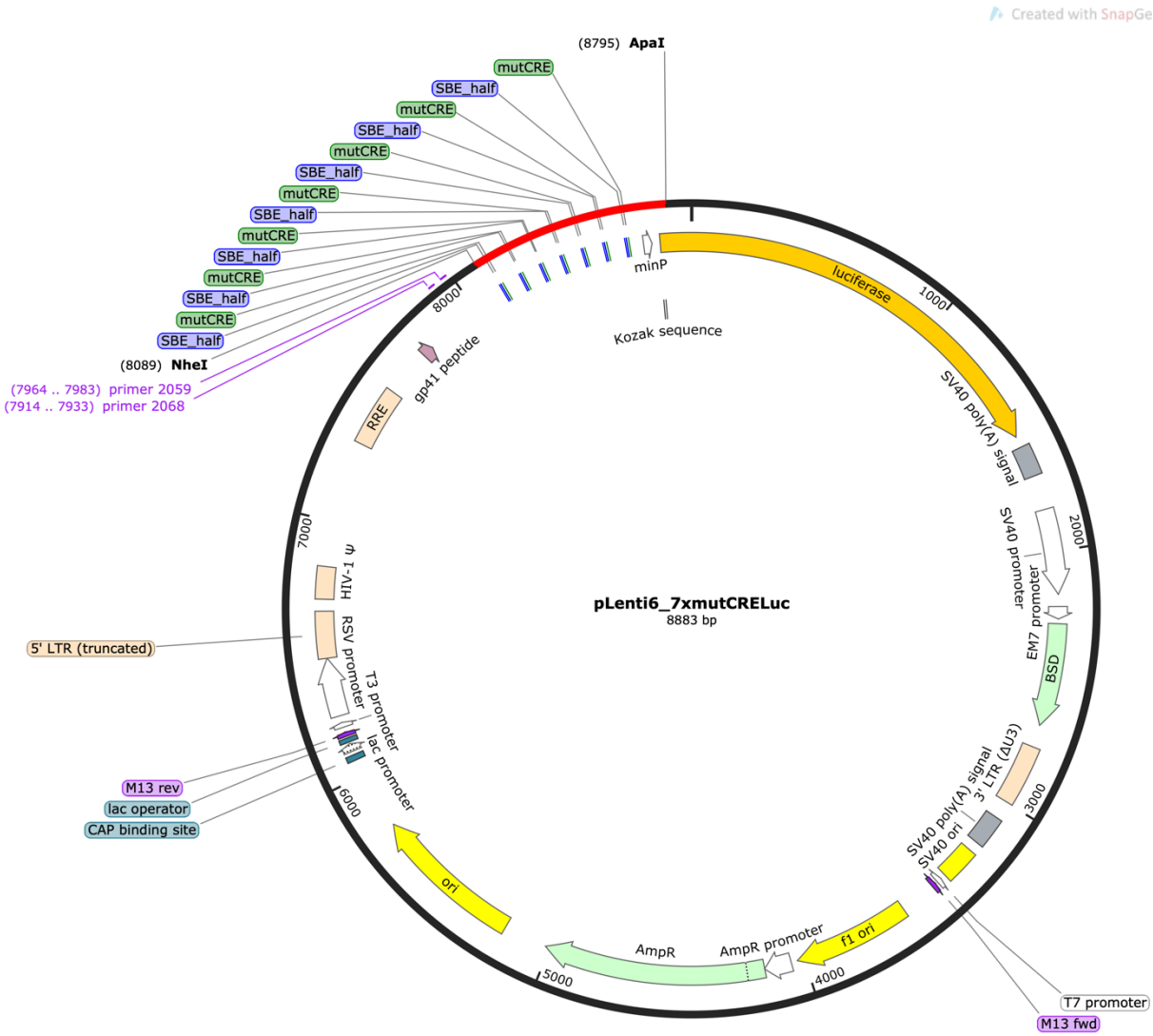

Figure 6-13: Vector map pLenti6_7xmutCRE:Luc

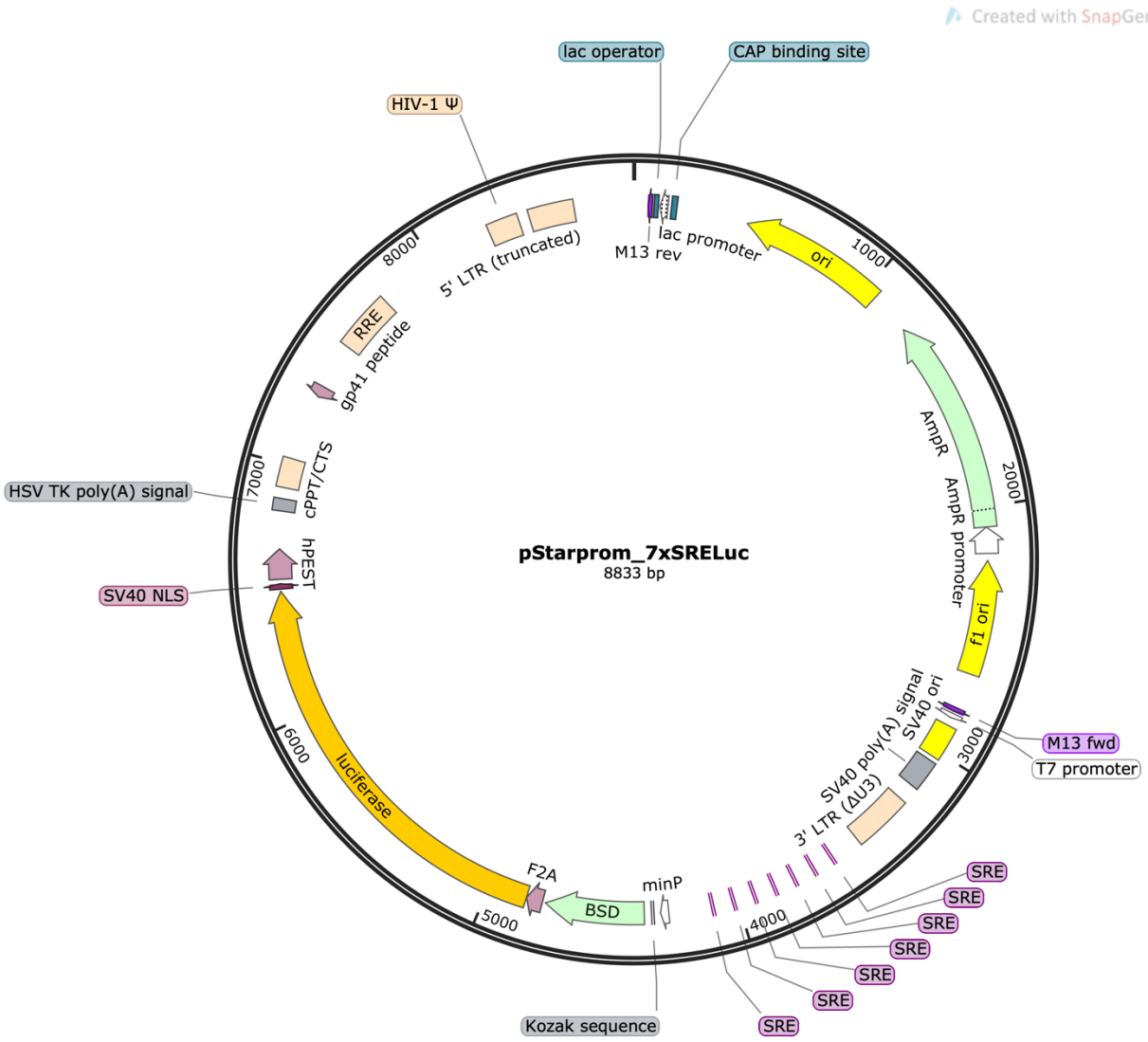

Figure 6-14: Vector map pStarprom_7xSRE:Luc

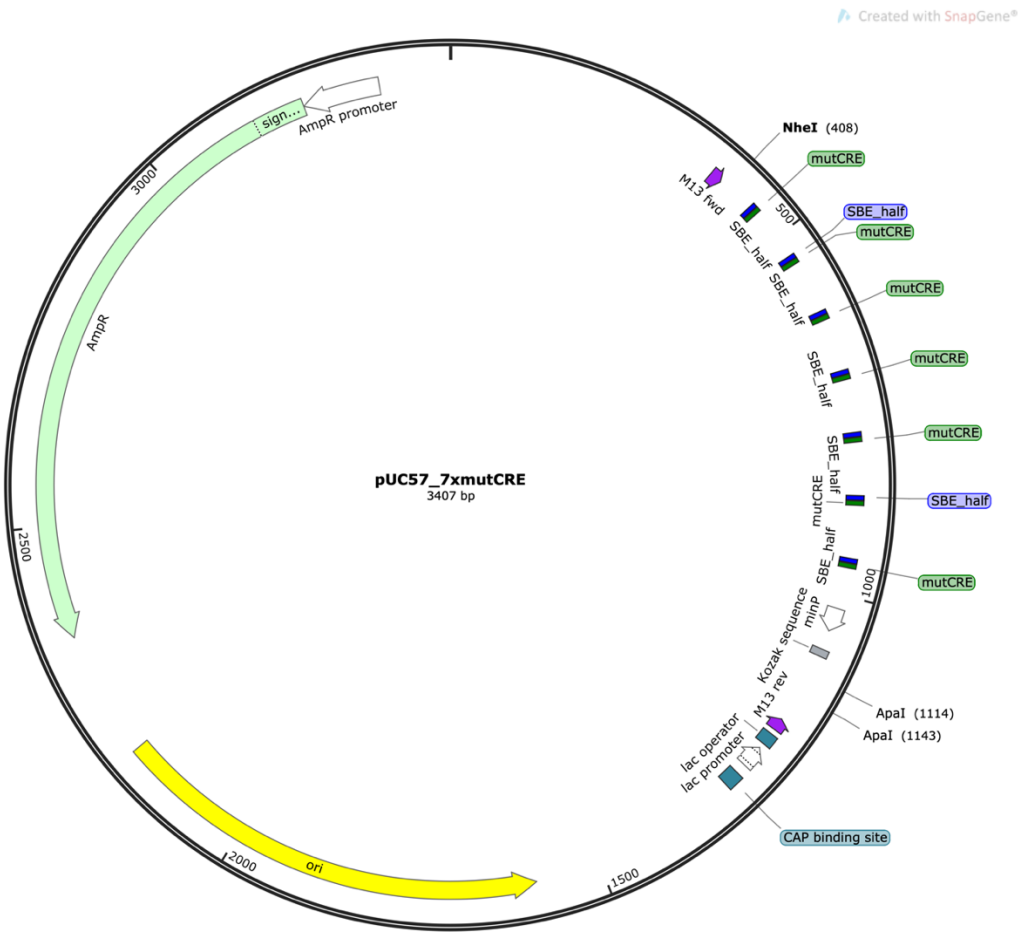

Figure 6-15: Vector map pUC57_7xmutCRE

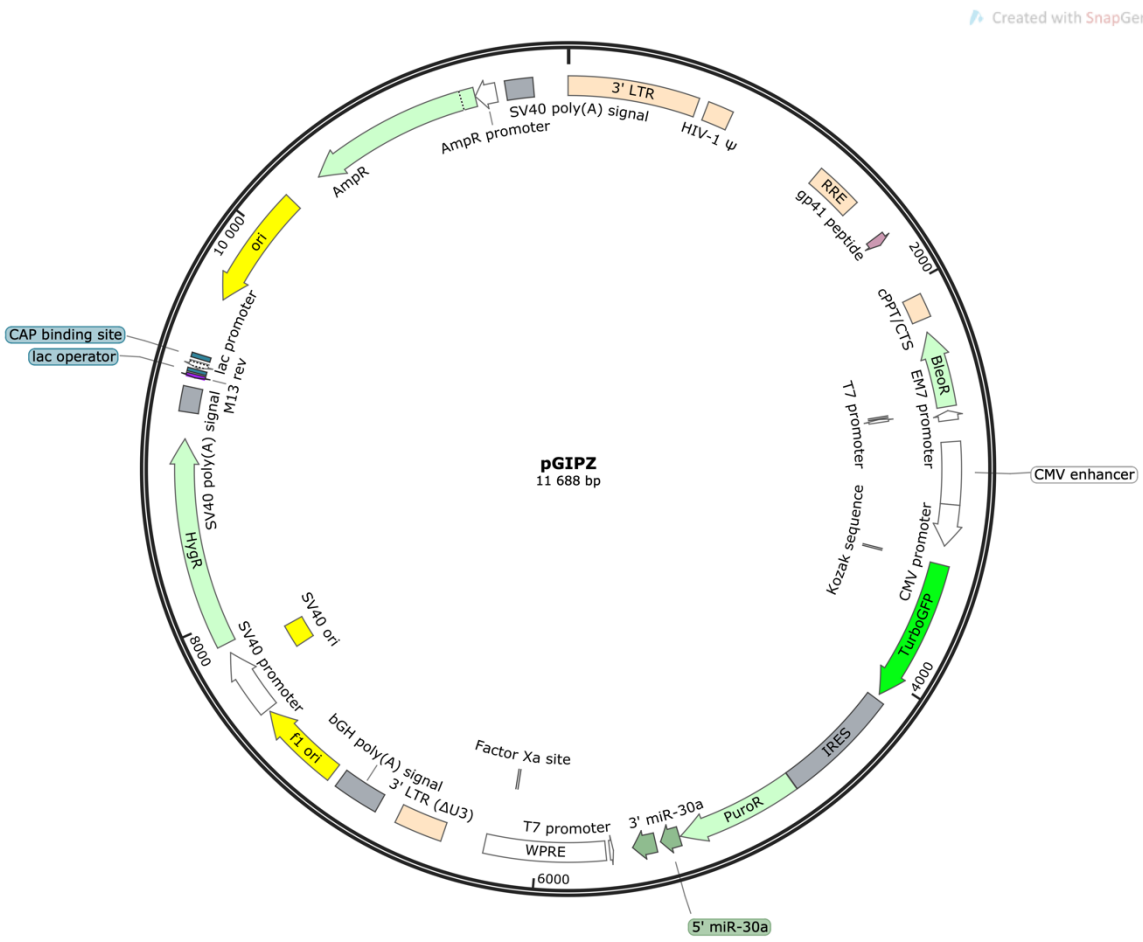

Figure 6-16: Vector map pGIPZ

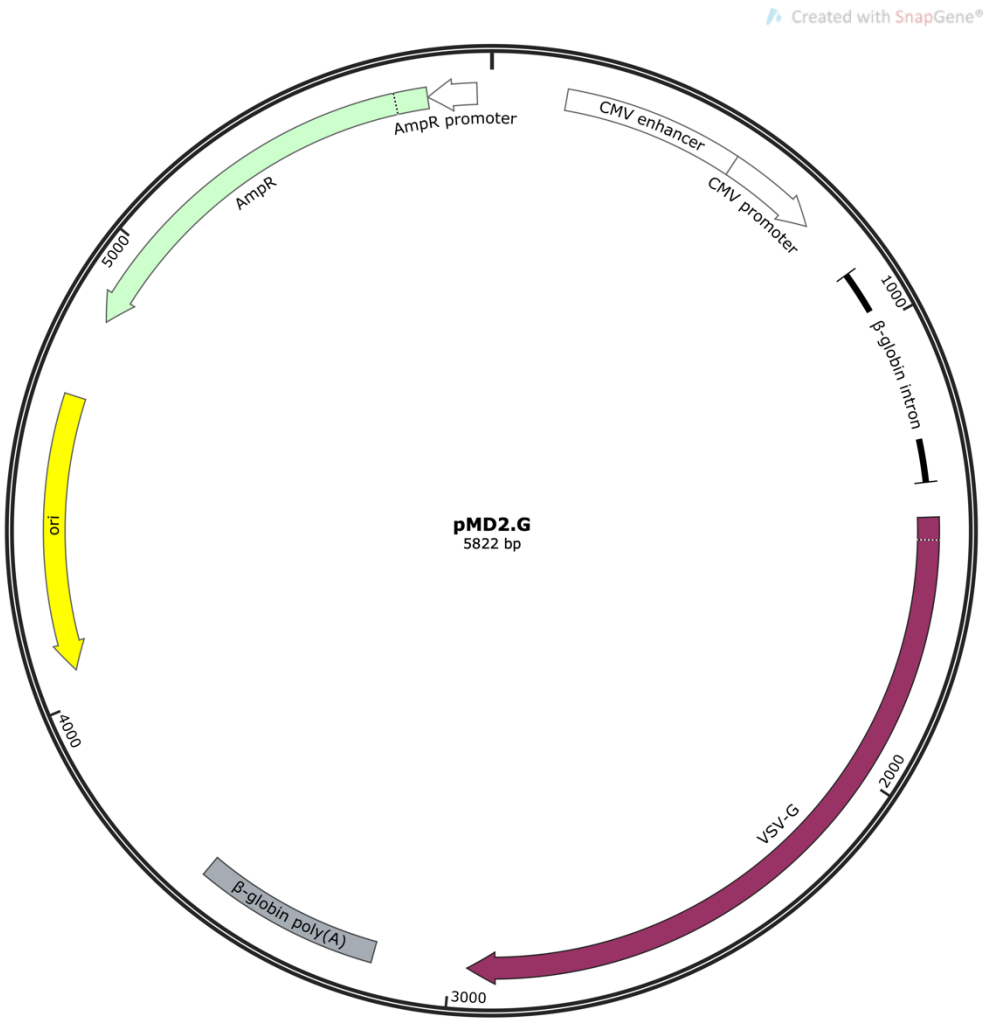

Figure 6-17: Vector map pMD2G

Figure 6-18: Vector map psPAX

List of Abbreviations

°	Degree
1°	Primary
°C	Degree Celsius
%	Percent
ψ	Phase of entrainment
τ	Intrinsic or free-running period
~	Approximately, nearly or circa
X(ϕ)	Influence Function (according to [209])
Z(ϕ))	Sensitivity Function (according to [209])
λ	Amplitude relaxation rate
AC	Adenylyl cyclase
ACN	Acetonitrile
ALK	Anaplastic lymphoma kinase receptor
AMH	Anti-Müllerian hormone
AMP	Adenosine monophosphate
AMPK	Adenosine monophosphate-activated protein kinase
Aq. dest	Aqua destillata
ATCC	American type culture collection
ATF	Activating transcription factor
ATP	Adenosine triphosphate
AUC	Area under the induction curve
AVP	Argenine Vasopressin (protein)
Arntl, ARNTL, ARNTL	Aryl hydrocarbon receptor nuclear translocator like (m_gene, h_gene, protein)
BCA	Bicinchoninic acid
bHLH	Basic helix-loop-helix
Bmal1, BMAL1, BMAL1	Brain and muscle Arntl-like 1 (m_gene, h_gene, protein)
Bmal1:Luc	Mouse *Bmal1* promotor driven luciferase
BMP	Bone morphogenic protein
bp	Base pairs

BSA	Bovine serum albumin
bZip	Basic leucine zipper
Ca^{2+}	Calcium
C2C12	Mouse myoblast cell line
CBP	CREB binding protein
CCG	Clock-controlled genes
cAMP	Cyclic adenosine monophosphate
CDMP	Cartilage-derived morphogenetic protein
cDNA	Complementary DNA
C/EBP	CCAAT/enhancer binding protein
c-fos, c-FOS	Fos proto-oncogene, AP-1 transcription factor subunit (m_gene, protein)
c-myc, MYC	MYC proto-oncogene, bHLH transcription factor (m_gene, protein)
c-jun, c-JUN	Jun proto-oncogene, AP-1 transcription factor subunit (m_gene, protein)
CAMK	Calmodulin-dependent protein kinase
Clock,CLOCK, CLOCK	Circadian locomotor output cycles protein kaput (m_gene, h_gene, protein)
cm, cm^2	Centimeter, square centimeter
CO_2	Carbon dioxide
CRE	cAMP response element
CREB	cAMP response element binding protein
CRH	Corticotropin releasing hormone
CT	Circadian time
CTGF	Connective tissue growth factor
Cry, *CRY*, CRY	Cryptochrome circadian regulator (m_gene, h_gene, protein)
Cx36	Connexin-36
D	Dalton
Dbp, DBP, DBP	D-box binding PAR bZIP transcription factor or D site albumin promoter binding protein (m_gene, h_gene, protein)
D-Box	D-box enhancer element

Dec1, DEC1, DEC1	bHLH family member E40 (m_gene, h_gene, protein)
ddH_2O	Double-distilled water
DGE	Differential gene expression
DMEM	Dulbecco's modified eagle's medium
DMSO	Dimethyl sulfoxide
DNA	Deoxyribonucleic acid
DNase	Deoxyribonuclease
dNTP	Deoxyribose nucleoside triphosphate
DTT	Dithiothreitol
E. coli	Escheria coli (bacteria)
E-Box	E-box enhancer element
ECM	Extracellular matrix
E4bp4, E4BP4	*Nfil3*, NFIL3 (m_gene, protein)
EDTA	Ethylenediaminetetraacetic acid
ERK	Extracellular signal regulated kinases
et al.	and others
EtOH	Ethanol
FA	Formic acid
FBS	Fetal bovine serum
FEO	Food entrainable oscillator
fos-B, FOSB	FosB proto-oncogene, AP-1 transcription factor (m_gene, protein)
g	Grams
$G\alpha$	G alpha subunit of GPCRs
GABA	Gamma-aminobutyric acid
GDF	Growth differentiation factor
GDF8	Myostatin
GluR	Glutamate receptor
GO	Gene ontology
GPCR	G-protein coupled receptor
GRP	Gastrin-releasing peptide
GRE	Glucocorticoid response elements
hs	Hours

HBS	HEPES-buffered saline
HCT116	Human colon colorectal cancer cell line
HEK293T	Human embryonic kidney, SV40 large T antigen cell line
HEPES	4-(2-hydroxyethyl)-1-piperazineethanesulfonic acid
h_gene	Human gene name
HSL	hormone sensitive lipase
HSF1	heat shock transcription factor 1
HSE	Heat shock element
IEG	Immediate early genes
ipRGC	Intrinsically photosensitive retinal ganglion cells
Itgav, ITGAV, ITGAV	Integrin alpha subunit V (m_gene, h_gene, protein)
Itgb6/8, ITGB6/8, ITGB6/8	Integrin subunit beta 6/8
IVIS	In vivo imaging system
JNK	c-jun N-terminal kinase
jun-B, JUNB	Jun B proto-oncogene, AP-1 transcription factor subunit (m_gene, protein)
k	Coupling strength
kb	Kilo bases
kD	Kilo Dalton
LAP	Latency associated peptide
LLC	Large latent complex
Ltbp, *LTBP*, LTBP	Latent TGF-β binding protein (m_gene, h_gene, protein)
Luc	Luciferase
LY2109761	TGF-β receptor inhibitor
µg	Microgram
µL	Microliter
µM	Micromole
M	Mole
mM	Millimole
MAPK	Mitogen-activated protein kinase 1
MDSEC	Majority decision-based method for secreted proteins

mg	Milligram
m_gene	Mouse gene name
MH1	SMAD mad homology 1 domain
mins	Minutes
MIS	Müllerian-inhibiting substance
MMP	Matrix metalloprotease
mL	Milliliter
MS	Mass spectrometry
mRNA	Messenger RNA
mut	mutated
NAD/NADH	Nicotinamide dinucleotide
NADP/NADPH	Nicotinamide dinucleotide phosphate
Nfil3, NFIL3	Nuclear factor interleukin 3 regulated (m_gene, protein)
NF-κB	Nuclear factor 'kappa-light-chain-enhancer' of activated B-cells
ng	Nano gram
NIH3T3	Mouse embryonic fibroblast cell line
nM	Nano Molar
Nr1d1/2, NR1D1/2, NR1D1/2	Nuclear receptor subfamily 1 group D member 1/2 (m_gene, h_gene, protein)
OP	Osteogenic protein
p300	Histone acetyltransferase
PACAP	Pituitary adenylate cyclase activating polypeptide
PAC1	Pituitary adenylate cyclase-activating polypeptide type I receptor
PAR bZip	Proline and acidic amino acid-rich basic leucine zipper
PBS	phosphate-buffered saline
PCR	polymerase chain reaction
Per, *PER*, PER	Period circadian regulator (m_gene, h_gene, protein)
Per2:Luc	Mouse *Per2* promotor driven luciferase
PER2::LUC	Mouse PER2 luciferase fusion protein

pH	potential of hydrogen
PKA	Protein kinase A
pmol	Picomol
Post-sync	Post-synchronization
PRC	Phase response curve
PSG	Pregnancy-Specific Glycoprotein
PTC	Phase transition curve
PVN	Paraventricular nucleus
qPCR	Quantitative polymerase chain reaction
qRT-PCR	Quantitative real-time polymerase chain reaction
Ras	Rat sarcoma
Rev-erbα/β, *REV-ERB*α/β, REV-ERBα/β	*Nr1d1/2*, *NR1D1/2*, NR1D1/2
RevDR2	Direct repeat 2 response element
RGD	Integrin recognition motif
RhoA	Ras homolog family member A
RHT	Retinohypothalamic tract
RNA	Ribonucleic acid
RNAseq	RNA sequencing
Ror, ROR,	RAR-related orphan receptors (m_gene, protein)
ROS	Reactive oxygen species
RORE	ROR response element
RSPO1	Rspondin-1
RXXR	Furin convertase motif
RT	Reverse transcription
SCN	Suprachiasmatic nucleus
SD	Standard deviation
Shc	Src homology domain containing transforming protein
shRNA	Small hairpin RNA
SFRP	Selected frizzled-related protein
Ski, SKI, SKI	SKI oncogene (m_gene, h_gene, protein)
Smad, *SMAD*, SMAD	Mothers against decapentaplegic homolog (m_gene, h_gene, protein)

α-SMA	Contractile protein α-smooth muscle actin
SMOC	SPARC-related modular calcium binding protein
SRE	Serum response element
SRF	Serum response factor
SYBR-green	Cyanine dye
t	Time
TAE	Tris-acetate-ETDA buffer
TE	Tris-EDTA
TF	Transcription factor
TFA	Trifluoroacetic acid
THSB1	Thrombospondin-1
TNPO1, TNPO1	Transportin-1 (h_gene, protein)
TTFL	Transcriptional-translational feedback loop
Tgfb, TGFB, TGFB (TGF-β)	Transforming growth factor beta (m_gene, h_gene, protein)
Tgfbr1, TGFBR1, TGFBR1 (ALK5)	TGF-β receptor type 1 (m_gene, h_gene, protein)
Tgfbr2, TGFBR2, TGFBR2	TGF-β receptor type 2 (m_gene, h_gene, protein)
TSS	Transcriptional starting site
SLC	Small latent complex
U-2 OS	Human osteosarcoma cell line
V	Volt
Vipr2, VPAC2	Vasoactive intestinal peptide receptor 2
Vip, VIP	Vasoactive intestinal polypeptide (gene, protein)
VRC	Velocity response curve
WNT3A	Wnt-3A protein
ZT	Zeitgeber time

Publications and distinctions

Publications

B. Maier, S. Lorenzen, A. M. Finger, H. Herzel, A. Kramer, “Searching novel clock genes using RNAi-based screening”, in *Springer Methods in Molecular Biology: Circadian Clocks, Methods and Protocols*, 2130, S. A. Brown, Springer US, 2020, DOI: 10.1007/978-1-0716-0381-9

Conference contributions

A. M. Finger, S. Jäschke, A. Kramer, Secretory pathways are required for circadian oscillations, poster presentation at the Chronobiology Gordon Research Seminar and Conference, Vermont, USA, 2017

A. M. Finger, S. Jäschke, A. Kramer, Intercellular communication between peripheral circadian oscillators, scientific talk at the German Clock Club, Würzburg, GER, 2018

A. M. Finger, S. Jäschke, A. Kramer, Mechanisms of Intercellular Communication between Peripheral Circadian Oscillators, poster presentation at the IMB Workshop: Molecular Mechanisms of Circadian Clocks, Mainz, GER, 2018

A. M. Finger, S. Jäschke, R. Hurwitz, H. Herzel, A. Kramer, Mechanisms of Intercellular Communication between Peripheral Circadian Oscillators, scientific talk and poster presentation at the Chronobiology Gordon Research Seminar, Barcelona, ESP, 2019

A. M. Finger, S. Jäschke, R. Hurwitz, H. Herzel, A. Kramer, Mechanisms of Intercellular Communication between Peripheral Circadian Oscillators, poster presentation at the Chronobiology Gordon Research Conference, Castelldefels, ESP, 2019

A. M. Finger, S. Jäschke, R. Hurwitz, H. Herzel, A. Kramer, A Potential Mechanism of Intercellular Coupling in Peripheral Circadian Clocks, scientific talk at the CARE conference, Munich, GER, 2019

Fellowships, and awards

Add-On Fellowship for Interdisciplinary Life Science, Joachim Herz Stiftung, Hamburg, GER, 2018-2020

FEBS Letters Poster Prize, awarded at the Chronobiology Gordon Research Conference, Castelldefels, ESP, 2019

“Förderprogramm Begegnungszonen” Grant, Joachim Herz Stiftung, Hamburg, GER, 2019

Professional experiences

Reviewer, Journal of Molecular Biology, 2019

Chair of the Summer School of Circadian Sciences, Charité University Medicine, Berlin, GER, 2020

Chair of the Chronobiology Gordon Research Seminar, Gordon Research Conferences, Maine, USA, 2021

Acknowledgement

Herein, I would like to express my deepest gratitude and acknowledgment to all the people and supporting institutes that made the accomplishment of this thesis possible.

Foremost I would like to thank Prof. Dr. Achim Kramer and Prof. Dr. Hanspeter Herzel for their continuous scientific and personal supervision. They have accepted me as their doctoral student and have given me the opportunity to work on a highly interesting and interdisciplinary topic combining experimental and theoretical research. The part of chronobiology linking biological with mathematical/physical phenomena has always fascinated me the most. Therefore, studying coupling among oscillators was the perfect fit for me. I thank Achim for his eminent scientific guidance, motivational advice, and our challenging discussions regarding future projects. I thank Hanspeter for his constant academic and personal input, his patience with my reoccurring confusion about theoretical concepts, as well as for making this last year of my Ph.D. possible. I thank both of my supervisors for putting trust in me, pushing me and encouraging me to develop into an independent scientist and become a part of the Chronobiology community. We have gone where the dust is, so where do we go next?

I also would like to thank Dr. Robert Hurwitz and Ralf Winter for their cooperation, support, advice, and constant work. Without you this project would not have developed the way it did.

A very special thanks goes to all my colleagues from the Kramer and Herzel laboratories, who have become friends over the last years. Scientifically but also personally I have benefited a lot from becoming part of their teams. They have always given me well-experienced scientific advice and had an open ear for interesting academic and non-academic discussions, especially when times were challenging. I would also like to thank Sebastian Jäschke for his work leading up to my project.

Last but not least, I would like to thank my family for their never ending support, for believing in me even when I don’t, for telling me to pull myself together when I don’t want to hear it, and for always being there. Thank you.

Declaration of Authorship

I, Anna-Marie Finger, hereby declare that this thesis: “Molecular Mechanisms of Intercellular Coupling among Peripheral Circadian Oscillators” and the work presented are my own. I confirm that I have not used any sources other than those listed in the bibliography and identified references. I further declare that I have not submitted this thesis at any other institution in order to obtain a research degree.

Ich, Anna-Marie Finger, erkläre, dass ich die vorliegende Arbeit mit dem Titel: “Molecular Mechanisms of Intercellular Coupling among Peripheral Circadian Oscillators“ selbst verfasst, sowie die darin präsentierten Ergebnisse selbständig erarbeitet habe. Ich bestätige weiterhin, keine anderen als die hier angegebenen Literaturquellen und Hilfsmittel verwendet zu haben. Ich habe diese Dissertation an keiner anderen Hochschule zur Erlangung des akademischen Grades Ph.D. eingereicht.

_____

Date/Datum, Signature/Unterschrift